

Utah State University

DigitalCommons@USU

All Graduate Theses and Dissertations

Graduate Studies

5-2012

The Mechanisms of Hydride Exchange, Organic Combination and Displacement Reactions

Weifang Hao
Utah State University

Follow this and additional works at: <https://digitalcommons.usu.edu/etd>



Part of the [Chemistry Commons](#), and the [Philosophy Commons](#)

Recommended Citation

Hao, Weifang, "The Mechanisms of Hydride Exchange, Organic Combination and Displacement Reactions" (2012). *All Graduate Theses and Dissertations*. 1226.
<https://digitalcommons.usu.edu/etd/1226>

This Dissertation is brought to you for free and open access by the Graduate Studies at DigitalCommons@USU. It has been accepted for inclusion in All Graduate Theses and Dissertations by an authorized administrator of DigitalCommons@USU. For more information, please contact digitalcommons@usu.edu.



THE MECHANISMS OF HYDRIDE EXCHANGE, ORGANIC COMBINATION
AND DISPLACEMENT REACTIONS

by

Weifang Hao

A dissertation submitted in partial fulfillment
of the requirements for the degree

of

DOCTOR OF PHILOSOPHY

in

Chemistry

Approved:

Vernon D. Parker, Ph.D.
Major Professor

Alvan C. Hengge, Ph.D.
Committee Member

Cheng-Wei Tom Chang, Ph.D.
Committee Member

Lance C. Seefeldt, Ph.D.
Committee Member

Roger A. Coulombe, Jr., Ph.D.
Committee Member

Mark R. McLellan
Vice President for Research and
Dean of the School of Graduate Studies

UTAH STATE UNIVERSITY
Logan, Utah

2012

Copyright © Weifang Hao 2012

All Rights Reserved

ABSTRACT

The Mechanisms of Hydride Exchange, Organic Combination
and Displacement Reactions

by

Weifang Hao, Doctor of Philosophy
Utah State University, 2012

Major Professor: Dr. Vernon D. Parker
Department: Chemistry and Biochemistry

The primary aim of this dissertation was to seek the answer to the question: “Is the single transition-state model appropriate for the fundamental reactions in organic chemistry?” The goal was accomplished by performing enormous kinetic data collection and detailed mechanistic analysis on several typical fundamental organic chemical reactions.

Three new methodologies for differentiating between a simple one-step and complex multi-step mechanism were developed and extensively confirmed during the application in the kinetic studies of all of the reaction discussed in this dissertation. The three methods consist of (1) half-life dependence of k_{app} , (2) sequential linear pseudo-first-order correlation, and (3) revised instantaneous rate constant analysis.

A detailed kinetic investigation of the formal hydride transfer reaction of NADH models [*N*-benzyl-1,4-dihydronicotinamide (BNAH)] with *N*-

methylacridinium (MA^+) and *N*-methyl-9,10-dihydroacridine (MAH) with tropylium ion (Tr^+)] confirmed that both these reactions take place in more than one step and involve kinetically significant reactant complex intermediates, which are noncovalently bound intermediates. Computations at the M06-2x/6-311++G(d,p) level provided the structure of the reactant complex intermediate. A reinvestigation of the formal hydride transfer reaction of 1-benzyl-3-cyanoquinolinium ion (BQCN^+) with *N*-methyl-9,10-dihydroacridine (MAH) in acetonitrile (AN) confirmed that the reaction takes place in more than one step and revealed a new mechanism that had not previously been considered. It was observed that even residual oxygen under glove box conditions initiates a chain process leading to the same products.

The combination reactions studied include the reaction between a carbocation and an anion as well as the reaction of *trans*- β -nitrostyrene with nitroethide ion. Conventional pseudo-first-order analysis as well as instantaneous rate constant analysis confirmed that the combination reactions do not follow the simple one-step mechanism. The $\text{S}_{\text{N}}2$ displacement of halide ions by the 4-nitrophenoxide ion was also investigated and the kinetic data are inconsistent with the concerted single transition-state model.

(249 pages)

PUBLIC ABSTRACT

The Mechanisms of Hydride Exchange, Organic Combination
and Displacement Reactions

by

Weifang Hao, Doctor of Philosophy

Utah State University, 2012

In chemical reactions, kinetics is the study of the rates of chemical processes. Reaction mechanisms are the detailed processes by which chemical substances are transformed into other substances. A mechanism describes in detail exactly what takes place at each stage of a chemical transformation.

The work outlined in this dissertation was carried out in order to find out the actual mechanisms for three classes of fundamental organic reactions by means of a series of novel kinetic techniques and analysis methods. They include the hydride exchange between NADH model compounds, organic combination, and S_N2 displacement reactions.

Rigorous kinetic investigations have found that these reactions actually take place by multi-step mechanisms involving kinetically significant intermediates. This result challenges the long-held assumption that these reactions follow a simple one-step mechanism. Although the assumption of the one-step mechanism can be applied to evaluate the magnitude of the rate of the overall reaction, it fails to provide a detailed description of the chemical reactions.

However, adopting the multi-step mechanisms proposed in this dissertation should end this chapter of organic chemistry.

Reaction mechanism is a primary topic for organic chemical studies and is able to provide a framework for appropriate application in pharmacy, industry, and agriculture. An essential objective of this work is to point out more attention to the importance of reaction mechanism in the field of organic chemistry. A broad impact of this work on academic studies may be achieved via promoting a revision of the mechanisms believed to be established over the past seventy years. It will have a broad effect in other branches of chemistry as well as in biochemistry.

This work is a sub-project of the three-year \$665,000 international cooperative project with the question, "Is the single transition state model appropriate for the fundamental reactions of organic chemistry?" initiated by Professor Vernon D. Parker at USU, collaborating with Professors Jin-Pei Cheng and Xiao-Qing Zhu at Nankai University in China. This international project, supported by both NSF (National Science Foundation) and NSFC (National Natural Science Foundation of China), has been fostering cooperation and good will between the scientific communities of the United States and China.

ACKNOWLEDGMENTS

I would like to express my sincere gratitude to my supervisor, Dr. Vernon D. Parker, for all that I have learned from him throughout my academic program at Utah State University. He helped me greatly to develop my skills in the study of chemical kinetics, to improve my understanding of the field of physical organic chemistry, and to gain a deep appreciation for the tenacity required to perform such research. The joy and enthusiasm he has for his research was contagious and motivational for me during the entire time of my Ph.D. pursuit.

I thank all of the members of my supervisory committee: Dr. Cheng-Wei Tom Chang, Dr. Roger A. Coulombe, Jr., Dr. Alvan C. Hengge, and Dr. Lance C. Seefeldt. I appreciate their support, encouragement, and suggestions, which greatly influenced my progress and professional growth.

I also would like to thank all of my labmates, e.g., Justin Holm and Mike Helms for teaching me how to use the instruments; Zhao Li for discussing the research and solving so many problems with me together; Xiaosong Xue for the computation work that he has done for my reaction systems; and Rui Cao, Russell Scow, and Xiaozhen Han, for their contribution to my research.

I am also grateful to Dr. Yun Lu, a former postdoctoral fellow in our group, for his generosity to send me several organic compounds for my preliminary tests and also for giving me valuable suggestions to my research.

I express my deep appreciation to my husband, Tao, for his love and support during all of years we have gone through together. I also thank my parents and my parents-in-law for their support and encouragement.

I especially thank Monica for her kindness and friendliness. She is always a good friend to me, giving me suggestions and support at all the time. We had a really great time together.

Finally, I thank Professor Jin-Pei Cheng and Prof. Xiao-Qing Zhu, our collaborators and my former supervisors at Nankai University, for establishing the USU-Nankai International Cooperative Graduate Program and their efforts in international funding application. I thank the Department of Chemistry and Biochemistry for giving me the opportunity to pursue my second Ph.D. at Utah State University.

Weifang Hao

CONTENTS

	Page
ABSTRACT	iii
PUBLIC ABSTRACT	v
ACKNOWLEDGMENTS	vii
LIST OF TABLES	xi
LIST OF FIGURES	xviii
LIST OF SCHEMES	xxiv
CHAPTER	
1. INTRODUCTION	1
2. THE DEVELOPMENT OF NEW METHODOLOGIES FOR DIFFERENTIATING BETWEEN THE SIMPLE ONE-STEP AND COMPLEX MULTI-STEP MECHANISMS	17
3. MECHANISM STUDY OF HYDRIDE TRANSFER BETWEEN N-BENZYL- 1,4-DIHYDRONICOTINAMIDE AND N-METHYLACRIDINIUM ION IN ACETONITRILE	28
4. MECHANISM STUDY OF HYDRIDE TRANSFER BETWEEN N-METHYL- 9,10-DIHYDROACRIDINE AND TROPYLIUM ION IN ACETONITRILE ..	48
5. OXYGEN INITIATED CHAIN MECHANISM FOR HYDRIDE TRANSFER BETWEEN NADH AND NAD ⁺ MODELS. THE REACTION OF 1- BENZYL-3-CYANOQUINOLINIUM ION WITH N-METHYL-9,10- DIHYDROACRIDINE IN ACETONITRILE	60
6. RAPID FORMATION AND SLOW COLLAPSE OF A CARBOCATION- ANION PAIR TO A NEUTRAL MOLECULE	95
7. THE MECHANISM OF COVALENT BOND FORMATION DURING THE COMBINATION OF NITROSTYRENE WITH NUCLEOPHILES	122
8. THE S _N 2 DISPLACEMENT OF HALIDE IONS BY 4-NITROPHENOXIDE ION	137
9. CONCLUSIONS	152
APPENDICES	155

CURRICULUM VITAE	220
------------------------	-----

LIST OF TABLES

Table	Page
1-1. The Rate Constant and Time Ratios for the Elimination Reactions of 2-(<i>p</i> -Nitrophenyl)ethyl Bromide in Alcohols Containing the Corresponding Alkoxide Ions at 293K.....	8
2-1. Changes in the Slopes and the Intercepts with the Extent of Reaction During Conventional Pseudo-First-Order Analysis for the Reaction of BrAN (5.0 mM) with PO ⁻ (0.50 mM) in Acetonitrile at 298 K.....	21
2-2. Point Segment Set for Sequential Pseudo-First-Order Linear Correlation Analysis.....	21
2-3. Apparent Rate Constants and Standard Deviations Obtained by the 24-Point Sequential Analysis for the Reaction of BrAN (5.0 mM) with PO ⁻ (0.50 mM) in Acetonitrile at 298 K.....	22
3-1. Time and Rate Constant Ratios for the Hydride Transfer Reactions Between BNAH/BNAH- <i>d</i> ₂ and MA ⁺ in Acetonitrile at 298K over a Range of Wavelengths.....	31
3-2. Apparent Rate Constants for the Hydride Transfer Reaction Between BNAH and MA ⁺ in Acetonitrile over the First Half-Life at 298K as a Function of Wavelengths.....	33
3-3. Apparent Rate Constants for the Hydride Transfer Reaction Between BNAH- <i>d</i> ₂ and MA ⁺ in Acetonitrile over the First Half-Life at 298K as a Function of Wavelengths.....	34
3-4. Apparent KIE for the Reactions Between BNAH/BNAH- <i>d</i> ₂ and MA ⁺ in Acetonitrile at 298K under Different Wavelengths.....	37
4-1. Changes in the Slopes and the Intercepts with the Extent of Reaction During Conventional Pseudo-First-Order Analysis for the Reactions of MAH/MAH- <i>d</i> ₂ (0.4 mM) with Tr ⁺ (0.05 M) in Acetonitrile at 298K and 450 nm.....	50
4-2. Apparent Rate Constants for the Reaction of MAH with Tr ⁺ in Acetonitrile over the First Half-Life at 298K as a Function of Wavelengths.....	51
4-3. Apparent Rate Constants for the Reaction of MAH- <i>d</i> ₂ with Tr ⁺ in Acetonitrile over the First Half-Life at 298K as a Function of Wavelengths.....	52

4-4.	Time and Rate Constant Ratios for the Hydride Transfer Reaction Between MAH and Tr^+ in Acetonitrile at 298K over a Range of Wavelengths.....	54
5-1.	Changes in the Apparent Pseudo-First-Order Rate Constants (k_{app}) as a Function of the Degree of Reaction Analyzed for the Reactions of MAH with BQCN^+ in AN at 298 K under Various Conditions and 430 nm.....	70
5-2.	Changes in k_{app} and Standard Deviations (S.D.) as a Function of the Degree of Reaction Analyzed for the Reactions of MAH /MAH- d_2 (40 mM) with BQCN^+ (0.5 mM) in AN at 298K in the Presence of Residual Oxygen and 430 nm.....	72
5-3.	Changes in k_{app} and Standard Deviations (S.D.) as a Function of the Degree of Reaction Analyzed for the Reactions of MAH /MAH- d_2 (40 mM) with BQCN^+ (0.5 mM) in AN at 298K Half-Saturated with Air and 430 nm.....	73
5-4.	Changes in k_{app} and Standard Deviations (S.D.) as a Function of the Degree of Reaction Analyzed for the Reactions of MAH /MAH- d_2 (0.5 mM) with BQCN^+ (40 mM) in AN at 298K in the Presence of Residual Oxygen and 450 nm.....	74
5-5.	Changes in k_{app} and Standard Deviations (S.D.) as a Function of the Degree of Reaction Analyzed for the Reaction of MAH (0.5 mM) with BQCN^+ (40 mM) in AN at 298K Half-Saturated with Air and 430nm.....	75
5-6.	Apparent Rate Constants and Apparent Kinetic Isotope Effects at Short Times for the Reactions of MAH/MAH- d_2 (10 mM) with BQCN^+ (40 mM) in AN at 298 K in the Presence of Residual Oxygen at 440nm (Over the First 0.3% Reaction).....	76
5-7.	Changes in k_{app} and Standard Deviations (S.D.) as a Function of the Degree of Reaction Analyzed for the Reaction of MAH (10 mM) with BQCN^+ (0.5 mM) in AN at 298K in the Presence of Residual Oxygen at 450nm over 1 HL.....	79
5-8.	Changes in k_{app} and KIE_{app} as a Function of the Degree of Reaction (Over the First 0.6% Reaction) Analyzed for the Reactions of MAH/MAH- d_2 (10 mM) with BQCN^+ (40 mM) in AN in the Presence of Residual Oxygen and 440 nm.....	80
6-1.	Effect of Sodium Acetate Concentration on the Apparent Steady-State Rate Constant for the Reaction of TMT^+ with Sodium Acetate in Acetic Acid at 298 K.....	101

6-2.	Apparent Steady-State Rate Constants for the Reaction Between TMT ⁺ and Acetate Ion as a Function of [Bu ₄ N ⁺ HOAc/AcO ⁻] in Acetic Acid at 298 K.....	101
6-3.	Ratios of Conventional Pseudo-First-Order Rate Constants Evaluated over Initial Data Segments Divided by the Apparent Steady-State Rate Constant ($k_{s.s.} = 0.0650 \text{ s}^{-1}$) for the Reaction of TMT ⁺ (0.02 mM) with Na ⁺ HOAc/AcO ⁻ (0.5 M) in Acetic Acid at 298 K and 510 nm.....	103
6-4.	Time and Rate Constant Ratios Observed for the Reaction of TMT ⁺ with NaOAc (0.50 M) in Acetic Acid at 298 K.....	104
6-5.	Ratios of Conventional Pseudo-First-Order Rate Constants Evaluated over Initial Data Segments Divided by $k_{s.s.}$ (0.0155 s^{-1}) for the Reaction of TMT ⁺ (0.02 mM) with Acetate Ion (0.005 M) in HOAc/AN (1/1, v/v) at 298 K and 480 nm.....	106
6-6.	Kinetic and Thermodynamic Parameters for the Collapse of {TMT ⁺ HOAc/AcO ⁻ }.....	106
7-1.	Rate and Equilibrium Constants for the Reactions of BMN with CH(CN) ₂ ⁻ , Piperidine, and Morpholine.....	123
7-2.	Changes in the Slopes and the Intercepts with the Extent of Reaction During Conventional Pseudo-First-Order Analysis for the Reaction of BNS with Nitroethide Ion in Two Different Solvents at 298K and 310 nm.....	126
7-3.	Time Ratios and Second-Order Rate Constants for the Combination Reaction of BNS with Nitroethide Ion in AN/Water (3/1, v/v) and DMSO/Water (3/1, v/v) at 298K over a Range of Wavelengths.....	128
7-4.	Apparent Rate Constants and Standard Deviations Obtained by the Sequential Pseudo-First-Order Analysis for the Reaction of BNS with Nitroethide Ion in AN/Water (3/1, v/v) and DMSO /Water (3/1, v/v) over the First Half-Life at 298K and 320 nm.....	130
8-1.	Time and Rate Constant Ratios for the Displacement Reaction Between MNBB ⁺ and PNPO ⁻ in AN at 298K over a Range of Wavelengths.....	142
8-2.	Time and Rate Constant Ratios for the Displacement Reaction Between PNBB ⁺ and PNPO ⁻ in AN at 298K over a Range of Wavelengths.....	143
8-3.	Apparent Rate Constants for the Displacement Reaction Between MNBB ⁺ (0.04 M) and PNPO ⁻ (0.06 mM) in AN over the First	

Half-Life at 298K as a Function of Wavelengths.....	145
8-4. Apparent Rate Constants for the Displacement Reaction Between PNBB ^r (0.04 M) and PNPO ⁻ (0.06 mM) in AN over the First Half-Life at 298K as a Function of Wavelengths.....	146
A-1. Apparent Rate Constants and Standard Deviations for 3 Sets of Experiments (20 Stopped-Flow Shots Each) on the Reaction Between BNAH (7.2 mM) and MA ⁺ (0.3 mM) in Acetonitrile at 298 K and 410 nm.....	157
A-2. Apparent Rate Constants and Standard Deviations for 3 Sets of Experiments (20 Stopped-Flow Shots Each) on the Reaction Between BNAH (7.2 mM) and MA ⁺ (0.3 mM) in Acetonitrile at 298 K and 420 nm.....	158
A-3. Apparent Rate Constants and Standard Deviations for 3 Sets of Experiments (20 Stopped-Flow Shots Each) on the Reaction Between BNAH (7.2 mM) and MA ⁺ (0.3 mM) in Acetonitrile at 298 K and 430 nm.....	159
A-4. Apparent Rate Constants and Standard Deviations for 3 Sets of Experiments (20 Stopped-Flow Shots Each) on the Reaction Between BNAH (7.2 mM) and MA ⁺ (0.6 mM) in Acetonitrile at 298 K and 440 nm.....	160
A-5. Apparent Rate Constants and Standard Deviations for 3 Sets of Experiments (20 Stopped-Flow Shots Each) on the Reaction Between BNAH (7.2 mM) and MA ⁺ (0.6 mM) in Acetonitrile at 298 K and 450 nm.....	161
A-6. Rate Constants for the Reaction Between BNAH (7.2 mM) and MA ⁺ (0.6 mM) in Acetonitrile at Various Temperatures.....	166
A-7. Changes in the Slopes and the Intercepts with the Extent of Reaction During Conventional Pseudo-First-Order Analysis for the Reaction of MAH (0.2 mM) with Tr ⁺ (0.05 M) in Acetonitrile at 298K and 400 nm.....	166
A-8. Changes in the Slopes and the Intercepts with the Extent of Reaction During Conventional Pseudo-First-Order Analysis for the Reaction of MAH (0.2 mM) with Tr ⁺ (0.05 M) in Acetonitrile at 298K and 410 nm.....	166
A-9. Changes in the Slopes and the Intercepts with the Extent of Reaction During Conventional Pseudo-First-Order Analysis for the Reaction of MAH (0.2 mM) with Tr ⁺ (0.05 M) in Acetonitrile at 298K and 420 nm.....	167

A-10.	Changes in the Slopes and the Intercepts with the Extent of Reaction During Conventional Pseudo-First-Order Analysis for the Reaction of MAH (0.4 mM) with Tr^+ (0.05 M) in Acetonitrile at 298K and 430 nm.....	167
A-11.	Changes in the Slopes and the Intercepts with the Extent of Reaction During Conventional Pseudo-First-Order Analysis for the Reaction of MAH (0.4 mM) with Tr^+ (0.05 M) in Acetonitrile at 298K and 440 nm.....	167
A-12.	Apparent Rate Constants and Standard Deviations for 3 Sets of Experiments (20 Stopped-Flow Shots Each) on the Reaction Between MAH (0.2 mM) and Tr^+ (0.05 M) in Acetonitrile at 298 K and 400 nm.....	168
A-13.	Apparent Rate Constants and Standard Deviations for 3 Sets of Experiments (20 Stopped-Flow Shots Each) on the Reaction Between MAH (0.2 mM) and Tr^+ (0.05 M) in Acetonitrile at 298 K and 410 nm.....	169
A-14.	Apparent Rate Constants and Standard Deviations for 3 Sets of Experiments (20 Stopped-Flow Shots Each) on the Reaction Between MAH (0.2 mM) and Tr^+ (0.05 M) in Acetonitrile at 298 K and 420 nm.....	170
A-15.	Apparent Rate Constants and Standard Deviations for 3 Sets of Experiments (20 Stopped-Flow Shots Each) on the Reaction Between MAH (0.4 mM) and Tr^+ (0.05 M) in Acetonitrile at 298 K and 430 nm.....	171
A-16.	Apparent Rate Constants and Standard Deviations for 3 Sets of Experiments (20 Stopped-Flow Shots Each) on the Reaction Between MAH (0.4 mM) and Tr^+ (0.05 M) in Acetonitrile at 298 K and 440 nm.....	172
A-17.	Apparent Rate Constants and Standard Deviations for 3 Sets of Experiments (20 Stopped-Flow Shots Each) on the Reaction Between MAH (0.4 mM) and Tr^+ (0.05 M) in Acetonitrile at 298 K and 450 nm.....	173
A-18.	Rate Constants for the Reaction Between MAH (0.4 mM) and Tr^+ (0.05 M) in Acetonitrile at Various Temperatures.....	176
A-19.	Apparent Steady-State Rate Constants for 3 Sets of Experiments (20 Stopped-Flow Shots Each) on the Reaction Between TMT^+ (0.02 mM) and NaOAc (0.5 M) in Acetic Acid at Various Temperatures and 480 nm.....	189

A-20.	Equilibrium Constants (K_4) for 3 Sets of Experiments (20 Stopped-Flow Shots Each) on the Reaction Between TMT^+ (0.02 mM) and NaOAc (0.5 M) in Acetic Acid at Various Temperatures and 480 nm.....	189
A-21.	Apparent Steady-State Rate Constants for 3 Sets of Experiments (20 Stopped-Flow Shots Each) on the Reaction Between TMT^+ (0.02 mM) and $\text{Bu}_4\text{N}^+ \text{HOAc}/\text{AcO}^-$ (0.005 M) in HOAc/AN (1/1, v/v) at Various Temperatures and 480 nm.....	189
A-22.	Equilibrium Constants (K_4) for 3 Sets of Experiments (20 Stopped-Flow Shots Each) on the Reaction Between TMT^+ (0.02 mM) and $\text{Bu}_4\text{N}^+ \text{HOAc}/\text{AcO}^-$ (0.005 M) in HOAc/AN (1/1, v/v) at Various Temperatures and 480 nm.....	190
A-23.	Changes in the Slopes and the Intercepts with the Extent of Reaction During Conventional Pseudo-First-Order Analysis for the Reaction of BNS with Nitroethide Ion in Two Different Solvents at 298K and 320 nm.....	194
A-24.	Changes in the Slopes and the Intercepts with the Extent of Reaction During Conventional Pseudo-First-Order Analysis for the Reaction of BNS with Nitroethide Ion in Two Different Solvents at 298K and 330 nm.....	194
A-25.	Changes in the Slopes and the Intercepts with the Extent of Reaction During Conventional Pseudo-First-Order Analysis for the Reaction of BNS with Nitroethide Ion in Two Different Solvents at 298K and 340 nm.....	195
A-26.	Changes in the Slopes and the Intercepts with the Extent of Reaction During Conventional Pseudo-First-Order Analysis for the Reaction of BNS with Nitroethide Ion in Two Different Solvents at 298K and 350 nm.....	195
A-27.	Changes in the Slopes and the Intercepts with the Extent of Reaction During Conventional Pseudo-First-Order Analysis for the Reaction of BNS with Nitroethide Ion in Two Different Solvents at 298K and 360 nm.....	195
A-28.	Apparent Rate Constants and Standard Deviations Obtained by the Sequential Pseudo-First-Order Analysis for the Reaction of BNS with Nitroethide Ion in AN/Water (3/1, v/v) and DMSO/Water (3/1, v/v) over the First Half-Life at 298K and 330 nm.....	196
A-29.	Apparent Rate Constants and Standard Deviations Obtained by the Sequential Pseudo-First-Order Analysis for the Reaction of BNS with Nitroethide Ion in AN/Water (3/1, v/v) and DMSO	

	/Water (3/1, v/v) over the First Half-Life at 298K and 340 nm.....	197
A-30.	Apparent Rate Constants and Standard Deviations Obtained by the Sequential Pseudo-First-Order Analysis for the Reaction of BNS with Nitroethide Ion in AN/Water (3/1, v/v) and DMSO /Water (3/1, v/v) over the First Half-Life at 298K and 350 nm.....	198
A-31.	Apparent Rate Constants and Standard Deviations Obtained by the Sequential Pseudo-First-Order Analysis for the Reaction of BNS with Nitroethide Ion in AN/Water (3/1, v/v) and DMSO /Water (3/1, v/v) over the First Half-Life at 298K and 360 nm.....	199
A-32.	Second-Order Rate Constants for 3 Sets of Experiments (20 Stopped-Flow Shots Each) on the Reaction Between BNS (0.1 mM) and Nitroethide Ion (0.04 M) in AN/Water (3/1, v/v) at Various Temperatures and 320 nm.....	202
A-33.	Apparent Rate Constants for the Displacement Reaction Between MNBBBr (0.04 M) and PNPO ⁻ (0.06 mM) in AN over the First Half-Life at 298K as a Function of Wavelengths.....	202
A-34.	Apparent Rate Constants for the Displacement Reaction Between PNBBBr (0.04 M) and PNPO ⁻ (0.06 mM) in AN over the First Half-Life at 298K as a Function of Wavelengths.....	203
A-35.	Apparent Rate Constants for the Displacement Reaction Between MNBBBr (0.08 M) and PNPO ⁻ (0.06 mM) in AN over the First Half-Life at 298K as a Function of Wavelengths (1).....	204
A-36.	Apparent Rate Constants for the Displacement Reaction Between MNBBBr (0.08 M) and PNPO ⁻ (0.06 mM) in AN over the First Half-Life at 298K as a Function of Wavelengths (2).....	205
A-37.	Apparent Rate Constants for the Displacement Reaction Between PNBBBr (0.08 M) and PNPO ⁻ (0.06 mM) in AN over the First Half-Life at 298K as a Function of Wavelengths (1).....	206
A-38.	Apparent Rate Constants for the Displacement Reaction Between PNBBBr (0.08 M) and PNPO ⁻ (0.06 mM) in AN over the First Half-Life at 298K as a Function of Wavelengths (2).....	207
A-39.	Apparent Rate Constants for the Displacement Reaction Between PNBBBr (0.16 M) and PNPO ⁻ (0.06 mM) in AN over the First Half-Life at 298K as a Function of Wavelengths (1).....	208
A-40.	Apparent Rate Constants for the Displacement Reaction Between PNBBBr (0.16 M) and PNPO ⁻ (0.06 mM) in AN over the First Half-Life at 298K as a Function of Wavelengths (2).....	209

LIST OF FIGURES

Figure	Page
1-1. Physical organic chemistry relationships.....	1
1-2. Steady-state vs. non-steady-state.....	4
1-3. Mechanism probes.....	4
1-4. Graphical representation of kinetic data.....	6
1-5. Mechanism probe values.....	7
1-6. Instantaneous rate constants (k_{inst}) – time profiles for simple one-step irreversible mechanism (a) and two-step reversible consecutive mechanism (b)	12
2-1. Apparent rate constants (k_{app}) – time plot for the reaction between phenoxide ion and BrAN in acetonitrile at 298 K (1.0 HL = 27.5 s).....	23
2-2. Apparent rate constants (k_{app}) – time plots for simple one-step mechanism (a) and complex mechanism (b).....	24
2-3. Apparent instantaneous rate constants (k_{IRC}) – time plot for the reaction of BrAN (5.0 mM) with PO^- (0.50 mM) in acetonitrile at 298 K (1.0 HL = 27.5 s).....	25
3-1. Apparent rate constants (k_{app}) – time plots for the reactions between BNAH (a)/BNAH- d_2 (b) and MA^+ in acetonitrile at 298K and 430 nm...34	34
3-2. Apparent instantaneous rate constants (k_{IRC}) – time plots for the reactions between BNAH(a)/BNAH- d_2 (b) and MA^+ in acetonitrile at 298K and 430 nm.....	35
3-3. Apparent KIE for the reactions between BNAH/BNAH- d_2 and MA^+ in acetonitrile at 298K and 430 nm as a function of reaction time.....	37
3-4. Electronic absorbance spectrum of the charge-transfer complex for the reaction between BNAH (0.1 M) and MA^+ (0.08 M) in acetonitrile at 298 K (left) and the absorbance – time decay curve at 560 nm (right).....	38
3-5. Calculated structures of complex 1, complex 2, and	

transition state in acetonitrile.....	41
3-6. The reaction coordinate for the reaction of BNAH and MA ⁺ in acetonitrile at 298.15 K calculated using the M06-2x/6-311++G(d,p)/SMD functional.....	42
4-1. Apparent instantaneous rate constants (k_{IRC}) – time plot for the reaction between MAH and Tr ⁺ in acetonitrile at 298K and 450nm.....	53
4-2. Optimized structures of reactant complex and transition state in acetonitrile with the M06-2x/6-311++(d,p)/SMD method.....	56
4-3. The reaction coordinate for the reaction of MAH and Tr ⁺ in acetonitrile at 298.15K calculated using the M06-2x/6-311++G(d,p)/SMD functional.....	56
5-1. UV/Vis absorption spectra for the reaction of BQCN ⁺ (0.04 M) with MAH (0.01 M) in AN at 298 K. (a) Time between spectra equals 30 s. (b) Time between spectra equals 25 min. Insert: Absorbance – time decay curve recorded at 525 nm under the same conditions.....	66
5-2. Pseudo-first-order plots for the reactions of BQCN ⁺ (0.50 mM) with MAH (40 mM) (a and b) and BQCN ⁺ (40 mM) with MAH (0.5 mM) (c and d) in AN half-saturated with air at 298 K and 430 nm.....	69
5-3. Apparent rate constants (k_{app}) – time plots for the reactions of BQCN ⁺ (40 mM) with MAH (a)/MAH- <i>d</i> ₂ (b) (10 mM) in AN containing residual air at 298 K and 440nm.....	76
5-4. Apparent instantaneous rate constants (k_{IRC}) – time and KIE _{IRC} plots for the reactions of BQCN ⁺ (0.5 mM) with MAH (MAH- <i>d</i> ₂) (40 mM) in AN half-saturated with air (a, b and c) and BQCN ⁺ (40 mM) with MAH (MAH- <i>d</i> ₂) (0.5 mM) containing residual oxygen (a', b' and c') at 298 K and 450nm.....	82
6-1. Apparent instantaneous rate constants (k_{inst}) – time plots for pre-association (a) and one-step (b) mechanisms.....	97
6-2. Diode-array visible absorption spectra of TMT ⁺ (0.02 mM) in acetic acid containing sodium acetate (0.01 M): start time, 0 s; cycle time, 2.5 s; total run time, 100 s.....	99
6-3. Eyring plot for the collapse of the ion pair in acetic acid (a) and Van't Hoff type plot for equilibrium (4) in HOAc (b).....	106

6-4.	Apparent instantaneous rate constants (k_{inst}) – time plots for the reaction of TMT ⁺ (0.02 mM) with sodium acetate (0.50 M) in acetic acid and 500 nm. Data for the first 3% of the reaction (a) and that over the first half-life (b).....	107
7-1.	UV/Vis spectra during the reaction of BNS (0.0001 M) with nitroethide ion (0.01 M) in AN/W (3/1, v/v) at 298 K. Time between spectra equals 20 s. The last spectrum shown is the 30 th recorded at 600s.....	125
7-2.	Pseudo-first-order plots for the reaction of BNS with nitroethide ion in AN/W (3/1, v/v) (a) and DMSO/Water (3/1, v/v) (b) at 298 K and 310 nm.....	127
7-3.	Apparent instantaneous rate constants (k_{IRC}) – time plots for the reaction between BNS and nitroethide ion in AN/Water (3/1, v/v) (a) and DMSO/Water (3/1, v/v) (b) at 298K and 320 nm.....	131
7-4.	Optimized structures of reactant complex and transition state as well as product in acetonitrile with the M06-2x/6-31+(d)/SMD method.....	133
7-5.	The reaction coordinate for the reaction of BNS and NE ⁻ in acetonitrile at 298.15K calculated using the M06-2x/6-31+G(d)/SMD method.....	133
8-1.	Calculated internal energies in the gas phase (short dashes) and the potential of mean force in DMF (long dashes) and in aqueous solution (solid curve) for the reaction of Cl ⁻ with CH ₃ Cl as a function of the reaction coordinate, R_c , in angstroms.....	138
8-2.	Comparison of gas-phase and solution-phase S _N 2 potential energy surfaces.....	139
8-3.	UV/Vis spectra during the reaction of PNPO ⁻ (0.06 mM) with MNBBBr (0.04 M) in acetonitrile at 298 K. Time between spectra equals 120 s. The last spectrum shown is the 20 th recorded at 2400s.....	141
8-4.	Apparent instantaneous rate constants (k_{IRC}) – time plots for the displacement reactions between MNBBBr (40 mM, a)/PNBBBr (80 mM, b) and PNPO ⁻ in acetonitrile at 298K.....	147
A-1.	Apparent instantaneous rate constants (k_{IRC}) – time plot for the reaction between BNAH and MA ⁺ in AN at 298K and 410 nm.....	162
A-2.	Apparent instantaneous rate constants (k_{IRC}) – time plot for the	

	reaction between BNAH and MA^+ in AN at 298K and 420 nm.....	162
A-3.	Apparent instantaneous rate constants (k_{IRC}) – time plot for the reaction between BNAH and MA^+ in AN at 298K and 440 nm.....	163
A-4.	Apparent instantaneous rate constants (k_{IRC}) – time plot for the reaction between BNAH and MA^+ in AN at 298K and 450nm.....	163
A-5.	Apparent KIE for the reactions between BNAH/BNAH- d_2 and MA^+ in AN at 298K and 410 nm as a function of reaction time.....	164
A-6.	Apparent KIE for the reactions between BNAH/BNAH- d_2 and MA^+ in AN at 298K and 420 nm as a function of reaction time.....	164
A-7.	Apparent KIE for the reactions between BNAH/BNAH- d_2 and MA^+ in AN at 298K and 440 nm as a function of reaction time.....	165
A-8.	Apparent KIE for the reactions between BNAH/BNAH- d_2 and MA^+ in AN at 298K and 450 nm as a function of reaction time.....	165
A-9.	Apparent instantaneous rate constants (k_{IRC}) – time plot for the reaction between MAH and Tr^+ in AN at 298K and 400 nm.....	174
A-10.	Apparent instantaneous rate constants (k_{IRC}) – time plot for the reaction between MAH and Tr^+ in AN at 298K and 410 nm.....	174
A-11.	Apparent instantaneous rate constants (k_{IRC}) – time plot for the reaction between MAH and Tr^+ in AN at 298K and 420 nm.....	175
A-12.	Apparent instantaneous rate constants (k_{IRC}) – time plot for the reaction between MAH and Tr^+ in AN at 298K and 430 nm.....	175
A-13.	Apparent instantaneous rate constants (k_{IRC}) – time plot for the reaction between MAH and Tr^+ in AN at 298K and 440 nm.....	176
A-14.	A comparison pseudo-first-order plots for the reactions of MAH (40 mM) with BQCN^+ (0.50 mM) (a, b and c) to those of MAH (0.5 mM) with BQCN^+ (40 mM) (a', b' and c') in AN in the presence of residual oxygen at 298 K and 430 nm.....	177
A-15.	Apparent KIE for the reactions of MAH/MAH- d_2 (10 mM) with BQCN^+ (40 mM) in AN in the presence of residual oxygen at 298 K and 440 nm as a function of reaction time.....	178
A-16.	Apparent KIE for the reactions of MAH/MAH- d_2 (40 mM) with BQCN^+ (0.50 mM) (a and b) and MAH/MAH- d_2 (0.5 mM) with BQCN^+ (40 mM) (a' and b') in AN in the presence of residual oxygen at 298 K and 430 nm or 450 nm	

	as a function of reaction time.....	179
A-17.	Apparent KIE for the reactions of MAH/MAH- d_2 (40 mM) with BQCN ⁺ (0.50 mM) in AN half-saturated with air at 298 K and 430 nm or 450 nm as a function of reaction time.....	180
A-18.	Apparent instantaneous rate constants (k_{IRC}) – time plots for the reaction of MAH (40 mM) with BQCN ⁺ (0.50 mM) in AN in the presence of residual oxygen at 298 K and 430 nm or 450nm (four sets).....	181
A-19.	Apparent instantaneous rate constants (k_{IRC}) – time plots for the reactions of MAH (40 mM) with BQCN ⁺ (0.50 mM) (a, b and c) and MAH (0.5 mM) with BQCN ⁺ (40 mM) (d) in AN half-saturated with air at 298 K and 430 nm or 450 nm.....	182
A-20.	Apparent instantaneous rate constants (k_{IRC}) – time plots for the reaction of MAH (0.5 mM) with BQCN ⁺ (40 mM) in AN in the presence of residual oxygen at 298 K and 430 nm or 450nm (three sets).....	183
A-21.	Apparent instantaneous rate constants (k_{IRC}) – time plots for the reaction of MAH- d_2 (40 mM) with BQCN ⁺ (0.50 mM) in AN in the presence of residual oxygen at 298 K and 430 nm or 450nm (three sets).....	184
A-22.	Apparent instantaneous rate constants (k_{IRC}) – time plots for the reactions of MAH- d_2 (40 mM) with BQCN ⁺ (0.50 mM) in AN half-saturated with air at 430nm or 450 nm (a and b) and MAH- d_2 (0.5 mM) with BQCN ⁺ (40 mM) in the presence of residual oxygen at 298 K and 450 nm (c and d).....	185
A-23.	KIE _{IRC} plots for the reactions of MAH/MAH- d_2 (40 mM) with BQCN ⁺ (0.50 mM) in AN in the presence of residual oxygen (a) and half-saturated with air (b) and MAH/MAH- d_2 (0.5 mM) with BQCN ⁺ (40 mM) in the presence of residual oxygen (c) at 298 K and 450 nm.....	186
A-24.	UV/Vis absorption spectra for the reactions of MAH with air (a) and MAH- d_2 with air (b) at 298K.....	187
A-25.	Absorbance – time curves (a) and KIE _{time} – time plot (b) for the reactions of MAH/MAH- d_2 with oxygen in AN half-saturated with air at 298K.....	188
A-26.	Eyring plot for the collapse of the ion pair in HOAc/AN (1/1, v/v) (a) and Van't Hoff type plot for equilibrium (4) in HOAc/AN (1/1, v/v) (b).....	190

A-27.	Sliding 51 point IRC analysis over the first half-life of the reaction of TMT ⁺ (0.1 mM) with NaOAc (0.5 M) at 298 K and 520 nm.....	190
A-28.	IRC analysis of the first 3% of the extent of reaction – time profile for the concentration jump experiment on the reaction of TMT ⁺ (0.22 mM) with NaOAc (0.5 M) carried out at 298 K and 520 nm.....	191
A-29.	¹ HNMR spectra of TMT ⁺ ClO ₄ ⁻ in CD ₃ CO ₂ D/CDCl ₃ (1/2).....	192
A-30.	¹ HNMR spectra of equilibrium reaction mixture in CD ₃ CO ₂ D/CDCl ₃ (1/2).....	193
A-31.	Apparent instantaneous rate constants (k_{IRC}) – time plots for the reaction between BNS and nitroethide ion in AN/Water (3/1, v/v) (a) and DMSO/Water (3/1, v/v) (b) at 298K and 330 nm.....	200
A-32.	Apparent instantaneous rate constants (k_{IRC}) – time plots for the reaction between BNS and nitroethide ion in AN/Water (3/1, v/v) (a) and DMSO/Water (3/1, v/v) (b) at 298K and 340 nm.....	200
A-33.	Apparent instantaneous rate constants (k_{IRC}) – time plots for the reaction between BNS and nitroethide ion in AN/Water (3/1, v/v) (a) and DMSO/Water (3/1, v/v) (b) at 298K and 350 nm.....	201
A-34.	Apparent instantaneous rate constants (k_{IRC}) – time plots for the reaction between BNS and nitroethide ion in AN/Water (3/1, v/v) (a) and DMSO/Water (3/1, v/v) (b) at 298K and 360 nm.....	201
A-35.	¹ HNMR spectra for the product of the displacement reaction between MNBBBr and PNPO ⁻ in CDCl ₃	210

LIST OF SCHEMES

Scheme	Page
1-1. The Simple Mechanism Based on Eigen's Study.....	2
1-2. The Simple One-Step Mechanism and the Complex Mechanism.....	2
1-3. The Proposed Structure for the Reactant Complex.....	13
1-4. The Proposed Ion-Dipole Complex.....	14
2-1. The Reaction of Bromoacetonitrile (BrAN) with Phenoxide ion (PO ⁻).....	19
3-1. The Simple One-Step Mechanism (1) and the Reversible Consecutive Mechanism (2).....	31
3-2. The Proposed Mechanism for the Reaction Between BNAH and MA ⁺	39
4-1. The Proposed Mechanism for the Reaction Between MAH and Tr ⁺	55
5-1. Proposed 3-Step Mechanism for the Reaction of MAH with BQCN ⁺ in AN. This Mechanism Was Proposed in 2003.....	62
5-2. Partial Structures of the CT Complex Between MAH- <i>d</i> ₁ and BQCN ⁺ in AN.....	63
5-3. The Complex Mechanism for the Reaction of MAH- <i>d</i> ₁ with BQCN ⁺ . The Formation of H- and D- Complexes Includes Formation of the Corresponding CT and "Reactant Complexes".....	64
5-4. Proposed Multi-Step Mechanism for the Reaction of MAH with BQCN ⁺ in AN in the Presence of Residual or Intentionally Added Air at 298 K. The Dashed Lines Connecting Structures in Steps (d and e) Are Between the Propagating Species in the Two Equations.....	87
6-1. The Pre-Association Mechanism.....	97
6-2. Reversible Reaction Between TMT ⁺ and Sodium HOAc/AcO ⁻ in Acetic Acid.....	99
6-3. Equilibria Involved in the Reaction of TMT ⁺ and HOAc/AcO ⁻	102

6-4.	Mechanism of the Combination Reaction.....	108
6-5.	Reaction Coordinate Diagram for the Pre-Association Mechanism.....	109
6-6.	Reaction Coordinate Diagram for the Intramolecular Collapse of {TMT ⁺ HOAc/AcO ⁻ } to TMT-OAc and Acetic Acid.....	111
6-7.	Winstein Solvolysis Scheme.....	111
6-8.	Comparison of Winstein Scheme to the TMT ⁺ System.....	112
7-1.	The Michael Addition Reaction.....	123
7-2.	The Proposed Mechanism for the Reaction Between BNS and Nitroethide Ion.....	131
8-1.	The Mechanism for the Reaction Between PNPO ⁻ and Methyl Iodide in Acetonitrile.....	140
8-2.	The Proposed Mechanism for the Reaction Between PNPO ⁻ and MNBBBr in Acetonitrile.....	147

CHAPTER 1

INTRODUCTION

A prominent goal of physical organic chemists in the 20th century was to develop theoretical relationships that shed light on the structures of the transition states of organic reactions. Much of the current theory of physical organic chemistry is embodied in the relationships, often based on observed structural effects on reactivity, shown in Figure 1-1. These are used to describe the results of the study of the kinetics and mechanisms of organic reactions. What all of these relationships have in common is that they are all most appropriate for the description of reactions that take place in a single step. For reactions involving more than a single transition state, parameters derived from these relationships necessarily become less reliable in describing transition-state structure.

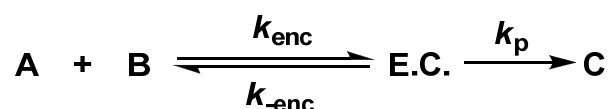
Hammett equation
Brønsted relationship
Hammond postulate
Variable transition-state theory
Marcus theory
Configuration mixing model
Principle of non-perfect synchronization

FIGURE 1-1. Physical organic chemistry relationships.

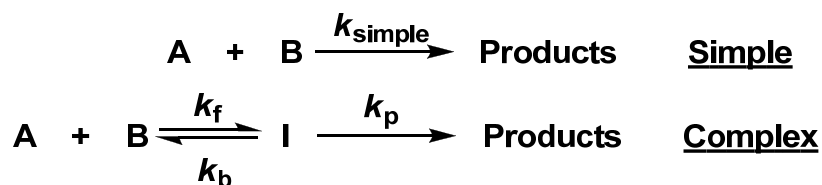
Since the work of Eigen,¹ it is an accepted fact that all bimolecular reactions in solution pass through an encounter complex (Scheme 1-1). Because the encounter complex is formed at diffusion-controlled rates, it is not considered to be kinetically significant for reactions taking place on the millisecond or second time scale. Thus, the simple irreversible second-order (simple) and the reversible

consecutive second-order (complex) mechanisms are described in Scheme 1-2 without involving the encounter complexes which are assumed, but not included, in the rate laws. These two mechanisms are kinetically indistinguishable once steady state for the complex mechanism is achieved.

SCHEME 1-1. The Simple Mechanism Based on Eigen's Study



SCHEME 1-2. The Simple One-Step Mechanism and the Complex Mechanism



In his classic book on physical organic chemistry, Hammett² recognized the difficulties in obtaining direct kinetic evidence for the presence of a multi-step reaction mechanism. However, he concluded that “it would require experimental data of more than ordinary precision to recognize effects of this magnitude with any assurance.” To my knowledge, there were no serious attempts during the last half of the 20th century to subject the fundamental reactions of organic chemistry, which are assumed to take place by a simple second-order mechanism, to a rigorous mechanism analysis designed to detect a more complex mechanism. During that period, enormous progress was made in digital

technology, which provided the tools necessary to undertake this task.

In 1998, Parker's group first realized that it is possible to kinetically distinguish between the simple and complex mechanisms shown in Scheme 1-2 during their studies of the proton-transfer reactions of methylantracene radical cations with nitrogen-centered bases.³⁻⁶ This is made possible by the observation that the reactions taking place by the complex mechanism do not quickly reach a steady state and in the *pre-steady-state* time period, the kinetic response deviates significantly from that expected for the simple one-step mechanism. Subsequently, Parker's group has employed non-steady-state kinetic methods to show that a number of fundamental organic reactions which include a nitroalkane proton transfer,⁷⁻⁹ an E2 elimination,¹⁰ an S_N2 reaction,¹¹⁻¹² a hydride exchange reaction between NADH models,¹³ a Diels-Alder reaction,¹⁴ an acyl transfer reaction,¹⁵ a carbocation-anion combination¹⁶ as well as an S_NAr reaction,¹⁷ long believed to take place by simple one-step mechanisms are actually more complex and proceed *via* kinetically significant reaction intermediates.

Methodology for Distinguishing Mechanisms

It is useful to define steady-state and non-steady-state in reactions following complex mechanisms in terms of the kinetic response as illustrated in Figure 1-2. For a reaction at steady state, the decay in reactant concentration is equal to the rise in product concentration at all times, while the decay in reactant concentration leads the rise in product concentration under non-steady-state conditions. These relationships assume that the reactant/product stoichiometry is equal to unity. The relationships in Figure 1-2 suggest a number of mechanism

probes to distinguish between the simple mechanism and the complex mechanism under non-steady-state conditions (Figure 1-3).

Steady-state (at all times):

$-d[R]/dt = d[P]/dt$, (R: Reactant, P: Product)

Non-steady-state (initial rates):

$-d[R]/dt > d[P]/dt$

$k_{\text{init}} > k_{\text{s.s.}}$ if reactant is monitored

$k_{\text{init}} < k_{\text{s.s.}}$ if product is monitored

(k_{init} : pseudo-first-order rate constants measured in the extent of reaction ranges from 0 to 0.05, $k_{\text{s.s.}}$: pseudo-first-order rate constants measured at steady state.)

FIGURE 1-2. Steady-state vs. non-steady-state.

Extent of reaction – time profiles

Rate constant ratio – $k_{\text{init}}/k_{\text{s.s.}}$

Time ratio – $t_{0.50}/t_{0.05}$

Extent of reaction – dependent deuterium KIE

Wavelength – dependent kinetic response

Instantaneous rate constants – time profiles

($t_{0.50}$: half-life, $t_{0.05}$: the time necessary to reach the extent of reaction equal to 0.05.)

FIGURE 1-3. Mechanism probes.

Practical Aspects of the Mechanism Analysis. At an early stage in the development of physical organic chemistry, Hammett² recognized that the kinetic response of the reversible consecutive second-order mechanism (Scheme 1-2) differs from that of the simple irreversible second-order mechanism at short times. However, he concluded that the deviations from simple mechanism behavior are small and differentiation of the mechanisms could not be done with the precision of kinetic measurements at that time. In 1974, Bunnett¹⁸ expressed the general belief that rate constants of organic reactions obtained by

spectrophotometric methods are reliable to about $\pm 5\%$. Obviously, precision in a set of measurements can be much greater than the expected reliability of a single measurement. When making multiple repetitions of a measurement, it is appropriate to use the standard error of the mean ($\sigma/N^{0.5}$), where σ is the standard deviation and N is the number of measurement, to express the uncertainty in the mean value.¹⁹ Thus, the best value of the quantity measured (X_{best}) is given by eq. 1-1, which shows that the uncertainty decreases with the square root of the number of measurements. The necessity of gathering large quantities of kinetic data in order to take advantage of this fact is readily accommodated when using stopped-flow spectrophotometry as the measurement technique. Parker²⁰ found that the precision in rate constant measurements of first-order reactions can be of the order of $\pm 0.5\%$ using that method. That means that when the numerical probes values differ from those for the simple mechanism by as much as 5%, the observed deviations are significantly large to confirm that the data are inconsistent with the simple mechanism.

$$X_{\text{best}} = X_{\text{mean}} \pm \sigma/N^{0.5} \quad (1-1)$$

Extent of Reaction – Time Profiles. The most common method used to evaluate absorbance – time profiles is to fit the experimental data to an exponential function and evaluate the resulting rate constant. Although this method of data analysis gives excellent results when it is known with certainty that the reaction follows first-order or pseudo-first-order kinetics, it has the very

serious drawback that small deviations from first-order kinetics are masked and go unnoticed.

This situation is clearly illustrated by the two different graphical treatments of the same data shown in Figure 1-4. The kinetic data are for the Diels-Alder reaction between anthracene (ANTH) and tetracyanoethylene (TCNE) in acetonitrile, which follows the complex mechanism. The figure on the left is the least-squares plot of theoretical $\ln [\text{Anthracene}]$ – time data under pseudo-first-order conditions. Small deviations from linearity are observed at short times, but it is obvious that in the presence of experimental scatter in the data these would be buried in noise and would go undetected. The figure on the right is for the same theoretical data plotted as an extent of reaction – time profile. The simple mechanism line is normalized to the theoretical data (solid circles) at extent of reaction equal to 0.05. The deviation of the simple mechanism line from the data points is obvious and can only lead to the conclusion that the data are inconsistent with the simple mechanism.

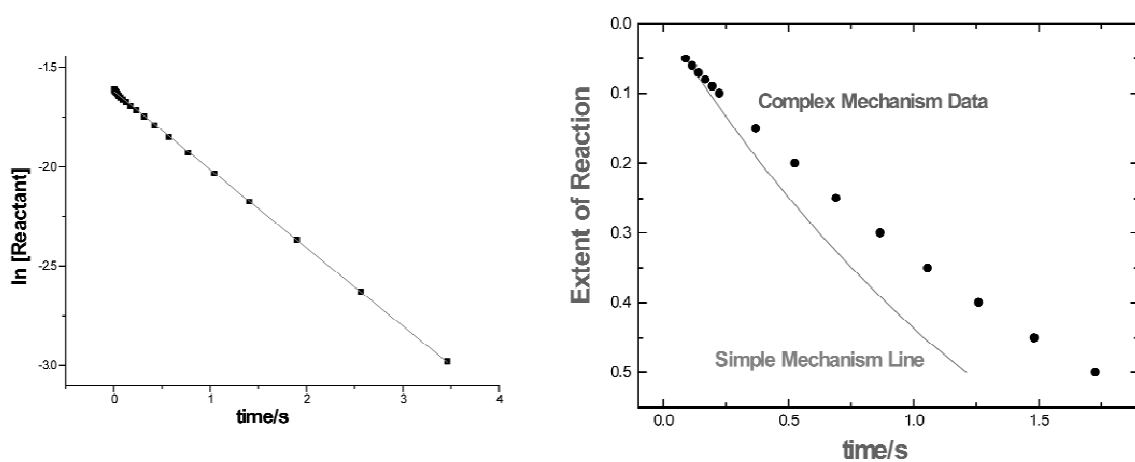


FIGURE 1-4. Graphical representation of kinetic data.

Numerical Mechanism Probes ($k_{\text{init}}/k_{\text{s.s.}}$ and $t_{0.50}/t_{0.05}$). The values of the numerical mechanism probes $k_{\text{init}}/k_{\text{s.s.}}$ (the ratio of pseudo-first-order rate constants measured in the extent of reaction ranges from 0 to 0.05 and steady state, respectively) and $t_{0.50}/t_{0.05}$ (the half-life divided by the time necessary to reach the extent of reaction equal to 0.05) are invariant at 1.00 and 13.5, respectively, for a reaction following the simple mechanism, but are dependent upon whether reactant or product is monitored for a reaction following the reversible consecutive second-order mechanism under pseudo-first-order conditions (Figure 1-5). In the limit where the two mechanisms are kinetically indistinguishable, the mechanism probe values for the complex mechanism are equal to those for the simple irreversible second-order mechanism (under pseudo-first-order conditions). Obviously, the ability to distinguish between the two mechanisms depends strongly on the precision of the measurements.

Irreversible second-order mechanism:

$$k_{\text{init}}/k_{\text{s.s.}} = 1.00$$

$$t_{0.50}/t_{0.05} = 13.5$$

Reversible consecutive second-order mechanism:

$$\text{Monitor reactant: } k_{\text{init}}/k_{\text{s.s.}} \geq 1.00$$

$$t_{0.50}/t_{0.05} \geq 13.5$$

$$\text{Monitor product: } k_{\text{init}}/k_{\text{s.s.}} \leq 1.00$$

$$t_{0.50}/t_{0.05} \leq 13.5$$

FIGURE 1-5. Mechanism probe values.

The elimination of HBr from 2-(*p*-nitrophenyl)ethyl bromide in alcohol/alkoxide media takes place by a two-step mechanism involving the intermediate formation of the carbanion.¹⁰ The values of the rate constant and time ratios for this reaction shown in Table 1-1 represent the complex

mechanism feature when monitoring the product evolution. The last two columns in Table 1-1 show that both $k_{\text{init}}/k_{\text{s.s.}}$ and $t_{0.50}/t_{0.05}$ deviate drastically from the theoretical values for simple one-step mechanisms, 1.00 and 13.5, respectively.

TABLE 1-1. The Rate Constant and Time Ratios for the Elimination Reactions of 2-(*p*-Nitrophenyl)ethyl Bromide in Alcohols Containing the Corresponding Alkoxide Ions at 293 K¹⁰

Substrate ^a	Solvent	[RO ⁻]/mM	$k_{\text{init}}/k_{\text{s.s.}}$	$t_{0.50}/t_{0.05}$
NPEB	EtOH	300	0.810	11.12
		150	0.763	10.52
NPEB- <i>d</i> ₂	EtOH	300	0.881	12.03
		150	0.929	12.61
NPEB	MeOH	300	0.840	11.58
		150	0.783	11.08
NPEB- <i>d</i> ₂	MeOH	300	0.714	8.72
		150	0.750	9.04

^a NPEB = 2-(*p*-nitrophenyl)ethyl bromide.

Extent of Reaction – Dependent Deuterium Kinetic Isotope Effects.

Because of the fact that the intermediate in the complex mechanism partitions between return to reactants and irreversible product formation, the apparent deuterium kinetic isotope effect (KIE_{app}) is attenuated and can be considerably smaller than the real value (KIE_{real}), which is equal to $k_{\text{p}}^{\text{H}}/k_{\text{p}}^{\text{D}}$, the ratio of the product-forming rate constants for H and D substrate, respectively.^{3,8} This has the important consequence that possible hydrogen atom, hydride or proton tunneling may be masked when evaluating KIE_{app} . The mechanism probe is readily applied with a high degree of precision, and its observation gives a clear indication of deviation of experimental data from that expected for the simple mechanism. It also has the advantage that when data from only one of the H or D substrates deviate significantly from simple mechanism behavior, the observation

of extent of reaction dependence of KIE_{app} allows for the resolution of the kinetics into the microscopic rate constants for the complex mechanism.

Wavelength – Dependent Kinetic Response.²⁰ For reactions following the simple mechanism (1 - E.R.) is expected to be independent on whether reactant or product is monitored and on the wavelength at which measurements are made. It is obvious from the mechanism probe values shown in Figure 1-5 that this is not the case for reactions following the complex mechanism. The ideal experimental situation is when measurements can be made at wavelengths where reactant and product are the only absorbing species. In any event, the observation that mechanism probe values are dependent upon the wavelength at which measurements are made is convincing evidence that the kinetics of the reaction are inconsistent with the simple mechanism.

Instantaneous Rate Constants – Time Profiles.¹⁵ The apparent instantaneous rate constant (k_{inst}) for a reaction taking place in a single microscopic step (simple mechanism) is time independent and equal to the microscopic rate constant for that step. However, for a reaction taking place in more than one consecutive step, the opportunity exists to observe time dependent k_{inst} . This opportunity can only be taken advantage of in the event that the *pre-steady-state* time period can be accessed. By definition, a k_{inst} is evaluated over an infinitesimally short time period. In practice, it is convenient to evaluate k_{inst} over a finite time period as the rate constant at the time of the midpoint of the time range. The validity of this procedure was readily established by

showing that the resultant value is independent of the magnitude of the time interval when the latter is small.

Most of the reactions of interest can be studied under pseudo-first-order conditions with the second reactant (B in Scheme 1-2) in large excess. Under these conditions the appropriate form of the rate law for the simple mechanism is Equation 1-2 in which E.R. represents the extent of reaction. Equation 1-2 transforms to Equation 1-3 when the decay of $[R]$ is monitored and to Equation 1-4 when evolution of $[P]$ is followed. The appropriate equations for evaluating instantaneous pseudo-first-order rate constants $(k_{\text{inst}})^{21}$ over a finite time interval (Δt) when monitoring reactant decay or product accumulation are Equations 1-5 and 1-6, respectively.

$$-\ln (1 - \text{E.R.}) = kt \quad (1-2)$$

$$-\ln ([R]/[R]_0) = kt \quad (1-3)$$

$$-\ln (1 - [P]/[R]_0) = kt \quad (1-4)$$

$$k_{\text{inst}} = -\Delta \ln ([R]/[R]_0) / \Delta t \quad (1-5)$$

$$k_{\text{inst}} = -\Delta \ln (1 - [P]/[R]_0) / \Delta t \quad (1-6)$$

A Sliding n -Point IRC Analysis.¹⁵ Due to the fact that there is always some scatter and noise in experimental kinetic data it is not practical to evaluate IRC directly from the raw data. The raw data have to be treated with a Savitsky-Golay smooth procedure²² before the calculation of IRC. The raw data consisted of a 2000-point absorbance – time profile. Conversion of the raw data to a $-\ln (1 - \text{E.R.})$ – time profile set the stage for evaluating a sliding n -point procedure ($n = 11, 21, 31, 51, \text{ or } 101$) for calculating k_{inst} – time arrays. The first step involves a

least-squares correlation of smoothed $\ln(1 - E.R.)$ – time over points 1 to n . The slope of this line is assigned to $-k_{\text{inst}}(N)$ where N is equal to $(n+1)/2$. The value of N is then incremented by taking points 2 to $n+1$ as the second correlation to obtain $-k_{\text{inst}}(N+1)$. The value $-k_{\text{inst}}(N+2)$ is obtained using points 3 to $n+2$. This procedure is continued until all points in the $\ln(1 - E.R.)$ – time profile have been used. For example when $n = 11$, the k_{inst} – time array consists of $-k_{\text{inst}}(6)$ to $-k_{\text{inst}}(1995)$. In order to incorporate the advantages of using different n values into a single IRC analysis, a procedure was devised to successively increase n with increasing time. A superior procedure was observed to involve an initial correlation over the first 3 points to give IRC(2), followed by correlations over 5 points (IRC(3)), 7 points (IRC(4)), and 9 points (IRC(5)). The 11-point sliding procedure was then used to give IRC(6) to IRC(50) and this was followed by application of the 101-point sliding procedure to generated IRC(51) to IRC(1950).

The instantaneous rate constants (k_{inst}) – time profiles for simple one-step mechanism are straight lines with zero slopes (Figure 1-6a) no matter whether reactant decay or product evolution is monitored. This reflects the fact that the instantaneous rate constant for this mechanism is also the microscopic rate constant for the process. However, the k_{inst} – time profiles for reactions taking place in more than one step depend upon whether decay of reactant or evolution of product concentration is monitored. In Figure 1-6b, the upper profile is for reactant decay and the lower one is for product evolution. When reactant decay is monitored, the k_{inst} – time plot extrapolated to zero time is equal to the rate constant for the initial step (k_f) in the reaction while the k_{inst} – time profile for

product evolution extrapolates to zero at $t = 0$. The intercept for the reactant decay plot suggests the possibility of evaluating the forward rate constant (k_f) directly from experimental data without the necessity of the complete resolution of the kinetics. The k_{inst} – time profiles for monitoring reactant decay and product evolution converge to a plateau value which can be equated to the rate constant under steady-state conditions ($k_{\text{s.s.}}$). Under the latter conditions, the profiles for both the simple mechanism and the complex mechanism are straight lines with zero slopes, so the two mechanisms become kinetically indistinguishable.

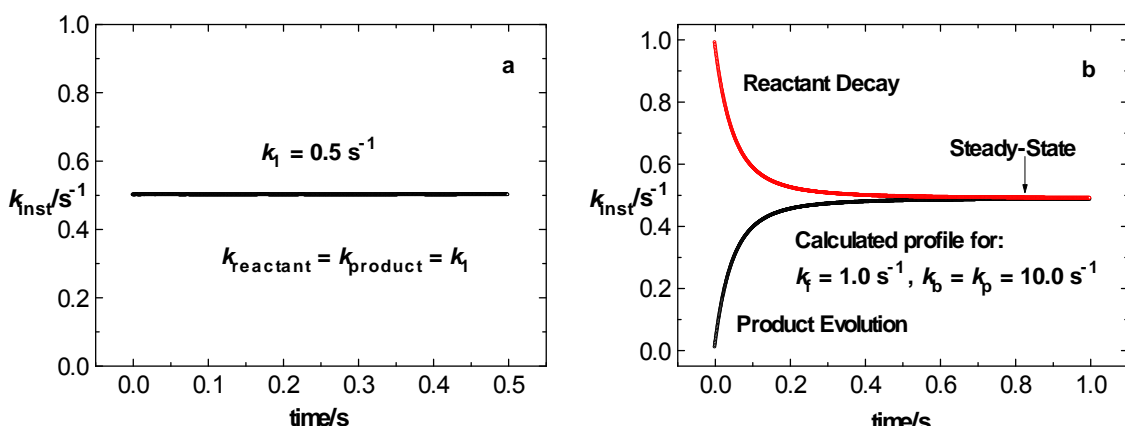


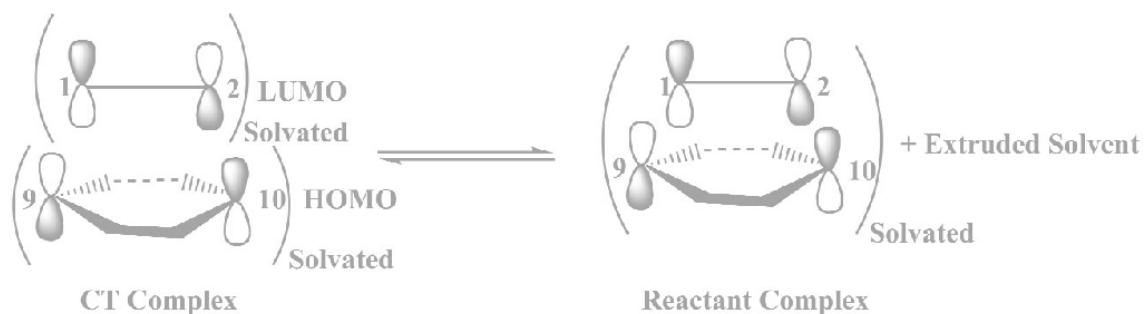
FIGURE 1-6. Instantaneous rate constants (k_{inst}) – time profiles for simple one-step irreversible mechanism (a) and two-step reversible consecutive mechanism (b).

Comments on the Structures of Intermediates in the Complex Mechanism

For the Diels-Alder reaction between anthracene (ANTH) and tetracyanoethylene (TCNE) in acetonitrile, Parker¹⁴ proposed that the intermediate (reactant complex) forming reactions, that necessarily take place on the same time scale as the overall reaction, do not involve the creation of new covalent bonds. Since the charge-transfer complex (CT) is formed on a much

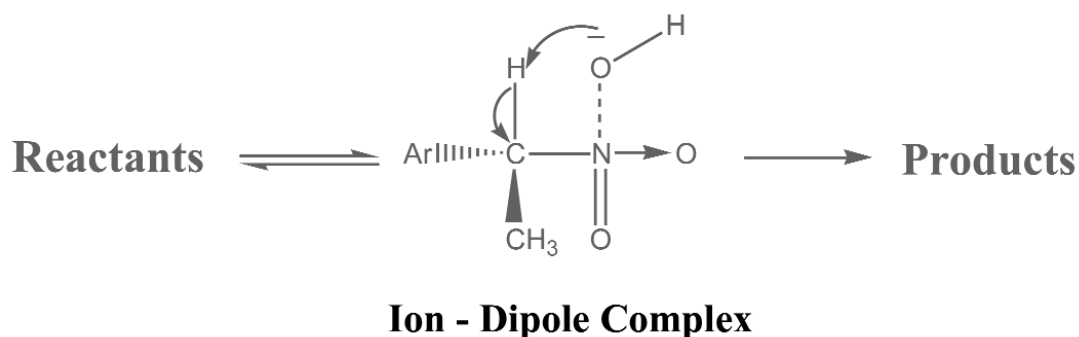
shorter time scale than the stopped-flow kinetic measurements and is in rapid equilibrium with the reactants, the CT complex is ruled out as the kinetically significant intermediate which is expected to affect the extent of reaction – time profiles. However, theoretical calculations²³ suggest that the CT complex lies on the product-forming reaction coordinate for the reaction carried out in chloroform. The barrier for CT complex formation appears to be very small, and density function calculations²⁴ suggest that the reactant moieties lie in parallel planes with an interplanar distance of 3.40 Å. Since the carbon atoms involved in bond formation have the proper orientation in the CT complex, it appears reasonable to assume the latter is indeed on the product-forming reaction coordinate. Parker¹⁴ proposed that the conversion of the CT complex to the “reactant complex” is accompanied by the shortening of the distances between the reaction centers and the extrusion of solvent, giving rise to a significant reaction barrier, as illustrated in Scheme 1-3. In Scheme 1-3, the interactions shown on the left are the lowest unoccupied molecular orbital (LUMO) of TCNE and the highest occupied molecular orbital (HOMO) of ANTH.

SCHEME 1-3. The Proposed Structure for the Reactant Complex



Similar considerations were employed to suggest the formation of the “reactant complex” in other reactions that involve significant reaction barriers. The ion-dipole complexes were suggested as the pertinent intermediates in nitroalkane proton-transfer reactions in aqueous solutions,⁷⁻⁹ in the S_N2 reaction between *p*-nitrophenoxide ion and methyl iodide in acetonitrile,¹¹⁻¹² and in the elimination reactions of *p*-nitrophenethylhalides in protic solvents.¹⁰ The ion-dipole complex formation for the proton-transfer reaction between an aryl nitroalkane and hydroxide ion⁷ in aqueous acetonitrile is illustrated in Scheme 1-4.

SCHEME 1-4. The Proposed Ion-Dipole Complex



The Objective of My Dissertation

The scientific objective of the work in this dissertation is to provide an answer to the question: “Is the single transition-state model appropriate for the fundamental reactions in organic chemistry?” It is aimed at challenging the very basis of much of the body of knowledge in physical organic chemistry developed over the past seventy years. The main efforts consist of (1) development of the new methodologies capable of differentiating between the simple one-step and

multi-step complex mechanisms and (2) investigation of the detailed mechanisms for several fundamental organic chemical reactions, which include the formal hydride transfer reactions between NADH model compounds, the combination reactions (a carbocation with an anion and a neutral molecule with an anion), and the S_N2 displacement reactions.

It is my opinion that our efforts will uncover the tip of the iceberg and that further probing of this area in the future may possibly bring about a profound change in the thinking of physical organic chemists and the way they approach the study of organic reaction mechanisms.

References

- (1) Eigen, M.; Johnson, J. S. *Annu. Rev. Phys. Chem.* **1960**, *11*, 309.
- (2) Hammett, L. P. *Physical Organic Chemistry*, 2nd ed.; McGraw-Hill: New York, 1940; Tokyo, 1970.
- (3) Parker, V. D.; Zhao, Y.; Lu, Y.; Zheng, G. *J. Am. Chem. Soc.* **1998**, *120*, 12720.
- (4) Lu, Y.; Zhao, Y.; Parker, V. D. *J. Am. Chem. Soc.* **2001**, *123*, 5900.
- (5) Zhao, Y.; Lu, Y.; Parker, V. D. *J. Chem. Soc., Perkin Trans. 2* **2001**, 1481.
- (6) Parker, V. D.; Lu, Y.; Zhao, Y. *J. Org. Chem.* **2005**, *70*, 1350.
- (7) Zhao, Y.; Lu, Y.; Parker, V. D. *J. Am. Chem. Soc.* **2001**, *123*, 1579.
- (8) Parker, V. D.; Zhao, Y. *J. Phys. Org. Chem.* **2001**, *14*, 604.
- (9) Li, Z.; Cheng, J.-P.; Parker, V. D. *Org. Biomol. Chem.* **2011**, *9*, 4563.
- (10) Handoo, K. L.; Lu, Y.; Zhao, Y.; Parker, V. D. *Org. Biomol. Chem.* **2003**,

1, 24.

- (11) Lu, Y.; Handoo, K. L.; Parker, V. D. *Org. Biomol. Chem.* **2003**, 1, 36.
- (12) Parker, V. D.; Lu, Y. *Org. Biomol. Chem.* **2003**, 1, 2621.
- (13) Lu Y.; Zhao, Y.; Handoo, K. L.; Parker, V. D. *Org. Biomol. Chem.* **2003**, 1, 173.
- (14) Handoo, K. L.; Lu, Y.; Parker, V. D. *J. Am. Chem. Soc.* **2003**, 125, 9381.
- (15) Parker, V. D. *J. Phys. Org. Chem.* **2006**, 19, 714.
- (16) Hao, W.; Parker, V. D. *J. Org. Chem.* **2008**, 73, 48.
- (17) Parker, V. D.; Li, Z.; Handoo, K. L.; Hao, W.; Cheng, J.-P. *J. Org. Chem.* **2011**, 76, 1250.
- (18) Bunnett, J. F. *Investigation of Rates and Mechanisms of Reactions, Part 1: General Considerations and Reactions at Conventional Rates*, 3rd ed.; Lewis, E. S. (ed.), Chapter 4; John Wiley: New York, 1974.
- (19) Taylor, J. T. *An Introduction to Error Analysis*, University Science Books; Oxford University Press: Mill Valley, CA, 1982.
- (20) Parker, V. D. *Pure Appl. Chem.* **2005**, 77, 1823.
- (21) For clarity k_{inst} is used to denote a single instantaneous rate constant and IRC denotes pseudo-first-order k_{inst} – time arrays.
- (22) Savitsky, A.; Golay, M. *Anal. Chem.* **1964**, 36, 1627.
- (23) Wise, K. E.; Wheeler, R. A. *J. Phys. Chem. A* **1999**, 103, 8279.
- (24) Liao, M.; Lu, Y.; Scheiner, S. *J. Comput. Chem.* **2003**, 24, 623.

CHAPTER 2

THE DEVELOPMENT OF NEW METHODOLOGIES FOR DIFFERENTIATING BETWEEN THE SIMPLE ONE-STEP AND COMPLEX MULTI-STEP MECHANISMS*

Abstract

Three new analysis procedures for pseudo-first-order kinetics are introduced and applied to the reaction of bromoacetonitrile (BrAN) with phenoxide ion (PO^-) in acetonitrile. The three methods consist of (1) half-life dependence of k_{app} , (2) sequential linear pseudo-first-order correlation, and (3) revised instantaneous rate constant analysis. Each of the three procedures is capable of distinguishing between simple one-step and multi-step mechanisms, and the combination of the three procedures provides a powerful strategy for differentiating between the two mechanistic possibilities, which has been extensively confirmed during the application in our kinetic studies of a wide variety of fundamental organic reactions discussed in the latter chapters.

Introduction

In 1997, Professor George S. Hammond published a short article entitled Physical Organic Chemistry after 50 years: “It has changed, but is it still there?”¹ In this article Hammond summarized the remarkable developments in the sub-discipline since it began with the work of Hammett.² No mention was made of the development of pseudo-first-order kinetic methods, which was the most important

* Coauthored by Vernon D. Parker, Weifang Hao, Zhao Li and Russell Scow. Reproduced with permission from *Int. J. Chem. Kinet.* **2012**, *44*(1), 2-12. Copyright © 2011, John Wiley and Sons.

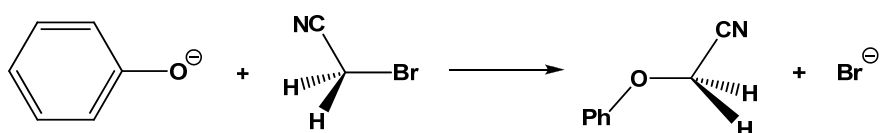
kinetic technique used by the vast majority of physical organic chemists. Aside from the development of very rapid kinetic techniques, essentially no improvements were made in the methods for which so many rate constants were measured for linear free-energy relationships. This is evident from the classic book *Kinetics and Mechanism*, by J. W. Moore and R. G. Pearson published in 1981.³ This deficiency continued for the remainder of the 20th century.

The digital revolution occurred during the time period of the development of physical organic chemistry. The latter had a great influence on the work of the physical chemists studying rapid kinetics but did not filter down to the physical organic chemists measuring rate constants of slower reactions. The objective of our work is to fill the gap by introducing work on the fundamental reactions of organic chemistry using new methods, which take advantage of modern digital acquisition of absorbance – time data and extensive new data analysis of pseudo-first-order kinetics. During the current century, several papers have appeared to deal with the inadequacy of a simple fit of an exponential curve to establish a simple one-step mechanism.⁴⁻⁷ The work of Kormányos and coworkers,⁵ entitled “Inherent Pitfalls in the Simplified Evaluation of Kinetic Curves,” is particularly relevant to the topic of this chapter. A more mathematical approach is presented for the analysis of the kinetics of complex systems in Bandstra’s work.⁶ The work of Nagy and Turányi⁴ deals with the effect of uncertainties in rate constants on the reliability of the corresponding activation parameters.

In this chapter, the kinetic data for the reaction of bromoacetonitrile (BrAN) with phenoxide ion (PO^-) (Scheme 2-1) in acetonitrile were chosen as samples to show how the new procedures work in practice. The results of the application of three different non-conventional pseudo-first-order procedures on the kinetic data of this reaction will be presented without mechanism discussions. But in the following chapters, the kinetic response of a wide variety of reactions, which include the formal hydride transfer reactions between NADH model compounds, the combination reactions, and the $\text{S}_{\text{N}}2$ displacement reactions, will be covered as well as the detailed mechanism analysis.

Bromoacetonitrile (BrAN) is not a common alkyl halide, but chloroacetonitrile (CIAN) has been used in recent publications concerned with the mechanism of the $\text{S}_{\text{N}}2$ reaction.⁸⁻⁹ The advantage of studying $\text{S}_{\text{N}}2$ reactions of BrAN is that it is much more reactive than a typical alkyl halide.

SCHEME 2-1. The Reaction of Bromoacetonitrile (BrAN) with Phenoxide ion (PO^-)



Experimental Methods and Data Processing

The methods discussed are limited to three general procedures, and the first is a more detailed application of the conventional pseudo-first-order kinetic relationship in a way that in some cases clearly distinguishes between simple one-step and complex multi-step mechanisms. When a complex mechanism is indicated, the other two procedures provide data, which give more details of the

kinetic response and can verify that the reaction follows a complex mechanism. The methods are discussed using experimental data for the reaction of bromoacetonitrile (BrAN) with phenoxide ion (PO^-) in acetonitrile at 298 K.

Half-Life Dependence of Conventional Pseudo-First-Order Rate Constants. The procedure involves converting absorbance – time profiles ($\text{Abs} - t$) to $-\ln(1 - \text{E.R.}) - \text{time}$ profiles, where E.R. is the extent of reaction. The latter are then subjected to linear least-squares analysis on five different segments of the data over time ranges corresponding to 0 – 0.5 half-lives (HL), 0 – 1 HL, 0 – 2 HL, 0 – 3 HL, and 0 – 4 HL. The data for the reaction of bromoacetonitrile (BrAN) with phenoxide ion (PO^-) in acetonitrile at 298 K are summarized in Table 2-1. In this case, the data show that the value of the apparent pseudo-first-order rate constant (k_{app}) over the first segment (0.5 HL) equals to 0.0350 s^{-1} . Values obtained for longer segments of the data (1.0 – 4.0 HL) steadily decreased with degree of conversion. While the changes in k_{app} observed are modest, the corresponding changes in the zero-time intercepts are much larger and suggest that this parameter is much more sensitive to the deviations from first-order kinetics than k_{app} is. Obviously, the response expected for the simple one-step mechanism is a constant value of k_{app} and an intercept independent of the number of HL taken into the linear least-squares correlation.

TABLE 2-1. Changes in the Slopes and the Intercepts with the Extent of Reaction During Conventional Pseudo-First-Order Analysis for the Reaction of BrAN (5.0 mM) with PO⁻ (0.50 mM) in Acetonitrile at 298 K

Number of HL	k_{app}/s^{-1}^a	Intercept/ s^{-1}^a
0.5	0.0350	0.0125
1.0	0.0346	0.0134
2.0	0.0336	0.0244
3.0	0.0318	0.0565
4.0	0.0289	0.1353

^a The error is $\pm 0.0002 s^{-1}$.

Sequential Pseudo-First-Order Linear Correlation. This analysis has been described in our recent papers.¹⁰⁻¹¹ The procedure involves recording a 2000-point absorbance – time profile over about the first HL of the reaction. After the conversion of the raw data to a $-\ln(1 - E.R.)$ – time profile, the linear least-squares analysis is then carried out over the following point segments: 1-11, 1-21, 1-31, 1-41, 1-51, 1-101, 1-201, . . . , 1-1801, and 1-1901, which gives 24 k_{app} values at the midpoints of the segments (Table 2-2). Standard deviations (S.D.) of the k_{app} evaluated for multiple (normally 20) stopped-flow shots are then recorded.

TABLE 2-2. Point Segment Set for Sequential Pseudo-First-Order Linear Correlation Analysis

Number	Segment	midpoint	Number	Segment	midpoint
1	1-11	6	13	1-801	401
2	1-21	11	14	1-901	451
3	1-31	16	15	1-1001	501
4	1-41	21	16	1-1101	551
5	1-51	26	17	1-1201	601
6	1-101	51	18	1-1301	651
7	1-201	101	19	1-1401	701
8	1-301	151	20	1-1501	751
9	1-401	201	21	1-1601	801
10	1-501	251	22	1-1701	851
11	1-601	301	23	1-1801	901
12	1-701	351	24	1-1901	951

TABLE 2-3. Apparent Rate Constants and Standard Deviations Obtained by the 24-Point Sequential Analysis for the Reaction of BrAN (5.0 mM) with PO⁻ (0.50 mM) in Acetonitrile at 298 K^a

time/s	k_{app}/s^{-1}	S.D./s ⁻¹	Segment
0.08	0.1293	0.0196	1
0.16	0.0870	0.0081	2
0.23	0.0669	0.0047	3
0.31	0.0553	0.0030	4
0.38	0.0479	0.0021	5
0.76	0.0334	0.0010	6
1.51	0.0284	0.0006	7
2.26	0.0272	0.0004	8
3.01	0.0266	0.0003	9
3.76	0.0262	0.0002	10
4.51	0.0259	0.0002	11
5.26	0.0257	0.0002	12
6.01	0.0255	0.0002	13
6.76	0.0254	0.0002	14
7.51	0.0252	0.0002	15
8.26	0.0251	0.0002	16
9.01	0.0249	0.0002	17
9.76	0.0248	0.0002	18
10.51	0.0247	0.0002	19
11.26	0.0246	0.0002	20
12.01	0.0245	0.0002	21
12.76	0.0243	0.0002	22
13.51	0.0242	0.0002	23
14.26	0.0241	0.0002	24

^a At least 20 stopped-flow shots.

The analysis is illustrated in Table 2-3 for the reaction of bromoacetonitrile (BrAN) with phenoxide ion (PO⁻) in acetonitrile at 298 K. The S.D. value for segment 1 is nearly 15% of the k_{app} value, and S.D. falls dramatically until it stabilizes to about 1% of the corresponding k_{app} from segments 9 to 24. The reason for the large S.D. in the early segments is related to the small number of points used in the linear correlations of the data in these segments. Each stopped-flow experiment is generally repeated at least three times. The expected

result (20 shots) of the 24-point procedure for the simple one-step mechanism is a rate constant, independent of time and of the particular time segment analyzed.

Although the primary purpose of this method is to estimate the errors in k_{app} , the plot shown in Figure 2-1 provides a convenient visual representation of the data, showing an initial high value and the subsequent decay to a plateau value as steady state is reached in about 3-4 s.

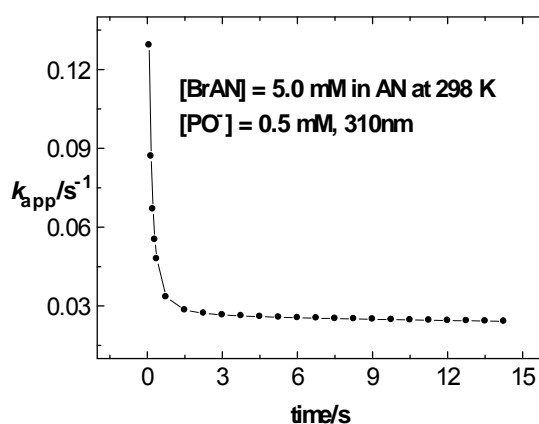


FIGURE 2-1. Apparent rate constants (k_{app}) – time plot for the reaction between phenoxide ion and BrAN in acetonitrile at 298 K (1.0 HL = 27.5 s).

The expected plot of the 24-point procedure for the simple one-step mechanism is illustrated in Figure 2-2a. For the reactions following the complex mechanism, the apparent rate constants derived from sequential correlation analysis steadily change with reaction time in different directions dependent upon whether reactant decay or product evolution is monitored. In Figure 2-2b, the upper profile is for reactant decay and the lower one is for product evolution.

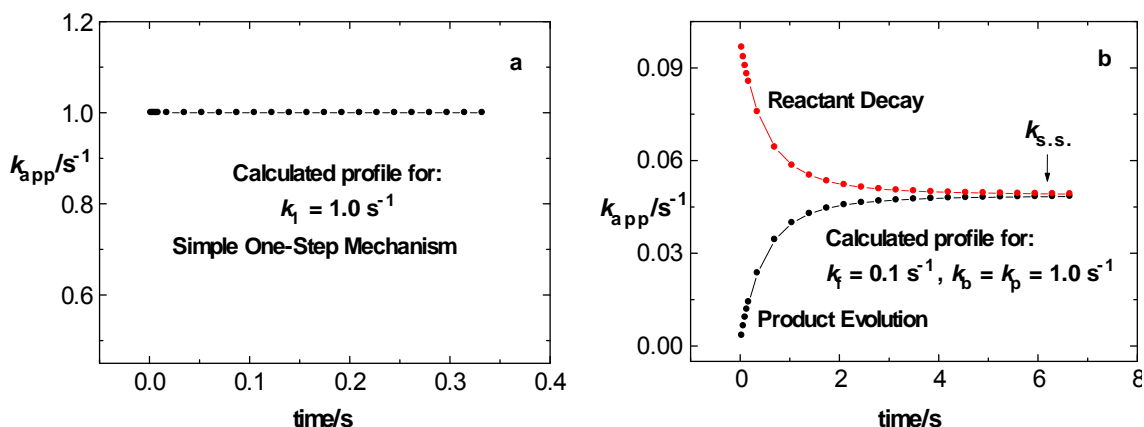


FIGURE 2-2. Apparent rate constants (k_{app}) – time plots for the simple one-step mechanism (a) and the complex mechanism (b).

A New Procedure for the Estimation of Instantaneous Rate Constants

– **Time Profiles.** Due to the use of a data smoothing procedure in the previous IRC analysis, we received the criticism for our method. So in this revised IRC analysis, we use the raw data directly obtained from the experiment. This method is actually an extension of the 24-point procedure. In this method, the points in the data segment are 1-3, 1-4, 1-5, 1-6, . . . , and 1-2000, and a 1998-point array of k_{app} – time data is obtained. The procedure was applied to calculated $-\ln(1 - E.R.)$ – time profiles, and the results were then compared to instantaneous rate constants (k_{inst}) – time profiles obtained at the midpoint between all points, as presented earlier.¹² The comparison showed that the k_{app} – time values at short times, as well as those near the end of the 1998-point array, were nearly identical to the corresponding k_{inst} – time values. The largest deviations (about 5%) were found in values near the center of the correlation. It was concluded that for all practical purposes the values obtained by the new procedure are equivalent to k_{inst} values, and the term k_{IRC} is appropriate to distinguish between the two

different instantaneous rate constants. The one advantage of k_{IRC} over k_{inst} is that since every value of the rate constant in the former case results from a linear correlation over several points (3 to 2000), there is a very large difference in the experimental precision as compared to the latter case. The other one is that the new procedure does not employ a data smoothing procedure. The plot in Figure 2-3 shows the application of the procedure outlined above.

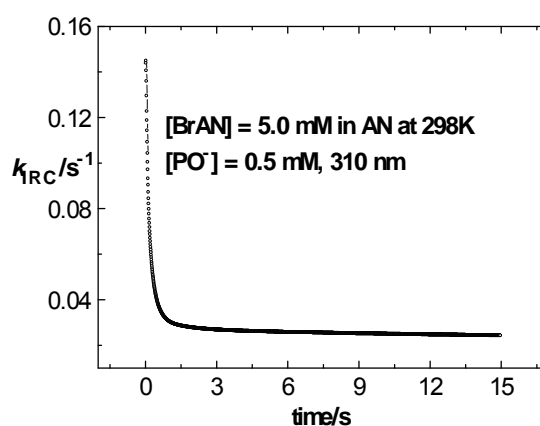


FIGURE 2-3. Apparent instantaneous rate constants (k_{IRC}) – time plot for the reaction of BrAN (5.0 mM) with PO^- (0.50 mM) in acetonitrile at 298 K (1.0 HL = 27.5 s).

Conclusion

Experimental absorbance – time profiles obtained from the reaction of bromoacetonitrile (BrAN) with phenoxide ion (PO^-) in acetonitrile were processed using three different non-conventional pseudo-first-order kinetic procedures, and the results are summarized. The procedures include (1) half-life dependence of k_{app} during conventional pseudo-first-order analysis, (2) sequential linear pseudo-first-order correlation, and (3) revised IRC analysis. Using these procedures, the determination as to whether a reaction follows a simple one-step or a more

complex mechanism can be made using a minimum of both time and materials. This, of course, is only the first step in the investigation of the mechanism of a reaction and should be followed by experiments under all applicable conditions, including changes in reactant concentrations, wavelengths at which absorbance – time data are obtained, temperature, and isotopic composition of reactants to name the most common variables.

References

- (1) Hammond, G. S. *Pure Appl. Chem.* **1997**, 69, 1919–1922.
- (2) Hammett, L. P. *Physical Organic Chemistry*, 2nd ed.; McGraw-Hill: New York, 1970.
- (3) Moore, J. W.; Pearson, R. G. *Kinetics and Mechanism*, 3rd ed.; Wiley: New York, 1981.
- (4) Nagy, T.; Turányi, T. *Int. J. Chem. Kinet.* **2011**, 43, 359–378.
- (5) Kormányos, B.; Horváth, A. K.; Peintler, G.; Nagypál, I. *J. Phys. Chem. A* **2007**, 111, 8104.
- (6) Bandstra, J. Z.; Tratnyek, P. G. *J. Math. Chem.* **2005**, 37, 409–422.
- (7) Vidaurre, G.; Vasquez, V. R.; Whiting, W. B. *Ind. Eng. Chem. Res.* **2004**, 43, 1395.
- (8) Vayner, G.; Houk, K. N.; Jorgensen, W. L.; Brauman, J. I. *J. Am. Chem. Soc.* **2004**, 126, 9054.
- (9) Chen, X.; Regan, C. K.; Craig, S. L.; Krenske, E. H.; Houk, K. N.; Jorgensen, W. L.; Brauman, J. I. *J. Am. Chem. Soc.* **2009**, 131, 16162–16170, and references cited.

- (10) Parker, V. D.; Li, Z.; Handoo, K. L; Hao, W.; Cheng, J.-P. *J. Org. Chem.* **2011**, 76, 1250.
- (11) Li, Z.; Cheng, J.-P.; Parker, V. D. *Org. Biomol. Chem.* **2011**, 9, 4563.
- (12) Parker, V. D. *J. Phys. Org. Chem.* **2006**, 19, 714.

CHAPTER 3
MECHANISM STUDY OF HYDRIDE TRANSFER BETWEEN N-BENZYL-1,4-
DIHYDRONICOTINAMIDE AND N-METHYLACRIDINIUM ION IN
ACETONITRILE

Abstract

A kinetic investigation of the formal hydride transfer reaction of *N*-benzyl-1,4-dihydronicotinamide (BNAH) with *N*-methylacridinium (MA^+) in acetonitrile (AN) confirmed that the reaction takes place in more than one step and involves a kinetically significant reactant complex intermediate, which is a non-covalent bound intermediate that is partially rate limiting during the course of this reaction. The methodology includes a numerical mechanism probe based on the ratio of times necessary to reach 50 and 5% reaction as well as quantitative pseudo-first-order kinetic analysis. The time-dependent apparent deuterium kinetic isotope effects (KIE_{app}) for the hydride transfer reaction approach unity at near zero time and increase with time toward plateau values as the reaction reaches a steady state. Computations at the M06-2x/6-311++G(d,p) level are consistent with the experimental study and provide the structures of two intermediates and confirm the free energy of the experimental rate-determining transition state.

Introduction

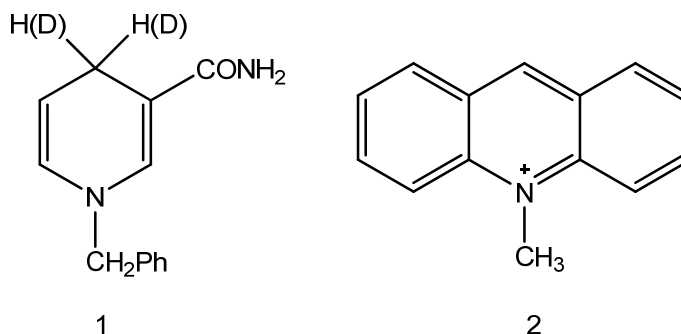
Hydride transfer is one of the fundamental chemical and biological reactions. The mechanism of the formal hydride transfer from the nicotinamide adenine dinucleotide coenzyme (NADH) and its analogues to the surrounding substrates has been a fascinating subject to chemists and biochemists and has

attracted the attention of many researchers around the world.¹⁻⁵ A controversy regarding the mechanism which began in the 1980's mainly focused on whether the hydride transfers takes place by direct hydride transfer or by a stepwise electron-proton-electron transfer and was eventually settled with the realization that which mechanism takes place depends upon the particular reaction in question.⁶⁻¹⁰ The studies of Sigman and co-workers¹¹⁻¹⁴ on the reduction of the *N*-methylacridinium cation (MA^+) by *N*-benzyl-1,4-dihydronicotinamide (BNAH) and of van Eikeren and co-workers¹⁵ on the transhydrogenation between BNAH and *N*-benzylnicotinamide cation (BNA^+) using suitable isotopic labels have both pointed to the possible generation of at least one intermediate species during these formal hydride transfers. In addition, several other publications also provided evidence for the formation of an intermediate in reactions between dihydronicotinamide and acceptors.¹⁶⁻¹⁸

In 1982, Bruice *et. al* reinvestigated the reaction between BNAH and MA^+ and claimed that the differences in kinetic ($k_{\text{H}}/k_{\text{D}}$) and product ($\text{Y}_{\text{H}}/\text{Y}_{\text{D}}$) isotope effects are invalid to determine the mechanism.⁶ They proposed a direct hydride transfer for this reaction. Since then, the direct one-step hydride transfer mechanism has been taken for granted for the reaction between BNAH and MA^+ .^{8,10}

The present work is a part of our general effort to determine the mechanisms of fundamental organic reactions. We have recently shown that the carbocation-anion combination reaction,¹⁹ the reaction of 2,4,6-trinitroanisole (TNA) with methoxide ion,²⁰ and the proton transfer reactions of simple

nitroalkanes with hydroxide ion²¹ take place by a reversible consecutive mechanism with kinetically significant intermediates using our recently developed methods.²²⁻²³ In this chapter, we report the kinetic data consistent with a complex mechanism which involves the existence of a kinetically significant intermediate during the hydride transfer reactions between BNAH/BNAH-*d*₂ (1) and MA⁺ (2) in acetonitrile.



Results and Discussion

Numerical Mechanism Probes. The time ratio ($t_{0.50}/t_{0.05}$) and apparent rate constant ratio ($k_{\text{init}}/k_{\text{s.s.}}$) are very useful mechanism probes in the analysis of reaction mechanisms.²⁴⁻²⁵ The time and rate constant ratios are equal to 13.5 and 1.00, respectively, for a pseudo-first-order reaction taking place in a simple one-step (Scheme 3-1, (1)) regardless of whether reactant or product is monitored. The data in Table 3-1 summarize the mechanism probe parameters observed for the hydride transfer reaction between BNAH/BNAH-*d*₂ and MA⁺ in acetonitrile at 298 K along with the values of the steady-state rate constants $k_{\text{s.s.}}$ as a function of the wavelengths of the measurement. The experimental data are inconsistent with the simple one-step mechanism for the hydride transfer. In all cases, $t_{0.50}/t_{0.05}$ are significantly greater than 13.5 and $k_{\text{init}}/k_{\text{s.s.}}$ are significantly

greater than unity while monitoring reactant decay. The observed results are consistent with the reversible consecutive second-order mechanism under pseudo-first-order conditions (Scheme 3-1, (2)).

SCHEME 3-1. The Simple One-Step Mechanism (1) and the Reversible Consecutive Mechanism (2)

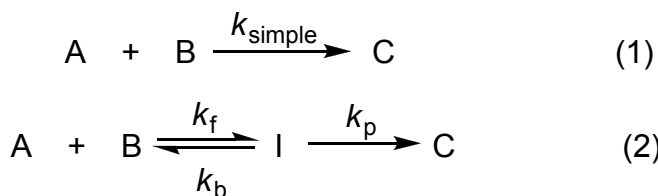


TABLE 3-1. Time and Rate Constant Ratios for the Hydride Transfer Reactions Between BNAH^a/BNAH-*d*₂^b and MA⁺ in Acetonitrile at 298K over a Range of Wavelengths

λ/nm	$t_{0.50}/t_{0.05}^a$	$k_{\text{init}}/k_{\text{s.s.}}^a$	$k_{\text{s.s.}}/\text{s}^{-1}^a$
410	15.9	1.36	0.515
420	16.7	1.57	0.518
430	18.2	1.67	0.475
440	18.6	1.74	0.503
450	16.7	1.26	0.504

λ/nm	$t_{0.50}/t_{0.05}^b$	$k_{\text{init}}/k_{\text{s.s.}}^b$	$k_{\text{s.s.}}/\text{s}^{-1}^b$
410	15.1	1.48	0.132
420	15.2	1.45	0.133
430	15.1	1.32	0.141
440	14.9	1.21	0.127
450	15.5	1.44	0.131

^a [BNAH] = 7.2 mM, [MA⁺] = 0.3 mM. ^b [BNAH-*d*₂] = 7.2 mM, [MA⁺] = 0.3 mM.

Pseudo-First-Order Kinetic Analysis. We recently developed a new method to carry out quantitative pseudo-first-order kinetic studies.²⁰ The experimental procedure involves recording a 2000-point absorbance – time (Abs – *t*) profile over about the first HL of the reaction and carrying out a sequential first-order analysis on specific point segments of the (1 - E.R.) – time (where E.R.

denotes extent of reaction) profiles. The procedure employs 24 different linear least-squares correlations over increasingly large point segments in the profile. These segments involve points 1-11, 1-21, 1-31, 1-41, 1-51, 1-101, 1-201, . . . , 1-1801, and 1-1901. Although the successive series of rate constants (k_{app}) obtained can then be plotted vs. the times at the midpoints of each segment, its primary value is that it provides average values and standard deviations (see Tables 3-2, 3-3 and A-1 to A-5) of apparent psuedo-first-order rate constants (k_{app}) for the midpoint of each segment. The times in this analysis are t_6 , t_{11} , t_{16} , t_{21} , t_{26} , t_{51} , t_{101} , . . . , t_{901} , and t_{951} where the subscript is the point number. This procedure gives a clear indication of any changes in the values of k_{app} as the reaction proceeds. If a reaction obeys pseudo-first-order kinetics, the values of k_{app} are constant for all of the point segments and are expected to be time independent and have the same value within experimental error.

The data in Tables 3-2 and 3-3 were obtained using the successive correlation method. It is obvious that the k_{app} – time profiles begin at relatively high values of k_{app} and decay with time toward steady-state values at all of the wavelengths. At 410 nm, the value of k_{app} in segment 1 was observed to be equal to 1.144 and then was observed to decrease steadily to 0.515 at segment 24 for the H-substrate. However, at 430 nm the value starts at 1.924 in segment 1 and decreases to 0.475 at segment 24. The wavelength-dependent rate constants for both of H- and D- substrates are inconsistent with the simple mechanism. The plots shown in Figure 3-1 provide a convenient visual representation of the data (Tables 3-2 and 3-3) showing an initial high value and the subsequent decay to a

plateau value as steady state is reached. The expected result of the sequential 24-point procedure for the one-step mechanism is a rate constant, independent of time and of the particular time segment analyzed.

TABLE 3-2. Apparent Rate Constants for the Hydride Transfer Reaction Between BNAH and MA⁺ in Acetonitrile over the First Half-Life at 298K as a Function of Wavelengths^a

410 nm		420 nm		430 nm		440 nm		450 nm		No.
k_{app}/s^{-1}	\pm^b	k_{app}/s^{-1}	\pm	k_{app}/s^{-1}	\pm	k_{app}/s^{-1}	\pm	k_{app}/s^{-1}	\pm	
1.144	0.193	1.190	0.088	1.924	0.114	1.347	0.141	1.424	0.107	1
0.974	0.105	1.010	0.105	1.729	0.074	1.112	0.178	1.288	0.052	2
0.893	0.110	0.896	0.084	1.593	0.046	0.986	0.181	1.144	0.012	3
0.819	0.080	0.812	0.057	1.422	0.073	0.908	0.171	1.047	0.016	4
0.761	0.066	0.756	0.040	1.282	0.099	0.845	0.154	0.966	0.024	5
0.638	0.030	0.640	0.015	0.912	0.137	0.691	0.089	0.783	0.016	6
0.580	0.010	0.592	0.032	0.702	0.084	0.610	0.029	0.687	0.012	7
0.551	0.004	0.558	0.038	0.603	0.058	0.570	0.015	0.624	0.008	8
0.538	0.002	0.543	0.038	0.557	0.044	0.552	0.014	0.590	0.006	9
0.531	0.004	0.536	0.038	0.533	0.035	0.540	0.016	0.570	0.004	10
0.526	0.004	0.531	0.039	0.520	0.026	0.533	0.018	0.556	0.003	11
0.523	0.004	0.530	0.042	0.511	0.022	0.529	0.020	0.547	0.002	12
0.521	0.005	0.528	0.043	0.504	0.019	0.526	0.020	0.539	0.002	13
0.519	0.006	0.527	0.043	0.498	0.016	0.523	0.020	0.533	0.002	14
0.518	0.006	0.525	0.044	0.494	0.014	0.520	0.020	0.528	0.002	15
0.517	0.006	0.524	0.045	0.490	0.013	0.518	0.020	0.524	0.002	16
0.517	0.006	0.523	0.045	0.487	0.012	0.515	0.020	0.520	0.002	17
0.517	0.007	0.521	0.045	0.485	0.011	0.513	0.020	0.517	0.002	18
0.517	0.007	0.520	0.046	0.483	0.011	0.511	0.020	0.514	0.002	19
0.517	0.008	0.520	0.046	0.481	0.010	0.509	0.020	0.511	0.002	20
0.517	0.008	0.520	0.046	0.479	0.009	0.507	0.020	0.509	0.002	21
0.516	0.008	0.519	0.046	0.478	0.009	0.506	0.021	0.508	0.002	22
0.516	0.009	0.518	0.046	0.476	0.009	0.505	0.021	0.506	0.001	23
0.515	0.009	0.518	0.047	0.475	0.009	0.503	0.021	0.504	0.001	24

^a [BNAH] = 7.2 mM, [MA⁺] = 0.3 mM, average of 3 sets of 20 stopped-flow repetitions. ^b \pm is the standard deviation of 3 sets of experiments.

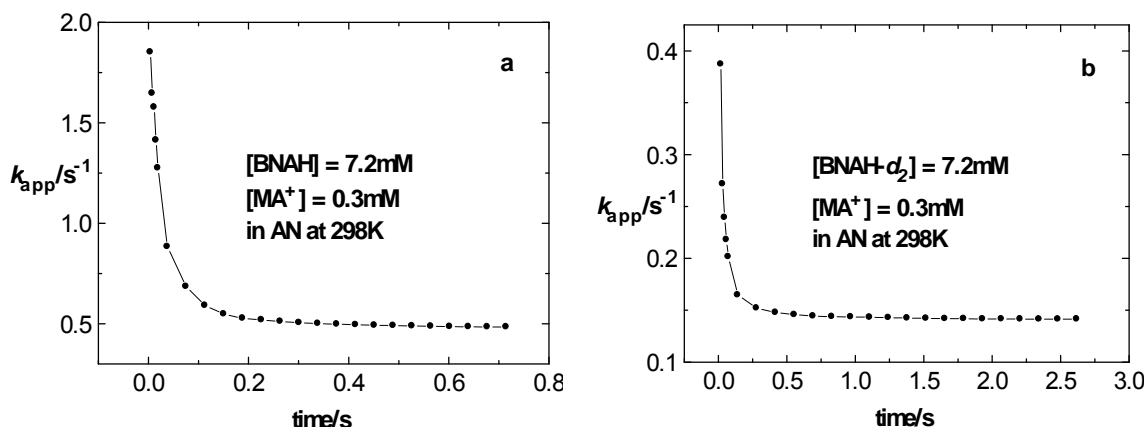


FIGURE 3-1. Apparent rate constants (k_{app}) – time plots for the reactions between BNAH (a)/BNAH- d_2 (b) and MA^+ in acetonitrile at 298K and 430 nm.

TABLE 3-3. Apparent Rate Constants for the Hydride Transfer Reaction Between BNAH- d_2 and MA^+ in Acetonitrile over the First Half-Life at 298K as a Function of Wavelengths^a

410 nm		420 nm		430 nm		440 nm		450 nm		No.
k_{app}/s^{-1}	\pm^b	k_{app}/s^{-1}	\pm	k_{app}/s^{-1}	\pm	k_{app}/s^{-1}	\pm	k_{app}/s^{-1}	\pm	
0.470	0.068	0.502	0.060	0.387	0.036	0.192	0.051	0.215	0.056	1
0.287	0.042	0.335	0.028	0.272	0.024	0.169	0.028	0.180	0.027	2
0.238	0.021	0.270	0.022	0.239	0.019	0.164	0.019	0.204	0.029	3
0.221	0.017	0.239	0.021	0.218	0.021	0.162	0.021	0.211	0.030	4
0.202	0.015	0.215	0.016	0.202	0.021	0.158	0.018	0.204	0.030	5
0.161	0.008	0.164	0.007	0.165	0.011	0.142	0.009	0.165	0.016	6
0.140	0.003	0.144	0.002	0.152	0.004	0.132	0.003	0.145	0.006	7
0.135	0.001	0.140	0.001	0.148	0.002	0.130	0.001	0.140	0.003	8
0.133	0.001	0.137	0.001	0.146	0.001	0.129	0.001	0.138	0.002	9
0.133	0.001	0.137	0.001	0.144	0.001	0.129	0.001	0.136	0.001	10
0.132	0.001	0.137	0.001	0.144	0.001	0.130	0.001	0.135	0.001	11
0.131	0.001	0.136	0.001	0.144	0.001	0.129	0.001	0.134	0.001	12
0.131	0.001	0.135	0.001	0.143	0.001	0.129	0.001	0.134	0.001	13
0.131	0.001	0.135	0.001	0.143	0.001	0.129	0.001	0.133	0.001	14
0.131	0.001	0.134	0.001	0.142	0.001	0.129	0.001	0.133	0.001	15
0.131	0.001	0.134	0.001	0.142	0.001	0.128	0.001	0.132	0.001	16
0.132	0.001	0.133	0.001	0.142	0.001	0.128	0.001	0.132	0.001	17
0.132	0.001	0.133	0.001	0.142	0.001	0.128	0.001	0.132	0.001	18
0.132	0.001	0.133	0.001	0.142	0.001	0.127	0.001	0.131	0.001	19
0.132	0.001	0.133	0.001	0.142	0.001	0.127	0.001	0.131	0.001	20
0.132	0.001	0.133	0.001	0.142	0.001	0.127	0.001	0.131	0.001	21
0.132	0.001	0.133	0.001	0.141	0.001	0.127	0.001	0.131	0.001	22
0.132	0.001	0.133	0.001	0.141	0.001	0.127	0.001	0.131	0.001	23
0.132	0.001	0.133	0.001	0.141	0.001	0.127	0.001	0.131	0.001	24

^a [BNAH- d_2] = 7.2 mM, [MA⁺] = 0.3 mM, average of 3 sets of 20 stopped-flow repetitions. ^b \pm is the standard deviation of 3 sets of experiments.

Instantaneous rate constant (IRC) analysis was reported several year ago,^{19,22} and required data smoothing due to the very small changes in signal from one point to the next in the 2000-point data profile, smaller than experimental noise. Recently, a variation of the successive correlation method was shown to give very nearly the same results without employing a data smoothing procedure.²³ The key feature of this analysis is that successive segments of the 2000-point $-\ln(1 - \text{E.R.}) - \text{time}$ profile; 1-3, 1-4, 1-5, . . . , and 1-2000 are subjected to linear least-squares correlation (the conventional first-order treatment) to give a 1998-point data array. A plot of the latter, $k_{\text{IRC}} - \text{time}$ then provides a smooth plot very similar to the original $k_{\text{inst}} - \text{time}$ plot.^{19,22}

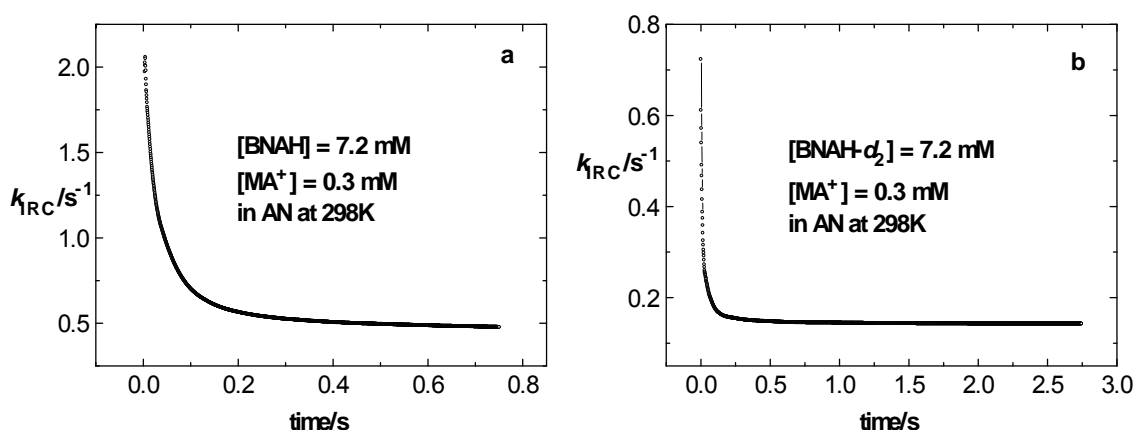


FIGURE 3-2. Apparent instantaneous rate constants (k_{IRC}) – time plots for the reactions between BNAH (a)/BNAH- d_2 (b) and MA^+ in acetonitrile at 298K and 430 nm.

The $k_{\text{IRC}} - \text{time}$ data for the reactions between BNAH/BNAH- d_2 and MA^+ in acetonitrile are illustrated by the plots in Figures 3-2 and A-1 to A-4. The $k_{\text{IRC}} - \text{time}$ profiles have the form expected for monitoring the reactant decay in a complex mechanism decaying rapidly from an initial value of close to 2.0 s^{-1} for

the H-substrate (a) and 0.8 s^{-1} for the D-substrate (b), respectively, toward steady-state values, while that expected for the one-step mechanism is a straight line with zero slopes.

Apparent Kinetic Isotope Effects. The apparent kinetic isotope effects for the hydride transfer reactions between BNAH/BNAH- d_2 and MA^+ in acetonitrile were determined using the values of k_{app} obtained from the 24-point successive correlation method. KIE_{app} equals to the ratio of $k_{\text{app}}^{\text{H}}$ to $k_{\text{app}}^{\text{D}}$. The observation of time-dependent KIE_{app} has been shown to provide a very effective argument to establish the existence of a complex mechanism.²¹ The KIE_{app} observed for a simple one-step mechanism corresponding to the ratio of microscopic rate constants are time independent. It is particularly important in showing complex reaction behavior to attempt to estimate the KIE_{app} as zero time is approached since an extrapolated KIE_{app} equal to 1 is very strong evidence that there is no C-H bond breaking in any step prior to the rate-determining transition state in a multi-step mechanism. The time-dependent KIE_{app} at 430 nm is illustrated in Figure 3-3 (Figures A-5 to A-8 for other wavelengths) for the hydride transfer reactions between BNAH/BNAH- d_2 and MA^+ in acetonitrile at 298K. The KIE_{app} values rise from near unity at zero-time to approach a constant value equal to 3.6 as steady state is reached. The KIE_{app} values at wavelengths from 410 nm to 450 nm, at 10 nm intervals, are summarized in Table 3-4. In all cases the KIE_{app} values at short times are close to unity and increase with time to the steady-state KIE_{app} value.

TABLE 3-4. Apparent KIE for the Reactions Between BNAH/BNAH- d_2 and MA^+ in Acetonitrile at 298K under Different Wavelengths

time/s	410 nm	420 nm	430 nm	440 nm	450 nm	Segment
	KIE _{app}	KIE _{app}	KIE _{app}	KIE _{app}	KIE _{app}	
0.008	1.85	1.64	1.78	2.60	2.15	1
0.012	1.68	1.73	1.99	3.03	2.79	2
0.016	1.93	1.78	2.15	3.23	3.08	3
0.019	2.04	1.85	2.31	3.12	3.19	4
0.023	2.13	1.88	2.43	3.24	3.36	5
0.041	2.42	2.20	2.69	3.37	3.35	6
0.077	2.72	2.55	2.92	3.48	3.20	7
0.113	3.00	2.86	3.19	3.74	3.46	8
0.150	3.13	3.08	3.33	3.85	3.61	9
0.186	3.22	3.21	3.40	3.94	3.73	10
0.222	3.32	3.28	3.44	4.03	3.80	11
0.258	3.39	3.33	3.47	4.08	3.84	12
0.294	3.44	3.37	3.49	4.11	3.86	13
0.331	3.48	3.39	3.51	4.12	3.87	14
0.367	3.50	3.40	3.52	4.13	3.88	15
0.403	3.52	3.41	3.53	4.12	3.88	16
0.439	3.55	3.42	3.53	4.11	3.88	17
0.475	3.57	3.43	3.53	4.10	3.88	18
0.512	3.57	3.44	3.53	4.09	3.89	19
0.548	3.57	3.46	3.54	4.09	3.89	20
0.584	3.57	3.47	3.54	4.09	3.89	21
0.620	3.57	3.48	3.54	4.09	3.89	22
0.656	3.58	3.47	3.54	4.08	3.89	23
0.693	3.58	3.46	3.55	4.07	3.90	24

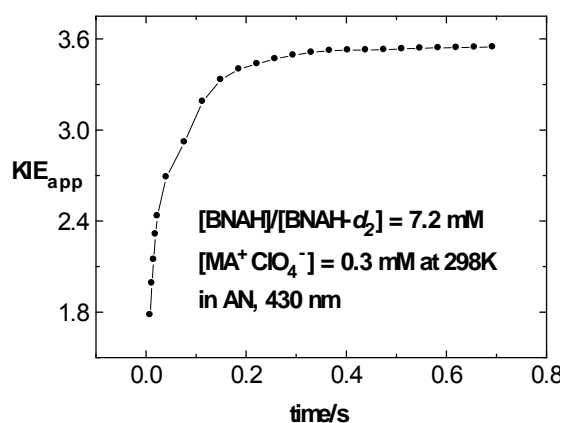


FIGURE 3-3. Apparent KIE for the reactions between BNAH/BNAH- d_2 and MA^+ in acetonitrile at 298K and 430 nm as a function of reaction time.

Electronic Absorbance Spectral Evidence for a Charge-Transfer Complex During the Reaction Between BNAH and MA⁺. When high concentrations of BNAH (0.1 M) and MA⁺ (0.08 M) were allowed to react in acetonitrile, a new broad absorbance band at $\lambda_{\text{max}} = 560$ nm, which is characteristic of a charge-transfer (CT) complex, was observed in a stopped-flow spectrophotometer (Figure 3-4) upon mixing. The absorbance then decayed with time and disappeared as the reaction approached completion.

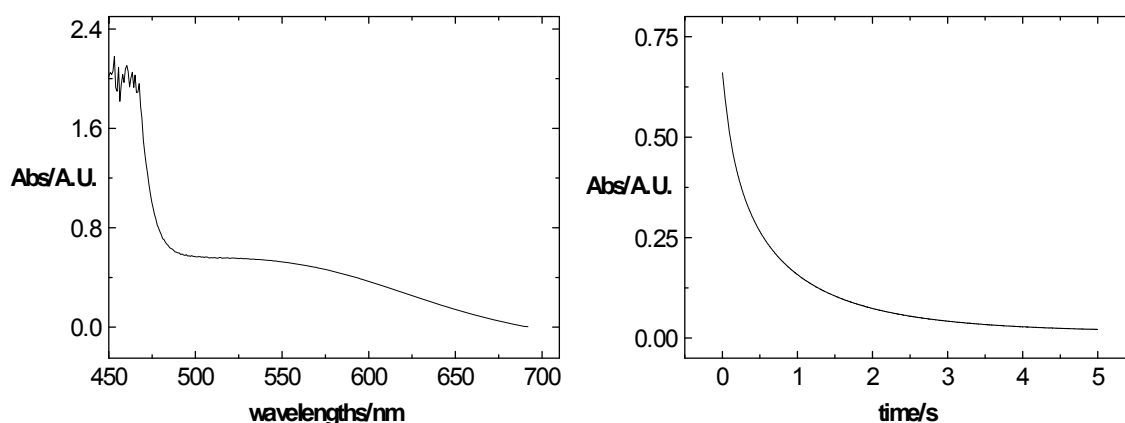
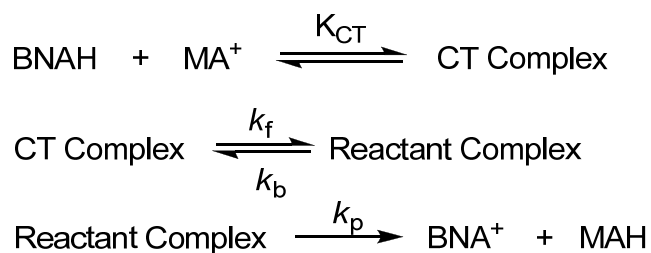


FIGURE 3-4. Electronic absorbance spectrum of the charge-transfer complex for the reaction between BNAH (0.1 M) and MA⁺ (0.08 M) in acetonitrile at 298 K (left) and the absorbance – time decay curve at 560 nm (right).

The data discussed in the previous paragraphs clearly rule out the simple one-step mechanism for the hydride transfer reactions between BNAH or BNAH-*d*₂ and MA⁺ in acetonitrile. Since the charge-transfer complex is formed immediately during the time of mixing, the rapid equilibrium between reactants and the CT complex is not expected to perturb the kinetics evaluated in the wavelength range from 410 nm to 450 nm during the reactions of BNAH or BNAH-*d*₂ and MA⁺ in acetonitrile. Due to the very rapid formation and

dissociation of the CT complex it can be ruled out as the kinetically significant intermediate required by the kinetics.²⁶⁻²⁷ Therefore, during the course of the reaction, there is necessarily another intermediate, which we call the “Reactant Complex,” giving rise to the time-dependent rate constants and time-dependent KIE_{app} ’s. The most probable mechanism for the reaction is shown in Scheme 3-2. The first step is the formation of the CT complex in rapid equilibrium with reactants, followed by the formation of a second intermediate, the “Reactant Complex” which is an intermediate without any new covalent bonds. Up to the latter step, there is no C-H bond breaking which contributes to the KIE_{app} . The final step is the actual hydride transfer process to produce the products. The multi-step mechanism for the hydride transfer fits our pseudo-first-order rate constant analysis and KIE_{app} observation.

SCHEME 3-2. The Proposed Mechanism for the Reaction Between BNAH and MA⁺



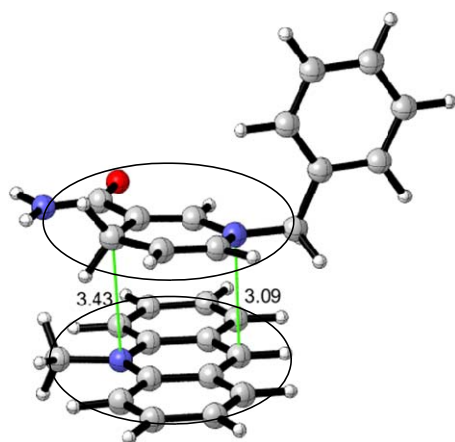
Furthermore, the preliminary computations show that there are two complexes on the reaction coordinate between the reactants and products. The structures of the complexes were optimized in solution (acetonitrile) using SMD/M06-2x/6-311++G(d,p) method. The M06-2x functional is particularly appropriate for these calculations since it has been shown to give very high

precision in energies when compared with a number of other DFT functionals.²⁸⁻

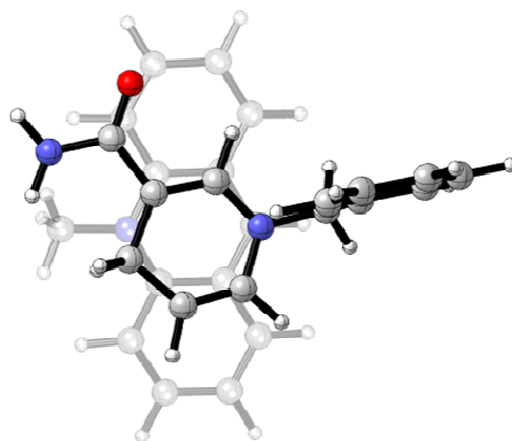
31

The optimized structures shown in Figure 3-5 were confirmed by frequency calculations to be minima on the reaction coordinate using the same level of theory. The calculations were carried out using the Gaussian 09 program package.³² Our kinetic results suggest that there are no covalent bound intermediates in this and related hydride transfer reactions from the reactants to the “Reactant Complexes.” We have previously proposed in a related reaction that the CT complex is rapidly formed and is in equilibrium with reactants in acetonitrile and that the CT complex undergoes intra-molecular rearrangement to another intermediate which we have called the “Reaction Complex.”²⁶

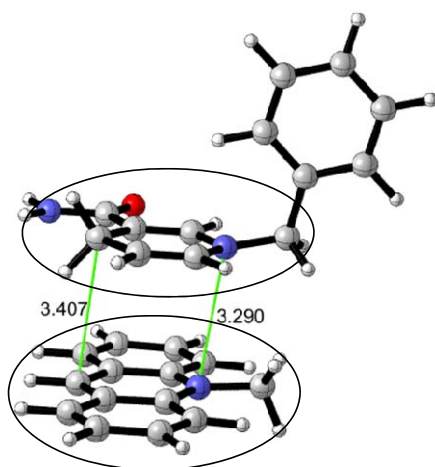
It is obvious that the reaction centers (circled in Figure 3-5) in the intermediate which we have labeled as Complex 1 are not in relative positions which make hydride transfer possible. So in this case Complex 1 functions in the same manner as the CT complex in our previously proposed²⁶ mechanism. Complex 2, which has a geometry conducive to bond formation between the reactive centers, is then equivalent to the “Reactant Complex” in the proposed mechanism. From the top view, we can see that Complex 2 is actually derived from the 180 degree rotation of Complex 1. We also present the calculated rate-determining transition state structure for the reaction.



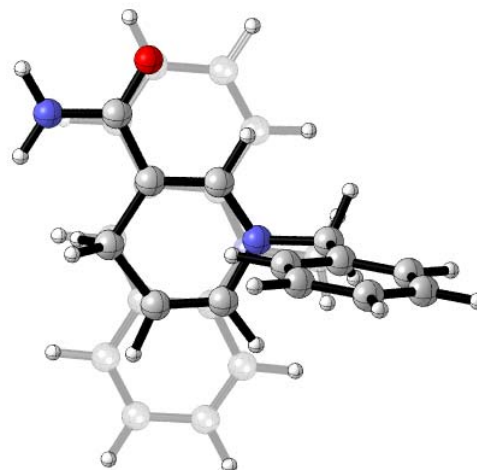
Complex 1, Side View



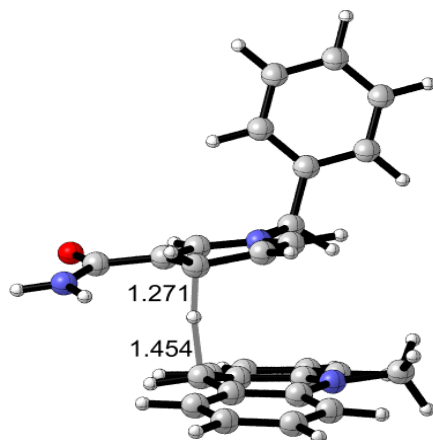
Complex 1, Top View



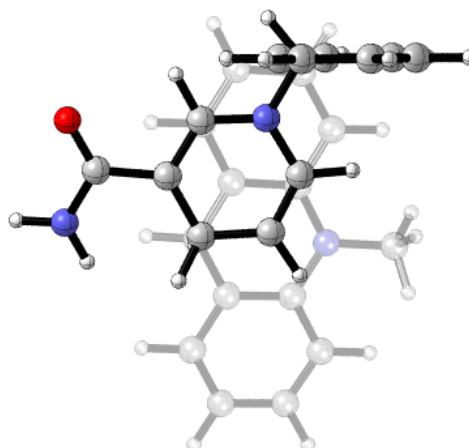
Complex 2, Side View



Complex 2, Top View



Transition State, Side View



Transition State, Top View

FIGURE 3-5. Calculated structures of complex 1, complex 2, and transition state in acetonitrile.

The reaction coordinate diagram for the reaction of BNAH and MA⁺ in acetonitrile is shown in Figure 3-6. A point of interest is that in acetonitrile, the reaction enthalpies (ΔH 's) for the formation of the transition state, the intermediates, and the products are significantly lower than the corresponding free energies (ΔG 's). The computations predict that the entropy changes (ΔS 's) will have a dominant effect on the kinetics of the reaction in solution. The latter compares favorably with the experimental activation parameters ($\Delta H^\ddagger = 6.47$ kcal mol⁻¹, $\Delta S^\ddagger = -28.3$ cal mol⁻¹ K⁻¹ and $\Delta G^\ddagger = 14.9$ kcal mol⁻¹, rate constants at various temperatures are listed in Table A-6).

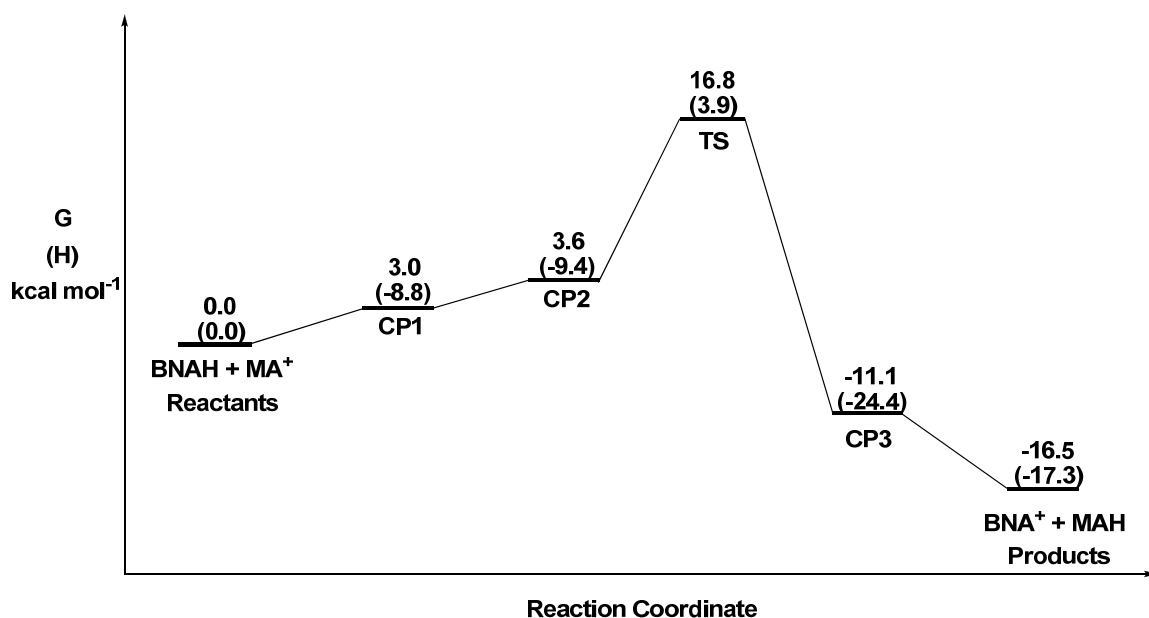


FIGURE 3-6. The reaction coordinate for the reaction of BNAH and MA⁺ in acetonitrile at 298.15 K calculated using the M06-2x/6-311++G(d,p)/SMD functional.

The calculated transition state free energy is 16.8 kcal mol⁻¹, close to the experimentally observed activation free energy for the reaction leading to product formation which is 14.9 kcal mol⁻¹. The CP1 and CP2 represent the CT complex

and the reactant complex, respectively. The “Reactant Complex” has a higher Gibbs free energy than the CT complex. Since we were unable to locate the transition state³³ for the formation of CP2, we are unable to compare the computed free energy of activation for its formation with the experimental value.

Conclusions

Our primary conclusion is that the hydride transfer reaction between BNAH and MA⁺ in acetonitrile takes place by a complex mechanism with a kinetically significant intermediate. This conclusion was arrived at from the experimental kinetic data which show that the k_{app} for the reactions of both BNAH and BNAH- d_2 is time dependent, with high values at short times and decreasing with time to steady-state values. The latter results in time-dependent KIE_{app} that approach unity near zero time and increase with time to a steady-state value.

Gaussian calculations at the M06-2x/6-311++G(d,p) level resulted in the observation of two intermediates, Complex 1 and Complex 2, on the reaction coordinate leading to hydride transfer. The two intermediates have no new covalent bonds and are held together by the overlap of π -orbitals in the two moieties. It was concluded that the geometry of Complex 1 is unsuitable for hydride transfer to occur at that stage of the reaction and the unimolecular rearrangement to Complex 2, in which the reactive sites are suitably close, is required before proceeding to the rate-determining transition state.

The calculations reveal that the enthalpies for the formation of the intermediates and the transition state are significantly lower than the corresponding free energies. This leads to the conclusion that the reaction from

reactants to the rate-determining transition state is driven to a large extent by the changes in entropy. The calculated rate-determining transition state energy is very close to the experimental free energy of activation available from the apparent rate constants at steady state.

Experimental Section

Materials. *N*-Benzyl-1,4-dihydronicotinamide (BNAH) and its 4,4'-dideuterated analogue (BNAH- d_2) were synthesized by reduction of the oxidized forms, *N*-benzylnicotinamide salt (BNA⁺) according to the standard literature procedure.³⁶⁻³⁷ The C-4 deuterium content of BNAH- d_2 was determined to be greater than 98% as indicated by ¹H NMR. *N*-methylacridinium perchlorate (MA⁺ClO₄⁻) was obtained from the ion exchange between *N*-methylacridinium iodide³⁸ and excess magnesium perchlorate. Acetonitrile was refluxed and distilled over P₂O₅ under a nitrogen atmosphere and past through an Al₂O₃ column before transferring into the glove box.

Kinetic Experiments. Kinetic experiments were carried out using a Hi-Tech SF-61 DX2 stopped-flow spectrophotometer installed in a glove box and kept under a nitrogen atmosphere. The temperature was controlled at 298 K using a constant temperature flow system connected directly to the reaction cell through a bath situated outside of the glove box. All stopped-flow experiments included the recording of at least 20 absorbance – time profiles over the entire applicable wavelengths range from 410 nm to 450 nm at 10 nm intervals. Each experiment was repeated at least three times. The 2000-point absorbance – time curve data were collected over one half-life.

References

- (1) Fukuzumi, S.; Suenbu, T.; Parz, M.; Hirasaka, T.; Itoh, S.; Fujitsuka, M.; Ito, O. *J. Am. Chem. Soc.* **1998**, *120*, 8060.
- (2) Anne, A.; Moiroux, J.; Saveant, J.-M. *J. Am. Chem. Soc.* **1993**, *115*, 10224.
- (3) Carlson, B. W.; Miller, L. L. *J. Am. Chem. Soc.* **1980**, *102*, 6533.
- (4) Zhu, X.-Q.; Liu, Y.; Zhao, B.-J.; Cheng, J.-P. *J. Org. Chem.* **2001**, *66*, 370.
- (5) Zhu, X.-Q.; Liu, Y.-C. *J. Org. Chem.* **1998**, *63*, 2786.
- (6) Powell, M. F.; Bruice, T. C. *J. Am. Chem. Soc.* **1982**, *104*, 5834.
- (7) Powell, M. F.; Bruice, T. C. *J. Am. Chem. Soc.* **1983**, *105*, 1014.
- (8) Powell, M. F.; Bruice, T. C. *J. Am. Chem. Soc.* **1983**, *105*, 7139.
- (9) Ohno, A.; Shio, T.; Yamamoto, H.; Oka, S. *J. Am. Chem. Soc.* **1981**, *103*, 2045.
- (10) Tanner, D. D.; Kharrat, A. *J. Org. Chem.* **1988**, *53*, 1646.
- (11) Creighton, D. J., Hajdu, J.; Mooser, G.; Sigman, D. S. *J. Am. Chem. Soc.* **1973**, *95*, 6855.
- (12) Creighton, D. J., Hajdu, J.; Sigman, D. S. *J. Am. Chem. Soc.* **1976**, *98*, 4619.
- (13) Hajdu, J.; Sigman, D. S. *J. Am. Chem. Soc.* **1976**, *98*, 6060.
- (14) Hajdu, J.; Sigman, D. S. *Biochemistry* **1977**, *16*, 2841.
- (15) van Eikeren, P.; Grier, D. L. *J. Am. Chem. Soc.* **1977**, *99*, 8057.
- (16) Steffens, J. J.; Chipman, D. M. *J. Am. Chem. Soc.* **1971**, *93*, 6694.

- (17) Bunting, J. W.; Sindhuatmadja, S. *J. Org. Chem.* **1981**, *46*, 4211.
- (18) Zhu, X.-Q.; Zhang, J.-Y.; Cheng, J.-P. *J. Org. Chem.* **2006**, *71*, 7007.
- (19) Hao, W.; Parker, V. D. *J. Org. Chem.* **2008**, *73*, 48.
- (20) Parker, V. D.; Li, Z.; Handoo, K. L.; Hao, W.; Cheng, J.-P. *J. Org. Chem.* **2011**, *76*, 1250.
- (21) Li, Z.; Cheng, J.-P.; Parker, V. D. *Org. Biomol. Chem.* **2011**, *9*, 4563.
- (22) Parker, V. D. *J. Phys. Org. Chem.* **2006**, *19*, 714.
- (23) Parker, V. D.; Hao, W.; Li, Z.; Scow, R. *Int. J. Chem. Kinet.* **2012**, *44*, 2.
- (24) Parker, V. D.; Zhao, Y. *J. Phys. Org. Chem.* **2001**, *14*, 604.
- (25) Parker, V. D. *Pure Appl. Chem.* **2005**, *77*, 1823.
- (26) Lu, Y.; Zhao, Y.; Handoo, K. L.; Parker, V. D. *Org. Biomol. Chem.* **2003**, *1*, 173.
- (27) Handoo, K. L.; Lu, Y.; Parker, V. D. *J. Am. Chem. Soc.* **2003**, *125*, 9381.
- (28) Zhao, Y.; Truhlar, D. G. *Theo. Chem. Acc.* **2008**, *120*, 215.
- (29) Zhao, Y.; Truhlar, D. G. *Chem. Acc. Res.* **2008**, *41*, 157.
- (30) Marenich, A. V.; Cramer, C. J.; Truhlar, D. G. *J. Phys. Chem. B.* **2009**, *113*, 6378.
- (31) Zhao, Y.; Truhlar, D. G. *Chem. Phys. Lett.* **2011**, *502*, 1.
- (32) Frisch, M. J.; Trucks, G. W.; Schlegel, H. B.; Scuseria, G. E.; Robb, M. A.; Cheeseman, J. R.; Scalmani, G.; Barone, V.; Mennucci, B.; Petersson, G. A.; Nakatsuji, H.; Caricato, M.; Li, X.; Hratchian, H. P.; Izmaylov, A. F.; Bloino, J.; Zheng, G.; Sonnenberg, J. L.; Hada, M.; Ehara, M.; Toyota, K.; Fukuda, R.; Hasegawa, J.; Ishida, M.; Nakajima,

T.; Honda, Y.; Kitao, O.; Nakai, H.; Vreven, T.; Montgomery, J. A., Jr.; Peralta, J. E.; Ogliaro, F.; Bearpark, M.; Heyd, J. J.; Brothers, E.; Kudin, K. N.; Staroverov, V. N.; Kobayashi, R.; Normand, J.; Raghavachari, K.; Rendell, A.; Burant, J. C.; Iyengar, S. S.; Tomasi, J.; Cossi, M.; Rega, N.; Millam, J. M.; Klene, M.; Knox, J. E.; Cross, J. B.; Bakken, V.; Adamo, C.; Jaramillo, J.; Gomperts, R.; Stratmann, R. E.; Yazyev, O.; Austin, A. J.; Cammi, R.; Pomelli, C.; Ochterski, J. W.; Martin, R. L.; Morokuma, K.; Zakrzewski, V. G.; Voth, G. A.; Salvador, P.; Dannenberg, J. J.; Dapprich, S.; Daniels, A. D.; Farkas, O.; Foresman, J. B.; Ortiz, J. V.; Cioslowski, J.; Fox, D. J. *Gaussian 09, Revision B.01*; Gaussian, Inc., Wallingford, CT, 2009.

- (33) It is not uncommon to fail to locate transitions between two stationary points on a PES (for example, see ref. 34 and 35), but when the latter are minima it is clear that the TS in question is of higher energy than either of the two stationary points.
- (34) Clemente, F. R.; Houk, K. N. *Angew. Chem. Int. Ed.* **2004**, *43*, 5766.
- (35) Paton, R. S.; Steinhardt, S. E.; Vanderwal, C. D.; Houk, K. N. *J. Am. Chem. Soc.* **2011**, *133*, 3895.
- (36) Mauzerall, D.; Westheimer, F. W. *J. Am. Chem. Soc.* **1955**, *77*, 2261.
- (37) Bunting, J. W.; Sindhuatmadja, S. *J. Org. Chem.* **1981**, *46*, 4211.
- (38) Roberts, R. M. G.; Ostovic, D.; Kreevoy, M. M. *J. Org. Chem.* **1983**, *48*, 2053.

CHAPTER 4

MECHANISM STUDY OF HYDRIDE TRANSFER BETWEEN N-METHYL-9,10-DIHYDROACRIDINE AND TROPYLIUM ION IN ACETONITRILE

Abstract

A kinetic analysis of the hydride transfer reaction of *N*-methyl-9,10-dihydroacridine (MAH) with tropylium ion (Tr^+) in acetonitrile (AN) revealed that the reaction takes place in more than one step and involves a kinetically significant intermediate. Computations at the M06-2x/6-311++G(d,p) level are consistent with the experimental study and provide the structure of the reactant complex intermediate.

Introduction

The mechanism of the formal hydride transfer from the nicotinamide adenine dinucleotide coenzyme (NADH) and its analogues to the surrounding substrates has been a fascinating subject to chemists and biochemists and has attracted the attention of many researchers around the world.¹⁻⁵ The direct one-step hydride transfer mechanism has been reported for the oxidation of Hantzsch 4-aryl-1,4-dihydropyridines by tropylium ion (Tr^+) based on the kinetic and thermodynamic analysis.⁶ The detailed kinetics of the reduction of the tropylium cation by *N*-methyl-9,10-dihydroacridine (MAH) in 20% acetonitrile – 80% water were studied.⁷ But all of the kinetic analyses inside were based on the assumption that the reaction takes place by a direct one-step hydride transfer mechanism.

The present work is a part of our general effort to determine the mechanisms of fundamental organic reactions. In this chapter, we report the kinetic data consistent with a complex mechanism which involves the existence of a kinetically significant intermediate during the hydride transfer reactions between MAH/MAH- d_2 and Tr^+ in acetonitrile. In order to reduce the complexity of the reaction, pure acetonitrile was used instead of aqueous solution because tropylium ion exists in equilibrium with its hydroxide adduct in aqueous solution.

Results and Discussion

Detailed Pseudo-First-Order Kinetics Analysis. The detailed pseudo-first-order analysis⁸ of the reactions of *N*-methyl-9,10-dihydroacridine (MAH) and *N*-Methyl-9,10-dihydroacridine-9,9- d_2 (MAH- d_2) with Tr^+ in acetonitrile is illustrated by the data in Table 4-1 and Tables A-7 to A-11. In the Table 4-1, the values of the apparent pseudo-first-order rate constants (k_{app}) for MAH steadily decreased from 0.210 over the first 0.5 HL to 0.135 at 4.0 HL, approximately with a change of 36%. Under comparable conditions, except that MAH- d_2 instead of MAH, a similar pattern of k_{app} as a function of the degree of reaction encompassed in the analysis was observed (column 3), and the variations were almost the same (about a change of 38%), from 0.0383 to 0.0237 s^{-1} (at $[\text{substrate}] = 0.4 \text{ mM}$) over the same range of degree of reaction. While the changes in k_{app} observed are modest, the corresponding changes in the zero-time intercepts are much more remarkable, which indicates that this parameter is much more sensitive to the deviations from the first-order kinetics than k_{app} is. These values are also listed in the Table 4-1. Obviously, the response expected

for the simple one-step mechanism is a constant value of k_{app} with an intercept independent of the number of HL taken into the linear least-squares correlation.

TABLE 4-1. Changes in the Slopes and the Intercepts with the Extent of Reaction During Conventional Pseudo-First-Order Analysis for the Reactions of MAH/MAH- d_2 (0.4 mM) with Tr^+ (0.05 M) in Acetonitrile at 298K and 450 nm

Number of HL	MAH		MAH- d_2	
	k_{app}/s^{-1}	intercept/ s^{-1}	k_{app}/s^{-1}	intercept/ s^{-1}
0.5	0.210	0.00237	0.0383	-0.00196
1.0	0.199	0.0108	0.0371	0.00354
2.0	0.185	0.0366	0.0347	0.0263
3.0	0.168	0.0945	0.0312	0.0905
4.0	0.135	0.275	0.0237	0.322

Sequential Pseudo-First-Order Kinetics Analysis. The 24-point sequential pseudo-first-order kinetics analysis has been described in Chapters 2 and 3. The apparent rate constants for the reactions of MAH/MAH- d_2 with Tr^+ in acetonitrile obtained using the successive correlation method are summarized in Tables 4-2, 4-3 and A-12 to A-17. It is obvious that the k_{app} – time profiles begin at relatively high values of k_{app} and decay with time toward steady-state values at all of the wavelengths for H- substrate. At 450 nm, the value of k_{app} in segment 1 was observed to be equal to 0.237 and then to decrease steadily to 0.196 at segment 24 for the H- substrate. But for the D-substrate at all of the wavelengths, the k_{app} – time profiles show the initial values close to $0.046 s^{-1}$, decrease sharply to about $0.040 s^{-1}$ at about 0.5 s, and then rise more slowly to $0.041 s^{-1}$ at about 1 s and are approximately constant for the remainder of the reaction period analyzed. The expected result of the sequential 24-point procedure for the simple one-step mechanism is a rate constant, independent of time and of the particular time segment analyzed.

TABLE 4-2. Apparent Rate Constants for the Reaction of MAH with Tr^+ in Acetonitrile over the First Half-Life at 298K as a Function of Wavelengths^a

400 nm		410 nm		420 nm		430 nm		440 nm		450 nm		No.
$k_{\text{app}}/\text{s}^{-1}$	\pm^b	$k_{\text{app}}/\text{s}^{-1}$	\pm	$k_{\text{app}}/\text{s}^{-1}$	\pm	$k_{\text{app}}/\text{s}^{-1}$	\pm	$k_{\text{app}}/\text{s}^{-1}$	\pm	$k_{\text{app}}/\text{s}^{-1}$	\pm	
0.236	0.030	0.229	0.008	0.241	0.020	0.229	0.016	0.231	0.012	0.237	0.026	1
0.234	0.014	0.229	0.007	0.228	0.016	0.228	0.014	0.229	0.012	0.232	0.021	2
0.230	0.010	0.225	0.007	0.227	0.013	0.228	0.012	0.228	0.012	0.230	0.017	3
0.226	0.012	0.222	0.010	0.224	0.009	0.225	0.011	0.226	0.013	0.225	0.015	4
0.222	0.011	0.218	0.007	0.221	0.008	0.222	0.011	0.223	0.013	0.221	0.016	5
0.211	0.006	0.208	0.004	0.209	0.008	0.213	0.010	0.213	0.011	0.207	0.012	6
0.206	0.004	0.203	0.003	0.205	0.005	0.208	0.010	0.208	0.010	0.202	0.012	7
0.205	0.003	0.203	0.002	0.204	0.004	0.207	0.009	0.207	0.010	0.201	0.012	8
0.204	0.002	0.203	0.002	0.203	0.004	0.207	0.009	0.206	0.009	0.201	0.011	9
0.204	0.001	0.204	0.003	0.203	0.004	0.207	0.008	0.206	0.009	0.200	0.011	10
0.204	0.001	0.204	0.003	0.203	0.004	0.206	0.008	0.206	0.008	0.200	0.011	11
0.204	0.002	0.204	0.003	0.203	0.004	0.206	0.008	0.206	0.008	0.200	0.011	12
0.204	0.002	0.205	0.003	0.203	0.004	0.206	0.008	0.205	0.008	0.200	0.011	13
0.203	0.003	0.205	0.003	0.203	0.004	0.206	0.008	0.205	0.008	0.199	0.011	14
0.203	0.003	0.205	0.003	0.203	0.005	0.205	0.008	0.205	0.008	0.199	0.011	15
0.203	0.004	0.204	0.003	0.202	0.005	0.205	0.008	0.205	0.008	0.199	0.011	16
0.203	0.004	0.204	0.003	0.202	0.005	0.205	0.008	0.204	0.008	0.198	0.011	17
0.203	0.004	0.204	0.003	0.202	0.005	0.205	0.008	0.204	0.008	0.198	0.012	18
0.203	0.005	0.204	0.003	0.202	0.005	0.205	0.008	0.204	0.008	0.198	0.012	19
0.202	0.005	0.204	0.003	0.202	0.006	0.204	0.008	0.204	0.008	0.197	0.012	20
0.202	0.005	0.204	0.003	0.202	0.006	0.204	0.009	0.204	0.008	0.197	0.012	21
0.202	0.005	0.204	0.003	0.201	0.006	0.204	0.009	0.203	0.008	0.197	0.012	22
0.202	0.005	0.204	0.003	0.201	0.006	0.204	0.009	0.203	0.008	0.196	0.012	23
0.202	0.005	0.204	0.003	0.201	0.006	0.203	0.009	0.203	0.008	0.196	0.012	24

^a [MAH] = 0.4 mM, $[\text{Tr}^+] = 0.05 \text{ M}$, average of 3 sets of 20 stopped-flow repetitions. ^b \pm is the standard deviation of 3 sets of experiments.

The instantaneous rate constants – time profile (IRC) analysis method was recently developed⁸⁻¹⁰ to distinguish between simple one-step and complex multi-step reaction mechanisms. The k_{IRC} – time profile for product formation during the reaction of MAH (0.4 mM) with Tr^+ (0.05 M) in acetonitrile shown in Figure 4-1 rapidly decreases from about 0.25 s^{-1} at short times to a more slowly decreasing profile near 0.20 s^{-1} at 1 HL. The expected result for the simple one-step mechanism is a straight line with zero slopes while that for a complex

mechanism during product evolution is expected to increase from zero at short times when only product absorbs at the experimental wavelength. Even though the product evolution was monitored under these wavelengths for this reaction, we found that the k_{IRC} – time profiles (Figure 4-1 and Figures A-9 to A-13) decrease from zero time. The latter implies that intermediate absorbance is significant under the conditions of the experiment.

TABLE 4-3. Apparent Rate Constants for the Reaction of MAH- d_2 with Tr^+ in Acetonitrile over the First Half-Life at 298K as a Function of Wavelengths^a

400 nm		410 nm		420 nm		430 nm		440 nm		450 nm		No.
$k_{\text{app}}/\text{s}^{-1}$	\pm^b	$k_{\text{app}}/\text{s}^{-1}$	\pm	$k_{\text{app}}/\text{s}^{-1}$	\pm	$k_{\text{app}}/\text{s}^{-1}$	\pm	$k_{\text{app}}/\text{s}^{-1}$	\pm	$k_{\text{app}}/\text{s}^{-1}$	\pm	
0.046	0.006	0.045	0.004	0.046	0.003	0.045	0.003	0.047	0.011	0.048	0.007	1
0.042	0.002	0.042	0.002	0.042	0.002	0.042	0.001	0.042	0.002	0.043	0.003	2
0.040	0.002	0.041	0.001	0.040	0.002	0.041	0.001	0.040	0.002	0.040	0.002	3
0.039	0.001	0.040	0.001	0.040	0.001	0.041	0.001	0.040	0.002	0.039	0.002	4
0.039	0.001	0.040	0.001	0.040	0.001	0.041	0.001	0.040	0.001	0.039	0.002	5
0.041	0.001	0.042	0.001	0.041	0.001	0.041	0.001	0.041	0.001	0.040	0.001	6
0.042	0.001	0.042	0.001	0.042	0.001	0.042	0.001	0.042	0.001	0.041	0.001	7
0.042	0.001	0.042	0.001	0.042	0.001	0.042	0.001	0.042	0.001	0.041	0.001	8
0.042	0.001	0.042	0.001	0.042	0.001	0.042	0.001	0.042	0.001	0.041	0.001	9
0.042	0.001	0.042	0.001	0.042	0.001	0.042	0.001	0.041	0.001	0.041	0.001	10
0.042	0.001	0.042	0.001	0.042	0.001	0.041	0.001	0.041	0.001	0.041	0.001	11
0.042	0.001	0.042	0.001	0.041	0.001	0.041	0.001	0.041	0.001	0.041	0.001	12
0.042	0.001	0.042	0.001	0.041	0.001	0.041	0.001	0.041	0.001	0.040	0.001	13
0.042	0.001	0.042	0.001	0.041	0.001	0.041	0.001	0.041	0.001	0.040	0.001	14
0.042	0.001	0.042	0.001	0.041	0.001	0.041	0.001	0.041	0.001	0.040	0.001	15
0.042	0.001	0.042	0.001	0.041	0.001	0.041	0.001	0.041	0.001	0.040	0.001	16
0.042	0.001	0.042	0.001	0.041	0.001	0.041	0.001	0.041	0.001	0.040	0.001	17
0.042	0.001	0.042	0.001	0.041	0.001	0.041	0.001	0.041	0.001	0.040	0.001	18
0.041	0.001	0.042	0.001	0.041	0.001	0.041	0.001	0.041	0.001	0.040	0.001	19
0.041	0.001	0.042	0.001	0.041	0.001	0.041	0.001	0.041	0.001	0.040	0.001	20
0.041	0.001	0.042	0.001	0.041	0.001	0.041	0.001	0.041	0.001	0.040	0.001	21
0.041	0.001	0.042	0.001	0.041	0.001	0.041	0.001	0.041	0.001	0.040	0.001	22
0.041	0.001	0.042	0.001	0.041	0.001	0.041	0.001	0.041	0.001	0.040	0.001	23
0.041	0.001	0.042	0.001	0.041	0.001	0.041	0.001	0.041	0.001	0.040	0.001	24

^a [MAH- d_2] = 0.4 mM, [Tr⁺] = 0.05 M, average of 3 sets of 20 stopped-flow repetitions. ^b \pm is the standard deviation of 3 sets of experiments.

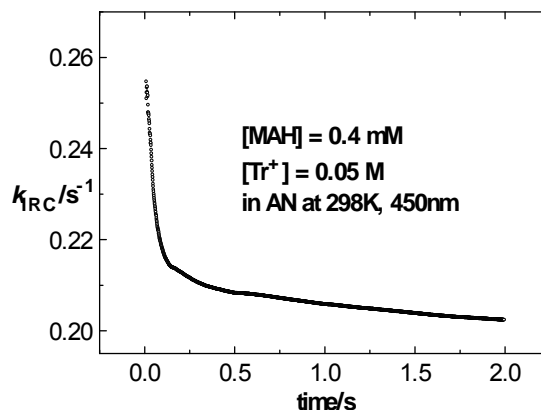


FIGURE 4-1. Apparent instantaneous rate constants (k_{IRC}) – time plot for the reaction between MAH and Tr^+ in acetonitrile at 298K and 450nm.

Numerical Mechanism Probes. In addition, we examined the time and rate constant ratios for the reaction of MAH with Tr^+ in acetonitrile. The time and rate constant ratios are equal to 13.5 and 1.00, respectively, for a pseudo-first-order reaction taking place in a one-step regardless of whether reactant or product is monitored.¹¹⁻¹² The data in Table 4-4 summarize the mechanism probe parameters observed for the hydride transfer reaction between MAH and Tr^+ in acetonitrile at 298 K along with the values of the steady-state rate constants $k_{s.s.}$ as a function of the wavelengths of the measurement. In all cases, $t_{0.50}/t_{0.05}$ are significantly greater than 13.5 and $k_{init}/k_{s.s.}$ are greater than unity, which are the expected features of a complex mechanism while monitoring reactant decay. The explanation for this data behavior for product evolution which is normal for reactant decay is that the intermediate absorbance is significant under these wavelengths, which is consistent with the 24-point sequential linear correlation analysis and the k_{IRC} – time profiles (Table 4-2 and Figure 4-1).

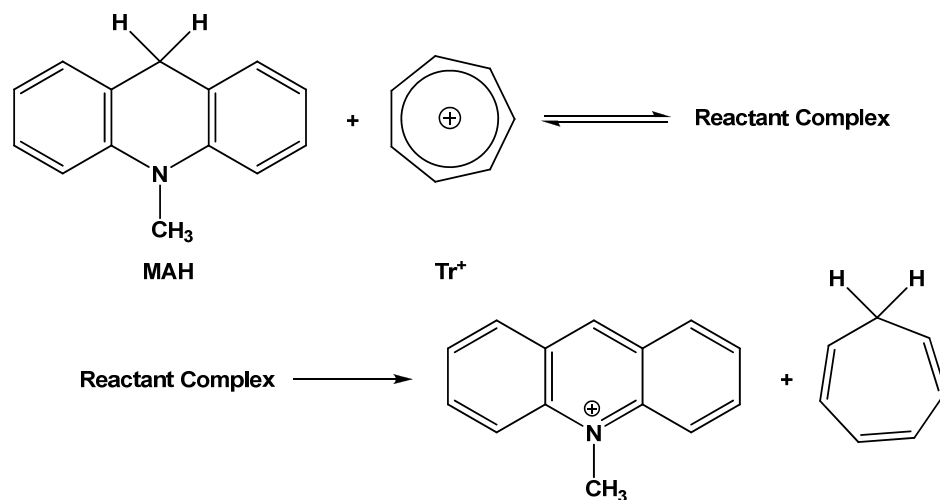
TABLE 4-4. Time and Rate Constant Ratios for the Hydride Transfer Reaction Between MAH and Tr^+ in Acetonitrile at 298K over a Range of Wavelengths^a

λ/nm	$t_{0.50}/t_{0.05}$	$k_{\text{init}}/k_{\text{s.s.}}$	$k_{\text{s.s.}}/\text{s}^{-1}$
400	14.8	1.20	0.202
410	13.8	1.10	0.204
420	15.0	1.23	0.201
430	14.4	1.13	0.203
440	14.4	1.16	0.203
450	14.3	1.12	0.196

^a $[\text{MAH}] = 0.4 \text{ mM}$, $[\text{Tr}^+] = 0.05 \text{ M}$.

All of the kinetic data shown in the previous paragraphs clearly rule out the simple one-step mechanism for the hydride transfer reaction between MAH and Tr^+ in acetonitrile. We were unable to find absorbance due to a charge-transfer complex in this case even though we attempted to use very high concentrations of both of reactants. Although we cannot rule out the participation of a CT complex, the mechanism for the hydride transfer reaction shown in Scheme 4-1 is consisted with the observed data. The first step is the formation of a kinetically significant reactant complex intermediate, which has significant absorbance at short times over the entire range of wavelengths experimentally available. The second step is the hydride transfer process to form the products. The proposed reversible consecutive mechanism for the hydride transfer fits all of the results of the pseudo-first-order rate constant analysis.

SCHEME 4-1. The Proposed Mechanism for the Reaction Between MAH and Tr⁺



The structures of the reactant complex and transition state were optimized in solution (acetonitrile) using SMD/M06-2x/6-311++G(d,p) method. The optimized structures shown in Figure 4-2 were confirmed by frequency calculations to be minima on the reaction coordinate using the same level of theory. The calculations were carried out using the Gaussian 09 program package.¹³ The calculated reaction coordinate diagram for the reaction of MAH with Tr⁺ in acetonitrile is shown in Figure 4-3 where CP1 represents the reactant complex. It is obvious that the entropy changes (ΔS 's) have a dominant effect on the kinetics of the reaction in solution, which is similar to the BNAH-MA⁺ system. Also we were unable to locate the transition state for the formation of the reactant complex. The calculated rate-determining transition state free energy is 21.1 kcal mol⁻¹, which deviates from the experimental overall activation Gibbs free energy (16.6 kcal mol⁻¹, rate constants at various temperatures are listed in Table A-18).

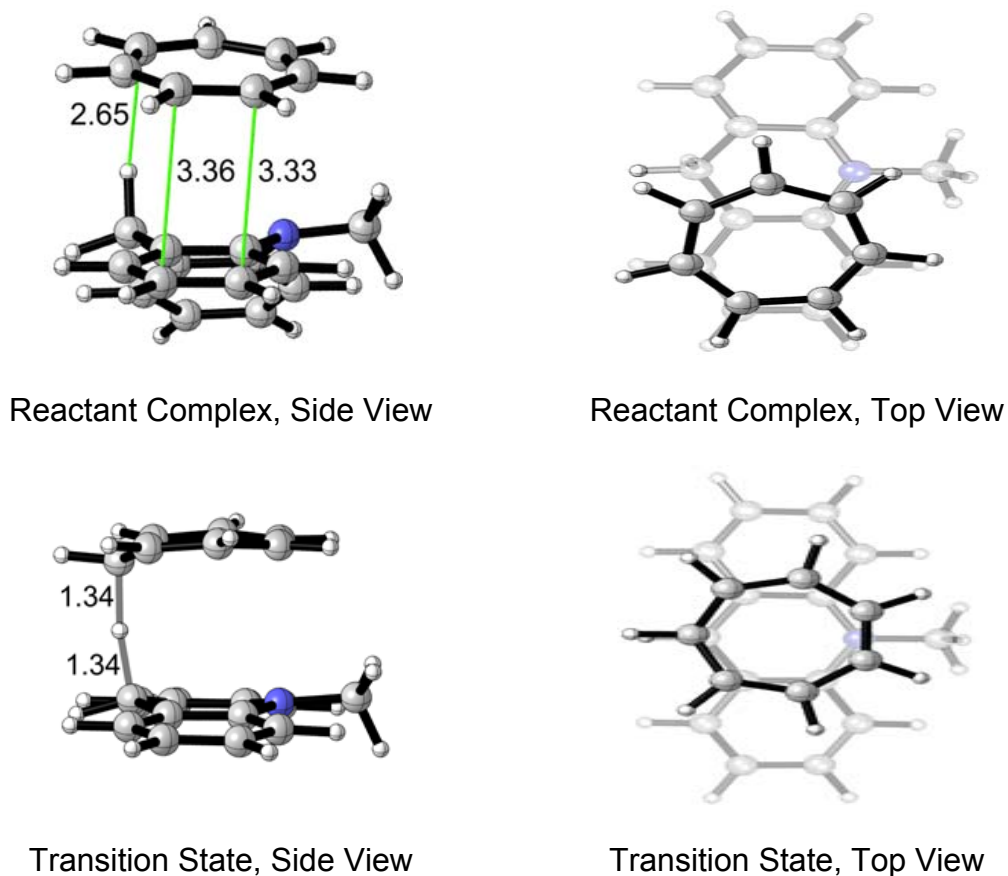


FIGURE 4-2. Optimized structures of reactant complex and transition state in acetonitrile with the M06-2x/6-311++(d,p)/SMD method.

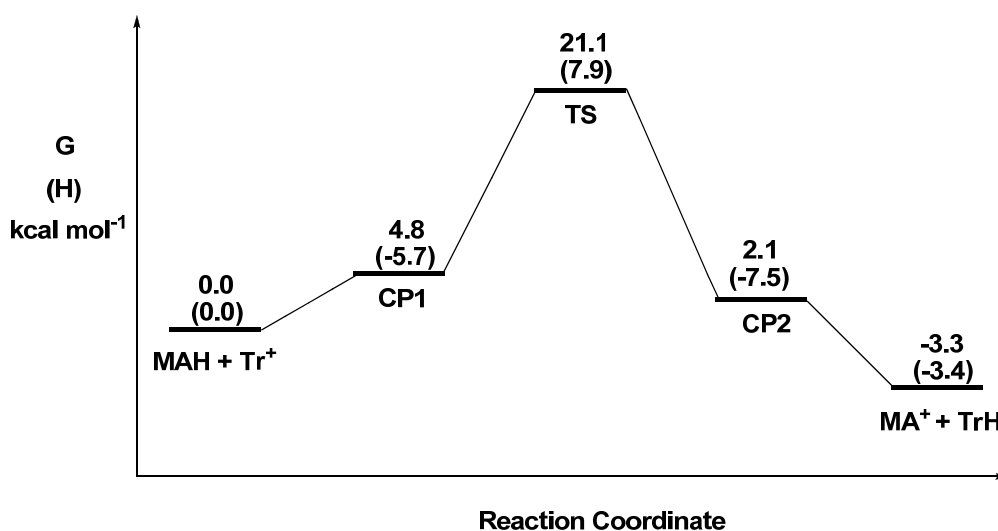


FIGURE 4-3. The reaction coordinate for the reaction of MAH and Tr⁺ in acetonitrile at 298.15K calculated using the M06-2x/6-311++G(d,p)/SMD functional.

Conclusions

Our primary conclusion is that the hydride transfer reaction between MAH and Tr^+ in acetonitrile takes place by a complex mechanism with a kinetically significant intermediate. This conclusion was arrived at from the experimental kinetic data which show that the values of k_{app} for the reactions of both MAH and MAH- d_2 are time dependent, with high values at short times and decreasing with time to steady-state values. Gaussian calculations at the M06-2x/6-311++G(d,p) level resulted in the observation of a reactant complex on the reaction coordinate leading to the transition state for hydride transfer.

Experimental Section

Materials. *N*-Methylacridinium iodide was prepared from acridine (Aldrich) and a 3-fold excess of methyl iodide in a minimum amount of acetone. *N*-Methyl-9,10-dihydroacridine was prepared by reduction of *N*-methylacridinium iodide using sodium borohydride in dry methanol, followed by recrystallization from absolute ethanol.¹⁴ *N*-Methyl-9,10-dihydroacridine 9,9- d_2 was prepared as described in the literature.¹⁵ Tropylium tetrafluoroborate was obtained from Aldrich and recrystallized from ethanol. Acetonitrile was refluxed and distilled over P_2O_5 under a nitrogen atmosphere and past through an Al_2O_3 column before transferring into the glove box.

Kinetic Experiments. Kinetic experiments were carried out using a Hi-Tech SF-61 DX2 stopped-flow spectrophotometer installed in a glove box and kept under a nitrogen atmosphere. The temperature was controlled at 298 K using a constant temperature flow system connected directly to the reaction cell

through a bath situated outside of the glove box. All stopped-flow experiments included the recording of at least 20 absorbance – time profiles over the wavelengths range from 400 nm to 450 nm at 10 nm intervals. Each experiment was repeated at least three times. The 2000-point absorbance – time curve data were collected over either 1+ or 4+ HL.

References

- (1) Fukuzumi, S.; Suenbu, T.; Parz, M.; Hirasaka, T.; Itoh, S.; Fujitsuka, M.; Ito, O. *J. Am. Chem. Soc.* **1998**, *120*, 8060.
- (2) Anne, A.; Moiroux, J.; Saveant, J.-M. *J. Am. Chem. Soc.* **1993**, *115*, 10224.
- (3) Carlson, B. W.; Miller, L. L. *J. Am. Chem. Soc.* **1980**, *102*, 6533.
- (4) Zhu, X.-Q.; Liu, Y.-C. *J. Org. Chem.* **1998**, *63*, 2786.
- (5) Zhu, X.-Q.; Liu, Y.; Zhao, B.-J.; Cheng, J.-P. *J. Org. Chem.* **2001**, *66*, 370.
- (6) Zhao, B.-J.; Zhu, X.-Q.; Lu, Y.; Xia, C.-Z.; Cheng, J.-P. *Tetrahedron Lett.* **2000**, *41*, 257.
- (7) Bunting, J. W.; Conn, M. M. *Can. J. Chem.* **1990**, *68*, 537.
- (8) Parker, V. D.; Hao, W.; Li, Z.; Scow, R. *Int. J. Chem. Kinet.* **2012**, *44*, 2.
- (9) Hao, W.; Parker, V. D. *J. Org. Chem.* **2008**, *73*, 48.
- (10) Parker, V. D. *J. Phys. Org. Chem.* **2006**, *19*, 714.
- (11) Parker, V. D.; Zhao, Y. *J. Phys. Org. Chem.* **2001**, *14*, 604.
- (12) Parker, V. D. *Pure Appl. Chem.* **2005**, *77*, 1823.
- (13) Frisch, M. J.; Trucks, G. W.; Schlegel, H. B.; Scuseria, G. E.; Robb, M.

A.; Cheeseman, J. R.; Scalmani, G.; Barone, V.; Mennucci, B.; Petersson, G. A.; Nakatsuji, H.; Caricato, M.; Li, X.; Hratchian, H. P.; Izmaylov, A. F.; Bloino, J.; Zheng, G.; Sonnenberg, J. L.; Hada, M.; Ehara, M.; Toyota, K.; Fukuda, R.; Hasegawa, J.; Ishida, M.; Nakajima, T.; Honda, Y.; Kitao, O.; Nakai, H.; Vreven, T.; Montgomery, J. A., Jr.; Peralta, J. E.; Ogliaro, F.; Bearpark, M.; Heyd, J. J.; Brothers, E.; Kudin, K. N.; Staroverov, V. N.; Kobayashi, R.; Normand, J.; Raghavachari, K.; Rendell, A.; Burant, J. C.; Iyengar, S. S.; Tomasi, J.; Cossi, M.; Rega, N.; Millam, J. M.; Klene, M.; Knox, J. E.; Cross, J. B.; Bakken, V.; Adamo, C.; Jaramillo, J.; Gomperts, R.; Stratmann, R. E.; Yazyev, O.; Austin, A. J.; Cammi, R.; Pomelli, C.; Ochterski, J. W.; Martin, R. L.; Morokuma, K.; Zakrzewski, V. G.; Voth, G. A.; Salvador, P.; Dannenberg, J. J.; Dapprich, S.; Daniels, A. D.; Farkas O.; Foresman, J. B.; Ortiz, J. V.; Cioslowski, J.; Fox, D. J. *Gaussian 09, Revision B.01*; Gaussian, Inc., Wallingford, CT, 2009.

- (14) Colter, A. K.; Charles, G. L.; Williamson, T. W.; Berry, R. E. *Can. J. Chem.* **1983**, *61*, 2544.
- (15) Karrer, P.; Szabo, L.; Krishan, H. J. V.; Schwyzer, R. *Helv. Chem. Acta.* **1950**, *33*, 294.

CHAPTER 5

OXYGEN INITIATED CHAIN MECHANISM FOR HYDRIDE TRANSFER
BETWEEN NADH AND NAD⁺ MODELS. THE REACTION OF 1-BENZYL-3-
CYANOQUINOLINIUM ION WITH N-METHYL-9,10-DIHYDROACRIDINE IN
ACETONITRILE

Abstract

A reinvestigation of the formal hydride transfer reaction of 1-benzyl-3-cyanoquinolinium ion (BQCN⁺) with *N*-methyl-9,10-dihydroacridine (MAH) in acetonitrile (AN) confirmed that the reaction takes place in more than one step and revealed a new mechanism that had not previously been considered. These facts are unequivocally established on the basis of conventional pseudo-first-order kinetics. It was observed that even residual oxygen under glove box conditions initiates a chain process leading to the same products and under some conditions is accompanied by a large increase in the apparent rate constant for product formation with time. The efficiency of the latter process, when reactions are carried out in AN with rigorous attempts to remove air, is low but appears to be much more pronounced when MAH is the reactant in large excess. On the other hand, the intentional presence of air in AN ([Air] = half-saturated) leads to a much greater proportion of the chain pathway which is still favored by high concentrations of MAH. The latter observation suggests that a reaction intermediate reacts with oxygen to initiate the chain process in which MAH participates. Kinetic studies at short times show that there is no kinetic isotope effect on the initial step in the reaction, which is the same for the two

competing processes. Our observation of the chain pathway of a NADH model compound under aerobic conditions is likely to be of importance in similar biological processes where air is always present.

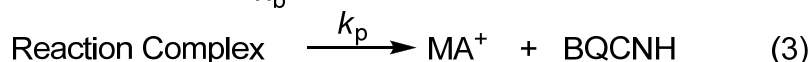
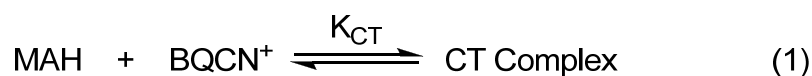
Introduction

The MAH-BQCN⁺ reaction in acetonitrile (AN) is of particular importance since it has been studied extensively and is considered to be a genuine example of a direct one-step hydride transfer reaction, mainly due to the work of Kreevoy and coworkers.¹⁻⁶ The outer sphere electron transfer (ET) mechanism can be considered to be unlikely due to the large standard potential difference (>1.2 V in AN) between that for the reduction of BQCN⁺ and the oxidation MAH.⁷ A review⁸ as well as a number of recent studies⁹⁻¹¹ of the mechanisms for the reactions of various cations with NADH model compounds illustrate that interest in these systems remains high.

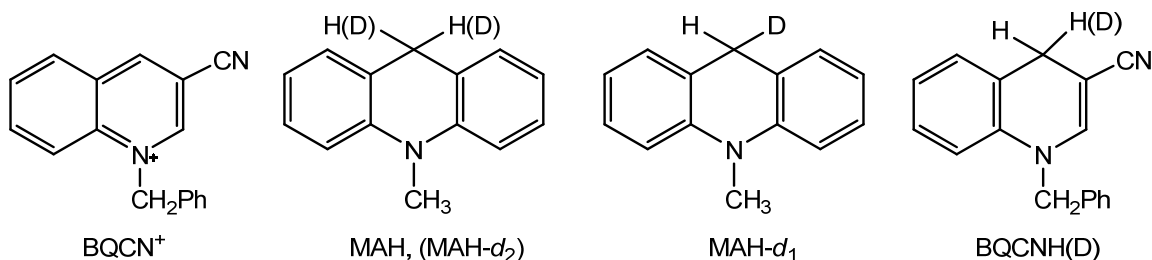
Earlier, we proposed a 3-step pre-association mechanism (Scheme 5-1) for the hydride transfer reaction between *N*-methyl-9,10-dihydroacridine (MAH) with 1-benzyl-3-cyanoquinolinium ion (BQCN⁺) in AN.¹² Recently, Perrin and Zhao¹³ presented a rejection of our mechanism (Scheme 5-1) and suggested that conclusions arrived at in other related papers¹⁴⁻²⁶ may be in error as well. Two main arguments were used in the rejection of our mechanism. The first argument was that the rate constants that we proposed for our mechanism require a slow dissociation of a weakly bound reaction complex (Scheme 5-1). The second argument was based upon intra-molecular deuterium kinetic isotope effects (IMKIE) for MAH-*d*₁. The following statement was made in reference to the

reactions of MAH- d_1 : “Regardless of mechanism, this kinetic isotope effect arises solely from the hydride transfer step. Even if the first step is partially rate-limiting, the second step is product determining. Therefore, even if eqn (2) (of ref. 13) is the mechanism, the KIE measured is k_p^H/k_p^D , without the necessity of extracting rate constants from two-step kinetics.”

SCHEME 5-1. Proposed 3-Step Mechanism for the Reaction of MAH with BQCN⁺ in AN. This Mechanism Was Proposed in 2003¹²



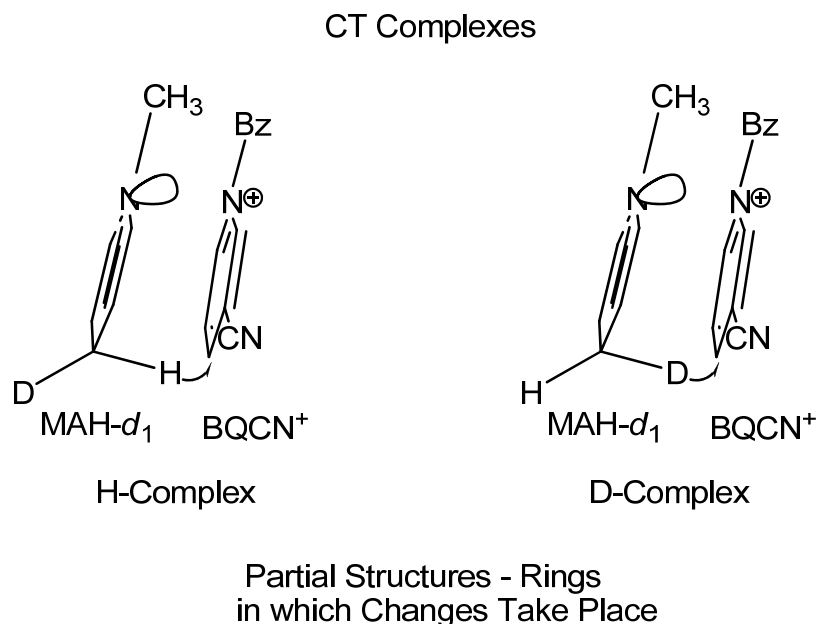
Mechanism 1



There is a fatal flaw in this argument. Charge transfer complexes of NADH model compounds with organic cations have sandwich type structures, with bonding between the π -orbitals of the two moieties.²⁷ Thus for mono-deuterium substrate (MAH- d_1) and BQCN⁺ there are two distinct charge transfer complexes:

the H-complex and the D-complex, illustrated in Scheme 5-2. These are expected to form initially in essentially equal concentrations.

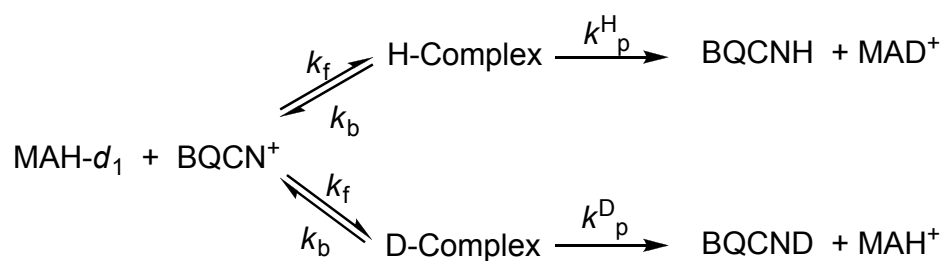
SCHEME 5-2. Partial Structures of the CT Complex Between MAH- d_1 and BQCN $^+$ in AN. The Positions of the Atoms Are in a Conformation where Hydride Transfer Is Possible. Since Solvent Isn't Included in This Representation the Structures More Accurately Represent What We Call the "Reactant Complex" Which Is Derived from Solvent Extrusion from the CT Complex in Our Mechanisms



The complexes differ according to which face of MAH- d_1 the cation (BQCN $^+$) is bound to. We proposed that considerable reorientation of the reactants in the CT complexes must take place along with loss of solvent to give "Reactant Complexes" with reaction centers poised for reaction (These complexes were called Reaction Complexes in ref. 12). The "Reactant Complexes," formed in reaction (2) in Scheme 5-1, are represented with the BQCN $^+$ moiety on either the same face as the 9-H of the nearly planar MAH- d_1 (H-Complex) or on the same face of the plane as the 9-D (D-complex).

The proposed mechanism of the reaction between MAH- d_1 with BQCN⁺ taking into account the H- and D-Complexes is shown in Scheme 5-3 in which the intermediate CT complexes are not shown for the sake of simplicity.

SCHEME 5-3. The Complex Mechanism for the Reaction of MAH- d_1 with BQCN⁺. The Formation of H- and D- Complexes Includes Formation of the Corresponding CT and “Reactant Complexes”



Mechanism 2

A closer examination of the expected result of the IMKIE¹³ experiment reveals that once steady state is achieved the reaction gives rise to the apparent kinetic isotope effect (KIE_{app}) rather than the real kinetic isotope effect (KIE_{real}). During the *pre-steady-state* period KIE_{app} is time dependent. The latter was verified by simulation of Mechanism 2 but the result is also obvious since the more rapid irreversible hydride transfer step will draw a disproportionate amount of substrate through the upper branch of the mechanism shown in Scheme 5-3.

In short, although Perrin's analysis¹³ appears to cast serious doubt on the details of our mechanism¹² his experimental data do not answer the question as to whether the reaction takes place by a complex or one-step mechanism. In our paper we clearly show that we were unable to detect any deviation from one-step kinetics at temperature below 308 K; the IMKIE¹³ were determined at only two

temperatures, 273 and 299 K, another serious flaw. We are confident that the claim¹³ that all our experimental data are erroneous is completely without foundation.

The present work is a part of our general effort to determine the mechanisms of fundamental organic reactions. Since the suggestion¹³ that all of our work^{12,14-26} in this general area is erroneous, we have adopted methodology for mechanism analysis based solely upon whether or not the experimental data are consistent with the pseudo-first-order relationship, *i.e.* the linearity of $\ln(1 - E.R.)$ – time arrays. Application of this methodology has resulted in conclusive evidence that neither the formation of the 1,1-dimethoxy Meisenheimer complex derived from the reaction of 2,4,6-trinitroanisole with methoxide ion²⁸ nor the proton transfer reactions of simple nitroalkanes with hydroxide ion in water²⁹ takes place by the mechanisms previously believed to be well-established.

In this chapter, we show that the reaction of MAH with $BQCN^+$ in AN is further complicated by a multi-step competing chain process under most circumstances. The chain process must be initiated by the reaction of oxygen with an intermediate, presumably the H- or D-Complex, since the reaction of O_2 with MAH is very slow, but is efficient even in the presence of residual oxygen under glove box conditions as long as $BQCN^+$ is present in the AN solution. We also attempt to clarify the mechanism at short times where the interference from the chain process is minimized.

Results

The spectra illustrated in Figure 5-1 were obtained during the reaction of

BQCN⁺ (0.04 M) with MAH (0.01 M) in AN at 298 K. The absorbance due to the product MA⁺ was indicated by the upward arrow in Fig. 5-1a. The peak with maximum absorbance at 525 nm, observed immediately after mixing, was observed to decay with time and disappear as the reaction approached completion shown in Fig. 5-1b. The species giving rise to the broad absorbance band at 525 nm is a charge-transfer complex. Similar spectra have been reported for MAH and related donors with a number of quinones as acceptor molecules.³⁰

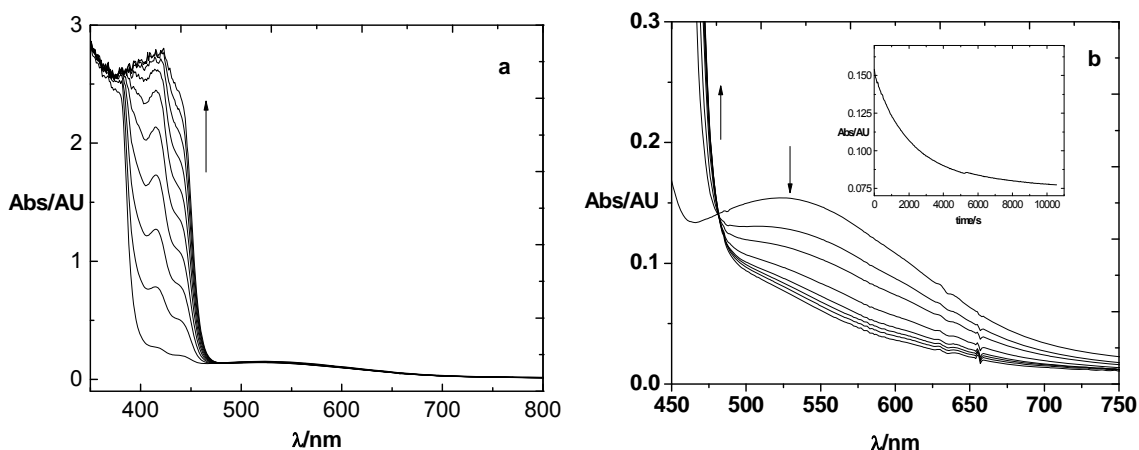


FIGURE 5-1. UV/Vis absorption spectra for the reaction of BQCN⁺ (0.04 M) with MAH (0.01 M) in AN at 298 K. (a) Time between spectra equals 30 s. (b) Time between spectra equals 25 min. Insert: Absorbance – time decay curve recorded at 525 nm under the same conditions.

The answer to the question of whether or not the reaction of BQCN⁺ with MAH in AN follows a one-step mechanism can readily be obtained using a modified conventional $\ln(1 - \text{E.R.})$ – time profiles, where E.R. is the extent of reaction. All of kinetic work here is based upon the conversion of absorbance – time profiles to $\ln(1 - \text{E.R.})$ – time profiles for the evolution of MA⁺.

Thus, whether or not the reactions conform to simple mechanism kinetics

will be assessed by the fit of the least-squares correlation lines to the experimental data. In addition to the visual inspection of pseudo-first-order plots, the latter is readily accomplished by the quantitative comparison of slopes and intercepts as a function of the interval in the data analyzed with the expected result for a one-step mechanism.

In addition, a second procedure we adopted is to divide the data arrays into up to 24 data segments on which the analysis is carried out. These segments involve points 1-11, 1-21, 1-31, 1-41, 1-51, 1-101, 1-201, . . . , 1-1801, and 1-1901. The successive series of rate constants (k_{app}) obtained can then be plotted vs. the times at the midpoints of each segment. The times in this analysis are t_6 , t_{11} , t_{16} , t_{21} , t_{26} , t_{51} , t_{101} , . . . , t_{901} , and t_{951} where the subscript is the point number. This procedure gives a clear indication of any changes in the values of the apparent pseudo-first-order rate constant (k_{app}) as the reaction proceeds and also provides standard deviations (S.D.) in data from multiple absorbance – time profiles. These methods are illustrated in the following sections.

Pseudo-First-Order Analysis of the Reactions of MAH and BQCN⁺ in which Either Reactant Acts as the Limiting or the Excess Reagent. The pseudo-first-order analyses of the reactions in which either BQCN⁺ or MAH is the limiting reactant are shown in Figure A-14. The comparison of the effect of which reactant is the limiting reagent is illustrated by the pseudo-first-order plots in which figures on the left (Fig. A-14a, A-14b and A-14c) are for the reaction in which [BQCN⁺] is limiting and those on the right (Fig. A-14a', A-14b', and A-14c')

are when [MAH] is limiting. The reactions were followed by monitoring evolution of product at 430 nm.

The most obvious result of a visual comparison of the pseudo-first-order plots on the left and the right of Fig. A-14 is that deviations from the experimental data from the least-squares correlation lines are significantly greater when the reaction rate is limited by $[BQCN^+]$ than when [MAH] is the limiting reactant. A close examination of the plots reveals that there are deviations in all cases but that in the case of the plots constructed for data over less than one half-life, the deviations appear to be so small that it might be considered to be "justifiable" to attribute them to experimental error.

The effect of the presence oxygen from air dissolved (half-saturated) in AN on the kinetic plots is illustrated in Figure 5-2 for the reactions of $BQCN^+$ (0.5 mM) with MAH (40 mM) and $BQCN^+$ (40 mM) with MAH (0.5 mM) over either 0.5 half-lives (HL) (Fig. 5-2a and 5-2c) or 4 HL (Fig. 5-2b and 5-2d). AN half-saturated with air was used for a practical reason, *i.e.* the $BQCN^+$ solution saturate with air was mixed with the MAH solution which was protected from air in order to insure that no reaction with oxygen takes place before mixing. The deviations of the correlation line from experimental data are obvious very early in the reaction in Fig. 5-2a and is extreme when the correlation was carried out over 4 HL (Fig. 5-2b) when [MAH] is in large excess. When $BQCN^+$ is the reactant in excess, deviation from the correlation is barely visible during the first HL (Fig. 5-2c) and not nearly so severe at 4 HL (Fig. 5-2d) as was observed in the previous case.

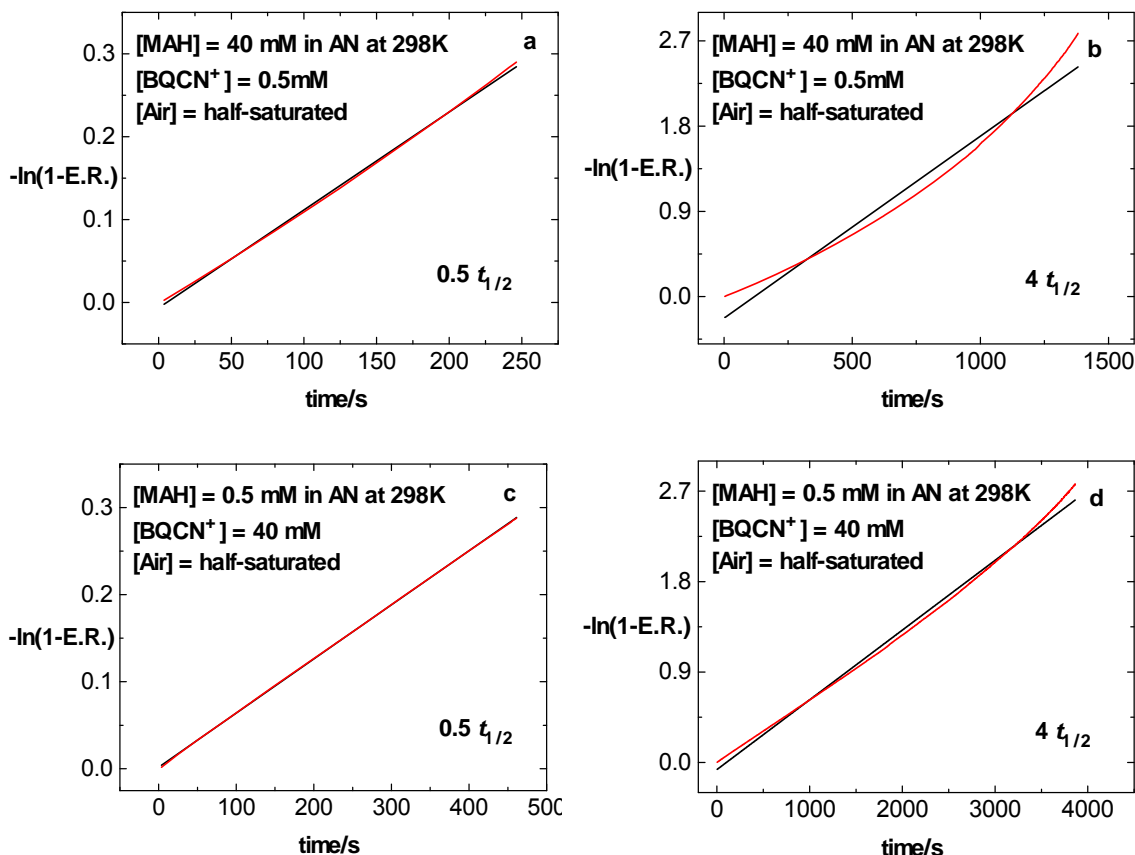


FIGURE 5-2. Pseudo-first-order plots for the reactions of BQCN⁺ (0.50 mM) with MAH (40 mM) (a and b) and BQCN⁺ (40 mM) with MAH (0.5 mM) (c and d) in AN half-saturated with air at 298 K and 430 nm.

The data in Table 5-1 allow for a closer examination of deviations from pseudo-first-order behavior of the reactions of BQCN⁺ with MAH in AN at 298 K and 430 nm. The data in column 2 shows the change in k_{app} for the reaction of excess MAH (40 mM) with BQCN⁺ (0.5 mM) in AN under an attempt to exclude air. The k_{app} measured over the first 0.5 HL was observed to be equal to 0.000827 s⁻¹ and to vary uniformly to 0.000981 s⁻¹ as the data segment was increased to 4.0 HL. Under comparable conditions, except that the reaction solution was half-saturated with air, a similar pattern of k_{app} as a function of the degree of reaction encompassed in the analysis was observed but in this case

(column 3), the variations were greater, 0.00118 to 0.00192 s⁻¹ over the same range of degree of reaction. A very similar trend was observed for the case (column 4) when BQCN⁺ was the excess reagent (40 mM) reacting with MAH (0.5 mM), in AN under conditions where rigorous attempts were made to exclude air. In this case, k_{app} varied between 0.000664 and 0.000716 s⁻¹ in the same range of the other analyses. The values of k_{app} in last column changed from 0.000622 s⁻¹ at 0.5 HL to 0.000694 s⁻¹ at 4.0 HL when the reaction solution was half-saturated with air and BQCN⁺ was the excess reagent (40 mM). The values of the intercepts of the least-squares correlations are even more sensitive to deviations from the pseudo-first-order relationship. These values are also listed in the Table 5-1 and the above concentration effects are explained in the discussion section.

TABLE 5-1. Changes in the Apparent Pseudo-First-Order Rate Constants (k_{app}) as a Function of the Degree of Reaction Analyzed for the Reactions of MAH with BQCN⁺ in AN at 298 K under Various Conditions and 430 nm

Number HL analyzed	[BQCN ⁺] ^a		[BQCN ⁺]/air ^b		[MAH] ^c		[MAH]/air ^d	
	k_{app}/s^{-1}	intercept	k_{app}/s^{-1}	intercept	k_{app}/s^{-1}	intercept	k_{app}/s^{-1}	intercept
0.5	0.000827	-0.00230	0.00118	-0.00658	0.000664	-0.000284	0.000622	0.00182
1.0	0.000858	-0.00817	0.00132	-0.0244	0.000664	-0.000496	0.000619	0.00226
2.0	0.000904	-0.0262	0.00153	-0.0737	0.000673	-0.00564	0.000632	-0.00529
3.0	0.000945	-0.0520	0.00173	-0.144	0.000691	-0.0206	0.000659	-0.0299
4.0	0.000981	-0.0825	0.00192	-0.227	0.000716	-0.0495	0.000694	-0.0714

^a [BQCN⁺] = 0.5 mM, [MAH] = 40 mM in AN containing only residual oxygen. ^b [BQCN⁺] = 0.5 mM, [MAH] = 40 mM in AN half-saturated with air. ^c [BQCN⁺] = 40 mM, [MAH] = 0.5 mM in AN containing only residual oxygen. ^d [BQCN⁺] = 40 mM, [MAH] = 0.5 mM in AN half-saturated with air.

The Successive Correlation Analysis of the Reactions of BQCN⁺ with MAH/MAH-*d*₂ in AN at 298 K. The application of the successive correlation method (24-point procedure) to data obtained under the four different sets of reactant concentrations used for the data in Table 5-1 is illustrated in Tables 5-2 to 5-5 for data gathered over 1 HL while monitoring product formation in the range from 430 to 450 nm. The data in Table 5-2 for the reaction of BQCN⁺ (0.5 mM) with MAH (40 mM) at 298K in the presence of residual oxygen show very little variation in k_{app} during the early stages of the reaction but continuously increase as the first HL is approached. The other new information available from the data in Table 5-2 is the magnitude of S.D. of data from repetitive stopped-flow shots. In this case the S.D. is of the order of 3 to 5 % of the k_{app} values. On the other hand, in AN half-saturated with air the successive k_{app} in Table 5-3 for the reaction of BQCN⁺ (0.5 mM) with MAH (40 mM) at 298 K vary considerably, from 0.000823 in segment 1 to 0.00134 s⁻¹ in segment 24. The increase in k_{app} with segment number can be attributed to a chain reaction initiated by oxygen in which oxygen intercepts an intermediate in the reaction resulting in the increase in the rate of product formation.

In the presence of residual air k_{app} obtained from the reactions of MAH/MAH-*d*₂ (0.5 mM) with BQCN⁺ (40 mM) in AN were observed (Table 5-4) to be nearly independent of segment number. Earlier¹² using lower [MAH/MAH-*d*₂] we found no deviations in reactions of MAH or MAH-*d*₂ over the first HL at temperatures lower than 308K. The latter observation is confirmed by the data in Table 5-4. The values of k_{app} in Table 5-5 are for the reaction of MAH (0.5 mM)

with BQCN⁺ (40 mM) in AN half-saturated with air. It should be noted that the S.D. at the top of the columns 2, 4 and 6 in Table 5-2 to 5-4 are significant and decrease progressively to very small values. The reason for this trend is that S.D. decrease directly in proportion to the increase in the number of points taken into the correlation.

TABLE 5-2. Changes in k_{app} and Standard Deviations (S.D.) as a Function of the Degree of Reaction Analyzed for the Reactions of MAH/MAH- d_2 (40 mM) with BQCN⁺ (0.5 mM) in AN at 298K in the Presence of Residual Oxygen and 430 nm

time	MAH-Data Set 1		MAH-Data Set 2		MAH- d_2		KIE _{app} (1)	KIE _{app} (2)	No.
	10^4 k_{app}/s^{-1}	10^4 S.D. (10 shots)	10^4 k_{app}/s^{-1}	10^4 S.D. (10 shots)	10^4 k_{app}/s^{-1}	10^4 S.D. (10 shots)			
2.47	7.10	0.18	8.42	0.34	2.14	0.41	3.32	3.93	1
4.72	6.95	0.23	8.77	0.26	1.80	0.28	3.86	4.87	2
6.97	6.87	0.10	8.80	0.11	1.68	0.28	4.09	5.24	3
9.22	6.83	0.07	8.87	0.10	1.59	0.23	4.30	5.58	4
11.47	6.88	0.08	8.85	0.08	1.54	0.13	4.47	5.75	5
22.72	6.88	0.07	8.80	0.05	1.35	0.12	5.10	6.52	6
45.22	6.86	0.07	8.84	0.03	1.32	0.04	5.20	6.70	7
67.72	6.87	0.07	8.93	0.03	1.30	0.01	5.28	6.87	8
90.22	6.87	0.08	9.00	0.03	1.29	0.01	5.33	6.98	9
112.7	6.88	0.09	9.07	0.04	1.28	0.01	5.38	7.09	10
135.2	6.89	0.11	9.12	0.04	1.28	0.01	5.38	7.13	11
157.7	6.89	0.13	9.18	0.04	1.28	0.01	5.38	7.17	12
180.2	6.91	0.14	9.24	0.04	1.28	0.01	5.40	7.22	13
202.7	6.93	0.16	9.29	0.04	1.28	0.01	5.41	7.26	14
225.2	6.96	0.17	9.34	0.04	1.28	0.01	5.44	7.30	15
247.7	7.02	0.18	9.39	0.04	1.28	0.01	5.48	7.34	16
270.2	7.09	0.18	9.44	0.05	1.28	0.01	5.54	7.38	17
292.7	7.16	0.18	9.50	0.05	1.28	0.01	5.59	7.42	18
315.2	7.24	0.18	9.56	0.05	1.28	0.01	5.66	7.47	19
337.7	7.33	0.18	9.63	0.05	1.28	0.01	5.73	7.52	20
360.2	7.42	0.17	9.69	0.06	1.28	0.01	5.80	7.57	21
382.7	7.52	0.17	9.75	0.06	1.28	0.01	5.88	7.62	22
405.2	7.62	0.17	9.82	0.07	1.28	0.01	5.95	7.67	23
427.7	7.72	0.16	9.89	0.08	1.28	0.01	6.03	7.73	24

TABLE 5-3. Changes in k_{app} and Standard Deviations (S.D.) as a Function of the Degree of Reaction Analyzed for the Reactions of MAH/MAH- d_2 (40 mM) with BQCN⁺ (0.5 mM) in AN at 298K Half-Saturated with Air and 430 nm

MAH-Data Set 1		MAH-Data Set 2		MAH- d_2		KIE _{app} (1)	KIE _{app} (2)	No.
10^4 k_{app}/s^{-1}	10^4 S.D. (10 shots)	10^4 k_{app}/s^{-1}	10^4 S.D. (10 shots)	10^4 k_{app}/s^{-1}	10^4 S.D. (10 shots)			
8.23	0.28	13.6	0.37	2.71	0.23	3.04	5.02	1
8.59	0.08	13.9	0.12	2.59	0.09	3.32	5.37	2
8.59	0.11	13.9	0.14	2.57	0.06	3.34	5.41	3
8.53	0.13	14.1	0.09	2.60	0.04	3.28	5.42	4
8.48	0.11	14.1	0.09	2.63	0.04	3.22	5.36	5
8.35	0.08	14.3	0.08	2.70	0.04	3.09	5.30	6
8.27	0.07	14.7	0.10	2.72	0.05	3.04	5.40	7
8.25	0.05	15.2	0.09	2.70	0.04	3.06	5.63	8
8.25	0.04	15.6	0.10	2.69	0.05	3.07	5.80	9
8.31	0.01	16.0	0.09	2.68	0.05	3.10	5.97	10
8.49	0.03	16.4	0.09	2.67	0.04	3.18	6.14	11
8.75	0.06	16.7	0.09	2.65	0.04	3.30	6.30	12
9.06	0.08	17.1	0.09	2.64	0.04	3.43	6.48	13
9.39	0.09	17.5	0.09	2.62	0.04	3.58	6.68	14
9.74	0.11	17.9	0.08	2.61	0.04	3.73	6.86	15
10.1	0.13	18.3	0.09	2.61	0.03	3.87	7.01	16
10.5	0.14	18.7	0.08	2.60	0.03	4.04	7.19	17
10.9	0.16	19.2	0.09	2.59	0.03	4.21	7.41	18
11.3	0.18	19.6	0.10	2.59	0.03	4.36	7.57	19
11.7	0.20	20.2	0.10	2.59	0.03	4.52	7.80	20
12.1	0.22	20.7	0.11	2.59	0.03	4.67	7.99	21
12.5	0.24	21.3	0.11	2.60	0.03	4.81	8.19	22
12.9	0.26	22.0	0.12	2.60	0.03	4.96	8.46	23
13.4	0.27	22.8	0.13	2.61	0.03	5.13	8.74	24

TABLE 5-4. Changes in k_{app} and Standard Deviations (S.D.) as a Function of the Degree of Reaction Analyzed for the Reactions of MAH/MAH- d_2 (0.5 mM) with BQCN⁺ (40 mM) in AN at 298K in the Presence of Residual Oxygen and 450 nm

MAH-Data Set 1		MAH-Data Set 2		MAH- d_2		KIE_{app} (1)	KIE_{app} (2)	No.
10^4 k_{app}/s^{-1} (10 shots)	10^4 S.D.	10^4 k_{app}/s^{-1} (10 shots)	10^4 S.D.	10^4 k_{app}/s^{-1} (10 shots)	10^4 S.D.			
5.95	0.54	6.25	0.36	1.15	0.34	5.17	5.43	1
6.06	0.47	6.36	0.23	1.23	0.13	4.93	5.17	2
6.01	0.38	6.34	0.15	1.10	0.08	5.46	5.76	3
5.99	0.31	6.32	0.12	1.06	0.08	5.65	5.96	4
5.98	0.24	6.31	0.08	1.07	0.09	5.59	5.90	5
5.99	0.12	6.32	0.04	1.12	0.05	5.35	5.64	6
6.03	0.07	6.33	0.04	1.14	0.02	5.29	5.55	7
6.06	0.05	6.31	0.03	1.13	0.02	5.36	5.58	8
6.07	0.04	6.29	0.03	1.14	0.02	5.32	5.52	9
6.07	0.03	6.28	0.02	1.14	0.02	5.32	5.51	10
6.07	0.02	6.27	0.02	1.13	0.02	5.37	5.55	11
6.06	0.02	6.26	0.02	1.13	0.02	5.36	5.54	12
6.05	0.02	6.25	0.02	1.13	0.02	5.35	5.53	13
6.05	0.02	6.25	0.02	1.13	0.02	5.35	5.53	14
6.04	0.03	6.24	0.02	1.13	0.02	5.35	5.52	15
6.04	0.03	6.23	0.02	1.13	0.02	5.35	5.51	16
6.03	0.04	6.21	0.02	1.13	0.02	5.34	5.50	17
6.03	0.04	6.21	0.02	1.13	0.02	5.34	5.50	18
6.03	0.04	6.20	0.02	1.13	0.02	5.34	5.49	19
6.02	0.04	6.19	0.02	1.13	0.02	5.33	5.48	20
6.02	0.04	6.18	0.02	1.13	0.02	5.33	5.47	21
6.02	0.05	6.17	0.02	1.13	0.02	5.33	5.46	22
6.02	0.05	6.16	0.02	1.13	0.02	5.33	5.45	23
6.01	0.05	6.15	0.02	1.13	0.02	5.32	5.44	24

Under these conditions the $[MA^+]$ which was monitored at 430 nm are low, so the concentration of the limiting reagents (MAH/MAH- d_2) was increased to 10 mM from 0.5 mM. This increase in [substrate] resulted in absorbance changes which could be monitored with a high degree of accuracy. Although these conditions are not strictly pseudo-first-order, only the first 0.3% of the reaction was followed. The tabulated data for these experiments are shown in Table 5-6. The data in Table 5-6 and Fig. 5-3 suggest the formation of an intermediate at

very short times.

TABLE 5-5. Changes in k_{app} and Standard Deviations (S.D.) as a Function of the Degree of Reaction Analyzed for the Reaction of MAH (0.5 mM) with BQCN⁺ (40 mM) in AN at 298K Half-Saturated with Air and 430nm

time	$10^4 k_{app}/s^{-1}$	10^4 S.D. (10 shots)	Segment
2.47	6.20	0.21	1
4.72	6.20	0.17	2
6.97	6.30	0.17	3
9.22	6.33	0.13	4
11.5	6.34	0.13	5
22.7	6.26	0.07	6
45.2	6.11	0.01	7
67.7	6.03	0.02	8
90.2	6.00	0.03	9
112.7	5.97	0.04	10
135.2	5.95	0.04	11
157.7	5.93	0.03	12
180.2	5.92	0.03	13
202.7	5.91	0.03	14
225.2	5.90	0.03	15
247.7	5.88	0.03	16
270.2	5.87	0.03	17
292.7	5.86	0.03	18
315.2	5.85	0.02	19
337.7	5.84	0.02	20
360.2	5.83	0.02	21
382.7	5.82	0.02	22
405.2	5.80	0.02	23
427.7	5.79	0.01	24

TABLE 5-6. Apparent Rate Constants and Apparent Kinetic Isotope Effects at Short Times for the Reactions of MAH/MAH- d_2 (10 mM) with BQCN⁺ (40 mM) in AN at 298 K in the Presence of Residual Oxygen at 440nm (Over the First 0.3% Reaction)

time/s	Data Set 1			Data Set 2			Data Set 3			No.
	k_{app}^{H1}/s^{-1}	k_{app}^{D1}/s^{-1}	KIE_{app}^1	k_{app}^{H2}/s^{-1}	k_{app}^{D2}/s^{-1}	KIE_{app}^2	k_{app}^{H3}/s^{-1}	k_{app}^{D3}/s^{-1}	KIE_{app}^3	
0.019	0.001312	0.001023	1.28	0.001234	0.000593	2.08	0.001122	0.001156	0.97	1
0.031	0.001021	0.000336	3.04	0.001020	0.000517	1.97	0.000775	0.000683	1.13	2
0.044	0.000878	0.000396	2.22	0.000904	0.000314	2.88	0.000841	0.000525	1.60	3
0.056	0.000852	0.000423	2.01	0.000861	0.000321	2.68	0.000807	0.000501	1.61	4
0.069	0.000822	0.000323	2.54	0.000860	0.000340	2.53	0.000758	0.000475	1.60	5
0.131	0.000620	0.000176	3.52	0.000618	0.000181	3.41	0.000577	0.000265	2.18	6
0.256	0.000554	0.000111	4.99	0.000521	0.000076	6.86	0.000514	0.000108	4.76	7
0.381	0.000549	0.000087	6.31	0.000506	0.000068	7.44	0.000498	0.000083	6.00	8
0.506	0.000552	0.000085	6.49	0.000511	0.000074	6.91	0.000503	0.000083	6.06	9
0.631	0.000554	0.000089	6.22	0.000514	0.000081	6.35	0.000508	0.000088	5.77	10
0.756	0.000559	0.000095	5.88	0.000517	0.000088	5.88	0.000514	0.000092	5.59	11
0.881	0.000562	0.000099	5.68	0.000520	0.000093	5.59	0.000519	0.000097	5.35	12
1.006	0.000564	0.000101	5.58	0.000521	0.000097	5.37	0.000521	0.000099	5.26	13
1.131	0.000566	0.000104	5.44	0.000522	0.000099	5.27	0.000522	0.000101	5.17	14
1.256	0.000567	0.000106	5.35	0.000524	0.000101	5.19	0.000524	0.000102	5.14	15
1.381	0.000567	0.000107	5.30	0.000525	0.000102	5.15	0.000525	0.000103	5.10	16
1.506	0.000568	0.000108	5.26	0.000525	0.000103	5.10	0.000525	0.000104	5.05	17
1.631	0.000568	0.000109	5.21	0.000525	0.000103	5.10	0.000526	0.000105	5.01	18
1.756	0.000568	0.000110	5.16	0.000526	0.000104	5.06	0.000526	0.000105	5.01	19
1.881	0.000569	0.000110	5.17	0.000526	0.000105	5.01	0.000526	0.000106	4.96	20
2.006	0.000569	0.000111	5.13	0.000526	0.000105	5.01	0.000527	0.000106	4.97	21
2.131	0.000569	0.000111	5.13	0.000526	0.000106	4.96	0.000527	0.000107	4.93	22
2.256	0.000570	0.000111	5.14	0.000526	0.000106	4.96	0.000527	0.000107	4.93	23
2.381	0.000571	0.000111	5.14	0.000526	0.000106	4.96	0.000527	0.000107	4.93	24

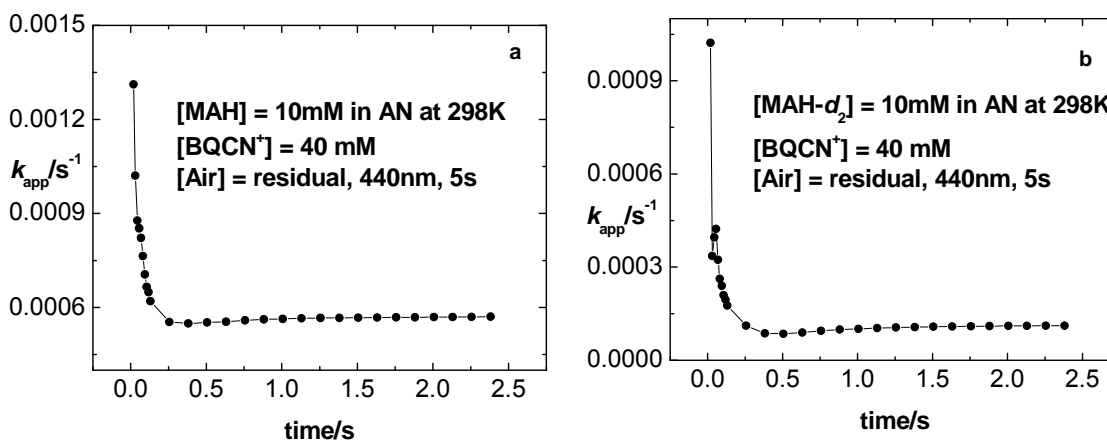


FIGURE 5-3. Apparent rate constants (k_{app}) – time plots for the reactions of BQCN⁺ (40 mM) with MAH (a)/(MAH- d_2) (b) (10 mM) in AN containing residual air at 298 K and 440nm.

Kinetic Isotope Effects for the Reaction of BQCN⁺ with MAH in AN at 298 K at Short Times. The observation of time-dependent KIE has been shown to be a very effective tool in mechanism analysis.²⁹ It is particularly important to attempt to estimate the KIE as zero-time is approached since an extrapolated KIE equal to 1 is very strong evidence that there is no C-H bond breaking in the first step of a multi-step mechanism. The time-dependence of KIE is only observed at times before steady state is reached. This implies that a plot of KIE_{app} vs. time can be used to estimate the time necessary to reach steady state. Although the latter is correct, it should be pointed out that a much more accurate analysis can be carried out using plots of k_{app}^H and k_{app}^D . This allows for the fact the time necessary for steady state to be reached may differ for the two different substrates.

The determination of the time necessary to reach steady state for the reactions of BQCN⁺ (40 mM) with MAH/MAH-*d*₂ (10 mM) in AN at 298K in the presence of residual air is illustrated in Figure 5-3. The time to reach steady state under these conditions can be estimated to be of the order of 0.5 ms for both isotopic substrates (MAH (Fig. 5-3a) and MAH-*d*₂ (Fig. 5-3b)).

A fact that must be considered when analyzing data obtained at very low conversions is that absorbance due to products is very low under these conditions. As a consequence of this, parameters based on changes in product absorbance are subject to much greater uncertainty than those observed at higher conversions. This is demonstrated by a comparison of the data from three identical sets of experiments in Table 5-6. The first set of experiments resulted in

KIE_{app} ranging from 1.28 to 5.14, in the second set from 2.08 to 4.96, and for the third set the values ranged from 0.97 to 4.93 (KIE_{app} vs. time plots shown in Figure A-15). The differences in the three ranges are almost entirely due to the large differences in the initial values. Under the reaction conditions that the data in Table 5-6 were gathered, the corresponding half-lives for the reaction of MAH was about 1000 s and that for MAH- d_2 was close to 5000 s.

The data for the reaction of MAH (10 mM) with BQCN⁺ (0.5 mM) in AN in the presence of residual oxygen shown in Table 5-7 are for three identical sets of reactions. The data not only show relatively small S.D. values but also only small differences in the values of k_{app} over the entire range of segments.

The data in Table 5-8 for the isotopic substrates encompass conversion in the range from 0 to 0.6%. In connection with the point we are making concerning reliability of data depending upon the concentration of product [MA⁺] analyzed is clearly illustrated by the columns labelled 10^4 S.D. are most pertinent. The S.D. values in the first row (segment 1) are of the order of 40% of the pertinent k_{app} values while those in segment 24 are only 0.3% of the corresponding k_{app} values.

Kinetic Isotope Effects over Several Half-Lives. Instantaneous rate constant (IRC) analysis²⁶ of the reactions between MAH/MAH- d_2 and BQCN⁺ in AN under two extreme sets of conditions are illustrated by the plots in Figure 5-4. New aspects of the analysis are summarized in the appendices from Figures A-18 to A-23.

We have seen from the data in Fig. 5-2 and Tables 5-1 that the conditions which favour the oxygen catalyzed reaction are those in which [MAH] is the

reagent in excess and $[BQCN^+]$ is limiting. The plots in the left-hand column of Fig. 5-4 (a, b and c) from reactions of MAH/MAH- d_2 (40 mM) with $BQCN^+$ (0.50 mM) are from conditions which favor the catalyzed reaction. The right-hand column of plots in Fig. 5-4 (a', b' and c') are from reactions of MAH/MAH- d_2 (0.5 mM) with $BQCN^+$ (40 mM) conditions under which the catalyzed reaction contributes minimally to the kinetic response.

TABLE 5-7. Changes in k_{app} and Standard Deviations (S.D.) as a Function of the Degree of Reaction Analyzed for the Reaction of MAH (10 mM) with $BQCN^+$ (0.5 mM) in AN at 298K in the Presence of Residual Oxygen at 450nm over 1 HL

MAH-Data Set 1		MAH-Data Set 2		MAH-Data Set 3		Average		No.
10^4 k_{app}/s^{-1}	10^4 S.D. (10 shots)	10^4 k_{app}/s^{-1}	10^4 S.D. (10 shots)	10^4 k_{app}/s^{-1}	10^4 S.D. (10 shots)	10^4 k_{app}/s^{-1}	\pm	
1.69	0.08	1.75	0.07	1.66	0.07	1.70	0.05	1
1.72	0.06	1.72	0.05	1.66	0.03	1.70	0.03	2
1.71	0.04	1.75	0.04	1.68	0.04	1.71	0.04	3
1.71	0.03	1.77	0.03	1.69	0.04	1.72	0.04	4
1.71	0.02	1.77	0.02	1.71	0.04	1.73	0.03	5
1.71	0.01	1.77	0.02	1.74	0.04	1.74	0.03	6
1.71	0.02	1.77	0.02	1.74	0.03	1.74	0.03	7
1.72	0.02	1.77	0.02	1.74	0.04	1.74	0.03	8
1.72	0.02	1.78	0.02	1.75	0.04	1.75	0.03	9
1.73	0.02	1.79	0.02	1.75	0.04	1.76	0.03	10
1.74	0.02	1.80	0.02	1.76	0.04	1.77	0.03	11
1.75	0.03	1.81	0.03	1.78	0.05	1.78	0.03	12
1.77	0.03	1.83	0.03	1.79	0.05	1.80	0.03	13
1.78	0.03	1.85	0.04	1.81	0.06	1.81	0.04	14
1.80	0.04	1.87	0.04	1.82	0.07	1.83	0.04	15
1.81	0.04	1.88	0.05	1.83	0.07	1.84	0.04	16
1.82	0.05	1.89	0.05	1.84	0.08	1.85	0.04	17
1.83	0.05	1.90	0.05	1.85	0.08	1.86	0.04	18
1.84	0.06	1.91	0.05	1.86	0.09	1.87	0.04	19
1.84	0.06	1.92	0.06	1.87	0.09	1.88	0.04	20
1.85	0.06	1.93	0.06	1.87	0.09	1.88	0.04	21
1.85	0.07	1.93	0.06	1.88	0.09	1.89	0.04	22
1.85	0.07	1.94	0.06	1.88	0.10	1.89	0.05	23
1.85	0.07	1.94	0.06	1.88	0.10	1.89	0.05	24

TABLE 5-8. Changes in k_{app} and KIE_{app} as a Function of the Degree of Reaction (Over the First 0.6% Reaction) Analyzed for the Reactions of MAH/MAH- d_2 (10 mM) with BQCN⁺ (40 mM) in AN in the Presence of Residual Oxygen and 440 nm

time/s	MAH		MAH- d_2		KIE_{app}	Segment
	$10^4 k_{app}^H$	10^4 S.D. (10 shots)	$10^4 k_{app}^D$	10^4 S.D. (10 shots)		
0.032	10.26	4.02	8.24	2.73	1.25	1
0.057	7.99	2.93	4.59	1.97	1.74	2
0.082	7.16	1.79	2.49	1.40	2.88	3
0.107	6.84	1.33	1.71	1.11	4.00	4
0.132	6.60	0.92	1.34	0.89	4.93	5
0.257	5.80	0.29	0.69	0.47	8.41	6
0.507	5.89	0.16	0.77	0.26	7.65	7
0.757	6.07	0.08	0.90	0.14	6.74	8
1.007	6.10	0.06	0.98	0.10	6.22	9
1.257	6.13	0.04	1.02	0.09	6.01	10
1.507	6.15	0.03	1.06	0.08	5.80	11
1.757	6.16	0.03	1.07	0.07	5.76	12
2.007	6.16	0.02	1.08	0.05	5.70	13
2.257	6.17	0.02	1.08	0.04	5.71	14
2.507	6.17	0.02	1.08	0.04	5.71	15
2.757	6.17	0.01	1.08	0.04	5.71	16
3.007	6.16	0.02	1.09	0.04	5.65	17
3.257	6.17	0.02	1.10	0.04	5.61	18
3.507	6.17	0.02	1.10	0.03	5.61	19
3.757	6.17	0.02	1.11	0.03	5.56	20
4.007	6.18	0.02	1.11	0.03	5.57	21
4.257	6.18	0.02	1.12	0.03	5.52	22
4.507	6.18	0.02	1.12	0.03	5.52	23
4.757	6.18	0.02	1.12	0.02	5.52	24

Considering first the plots in the left-hand column we find in the profile (Fig. 5-4a) for the reaction of MAH the values of k_{IRC} increase with time until a maximum value is reached at 1075 s and then fall continually throughout the remainder of the reaction. On the other hand the k_{IRC} – time profile (Fig. 5-4b) for the corresponding reaction of MAH- d_2 is more normal and ascends rapidly at short times to a maximum followed by a slower increase in k_{IRC} for the remainder of the reaction. The latter is due to the effect of oxygen which is greatly

diminished when MAH- d_2 is the reactant as compared to the reaction of MAH. The KIE_{IRC} – time profile (Fig. 5-4c) increases from about 100 s to a maximum value close to 12.4 before decreasing for the remainder of the reaction to 7.5 at about 1900 s.

The k_{IRC} – time profiles for the reactions when MAH/MAH- d_2 is the limiting reagent (Figs. 5-4a' and 5-4b') show more conventional form and are relatively flat throughout the reaction period. That for MAH- d_2 (Fig. 5-4b') rises sharply at short times while that reaction period is not visible on the MAH profile (Fig. 5-4a'). These differences point out again how sensitive the reactions are to the O_2 concentration. These plots are the instantaneous rate constants – time profiles (IRC) and how these differ from those obtained by the earlier procedure is explained in the Chapter 2.

Discussion

The conventional kinetic data in Table 5-1 suffice to answer the question regarding whether or not the reactions follow a one-step or a complex mechanism. Under all conditions studied:

- (a) BQCN⁺ as limiting reagent in AN with residual oxygen
- (b) BQCN⁺ as limiting reagent in AN half-saturated with air
- (c) MAH as limiting reagent in AN with residual oxygen
- (d) MAH as limiting reagent in AN half-saturated with air

the rate constants derived and the intercepts of linear correlation plots varied as the degree of reaction of the analyses increased. This leaves little room for doubt that the reaction between MAH and BQCN⁺ in AN follows a multi-step

mechanism.

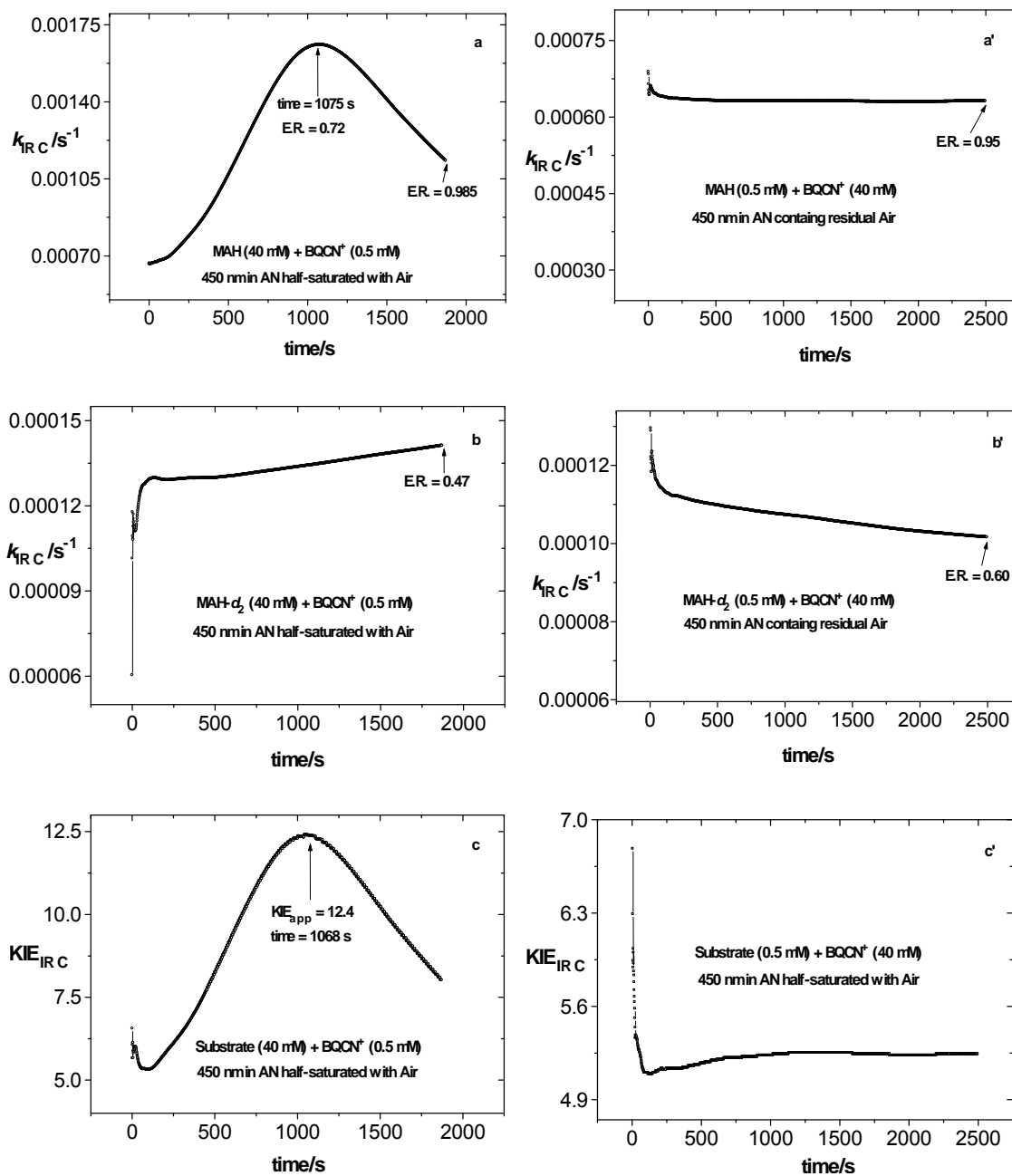


FIGURE 5-4. Apparent instantaneous rate constants (k_{IRC}) – time and KIE_{IRC} plots for the reactions of BQCN⁺ (0.5 mM) with MAH/MAH- d_2 (40 mM) in AN half-saturated with air (a, b and c) and BQCN⁺ (40 mM) with MAH/MAH- d_2 (0.5 mM) containing residual oxygen (a', b' and c') at 298 K and 450nm.

The successive correlation data in Table 5-2 (condition a) over about 1 HL

show that even in the absence of intentionally added air at 298 K there are significant changes in k_{app} with time. The data also show that under these conditions there are differences in k_{app} in the two sets of experiments. These differences could be a consequence of differences in the trace oxygen concentration. We have pointed out that in another comparison of three identical runs (Table 5-7) the differences observed in k_{app} are very small.

The data in Table 5-3 are under conditions (b) and once again we observe that the two different sets of k_{app}^H differ and give rise to 2 sets of KIE_{app} (using a single set of k_{app}^D) ranging from 3.04 to 5.13 for Set 1 and 5.02 to 8.74 for Set 2. Although the values of KIE are different in the two sets, most likely due to differences in $[O_2]$, the trends in the two KIE_{app} sets are similar beginning at short times at relatively low values and increasing by 69 and 74% over time for Sets 1 and 2, respectively.

In the absence of intentionally added air with MAH as limiting reagent (conditions c) the data are much more reproducible from one data set to the next. This is illustrated in Table 5-4. Under these conditions the variations in KIE_{app} are much smaller, settling down at about 5.33 for Set 1 and 5.44 for Set 2, respectively. The larger variations in values from segments 1-5 are consistent with the larger standard deviations observed for data in these segments.

The conditions for the reactions described by the data in Table 5-6 are quite different from those previously discussed. The concentration of the limiting reagents (MAH/MAH- d_2) was increased to 10 mM. The purpose of this was to allow the reactions to be analyzed with very low conversions (0.3%) and still

produce high enough product concentrations so that the precision in the rate constants would not suffer too greatly. Standard deviations for the three data sets are appreciably larger than for the data discussed above but the overall result, the time-dependent KIE_{app} are reasonably close for the three data sets again with the largest variations observed in the early reaction segments. The ranges of KIE_{app} were observed to be 1.28-5.14, 1.97-4.96 and 0.97-4.93 for Data Sets 1, 2, and 3, respectively, and the average value was 1.44.

The mechanistic significance of KIE_{app} approaching unity at near zero time is that it provides very strong evidence that there is no KIE in the first step of the reaction.²⁹ This would suggest that the mechanism of the reaction showing these kinetic characteristics must involve a minimum of three microscopic steps.

Data for another set of reactions under still different conditions, MAH (10 mM) and $BQCN^+$ (0.50 mM), are illustrated in Table 5-7. The data of most interest is in column 7 which shows that the average value of k_{app} changes smoothly from 1.70 to 1.89 over 1 HL with very small standard deviations. It is evident that under these conditions there is no problem with the precision of the measurements or the data, and that even in the presence of only residual concentrations of air, there is a definitive dependence of k_{app} on time.

This leads us once again to the dependence of KIE_{app} on the extent or time of reaction and to the data in Table 5-8. In this case the limiting reagents are MAH and $MAH-d_2$ (10 mM) in the presence of $BQCN^+$ (40 mM). We observed that high precision of the data was achieved (Table 5-8) under these conditions during the first 0.6% of the reaction. The data in Table 5-8 strengthen our case

that KIE_{app} for this reaction is time dependent and approaches unity as the time approaches 0. In this case KIE_{app} was observed to be equal to 1.25 at short times and to increase relatively rapidly to a maximum value of 8.41 and then slowly settle down to a value equal to 5.52 in the later segments of the reaction.

Before suggesting a mechanism that describes this massive amount of experimental data, it is helpful to summarize the mechanistic evidence. The most pertinent evidence is summarized below. The first and very important point is (1) which seems difficult to argue with.

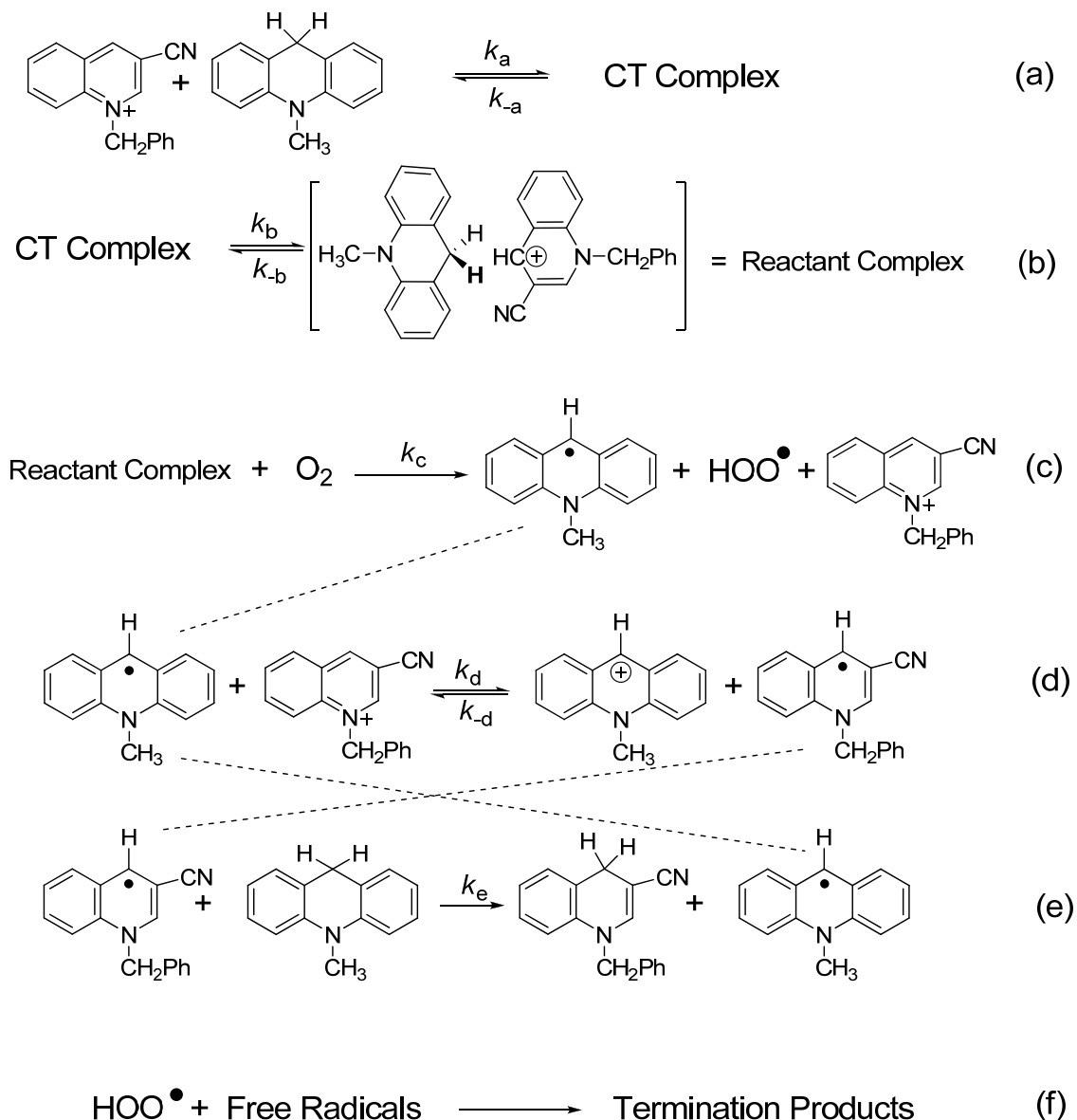
- (1) The conventional pseudo-first-order kinetics are inconsistent with a one-step mechanism.³¹
- (2) The rate of the reaction is dependent upon $[O_2]$ and the increase in k_{app} with time is even observed in the presence of only residual air in a glove box under a nitrogen atmosphere.
- (3) KIE_{app} under a variety of conditions, approach 1.0 at short times before proceeding to a maximum value and then slowly decreasing.
- (4) The air effect is much more prominent when $[MAH]$ is in large excess.
- (5) The kinetic data are reproducible and statistically significant.

The observation of the air effect requires that O_2 reacts with some species, either reactant or intermediate. The obvious possibility is that O_2 abstracts a hydrogen atom from the 10-position of MAH. This reaction apparently takes place but at a very low rate (Figure A-24 and A-25) in the absence of $BQCN^+$ in AN. It appears that the H atoms at the 10-position of MAH require activation to make the H-atom abstraction reaction feasible at rates high enough

to be significant in the product forming reaction of MAH with BQCN^+ . However, it is likely that the reaction does provide enough radicals to serve as an initiator in a chain process. The fact that KIE_{app} under conditions most favourable to the air effect rise to a maximum value before falling steadily for the remainder of the reaction could be explained as follows: The rise to the maximum is where initiation and propagation of the chains dominate over chain termination and also the non-chain process. After the maximum chain termination reduces the contribution of the radical process.

Finally, the approach of KIE_{app} toward unity as the time approaches zero suggest not only that there is no KIE in the first step of the reaction but also that the mechanism involves a minimum of three microscopic reactions. We believe that the chain mechanism illustrated in Scheme 5-4 takes into account all of the experimental data and the points listed above. The reaction between MAH and oxygen is not included in the scheme but must be considered to be an initiation step.

SCHEME 5-4. Proposed Multi-Step Mechanism for the Reaction of MAH with BQCN⁺ in AN in the Presence of Residual or Intentionally Added Air at 298 K. The Dashed Lines Connecting Structures in Steps (d and e) Are Between the Propagating Species in the Two Equations



We will begin the mechanism discussion by justifying each step in Scheme 5-4. In our previous investigation we found that the CT complex formed (step a) at a rate too rapid to follow by stopped-flow with an equilibrium constant

close to 1.0 at 298K.¹² The CT complex could be the intermediate reacting with oxygen. However, we don't believe that the loosely bound CT complex would change the reactivity of MAH sufficiently to enhance the rate of H-atom transfer to O₂ to the degree necessary for this reaction to take part in this mechanism. We view the formation of the "Reactant Complex" (step b) to involve the extrusion of solvent between the two entities in the CT complex and movement of atoms in the latter to an arrangement more conducive to the bond changes that must take place in going to the transition state for hydrogen atom (or hydride in Mechanism 1) transfer (step b). Once MAH radical is formed (step c), the chain mechanism (steps d and e) takes place. The dashed lines in Scheme 5-4 connect chain carriers in the two steps (d and e). The product formation step (step 3 in Scheme 5-1) of the polar mechanism takes place concurrently with the chain mechanism and under some conditions is expected to dominate, *i.e.* when the substrate is MAH-*d*₂ and when the limiting reagent is MAH. The radical reactions (steps d and e) are expected to take place very rapidly. During the *pre-steady-state* period of the overall reaction, steps a and b dominate and at times approaching zero, the mechanism predicts that KIE_{app} will approach unity as was observed experimentally.

Before concluding we would like to return to Perrin's¹³ apparently logical argument that the rate constant (k_b) that we reported¹² in Mechanism 1 is too small for the dissociation of a weakly bound complex. We do not know the structure of the "Reactant Complex" and therefore cannot use quantitative terms in describing its properties, in particular the Gibb's free energy of conversion to

the CT complex, not dissociation. But what we have argued before¹² and still believe is that the “Reactant Complex” is tight by the virtue of the structural and solvation changes that must take place to revert to the CT complex. The latter process may have a significant entropic contribution, especially if solvation changes lag behind bond changes as is often proposed. Perrin¹³ ignored the fact that we did not suggest that the “Reactant Complex” dissociates but rather, is converted back to the CT complex. In any event, the rate constants that we derived¹² on the basis of a two-step mechanism are no longer relevant and this renders Perrin’s¹³ comments irrelevant.

Conclusions

The most important conclusion for the “big picture” is that the reaction of MAH with BQCN⁺ in AN takes place by a multi-step mechanism. Another conclusion of some general importance is that oxygen takes part in a chain process during this reaction and is important even under conditions where it is rigorously attempted to eliminate oxygen by thorough degassing of the solutions before placing them in a glove box containing the stopped-flow instrument under an atmosphere of purified nitrogen. This leads to the conclusion that the chain pathway of formal hydride transfer in biological systems in nature may also involve the participation of oxygen.

Another important conclusion of this work as well as our other recent publications^{28,29} verify the value of the kinetic methods developed in our laboratory over the past fifteen years and continue to be developed.

Experimental Section

Materials. *N*-Methylacridinium iodide was prepared from acridine (Aldrich) and a 3-fold excess of methyl iodide in a minimum amount of acetone. 10-Methyl-9,10-dihydroacridine was prepared by reduction of *N*-methylacridinium iodide using sodium borohydride in dry methanol, followed by recrystallization from absolute ethanol.³² 10-Methyl-9,10-dihydroacridine 9,9-*d*₂ was prepared as described in the literature.³³ 1-Benzyl-3-cyanoquinolinium perchlorate was prepared by ion exchange of 1-benzyl-3-cyanoquinolinium bromide obtained from the reaction of 3-cyanoquinoline with benzyl bromide.³⁴ The bromide salt was dissolved in dry acetonitrile in the presence of a 50-fold excess of sodium perchlorate. After evaporation of the solvent the residue was washed with water and collected by filtration. The process was repeated twice to ensure complete exchange. The resulting solid was recrystallized from absolute ethanol to give the perchlorate salt. ¹H NMR (300 MHz, CD₃CN): δ 6.18 (2H, s), 7.43 (5H, m), 8.10 (1H, m), 8.32 (1H, m), 8.44(2H, d), 9.50(1H, s), 9.55 (1H, s). Acetonitrile was refluxed and distilled over P₂O₅ under a nitrogen atmosphere and past through an Al₂O₃ column before taking into the glove box.

Kinetic Experiments. Kinetic experiments were carried out using a Hi-Tech SF-61 DX2 stopped-flow spectrophotometer installed in a glove box and kept under a nitrogen atmosphere. The temperature was controlled at 298 K using a constant temperature flow system connected directly to the reaction cell through a bath situated outside of the glove box. All stopped-flow experiments included recording 10 absorbance – time profiles at 430 nm or 450 nm. Each

experiment was repeated at least three times. The 2000-point absorbance – time curve data were collected over either 1+ or 4+ HL.

Absorbance – time (Abs – t) profiles for product evolution were analyzed individually by two different procedures. The first step in both procedures was to convert the Abs – t profiles to $(1 - \text{E.R.})$ – time profiles, where E.R. denotes the extent of reaction. This was carried out by dividing each absorbance value by the infinity value obtained from the product extinction coefficient and the reactant concentration and subtracting the value from 1.0. This procedure gave $(1 - \text{E.R.})$ – time profiles that decayed from $(1 - \text{E.R.}) = 1$ for either one or four HL depending on which analysis procedure was used. For pseudo-first-order kinetic analysis, the $(1 - \text{E.R.})$ – time profiles were converted to $-\ln(1 - \text{E.R.})$ – time profiles. For further processing, the individual four HL $(1 - \text{E.R.})$ – time profiles were first averaged to give the average profiles. The first kinetic procedure used was simply a least-squares linear correlation of the $-\ln(1 - \text{E.R.})$ – time profiles to give the apparent pseudo-first-order rate constants over either one, two, three, or four HL. The second procedure involved recording the Abs – t profiles over slightly more than the first HL followed by the sequential 24 linear correlations described in the Results section.

References

- (1) Kim, Y.; Truhlar, D. G.; Kreevoy, M. M. *J. Am. Chem. Soc.* **1991**, *113*, 7837.
- (2) Kotchevar, A. T.; Kreevoy, M. M. *J. Phys. Chem.* **1991**, *95*, 10345.
- (3) Kreevoy, M. M.; Kotchevar, A. T. *J. Am. Chem. Soc.* **1990**, *112*, 3579.

- (4) Kreevoy, M. M.; Ostovic, D.; Lee, I. -S. H., Binder, D. A., King, G. W. *J. Am. Chem. Soc.* **1988**, *110*, 524.
- (5) Ostovic, D.; Lee, I.-S. H.; Roberts, R. M. G.; Kreevoy, M. M. *J. Org. Chem.* **1985**, *50*, 4206.
- (6) Kreevoy, M. M.; Lee, I.-S. H. *J. Am. Chem. Soc.* **1984**, *106*, 2550.
- (7) Anne, A. J.; Moiroux, J.; Saveänt, J.-M. *J. Org. Chem.* **2000**, *65*, 7213.
- (8) Schowen, R. L. "Model Studies of Hydrogen Transfer Reactions," Chapter 4 in "Hydrogen-Transfer Reactions," edited by Hynes, J. T.; Klinman, J. P.; Limbach, H. -H.; Schowen, R. L.; Wiley-VCH Verlag GmbH & Co.: Weinheim, 2007.
- (9) Cheng, J.-P; Lu, Y.; Zhu, X.-Q.; Mu, L. *J. Org. Chem.* **1998**, *63*, 6108.
- (10) Cheng, J.-P; Lu, Y. *J. Phys. Org. Chem.* **1997**, *10*, 577.
- (11) Zhu, X.-Q.; Zhang, J.-Y.; Cheng, J.-P. *J. Org. Chem.* **2006**, *71*, 7007.
- (12) Lu, Y.; Zhao, Y.; Handoo, K. L.; Parker, V. D. *Org. Biomol. Chem.* **2003**, *1*, 173.
- (13) Perrin, C. L.; Zhao, C. *Org. Biomol. Chem.* **2008**, *6*, 3349.
- (14) Parker, V. D.; Zhao, Y.; Lu, Y.; Zheng, G. *J. Am. Chem. Soc.* **1998**, *120*, 12720.
- (15) Lu, Y.; Handoo, K. L.; Parker, V. D. *Org. Biomol. Chem.* **2003**, *1*, 36.
- (16) Parker, V. D.; Lu, Y. *Org. Biomol. Chem.* **2003**, *1*, 2621.
- (17) Lu, Y.; Zhao, Y.; Parker, V. D. *J. Am. Chem. Soc.* **2001**, *123*, 5900.
- (18) Zhao, Y.; Lu, Y.; Parker, V. D. *J. Chem. Soc., Perkin Trans. 2* **2001**, 1481.

- (19) Parker, V. D.; Zhao, Y. *J. Phys. Org. Chem.* **2001**, 14, 604.
- (20) Zhao, Y.; Lu, Y.; Parker, V. D. *J. Am. Chem. Soc.* **2001**, 123, 1579.
- (21) Handoo, K. L.; Lu, Y.; Zhao Y.; Parker, V. D. *Org. Biomol. Chem.* **2003**, 1, 24.
- (22) Handoo, K. L.; Lu, Y.; Zhao, Y.; Parker, V. D. *J. Am. Chem. Soc.* **2003**, 125, 9381.
- (23) Parker, V. D.; Lu, Y.; Zhao, Y. *J. Org. Chem.* **2005**, 70, 1350.
- (24) Parker, V. D. *Pure Appl. Chem.* **2005**, 77, 1823.
- (25) Parker, V. D. *J. Phys. Org. Chem.* **2006**, 19, 714.
- (26) Hao, W.; Parker, V. D. *J. Org. Chem.* **2008**, 73, 48.
- (27) Liao, M. -S.; Lu, Y.; Parker, V. D.; Scheiner, S. J. *Phys. Chem. A* **2003**, 107, 8939.
- (28) Parker, V. D.; Li, Z.; Handoo, K. L.; Hao, W.; Cheng, J.-P. *J. Org. Chem.* **2011**, 76, 1250.
- (29) Li, Z.; Cheng, J.-P.; Parker, V. D. *Org. Biomol. Chem.* **2011**, 9, 4563.
- (30) Fukuzumi, S.; Ohkubo, K.; Tokuda, Y.; Suenubo, T. *J. Am. Chem. Soc.* **2000**, 122, 4286.
- (31) It could be argued that there is a one-step hydride transfer (obeying pseudo-first-order kinetics) accompanied by a radical chain mechanism to give the deviations from the pseudo-first-order rate law. However, the k_{app} – time plots in Fig. 5-3 reveal that the reaction kinetics become complex at times too short for the chain mechanism to contribute to the kinetic response.

- (32) Colter, A. K.; Charles, G. L.; Williamson, T. W.; Berry, R. E. *Can. J. Chem.* **1983**, *61*, 2544.
- (33) Karrer, P.; Szabo, L.; Krishan, H. J. V.; Schwyzer, R. *Helv. Chem. Acta.* **1950**, *33*, 294.
- (34) Roberts, R. M. G.; Ostovic, D.; Kreevoy, M. M. *J. Org. Chem.* **1983**, *48*, 2053.

CHAPTER 6
RAPID FORMATION AND SLOW COLLAPSE OF A CARBOCATION-ANION
PAIR TO A NEUTRAL MOLECULE*

Abstract

The 4,4',4''-trimethoxytrityl cation (TMT^+) was observed to react with acetate ion in acetic acid reversibly to give the corresponding ester (TMT-OAc). The rate of the reaction was found to be independent of $[\text{NaOAc}]$ over a 25000-fold range. Similar results were observed in the presence of Bu_4N^+ in acetic acid as well as in HOAc/AN (1/1, v/v). It was concluded that $\{\text{TMT}^+ \text{HOAc}/\text{AcO}^-\}$ is an ion pair that forms essentially completely from free TMT^+ and HOAc/AcO^- during the time of mixing under stopped-flow conditions. The process which was studied kinetically is the intramolecular collapse of the ion pair to TMT-OAc which takes place in two steps involving a kinetically significant intermediate. The remarkably close resemblance of this reaction to the Winstein scheme for solvolysis reactions is noted. In analogy to the Winstein scheme, it was proposed that the intermediate could be an intimate ion pair formed upon extrusion of solvent from the solvent separated ion pair. The product-forming step could then correspond to the intimate ion pair reacting further to form a covalent bond between the two moieties within the complex. The values of the thermodynamic and the activation parameters as well as the apparent rate constants for the reaction in the presence of either sodium or tetrabutylammonium ions suggest that these

*Coauthored by Weifang Hao and Vernon D. Parker. Reproduced with permission from *J. Org. Chem.* **2008**, 73(1), 48-55. Copyright © 2008, American Chemical Society.

counterions play insignificant roles in the reactions. However, the equilibrium constant for the intramolecular step (K_4) was observed to be two times greater in the presence of Bu_4N^+ than in the presence of Na^+ . The rate of the reaction in HOAc was observed to be about four times as great as that in HOAc/AN (1/1, v/v).

Introduction

The study of the reactions of carbocations with nucleophiles has been a topic of intense interest for more than half a century.¹⁻¹⁸ There appears to be general agreement that the reactions take place in a single rate-determining step accompanied by the formation of a covalent bond between the two moieties. The main recent interest in these reactions has been on developing reactivity scales for both the cations and the nucleophiles.¹⁹⁻²⁰

We regard the cation – anion combination reaction as one of the simplest covalent bond forming reactions possible. The reactions result in the formation of a single bond without disrupting any other covalent bonds. This suggests these reactions as an obvious target for our ongoing research,²¹⁻³² the results of which show that many fundamental organic reactions previously believed to take place in a one-step actually take place by a mechanism with more than one transition state.

The ability to distinguish between one-step and more complex reaction mechanisms has been enhanced by the development of instantaneous rate constants (IRC) analysis³³ which allows the course of the reaction to be analyzed in terms of the apparent instantaneous rate constants (k_{inst}) as a function of time.

For the one-step mechanism in the absence of any complications, k_{inst} is a true constant independent of time. On the other hand, k_{inst} varies with time in the *pre-steady-state* time period for a more complex mechanism and approaches the steady-state value ($k_{\text{s.s.}}$) with increasing time. These relationships are illustrated in Figure 6-1 for a reaction following the pre-association mechanism (Scheme 6-1) in which the intermediate reactant complex is kinetically significant. This mechanism was chosen for the illustration since it has been widely discussed³⁴ and is the simplest complex mechanism involving consecutive reactions.

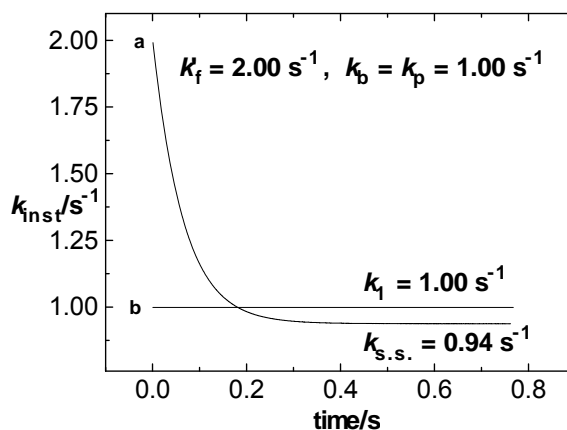
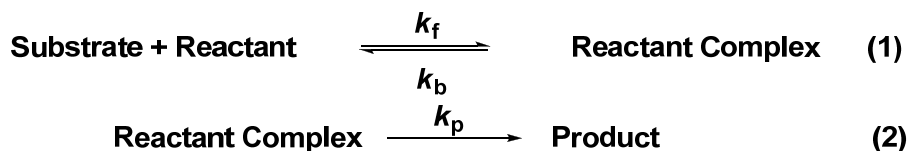


FIGURE 6-1. Apparent instantaneous rate constants (k_{inst}) – time plots for pre-association (a) and one-step (b) mechanisms.

SCHEME 6-1. The Pre-Association Mechanism



The k_{inst} – time profile for the pre-association mechanism (a) in Figure 6-1 intercepts the zero time axis at 2.00, which corresponds to k_f and approaches the

steady-state value (0.94 s^{-1}). That for the one-step mechanism (b) ($k_1 = 1.00 \text{ s}^{-1}$) is a straight line with zero slopes. The ease of distinguishing between the two mechanisms under the conditions of the calculated data is apparent from Figure 6-1.

The objective of this study was to determine the mechanism of a cation – anion combination reaction. We selected the 4,4',4''-trimethoxytrityl cation (TMT^+), a carbocation of moderate reactivity toward nucleophiles,¹² as the cationic reactant and acetate ion as the anionic reactant. In order to moderate the rate of the cation – anion combination reaction, we chose acetic acid as the solvent for this study. It is well-known that acetate ion exists in acetic acid as the hydrogen-bonded complex, hydrogen biacetate ion (HOAc/AcO^-),³⁵ and this is expected to markedly affect the nucleophilicity of the ion. Choosing conditions under which the rates of the anion – cation combinations are moderate is of special importance in attempting to determine whether the reactions follow a one-step or more complex reaction mechanisms. This is because of the fact that the initial portion of the reaction, *i.e.*, the *pre-steady-state* time period, must be accessed in order to differentiate between the mechanisms. Since cation – anion combination reactions are inherently rapid reactions, most of the previous kinetic studies have out of necessity been carried out under conditions where the initial time periods could not be accessed.

Results

The reaction between TMT^+ and NaOAc in acetic acid to form the corresponding ester is reversible. The approach to equilibrium is illustrated by the

spectra in Figure 6-2 for the decrease in $[\text{TMT}^+]$. The reversible reaction is illustrated in Scheme 6-2. No reaction between TMT^+ and acetic acid could be detected in the absence of acetate ion.

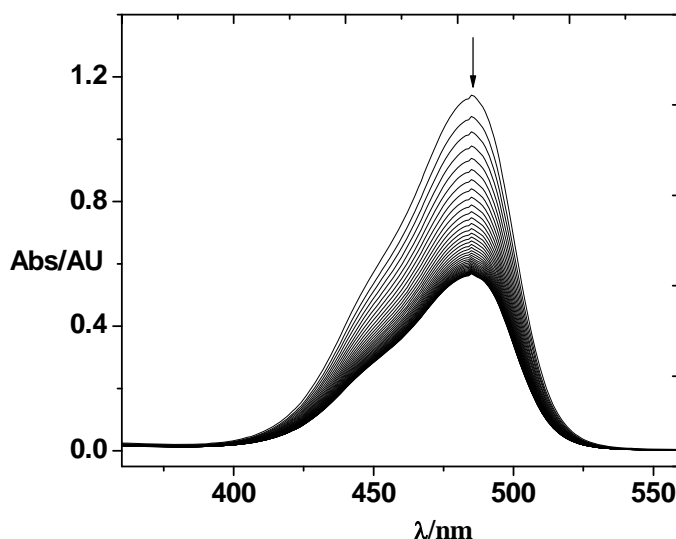
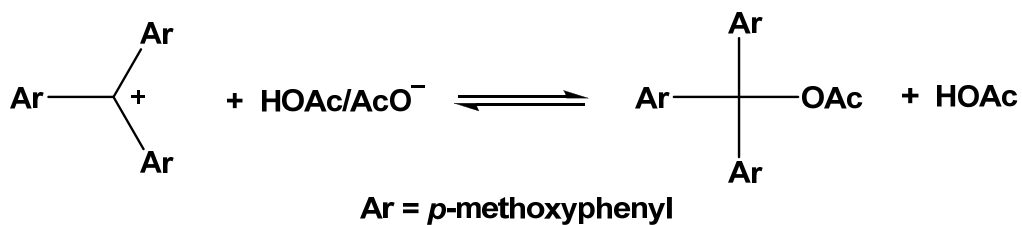


FIGURE 6-2. Diode-array visible absorption spectra of TMT^+ (0.02 mM) in acetic acid containing sodium acetate (0.01 M): start time, 0 s; cycle time, 2.5 s; total run time, 100 s.

SCHEME 6-2. Reversible Reaction Between TMT^+ and Sodium HOAc/AcO^- in Acetic Acid



Definitions of Rate Constants. A number of different methods were used to obtain rate constants in this work. In order to avoid confusion as to the

meaning of the abbreviations used to define the rate constants, the definitions are given below:

k_{inst} = An apparent pseudo-first-order rate constant obtained by an IRC procedure over short time intervals. These can be time dependent in the manner illustrated in Figure 6-1.

$k_{\text{s.s.}}$ = An apparent pseudo-first-order rate constant evaluated in the plateau region of the k_{inst} – time profile.

k_{N} = An apparent pseudo-first-order rate constant evaluated in the conventional way over a segment of the (1 - E.R.) – time profile where E.R. is the extent of reaction. The subscript N signifies the segment number, and k_{N} can be time dependent.

The Effect of Acetate Ion Concentration on the Reaction Rate. Kinetic experiments were carried out by stopped-flow spectrophotometry under a nitrogen atmosphere in a glove box. Our initial experiments in glacial acetic acid gave rise to remarkable results. The rate of the reaction was observed to be independent of sodium acetate concentration over a wide range for the reaction of TMT^+ with acetate ion in acetic acid at 298 K (Table 6-1). $[\text{NaOAc}]$ was varied over the entire applicable range, from 0.50 to 0.00002 M with only random variations in $k_{\text{s.s.}}$. The data in the last entry in Table 6-1 where $[\text{NaOAc}]$ and $[\text{TMT}^+]$ were equal to 0.02 and 0.01 mM, respectively, were subject to significant error due to the small absorbance change for the reaction. The latter data are included to show that the zero-order in $[\text{NaOAc}]$ appears to continue as long as there is enough acetate ion present for TMT^+ to completely react.

TABLE 6-1. Effect of Sodium Acetate Concentration on the Apparent Steady-State Rate Constant for the Reaction of TMT⁺ with Sodium Acetate in Acetic Acid at 298 K

λ/nm	$[\text{TMT}^+]/\text{mM}$	$[\text{NaOAc}]/\text{mM}$	$t_{0.50}/t_{0.05}$	$k_{\text{s.s.}}/\text{s}^{-1}{}^a$
520	0.20	500	20.2	0.0645
520	0.20	250	17.8	0.0586
520	0.20	125	19.5	0.0597
520	0.20	10.0	18.8	0.0529
520	0.20	2.50	23.2	0.0537
480	0.010	0.10	16.4	0.0593
480	0.010	0.020	19.7	0.0767

^a $k_{\text{s.s.}}$ was evaluated from 200 data points near the half-life of the reaction.

TABLE 6-2. Apparent Steady-State Rate Constants for the Reaction Between TMT⁺ and Acetate Ion as a Function of [Bu₄N⁺ HOAc/AcO⁻] in Acetic Acid at 298 K^a

$[\text{Bu}_4\text{N}^+ \text{HOAc/OAc}^-]/\text{mM}$	$t_{0.50}/t_{0.05}$	$k_{\text{s.s.}}/\text{s}^{-1}{}^b$	$[\text{TMT-OAc}]_{\text{equil}}/[\text{TMT}^+]_{\text{equil}}$ (= K_4)
20.0	15.0	0.0667	1.81
10.0	14.1	0.0701	1.89
5.0	14.3	0.0710	2.12
2.5	13.8	0.0679	1.97

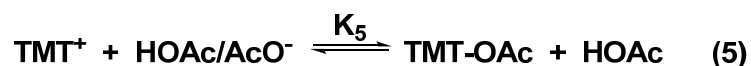
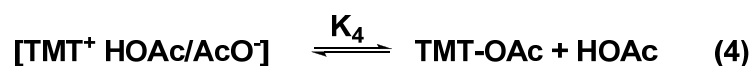
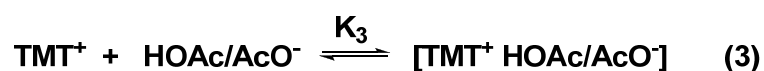
^a From absorbance – time data at 480 nm, $[\text{TMT}^+] = 0.02 \text{ mM}$. ^b $k_{\text{s.s.}}$ was evaluated from 200 data points near the half-life of the reaction.

The data in Table 6-2 show that the rate of the reaction of TMT⁺ with Bu₄N⁺ HOAc/AcO⁻ in acetic acid is also independent of the salt concentration. The value of $k_{\text{s.s.}}$ obtained at 480 nm was observed to be constant within experimental error as [Bu₄N⁺ HOAc/AcO⁻] was varied from 2.5 to 20 mM.

The data in Tables 6-1 and 6-2 suggest that TMT⁺ and HOAc/AcO⁻ in acetic acid react during the time of mixing. This reaction is reversible (see Scheme 6-3), but because of saturation of equilibrium (3) with respect to [HOAc/AcO⁻] there is not a direct relationship between the latter and the concentration of the product (TMT-OAc) at equilibrium. The most likely

explanation of zero-order kinetics in acetate ion for this reaction is that HOAc/AcO⁻ very rapidly interacts with TMT⁺ to form an ion-pair, *i.e.*, equilibrium (3) is saturated at all [HOAc/AcO⁻] in Table 6-1 and 6-2. The ion-pair then reversibly undergoes an intramolecular combination reaction (eq 4) resulting in the formation of the corresponding acetate ester. Since equilibrium (3) is established during the time of mixing in the stopped-flow spectrophotometer, the process that takes place during our kinetic experiments is illustrated by equilibrium (4) (Scheme 6-3).

SCHEME 6-3. Equilibria Involved in the Reaction of TMT⁺ and HOAc/AcO⁻



The Results of Conventional Kinetic Studies of the Combination Reaction in Acetic Acid. The method of data treatment involved evaluating pseudo-first-order rate constants over consecutive intervals consisting of three different series of segments. The 21-point procedure included the following segments: data points 1-21(1), 21-41(2), 41-61(3), 61-81(4), 81-101(5), 101-121(6), and 121-141(7) for absorbance – time data obtained by stopped-flow spectrophotometry. The 31- and 51-point segments were constructed in the same manner as those in the 21-point procedure. The pseudo-first-order rate constants (k_N) evaluated for each time segment are finally divided by the

apparent steady-state rate constant ($k_{s.s.}$) calculated from data at times approaching the half-life of the reaction resulting in dimensionless ratios.

TABLE 6-3. Ratios of Conventional Pseudo-First-Order Rate Constants Evaluated over Initial Data Segments Divided by the Apparent Steady-State Rate Constant ($k_{s.s.} = 0.0650 \text{ s}^{-1}$) for the Reaction of TMT^+ (0.02 mM) with Na^+ HOAc/AcO^- (0.5 M) in Acetic Acid at 298 K and 510 nm

Segment/N	$k_N/k_{s.s.}$ (21 point)	$k_N/k_{s.s.}$ (31 point)	$k_N/k_{s.s.}$ (51 point)
1	2.64	2.01	1.51
2	1.12	1.15	1.10
3	1.13	1.09	1.10
4	1.05	1.07	1.07
5	1.09	1.09	1.06
6	1.07	1.07	1.05
7	1.09	1.08	1.05

The initial rate data in Table 6-3 were obtained by the consecutive segment treatment of kinetic data for the pseudo-first-order reaction of TMT^+ (0.02 mM) with acetate ion (0.50 M) in acetic acid at 298 K. The expected result for a one-step mechanism is that all of the rate constant ratios (the value of the observed pseudo-first-order rate constant divided by $k_{s.s.}$) in Table 6-3 are expected to be the same and equal to 1.00 within experimental error, *i.e.*, pseudo-first-order rate constants for the one-step mechanism are expected to be time independent. This is equivalent to the straight line with zero slopes in Figure 6-1b. The observed result is that the rate constants in all three sets of data exceed $k_{s.s.}$ by 2.64, 2.01, and 1.51 for the initial 21-, 31-, and 51-point segments, respectively, and the ratios in all three columns approach unity in subsequent segments. The data rule out the simple one-step mechanism for the intramolecular combination reaction between TMT^+ and HOAc/AcO^- in acetic acid.

TABLE 6-4. Time and Rate Constant Ratios Observed for the Reaction of TMT⁺ with NaOAc (0.50 M) in Acetic Acid at 298 K

λ/nm	$[\text{TMT}^+]/\text{mM}$	$t_{0.50}/t_{0.05}^a$	$(k_1(21)/k_{s.s.})^b$	$k_{s.s.}/\text{s}^{-1}^c$	K_4
420	0.10	14.8	1.27	0.0646	0.77
430	0.04	14.9	1.35	0.0679	0.94
440	0.04	16.2	1.42	0.0681	0.83
450	0.02	15.2	1.43	0.0729	0.89
460	0.02	15.0	1.35	0.0725	0.90
470	0.02	15.2	1.39	0.0735	0.88
480	0.02	15.5	1.52	0.0711	0.92
490	0.02	15.8	1.73	0.0687	0.94
500	0.02	16.8	1.89	0.0730	0.91
510	0.02	19.2	2.64	0.0650	0.98
520	0.10	20.0	2.87	0.0698	0.78
One-step Mechanism		13.5	1.00		

^a The time ratio ($t_{0.50}/t_{0.05}$) is a very effect probe to test for (a) complex mechanism behavior and (b) whether or not the data are wavelength dependent. In the latter case, if the ratio is wavelength dependent, this is strong evidence that an intermediate absorbs over the same wavelength that the absorbance is monitored. Otherwise, in the absence of interference from an intermediate the ratio is expected to be independent of wavelength. ^b Pseudo-first-order rate constant over the first 21 data points in the 2000 point array divided by $k_{s.s.}$. ^c Evaluated from 200 points near the apparent half-life of the reaction.

When an intermediate absorbs in the same spectral region as that where the kinetics of a reaction is monitored, the kinetic results will usually be wavelength dependent. This is because the kinetic analysis assumes that only reactant or product absorb at the wavelength where measurements are made. Conducting kinetic measurements over a range of wavelength then becomes a very effective tool in demonstrating whether a reaction takes place in a one-step or by a more complex mechanism. The data in Table 6-4 summarize the results over the wavelength region from 420 to 520 nm for the reaction of TMT⁺ with NaOAc (0.50 M) in acetic acid at 298 K. The variation in the $k_1(21)/k_{s.s.}$ ratio with

wavelength suggests that there may be interference from absorbance due to an intermediate since the ratio is otherwise expected to be wavelength independent.

Estimation of the Equilibrium Constant for eq 4. The last columns in Tables 6-2 and 6-4 give estimates of K_4 (eq 4), the equilibrium constant for the reaction of the ion pair. These were obtained from the stopped-flow experiments and were evaluated as the difference in initial (A_{init}) and infinity absorbances (A_{inf}) divided by (A_{inf}): $(A_{\text{init}} - A_{\text{inf}})/A_{\text{inf}}$. It is of interest to note that K_4 in HOAc at 298 K is about two times as great in the presence of $\text{Bu}_4\text{N}^+ \text{HOAc}/\text{AcO}^-$ (1.95 ± 0.14) as compared to that in the presence of $\text{Na}^+ \text{HOAc}/\text{AcO}^-$ (0.89 ± 0.09).

Effect of Cosolvent on the Kinetics of the Reactions of TMT^+ with HOAc/AcO^- . Consecutive segment kinetic data for the reaction of TMT^+ (0.02 mM) with HOAc/AcO^- (5.0 mM) in HOAc/AN (1/1, v/v) where AN is acetonitrile are summarized in Table 6-5. The results in the mixed solvent are similar to those in acetic acid in terms of the decrease in the rate constant ratios with the extent of reaction. The greatest difference in the results in the two solvents is that $k_{\text{s.s.}}$ in HOAc is about four times greater than in the mixed solvent.

The Effect of Temperature on the Rate and Equilibrium for the Collapse of $\{\text{TMT}^+ \text{HOAc}/\text{AcO}^-\}$. The kinetics of the collapse of $\{\text{TMT}^+ \text{HOAc}/\text{AcO}^-\}$ were studied in HOAc and in mixed solvent HOAc/AN (1/1, v/v) in the temperature range from 293 to 323 K. The $k_{\text{s.s.}}$ and K_4 data for 3 sets of experiments in HOAc and HOAc/AN (1/1, v/v) at various temperatures are listed in Tables A-19 to A-22. The activation and thermodynamic parameters derived from these studies based upon $k_{\text{s.s.}}$ and K_4 data are summarized in Table 6-6.

The corresponding Eyring and Van't Hoff plots for the reactions carried out in HOAc are shown in Figure 6-3 and those obtained from data in mixed solvent are illustrated in Figures A-26.

TABLE 6-5. Ratios of Conventional Pseudo-First-Order Rate Constants Evaluated over Initial Data Segments Divided by $k_{s.s.}$ (0.0155 s^{-1}) for the Reaction of TMT^+ (0.02 mM) with Acetate Ion (0.005 M) in HOAc/AN (1/1, v/v) at 298 K and 480 nm

Segment/N	$k_N/k_{s.s.}$ (21 point)	$k_N/k_{s.s.}$ (31 point)	$k_N/k_{s.s.}$ (51 point)
1	1.31	1.26	1.21
2	1.24	1.18	1.12
3	1.21	1.11	1.01
4	1.17	1.04	0.98
5	1.04	1.01	0.99
6	1.03	0.98	1.00
7	1.01	0.99	0.99

TABLE 6-6. Kinetic and Thermodynamic Parameters for the Collapse of $\{\text{TMT}^+ \text{HOAc}/\text{AcO}^-\}$

Solvent	ΔH^\ddagger kcal mol^{-1}	ΔS^\ddagger $\text{cal mol}^{-1} \text{ K}^{-1}$	ΔH° kcal mol^{-1}	ΔS° $\text{cal mol}^{-1} \text{ K}^{-1}$
HOAc	12.2	-22.4	-4.22	-14.0
HOAc/AN (1/1)	13.7	-20.6	-1.40	-5.22

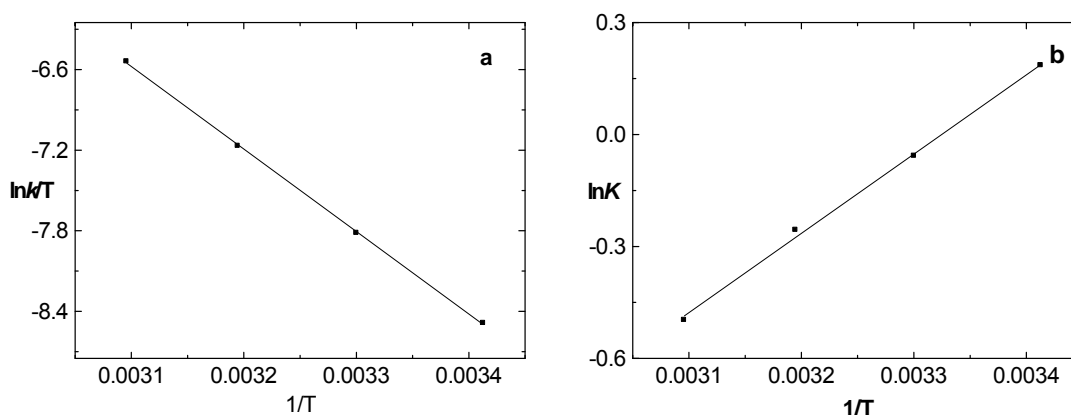


FIGURE 6-3. Eyring plot for the collapse of the ion pair in acetic acid (a) and Van't Hoff type plot for equilibrium (4) in HOAc (b).

Application of IRC Analysis to the Collapse of $\{\text{TMT}^+ \text{HOAc}/\text{AcO}^-\}$.

The IRC plots shown in Figure 6-4 are for reaction of TMT^+ (0.02 mM) with sodium acetate (0.5 M) in acetic acid at 298 K for decay of absorbance due to reactant measured at 500 nm. The k_{inst} – time profile (IRC) for the first 3% of reaction, which was obtained from the fifth order polynomial smoothed data is illustrated in Figure 6-4a and Figure A-28. The curve appears to intersect the zero time axis at about 0.24 s^{-1} which provides an estimate of k_f in Scheme 6-4. The k_{inst} – time profile begins to approach a plateau value at about 170 ms. The latter is more clearly illustrated by the k_{inst} – time profile shown in Figure 6-4b and Figure A-27. The latter was obtained using the 51-point sliding procedure described in the experimental section. The sine-wave-like behavior in the plateau portion of the k_{inst} – time profile in Figure 6-4a is often observed in these plots and is due to spectrometer output noise which is not completely smoothed out by the fifth order polynomial function. The effect of spectrometer output noise is illustrated even more clearly in the plateau regions of Figures 6-4b.

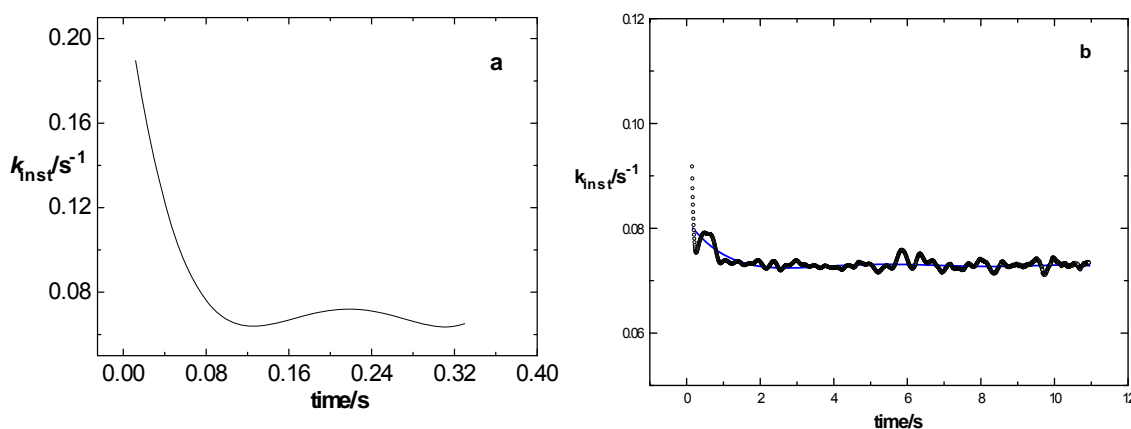
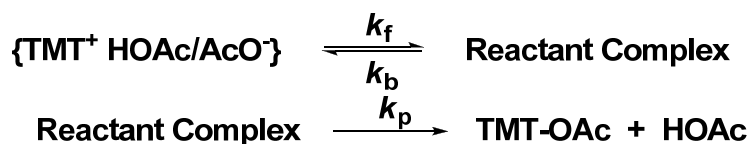


FIGURE 6-4. Apparent instantaneous rate constants (k_{inst}) – time plots for the reaction of TMT^+ (0.02 mM) with sodium acetate (0.50 M) in acetic acid and 500 nm. Data for the first 3% of the reaction (a) and that over the first half-life (b).

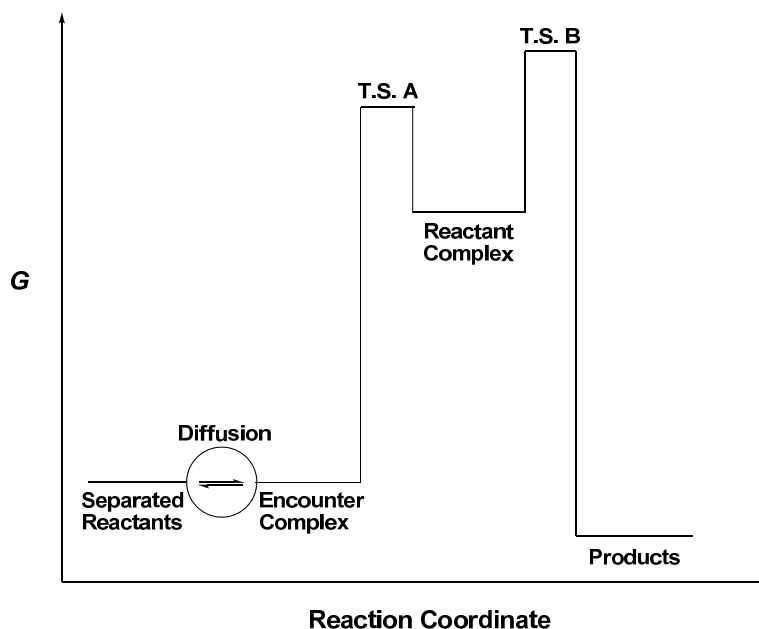
SCHEME 6-4. Mechanism of the Combination Reaction



Discussion

The reaction coordinate (RC) diagram for the pre-association mechanism is illustrated in Scheme 6-5. Beginning with separated reactants on the far left, reactant and substrate diffuse and begin to collide resulting in what is called the encounter complex, which amounts to the two reactants in a solvent cage where it is thought that up to about 10 collisions occur before the reactants separate.³⁴ The diffusion process is illustrated by a double arrow within a circle on the RC. The encounter complex, which has a lifetime of a nanosecond or less depending upon the solvent, is transformed through the first transition state (T.S. A) to the reactant complex. We believe that this transformation consists of solvation and geometry changes leading to a configuration ready for covalent bond formation. The latter then is transformed through the second transition state (T.S. B) to products. This presentation of the RC diagram for preassociation uses the bar graph approach employed by Guthrie³⁶ in his discussion of reactions passing through tetrahedral intermediates. We use the diffusion element to emphasize how the encounter complex³⁴ is defined.

SCHEME 6-5. Reaction Coordinate Diagram for the Pre-Association Mechanism



All of the kinetic data reported in Tables 6-1 to 6-5 and Figures 6-4 are inconsistent with a one-step mechanism for the reaction between TMT^+ with hydrogen biacetate ion either in the presence of Na^+ or Bu_4N^+ in acetic acid or in mixed solvents. Furthermore, the data are consistent with the pre-association mechanism under all circumstances. The data in Tables 6-1 and 6-2 show that the initial reaction takes place during the time of mixing in the stopped-flow spectrophotometer and that the process that can be studied kinetically is the intramolecular collapse of $\{\text{TMT}^+ \text{HOAc}/\text{AcO}^-\}$ to the product, TMT-OAc (eq 4). The degree of reversibility of this process depends strongly on the solvent composition. The data in Tables 6-3 to 6-5 and in Figure 6-4 show that the intramolecular collapse of $\{\text{TMT}^+ \text{HOAc}/\text{AcO}^-\}$ takes place in at least two steps

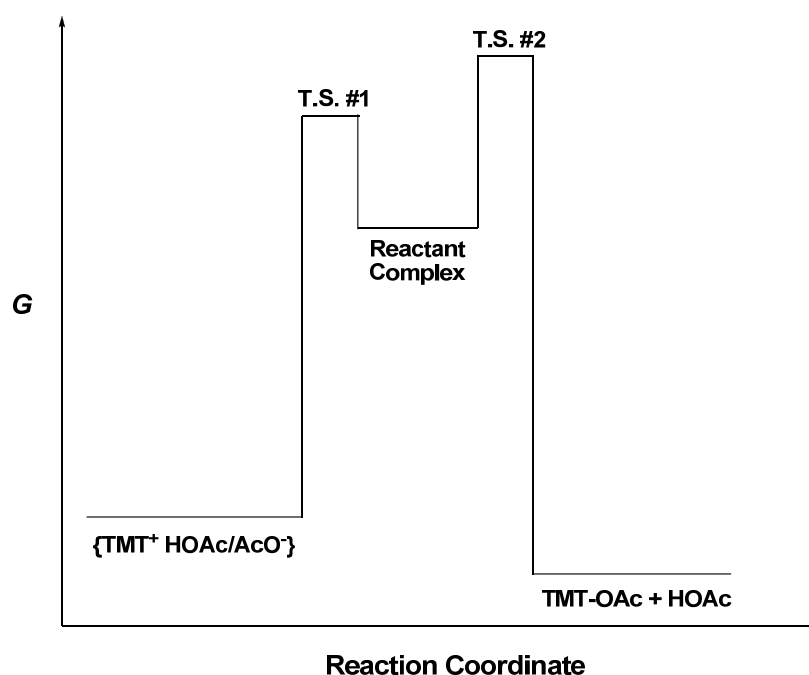
and that the data are consistent with the reversible consecutive two-step mechanism illustrated in Scheme 6-4.

Since the mechanism depicted in Scheme 6-4 is the simplest mechanism consistent with the data, we adopt it for the sake of simplicity since there is no evidence currently available for a more complex mechanism. With the latter in mind, the reaction coordinate diagram illustrated in Scheme 6-6 was constructed to describe the intramolecular reaction. The reactant in the lower left-hand corner of the diagram is $\{\text{TMT}^+ \text{HOAc}/\text{AcO}^-\}$. The first transition state (T.S. #1) lies between the reactant and an intermediate which we refer to as the "Reactant Complex" for which we have no structural data but it is required by the kinetics observed. In the following paragraphs we relate our work to Winstein's scheme for the dissociation of R-X , where R is an alkyl or an arylalkyl group and X is a leaving group, and provide a plausible suggestion for the structure of the "Reactant Complex." The second transition state (T.S. #2) lies between the "Reactant Complex" and the product TMT-OAc .

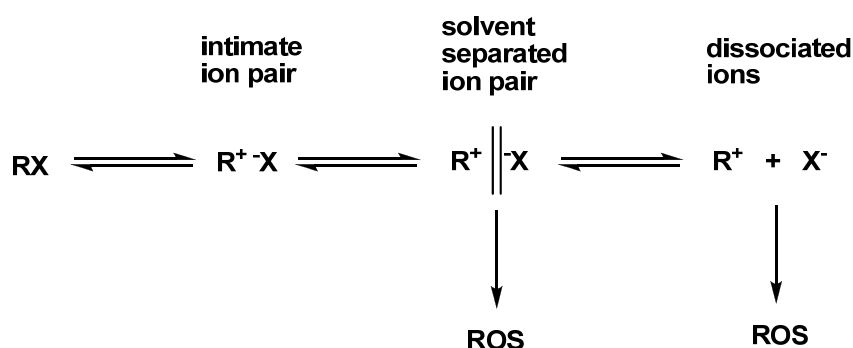
The concept of ion pairs in organic reactions owes much to the pioneering work of Winstein's group more than 50 years ago.³⁷ Using kinetic salt effects, they were able to provide convincing evidence for Scheme 6-7 for the solvolysis reactions of RX (X = halide or other leaving groups). Ionization to the intimate ion pair which does not undergo solvolysis is the first step in this process. The binding between the ions is weakened and solvent separates the two in the solvent separated ion pair. At this stage R^+ can react irreversibly with solvent to give the substitution product. Alternatively, the solvent separated ion pair can

dissociate to the free ions and R^+ can react to form the substitution product. The solvent separated ion pair was observed to undergo exchange with other anions intentionally incorporated in the solution for purposes of studying the process and the substitution reaction could be nearly completely suppressed in the presence of the common ion, X^- .

SCHEME 6-6. Reaction Coordinate Diagram for the Intramolecular Collapse of $\{TMT^+ HOAc/AcO^-\}$ to TMT-OAc and Acetic Acid

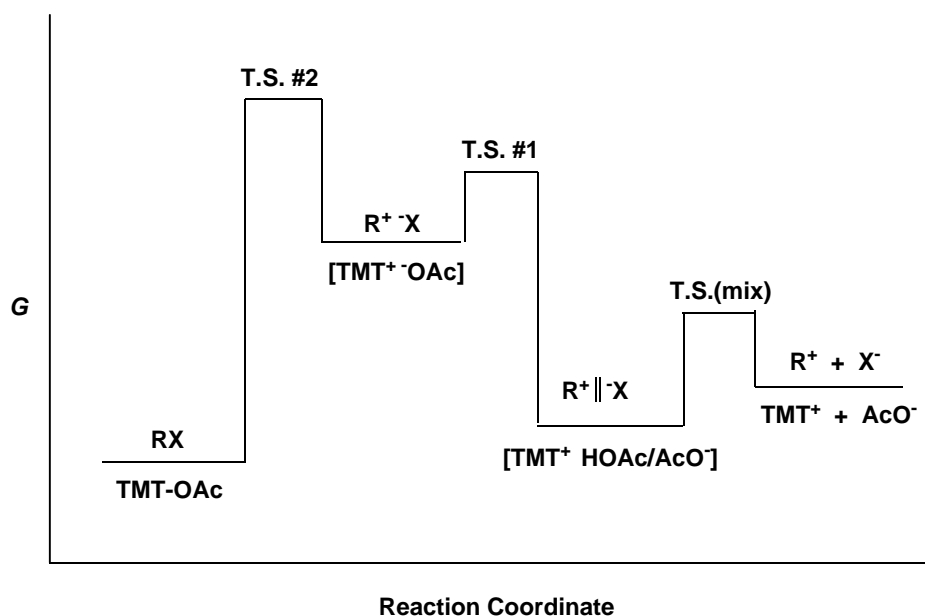


SCHEME 6-7. Winstein Solvolysis Scheme



The reaction coordinate diagram (Scheme 6-8) illustrates the reactions shown in the horizontal line in Scheme 6-7 compared to the dissociation of TMT-OAc. The free energies (G) of wide bars are drawn to approximately correspond to the relative energies of the various species which we are able to estimate from our kinetic data for the reaction of TMT^+ with acetate ion in acetic acid. The designation of the three transition states, T.S. (mix), T.S. #1, and T.S. #2, refer to the TMT^+ system and T.S. (mix) is labeled to show that this step takes place during the time of mixing in the stopped-flow experiments. The labeling of the other transitions states (T.S. #1 and T.S. #2) is consistent with that in Scheme 6-6.

SCHEME 6-8. Comparison of Winstein Scheme to the TMT^+ System



The correspondence of the reaction coordinate deduced from kinetic data for the dissociation of TMT-OAc in acetic acid to that for the Winstein scheme is

truly remarkable. This suggests that $\{\text{TMT}^+ \text{HOAc}/\text{AcO}^-\}$ is really a solvent (HOAc) separated ion pair and that the “Reactant Complex” is an intimate ion pair. All of our data can be reconciled with this formulation. When considered in this context this work can be considered to be a direct kinetic verification of the Winstein³⁷ scheme which was based on the more indirect evidence provided by the addition of three different types of salts: (a) a common ion salt (LiX for solvolysis of RX), (b) salts with nonreactive anions (LiY for solvolysis of RX) the effect of which can be attributed to increasing the ionic strength and (c) salts of reactive anions (for example, LiN_3 for the solvolysis of RX) which result in the formation of a stable compound.

Analysis of $k_{\text{s.s.}}$ data in the temperature range from 293 to 323 K resulted in ΔH^\ddagger and ΔS^\ddagger equal to 12.2 kcal/mol and -22.4 cal/mol K, respectively. Over the same temperature range, ΔH° and ΔS° for equilibrium (4) were observed to be equal to -4.22 kcal/mol and -14.0 cal/mol K, respectively. It is of interest to note that the cation – anion combination reaction between TMT^+ and NaOAc in acetic acid is exothermic ($\Delta H^\circ = -4.22$ kcal/mol) with a significantly large barrier ($\Delta H^\ddagger = 12.2$ kcal/mol, calculated from $k_{\text{s.s.}}$ data). Since our evidence strongly suggest that this cation – anion combination is a unimolecular reaction of the solvent separated ion-pair and takes place in two steps, the activation parameters refer to two consecutive transition states. The data are illustrated in Figure 6-3. The corresponding plots for the reactions in HOAc/AN (1/1, v/v) are shown in Figure A-26, from which ΔH^\ddagger and ΔS^\ddagger were found to be equal to 13.7 kcal/mol and -20.6 cal/mol K, respectively. Values of ΔH° and ΔS° for equilibrium (4) were observed

to be equal to -1.40 kcal/mol and -5.22 cal/mol K, respectively. The activation parameters in the mixed solvent in the presence of Bu_4N^+ ion are very nearly the same as those observed in HOAc in the presence of Na^+ ion. On the other hand, both thermodynamic parameters for equilibrium (4) are considerably more negative in the HOAc as solvent than were observed in mixed solvent.

It was mentioned earlier that the changes in the $k_N/k_{s.s.}$ ratios with wavelength in Tables 6-4 can be explained by interference from the absorbance by the intermediate. This appears to be consistent with the intermediate being the intimate ion pair $\{\text{TMT}^+ \text{ } ^-\text{OAc}\}$. We do not find any significant differences in the visible absorption spectrum of $\{\text{TMT}^+ \text{ HOAc/AcO}^-\}$ in HOAc/AN (1/1, v/v) and of $\{\text{TMT}^+ \text{ ClO}_4^-\}$ in CHCl_3 or of the former in HOAc. However, it is conceivable that the spectrum of $\{\text{TMT}^+ \text{ } ^-\text{OAc}\}$ is shifted slightly to lower wavelengths and that the observed absorbance at the higher wavelengths, during the reaction, is more reflective of that of the reactant, $\{\text{TMT}^+ \text{ HOAc/AcO}^-\}$.

Conclusions

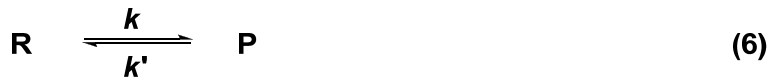
Our overall conclusion is that the cation – anion combination reactions of TMT^+ with acetate salts in acetic acid involve the formation of $\{\text{TMT}^+ \text{ HOAc/AcO}^-\}$, which we regard as a solvent separated ion-pair, during the time of mixing. The intramolecular collapse of the solvent separated ion-pair then takes place by a two-step mechanism (Scheme 6-4) involving the formation of a kinetically significant “Reactant Complex” as an intermediate which we propose to be the intimate ion pair, $\{\text{TMT}^+ \text{ } ^-\text{OAc}\}$. This mechanism conforms remarkably well to the

Winstein³⁷ scheme for the ionization of RX (TMT-OAc in this case) as shown in the comparison illustrated in Scheme 6-8.

In other work, we have proposed that the “Reactant Complex” is a tight complex formed by extrusion of solvent and appropriate geometry changes from the encounter complex or in other cases from the corresponding charge-transfer complex.^{26,30,32} It would appear that the latter description can apply equally well to conversion of a solvent separated ion pair to an intimate ion pair. Obviously, our findings are unexpected from studies of carbocation – anion combinations that have appeared in the interim between the 1950s and the present time. Our observation that the HOAc/AcO[−] solutions are ideal systems to obtain detailed kinetic and mechanism information on these important reactions will eventually provide the means to greatly increase our knowledge of how these reactions take place.

Experimental Section

Kinetic Analysis. The appropriate integrated rate law for the pseudo-first-order reversible reaction (6) is given by eq 7 where A_o^R , A_{eq}^R , and A_t^R are the reactant absorbances at zero time, at equilibrium and at time (t), respectively. Equation 7 is directly applicable at wavelengths where the reactant is the only absorbing species. Under these circumstances A_{eq}^R is directly measured as the plateau absorbance at long times.



$$\ln \left[\frac{A_o^R - A_{eq}^R}{A_t^R - A_{eq}^R} \right] = (k + k')t \quad (7)$$

The first step in our analysis is to convert the $(A_o^R - A_{eq}^R)$ – time profile to an extent of reaction – time profile by dividing $(A_t^R - A_{eq}^R)$ by $(A_o^R - A_{eq}^R)$ at each time point in the absorbance – time array. Any kinetic operations on the extent of reaction time profile defined in this way give results equivalent to those when using the pseudo-first-order relationship but in this case the apparent rate constant is equal to the sum of forward and reverse rate constants, $k_{app} = k + k'$.

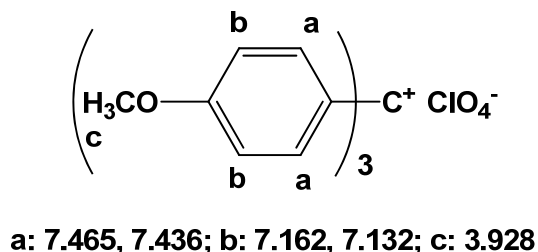
Experimental Procedure for Kinetic Studies. Solvents and Reactants.

Acetic acid and acetonitrile were of the highest purity level commercially available and distilled before use. Sodium acetate was ACS reagent grade and used without further purification.

Preparation of $Bu_4N^+(HOAc/AcO^-)$. A 40% aqueous solution of Bu_4NOH (0.008 mol) was allowed to react with 2 equiv of $HOAc$ (0.016mol) in CH_2Cl_2 at room temperature. After stirring for about 30 min, anhydrous sodium sulfate (about 10 g) was added to remove most of the water. The CH_2Cl_2 solution was filtered through anhydrous sodium sulfate before removing the solvent under vacuum. The resulting white solid ($Bu_4N^+ HOAc/OAc^-$, 0.0048 mol) was washed thoroughly with anhydrous ether and the residual ether was removed under vacuum.

Preparation of 4,4',4''-Trimethoxytrityl Perchlorate. 4,4',4''-Trimethoxytrityl chloride (1 mmol) was allowed to react with silver perchlorate (1 mmol) in acetonitrile (50 mL) at room temperature. After the precipitation of silver chloride, the solution was filtered to remove $AgCl$, and the solvent was removed under vacuum and dried to gave a red solid (0.89 mmol $TMT^+ClO_4^-$) identified by its

^1H NMR spectrum (solvent: $\text{CD}_3\text{CO}_2\text{D}/\text{CDCl}_3 = 1/2$). The signals at 1.881 to 1.856, 11.533 and 7.254 are due acetic acid and CHCl_3 , respectively. The ^1H NMR assignments are summarized below; and the spectrum is illustrated in Figure A-29. The ^1H NMR spectra for the equilibrium reaction mixture is illustrated in Figure A-30.



Kinetic Measurements. A Hi-Tech Scientific SF-61 Stopped-Flow Spectrophotometer with a Techne Flow Cooler FC-200 thermostat to control the temperature of the cell block within ± 0.2 K in a glove box under a nitrogen atmosphere was used for kinetic measurements. Data, 2000 points over a time range about 10% greater than the first half-life, were collected under pseudo-first-order conditions at 298 K.

Kinetic Procedure. The stopped-flow instrument used a single-beam light path. This necessitated subtraction of background absorbance which was obtained by having pure solvent in the reactant syringe and the excess reagent in the other syringe in the same concentration used in the kinetic experiments. Three background shots were recorded before each set of kinetic shots and all data points were averaged. A minimum of twenty shots under kinetic conditions were recorded in each set of measurements. The kinetic absorbance – time curves were first averaged, background absorbance was subtracted and the zero

time absorbance (Abs_0) was calculated by a linear least-squares procedure using the first seven data points. The absorbance – time arrays were converted to (1 - E.R.) – time profiles in the manner described in the previous section. The reactant extinction coefficient was calculated from Abs_0 and the known reactant concentration.

Data Handling Procedures. The procedures used have been described in detail.^{24,33} Additional information specific to the IRC procedure are presented here. The application of the IRC method on calculated data (Figure 5-1) was used to illustrate the response of the one-step and the pre-association mechanisms. The application of the method is somewhat more complex on experimental data since calculating IRC between successive points amplifies the effect of instrumental noise.³³ We have found that smoothing (1 - E.R.) – time profiles by fitting to fifth order polynomial equations does not give noticeable distortion in the data as long as the fit is limited to the first 3% of the profile (or if the initial 3% of the data are excluded and the remainder of the profile is fit precisely by that treatment).³³ An alternative method to approximate IRC is to carry out a sliding 51 point analysis in which the IRC for the midpoint of the initial interval (point 26) is estimated from the pseudo-first-order rate constant derived from the 51 data points. The IRC for subsequent points (27 to 1975 for a 2000 point array) are obtained by sequentially sliding the data segment analyzed by one point. The IRC for point 27 is obtained from the points ranging from 2 to 52 that for point 28 from points ranging from 3 to 53, and so forth until IRC for point 1976 are obtained from the data segment from point 1950 to 2000. The

disadvantage of the latter method is that IRC for short times are not available from the analysis.

References

- (1) Turgeon, V.C.; LaMer, V. K. *J. Am. Chem. Soc.* **1952**, *74*, 5988.
- (2) Duynstee, E. F. J.; Grunwald, E. *J. Am. Chem. Soc.* **1959**, *81*, 4342.
- (3) Diffenback, R. A.; Sano, K.; Taft, R. W. *J. Am. Chem. Soc.* **1966**, *88*, 4747.
- (4) Ritchie, C. D.; Skinner, G. A.; Badding, V. G. *J. Am. Chem. Soc.* **1967**, *89*, 2063.
- (5) Hill, E. A.; Mueller, W. J. *Tetrahedron Lett.* **1968**, 2565.
- (6) Noyce, D. S.; Brauman, S. K. *J. Am. Chem. Soc.* **1968**, *90*, 5218.
- (7) Brauman, J. I.; Archie, W. C., Jr. *J. Am. Chem. Soc.* **1970**, *92*, 5981.
- (8) Ritchie, C. D.; Virtanen, P. O. I. *J. Am. Chem. Soc.* **1972**, *94*, 4963, 4966.
- (9) Bunton, C. A.; Huang, S. K. *J. Am. Chem. Soc.* **1972**, *94*, 3536.
- (10) Ritchie, C. D. *Acc. Chem. Res.* **1972**, *5*, 348.
- (11) Ritchie, C. D.; Virtanen, P. O. I. *J. Am. Chem. Soc.* **1973**, *95*, 1882.
- (12) Bunton, C. A.; Huang, S. K. *J. Am. Chem. Soc.* **1974**, *96*, 515.
- (13) Ritchie, C. D. *J. Am. Chem. Soc.* **1975**, *97*, 1170.
- (14) Ritchie, C. D.; Sawada, M. *J. Am. Chem. Soc.* **1977**, *99*, 3754.
- (15) Ritchie, C. D.; Van Verth, J. E.; Virtanen, P. O. I. *J. Am. Chem. Soc.* **1982**, *104*, 3491.
- (16) Ritchie, C. D. *J. Am. Chem. Soc.* **1984**, *106*, 7187.
- (17) Ritchie, C. D. *Can. J. Chem.* **1986**, *64*, 2239.

- (18) Arnett, E. M.; Flowers, R. A.; Ludwig, R. T.; Meekhof, A.; Walek, S. *Pure Appl. Chem.* **1995**, 67, 729.
- (19) Mayr, H.; Kempf, B.; Ofial, A. R. *Acc. Chem. Res.* **2003**, 36, 66 and references cited therein.
- (20) Minegishi, S.; Mayr, H. *J. Am. Chem. Soc.* **2003**, 125, 286.
- (21) Parker, V. D.; Zhao, Y.; Lu, Y.; Zheng, G. *J. Am. Chem. Soc.* **1998**, 120, 12720.
- (22) Lu, Y.; Zhao, Y.; Parker, V. D. *J. Am. Chem. Soc.* **2001**, 123, 5900.
- (23) Zhao, Y.; Lu, Y.; Parker, V. D. *J. Chem. Soc., Perkin Trans. 2* **2001**, 1481.
- (24) Parker, V. D.; Zhao, Y. *J. Phys. Org. Chem.* **2001**, 14, 604.
- (25) Zhao, Y.; Lu, Y.; Parker, V. D. *J. Am. Chem. Soc.* **2001**, 123, 1579.
- (26) Lu, Y.; Zhao, Y.; Handoo, K. L.; Parker, V. D. *Org. Biomol. Chem.* **2003**, 1, 173.
- (27) Handoo, K. L.; Lu, Y.; Zhao, Y.; Parker, V. D. *Org. Biomol. Chem.* **2003**, 1, 24.
- (28) Lu, Y.; Handoo, K. L.; Parker, V. D. *Org. Biomol. Chem.* **2003**, 1, 36.
- (29) Parker, V. D.; Lu, Y. *Org. Biomol. Chem.* **2003**, 1, 2621.
- (30) Handoo, K. L.; Lu, Y.; Zhao, Y.; Parker, V. D. *J. Am. Chem. Soc.* **2003**, 125, 9381.
- (31) Parker, V. D.; Lu, Y.; Zhao, Y. *J. Org. Chem.* **2005**, 70, 1350.
- (32) Parker, V. D. *Pure Appl. Chem.* **2005**, 77, 1823.
- (33) Parker, V. D. *J. Phys. Org. Chem.* **2006**, 19, 714.

- (34) Ridd, J. H. *Adv. Phys. Org. Chem.* **1978**, 16, 1.
- (35) Clark, J. H.; Emsley, J. *J. Chem. Soc., Dalton Trans.* **1973**, 2760.
- (36) Guthrie, J. P. *J. Am. Chem. Soc.* **1978**, 100, 5892; **1974**, 96, 3608; **1973**, 95, 6999.
- (37) Winstein, S.; Clippenger, E.; Fainsberg, A. H.; Heck, R.; Robinson, G. C. *J. Am. Chem. Soc.* **1954**, 78, 328 and references cited.

CHAPTER 7

THE MECHANISM OF COVALENT BOND FORMATION DURING THE COMBINATION OF NITROSTYRENE WITH NUCLEOPHILES

Abstract

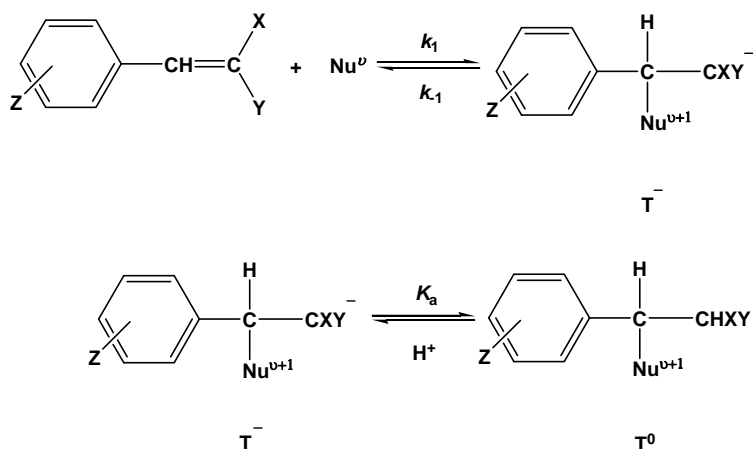
Trans- β -nitrostyrene undergoes a combination reaction with nitroethide ion in acetonitrile-water or DMSO-water resulting in the formation of the carbanionic adduct. The rate of the reaction in DMSO-water was observed to be about 160 folds of that of in acetonitrile-water. Conventional pseudo-first-order analysis as well as instantaneous rate constant analysis showed that the reaction takes place in two steps presumably by the pre-association mechanism. Computations at the M06-2x/6-31+G(d) level are consistent with the experimental study and provide the structure of the reactant complex intermediate.

Introduction

Trans- β -nitrostyrene (BNS) has long been known to undergo combination reactions with nucleophiles including thiolate ion,¹ alkoxide ions,²⁻³ hydroxide anions,⁴⁻⁷ carbon anions⁸⁻¹⁰ and secondary amines.¹¹⁻¹² In the case of ionic nucleophiles the products of the reactions were observed to be the carbanion resulting from the attack of the nucleophile upon the double bond accompanied by the formation of a single covalent bond. Bernasconi's group has devoted considerably effort in the study of nucleophilic addition to olefins reactions.⁵⁻⁹ The general mechanism for the Michael addition reactions shown in their work is illustrated in Scheme 7-1, where X and Y are electron-withdrawing groups. The

second step, acid – base equilibrium is usually rapid on the time scale of the first step, although in some cases it has been found to be (partially) rate limiting.¹³

SCHEME 7-1. The Michael Addition Reaction



They reported that the same rate was observed when monitoring reactants or products which shows that no intermediate accumulates during the Michael addition reactions studied and that excellent first-order behavior was observed in all cases. Table 7-1 summarizes the rate and equilibrium constants for the reaction of benzylidenemalononitrile (BMN) with $\text{CH}(\text{CN})_2^-$, piperidine, and morpholine disclosed in their kinetic study.⁸

TABLE 7-1. Rate and Equilibrium Constants for the Reactions of BMN with $\text{CH}(\text{CN})_2^-$, Piperidine, and Morpholine

constants	$\text{CH}(\text{CN})_2^-$		piperidine ¹³	morpholine ¹⁴
	Water, 298 K	DMSO/Water (1/1), 293 K	DMSO/Water (1/1), 293 K	DMSO/Water (1/1), 293 K
$k_1/\text{M}^{-1}\text{s}^{-1}$	3.44×10^5	9.50×10^5	2.10×10^5	5.9×10^4
k_{-1}/s^{-1}	7.69	6.52	1.36×10^4	2.6×10^5
$\text{p}K_a^{\text{CH } a}$	6.19	5.07	8.43	8.43
$\text{p}K_a^{\text{Nu } b}$	11.19	10.21	11.00	8.72

^a Refers to T^0 ; ^b Refers to $\text{CH}_2(\text{CN})_2$, piperidine H^+ and morpholine H^+ , respectively.

It is obvious they treated the first step of the Michael addition reactions as a simple one-step process. Over the past several years we have reported that a number of fundamental organic reactions, long believed to take place by one-step mechanisms, actually take place by more complex mechanisms involving the formation of kinetically significant intermediates. The reactions include an E₂ elimination reaction,¹⁵ a Diels-Alder reaction,¹⁶ the reaction of 2, 4, 6-trinitroanisole (TNA) with methoxide ion¹⁷ and proton transfer from simple nitroalkanes to hydroxide ion.¹⁸ In this chapter, we report the kinetics and mechanism of the reaction of BNS with nitroethide ion in acetonitrile-water (AN/W = 3/1, v/v) or DMSO-water (3/1, v/v) to give solutions of the corresponding stable carbanion. Our experimental data are inconsistent with the simple one-step mechanism and once more suggests the kinetically significant complex mechanism.

The simplest bimolecular organic reaction possible is the combination of two reactants resulting in the formation of only one covalent bond without an accompanying cleavage of any single bonds. The combination of anions with BNS to give the stable carbanions is an example of such reactions. These systems offer the possibility of studying the mechanism of a single covalent bond formation.

Results and Discussion

The spectra illustrated in Figure 7-1 were obtained during the reaction of BNS (0.0001 M) with nitroethide ion (0.01 M) in AN/W (3/1, v/v). The absorbance due to reactant indicated by the downward arrow decreases in the expected manner while that due to the carbanionic product was masked by the BNS

absorbance. The spectra suggest conversion of substrate to product without the intervention of significant side-reactions.

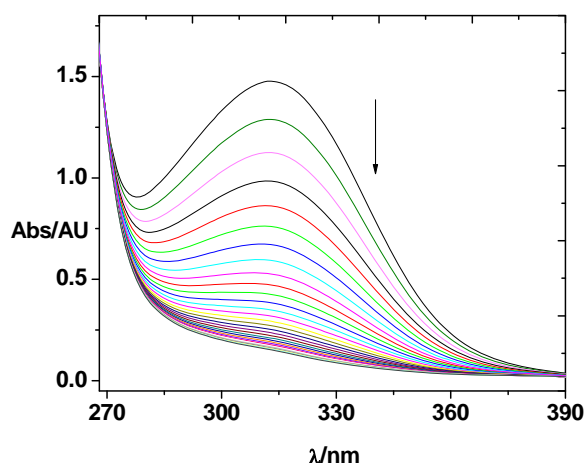


FIGURE 7-1. UV/Vis spectra during the reaction of BNS (0.0001 M) with nitroethide ion (0.01 M) in AN/W (3/1, v/v) at 298 K. Time between spectra equals 20 s. The last spectrum shown is the 30th recorded at 600s.

Half-Life Dependence of Conventional Pseudo-First-Order Rate

Constants. Whether or not the reactions conform to simple mechanism kinetics can be assessed by the conventional first-order analysis of $\ln(1 - \text{E.R.})$ – time profiles where E.R. is the extent of reaction. The data obtained from the conventional pseudo-first-order study for the reaction of BNS with nitroethide ion in two different solvents at 298K are summarized in Table 7-2 and Tables A-23 – A-27. When the solvent is AN/Water (3/1, v/v), the values of the apparent pseudo-first-order rate constant (k_{app}) steadily decreased from 0.0473 over the first 0.5 half-lives (HL) to 0.0368 at 4.0 HL, approximately with a change of 22%. A similar pattern of k_{app} as a function of the degree of reaction encompassed in the analysis was observed when the solvent is DMSO/Water (3/1, v/v) (column

3), but in this case the variations were much greater, 0.823 to 0.490 over the same range of degree of reaction, about a change of 40%. In contrast to the modest changes in k_{app} observed, the corresponding changes in the zero-time intercepts are much more remarkable, which indicates that this parameter is much more sensitive to the deviations from the first-order kinetics than k_{app} is. These values are also listed in the Table 7-2. Obviously, the response expected for the simple one-step mechanism is a constant value of k_{app} and an intercept independent of the number of HL taken into the linear least squares correlation.

TABLE 7-2. Changes in the Slopes and the Intercepts with the Extent of Reaction During Conventional Pseudo-First-Order Analysis for the Reaction of BNS with Nitroethide Ion in Two Different Solvents at 298K and 310 nm

No. HL	in AN/Water (3/1, v/v) ^a		in DMSO/Water (3/1, v/v) ^b	
	k_{app}/s^{-1}	intercept/ s^{-1}	k_{app}/s^{-1}	intercept/ s^{-1}
0.5	0.0473	-0.000384	0.823	-0.00733
1.0	0.0457	0.00480	0.807	-0.00412
2.0	0.0438	0.0196	0.770	0.0131
3.0	0.0413	0.0536	0.703	0.0685
4.0	0.0368	0.149	0.490	0.380

^a [BNS] = 0.1 mM, [Nitroethide] = 0.04 M; ^b [BNS] = 0.05 mM, [Nitroethide] = 5.0 mM.

The plots shown in Figure 7-2 allow visual inspection of pseudo-first-order analyses of the reaction of BNS with nitroethide ion. The large deviations between the experimental data using conventional first-order analysis and the least-squares linear fit for the simple one-step mechanism clearly reveal that the reaction does not conform to simple one-step mechanism kinetics. The left profile is for the reaction in AN/W (3/1, v/v) and the right one is in DMSO/W (3/1, v/v). The most obvious results of a visual comparison of the pseudo-first-order plots

on the left and the right of Figure 7-2 are that (1) the deviation of the experimental data from the least-squares correlation line is significantly greater when the solvent is DMSO/W (3/1, v/v) than AN/W (3/1, v/v) and (2) the slope of the correlation line is more than an order of magnitude greater for the former even though the [nitroethide] is a factor of 2 lower.

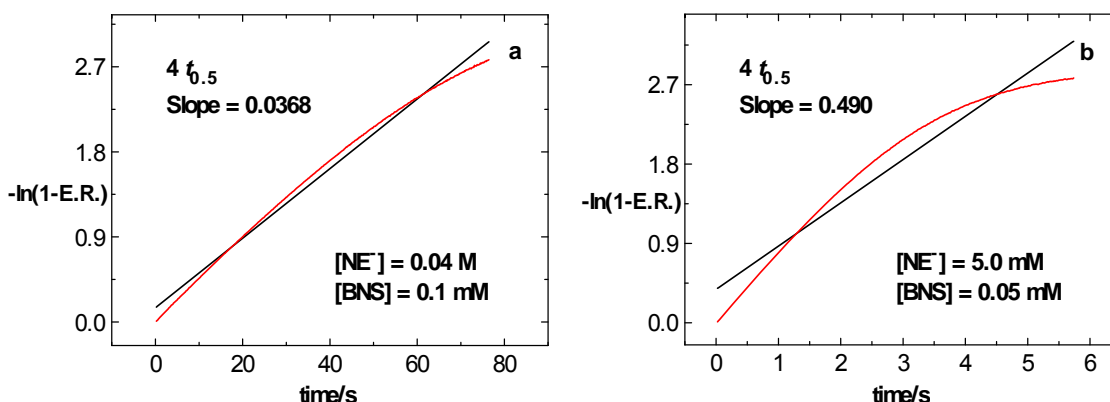


FIGURE 7-2. Pseudo-first-order plots for the reaction of BNS with nitroethide ion in AN/W (3/1, v/v) (a) and DMSO/Water (3/1, v/v) (b) at 298 K and 310 nm. Red line is our experimental data using conventional first-order analysis and dark line is the least square linear fit for simple one-step mechanism.

Numerical Mechanism Probes. The time ratio ($t_{0.50}/t_{0.05}$) is a very useful mechanism probe in the analysis of reaction mechanism.¹⁹⁻²⁰ The time ratio is equal to 13.5 for a pseudo-first-order reaction taking place in a simple one-step (1) regardless of whether reactant or product is monitored. The time ratio data for the reaction between BNS and nitroethide ion, along with second-order rate constants as a function of the wavelength of the measurement are summarized in Table 7-3. The value of the time ratio for a more complex mechanism, in particular for the “pre-association” mechanism (2) depends upon whether reactant decay (≥ 13.5) or product evolution (≤ 13.5) is monitored. The data in

Table 7-3 were obtained at wavelengths where reactant, but not product, has significant absorbance. At all wavelengths monitored, the time ratio is greater than 13.5 which is consistent with the decrease in reactant absorbance with time for complex mechanism. The variation in the time ratio may be a reflection of absorbance due to the intermediate which is present in low concentrations. There is a significant solvent effect: the reaction rate constants are much larger in aqueous DMSO than in aqueous acetonitrile. Considering the data observed at 340 nm, the second-order rate constant is about $1 \text{ M}^{-1}\text{s}^{-1}$ in aqueous acetonitrile while in aqueous DMSO the second-order rate constant is observed to be $169 \text{ M}^{-1}\text{s}^{-1}$. The solvent effect is most likely, in part, due to the fact that the more polar aqueous DMSO solvent more strongly destabilizes the anions. The effective [HOH] concentration may also be lower in DMSO due to its greater H-bonding ability.

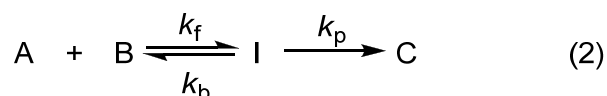
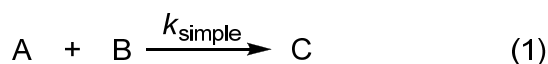


TABLE 7-3. Time Ratios and Second-Order Rate Constants for the Combination Reaction of BNS with Nitroethide Ion in AN/Water (3/1, v/v) and DMSO/Water (3/1, v/v) at 298K over a Range of Wavelengths

λ/nm	AN/W (3/1, v/v) ^a		DMSO/W (3/1, v/v) ^b	
	$t_{0.50}/t_{0.05}$	$k_2/\text{M}^{-1}\text{s}^{-1}$	$t_{0.50}/t_{0.05}$	$k_2/\text{M}^{-1}\text{s}^{-1}$
310	14.5	1.13	14.0	170
320	14.4	1.16	13.9	172
330	14.4	1.17	14.5	167
340	14.6	1.17	14.5	169
350	15.1	1.17	15.2	173
360	15.6	1.16	15.4	171

^a [BNS] = 0.1 mM, [Nitroethide] = 0.04 M; ^b [BNS] = 0.05 mM, [Nitroethide] = 5.0 mM.

Sequential Pseudo-First-Order Linear Correlation. The 24-point sequential non-conventional kinetics analysis has been described in previous chapters. The apparent rate constants for the reaction of BNS with nitroethide ion in two different solvents obtained using the successive correlation method are summarized in Table 7-4 and Tables A-28 – A-31. It is obvious that the k_{app} – time profiles begin at relatively high values of k_{app} and decay with time toward steady-state values at all of the wavelengths. At 320 nm, the value of k_{app} in segment 1 was observed to be equal to 0.0762 s^{-1} and then was observed to decrease steadily to 0.0450 s^{-1} at segment 24 when the solvent is AN/Water (3/1, v/v). A similar pattern of k_{app} as a function of time in the analysis was observed when the solvent is DMSO/Water (3/1, v/v), but in this case the k_{app} decreases from 1.026 s^{-1} to 0.802 s^{-1} over the same range of degree of reaction (over the first half-life). The expected result of the sequential 24-point procedure for the simple one-step mechanism is an apparent rate constant, independent of time and of the particular time segment analyzed.

The apparent instantaneous rate constants (k_{IRC}) – time profiles for the reaction between BNS and nitroethide ion in two different solvents are illustrated by the plots in Figure 7-3 and Figures A-31 – A-34. The k_{IRC} – time profiles have the form expected for reactant decay in a complex mechanism decreasing rapidly from an initial value of close to 0.09 s^{-1} when the solvent is AN/Water (3/1, v/v) (a) and 0.93 s^{-1} when the solvent is DMSO/Water (3/1, v/v) (b), respectively, toward steady-state values, while that expected for the simple one-step mechanism is a straight line with zero slopes.

TABLE 7-4. Apparent Rate Constants and Standard Deviations Obtained by the Sequential Pseudo-First-Order Analysis for the Reaction of BNS with Nitroethide Ion in AN/Water (3/1, v/v) and DMSO/Water (3/1, v/v) over the First Half-Life at 298K and 320 nm

time/s	AN/W (3/1, v/v) ^a		time/s	DMSO/W _b (3/1, v/v)		Segment
	k_{app}/s^{-1}	\pm		k_{app}/s^{-1}	\pm	
0.047	0.0762	0.0114	0.002	1.026	0.280	1
0.089	0.0687	0.0037	0.005	0.937	0.189	2
0.132	0.0606	0.0032	0.007	0.913	0.180	3
0.174	0.0569	0.0035	0.009	0.899	0.097	4
0.217	0.0542	0.0036	0.011	0.887	0.062	5
0.429	0.0495	0.0024	0.023	0.843	0.042	6
0.854	0.0475	0.0007	0.045	0.826	0.021	7
1.279	0.0467	0.0013	0.067	0.824	0.020	8
1.704	0.0462	0.0014	0.090	0.820	0.018	9
2.129	0.0459	0.0014	0.112	0.817	0.015	10
2.554	0.0457	0.0014	0.135	0.817	0.012	11
2.979	0.0456	0.0013	0.157	0.816	0.010	12
3.404	0.0455	0.0013	0.179	0.815	0.009	13
3.829	0.0454	0.0012	0.202	0.814	0.008	14
4.254	0.0454	0.0012	0.224	0.813	0.007	15
4.679	0.0453	0.0011	0.247	0.812	0.007	16
5.104	0.0453	0.0011	0.269	0.811	0.006	17
5.529	0.0453	0.0010	0.291	0.810	0.006	18
5.954	0.0452	0.0010	0.314	0.808	0.006	19
6.379	0.0452	0.0010	0.336	0.807	0.006	20
6.804	0.0451	0.0010	0.359	0.806	0.006	21
7.229	0.0451	0.0010	0.381	0.805	0.006	22
7.654	0.0451	0.0009	0.403	0.803	0.006	23
8.079	0.0450	0.0009	0.426	0.802	0.006	24

^a [BNS] = 0.1 mM, [Nitroethide] = 0.04 M; ^b [BNS] = 0.05 mM, [Nitroethide] = 5.0 mM. Average of 3 sets of 20 stopped-flow repetitions.

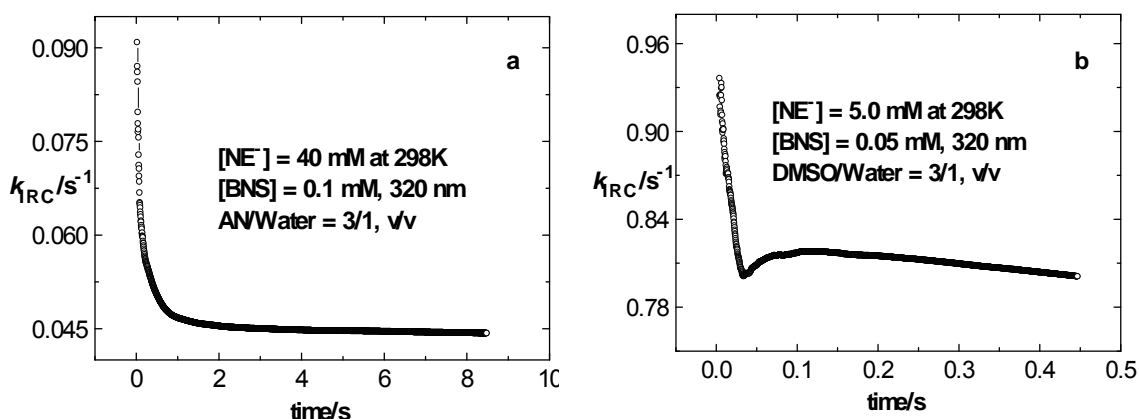
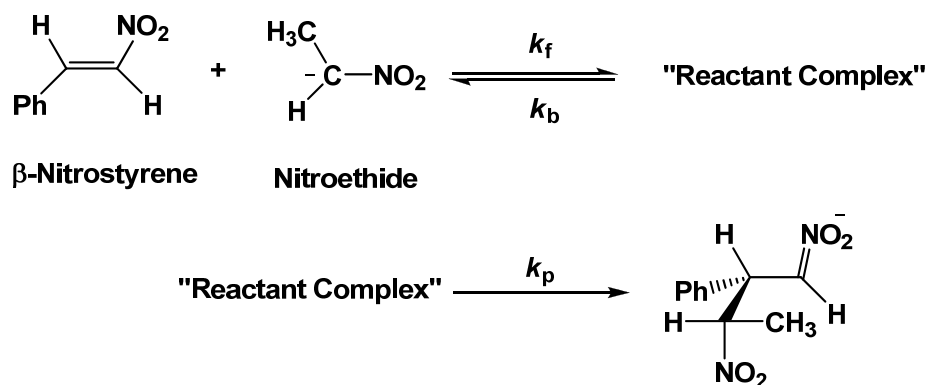


FIGURE 7-3. Apparent instantaneous rate constants (k_{IRC}) – time plots for the reaction between BNS and nitroethide ion in ion AN/Water (3/1, v/v) (a) and DMSO/Water (3/1, v/v) (b) at 298K and 320 nm.

All of the kinetic data for the reaction between BNS and nitroethide ion are consistent with the “pre-association” mechanism in which the intermediate (“Reactant Complex”) is kinetically significant (Scheme 7-2). The fact that the overall reaction is so simple, *i.e.*, the combination reaction only involves the formation of a covalent bond between nitroethide ion and the α -carbon of BNS, strongly suggests that the “Reactant Complex” is not covalently bonded but rather held together by non-bonded interactions between the two reactants.

SCHEME 7-2. The Proposed Mechanism for the Reaction Between BNS and Nitroethide Ion



Computations at the M06-2x/6-31+G(d) level were carried out for the reaction of BNS with nitroethide ion in acetonitrile and provided the structures of the reactant complex and the transition state. The optimized structures shown in Figure 7-4 were confirmed by frequency calculations to be minima on the reaction coordinate using the same level of theory. In addition, the calculated reaction coordinate diagram for the reaction of BNS with nitroethide ion in acetonitrile is shown in Figure 7-5 where CP represents the reactant complex. The calculated transition state free energy is 12.0 kcal mol⁻¹. The experimental overall activation Gibbs free energy in AN/Water (3/1, v/v) is 17.3 kcal mol⁻¹ (second-order rate constants at various temperatures for this reaction are listed in Table A-32).

Conclusions

The Michael addition reaction between BNS and nitroethide ion in two different solvents including aqueous acetonitrile and aqueous DMSO takes place by a pre-association mechanism in which the intermediate is kinetically significant (Scheme 7-2). This conclusion was derived from the experimental kinetic data which upon analysis revealed time dependent apparent rate constants for the reaction. Gaussian calculations at the M06-2x/6-31+G(d) level resulted in the observation of a reactant complex on the reaction coordinate leading to the transition state for the addition.

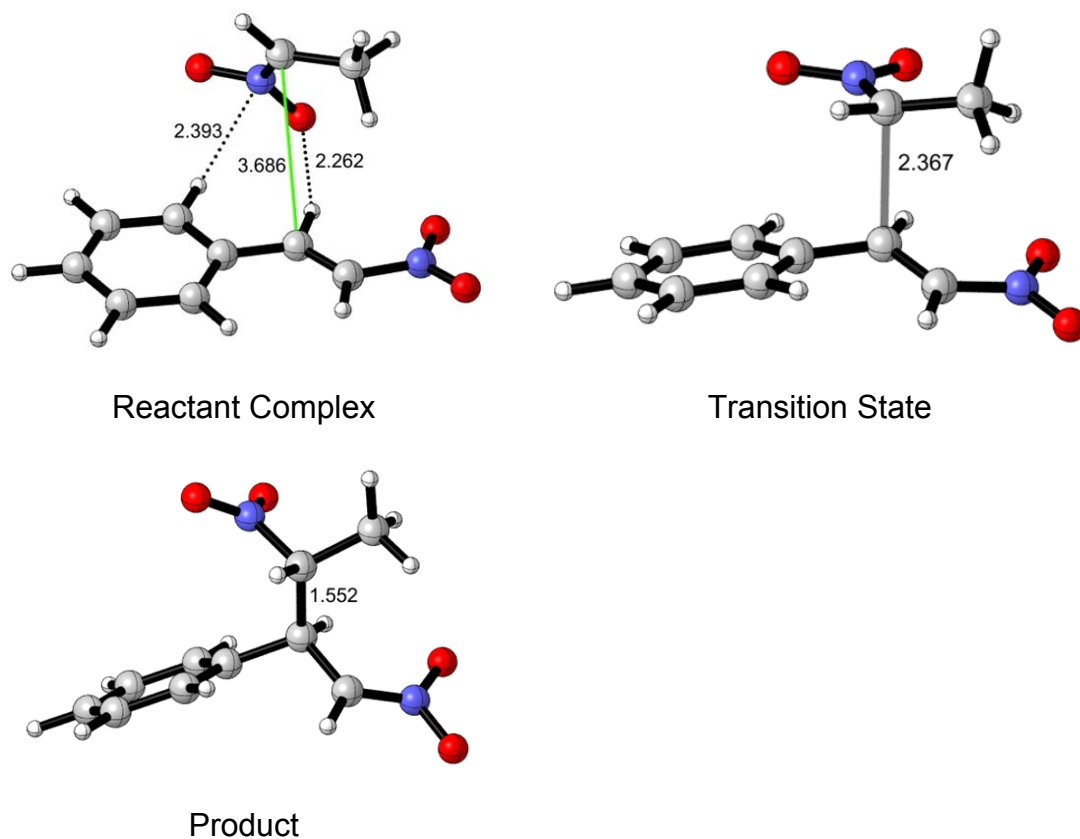


FIGURE 7-4. Optimized structures of reactant complex and transition state as well as product in acetonitrile with the M06-2x/6-31+(d)/SMD method.

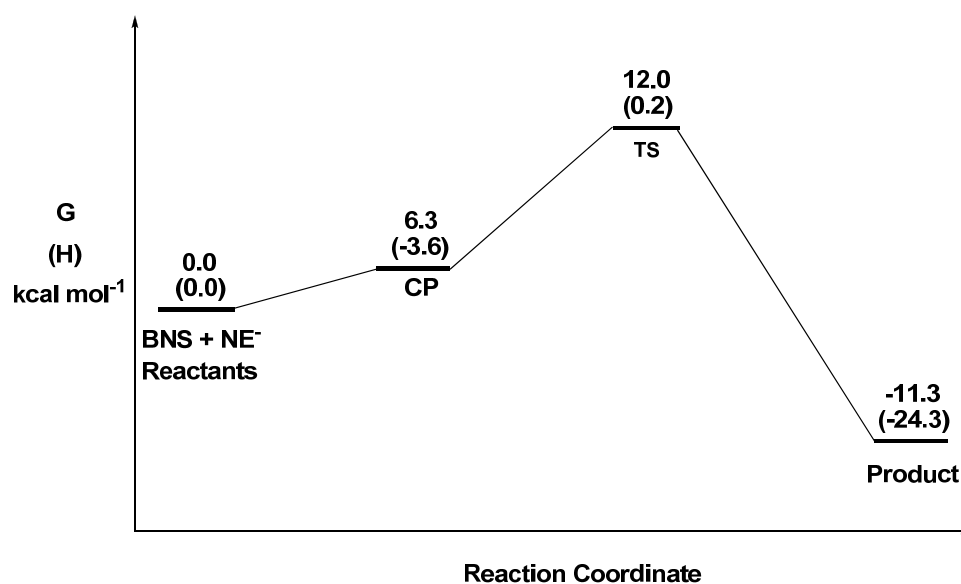


FIGURE 7-5. The reaction coordinate for the reaction of BNS and NE⁻ in acetonitrile at 298.15K calculated using the M06-2x/6-31+G(d)/SMD method.

Experimental Section

Materials. *Trans*- β -nitrostyrene was obtained commercially from Aldrich and recrystallized from isopropanol. Nitroethane was also obtained commercially from Aldrich and was redistilled at reduced pressure before use. Nitroethide ion was freshly prepared through the reaction of nitroethane with tetramethylammonium hydroxide for each experiment. Acetonitrile was refluxed and distilled over P_2O_5 under a nitrogen atmosphere and past through an Al_2O_3 column before transferring into the glove box. Distilled water was further purified by passing through a Barnsted Nanopure Water System. Commercial DMSO was redistilled at reduced pressure before use.

Kinetic Experiments. Kinetic experiments were carried out using a Hi-Tech SF-61 DX2 stopped-flow spectrophotometer installed in a glove box and kept under a nitrogen atmosphere. The temperature was controlled at 298 K using a constant temperature flow system connected directly to the reaction cell through a bath situated outside of the glove box. All stopped-flow experiments included the recording of at least 20 absorbance – time profiles over the wavelengths range from 310 nm to 360 nm at 10 nm intervals. Each experiment was repeated at least three times. The 2000-point absorbance – time curve data were collected over either 1+ or 4+ HL.

References

- (1) Bernasconi, C. F.; Schuck, D. F. *J. Org. Chem.* **1992**, 57, 2365.
- (2) Berry, R. W. H.; Mazza, R. J. *Polymer* **1973**, 14, 172-174.
- (3) Feit, B. A.; Bohor, L. J. *J. Chem. Soc., Perkin Trans. 2* **1974**, 1823.

- (4) Crowell, T. I., Kim, T.-R. *J. Am. Chem. Soc.* **1973**, 95, 6781.
- (5) Bernasconi, C. F.; Howard, K. A.; Kanavarioti, A. *J. Am. Chem. Soc.* **1984**, 106, 6827.
- (6) Bernasconi, C. F.; Paschalis, P. *J. Am. Chem. Soc.* **1989**, 111, 5893.
- (7) Bernasconi, C. F.; Flores, F. X.; Claus, J. J.; Dvorak, D. *J. Org. Chem.* **1994**, 59, 4917.
- (8) Bernasconi, C. F.; Zitomer, J. L.; Fox, J. P.; Howard, K. A. *J. Org. Chem.* **1984**, 49, 482.
- (9) Bernasconi, C. F.; Laibelman, A.; Zitomer, J. L. *J. Am. Chem. Soc.* **1985**, 107, 6570.
- (10) Zenz, I.; Mayr, H. *J. Org. Chem.* **2011**, 76, 9370.
- (11) Bernasconi, C. F.; Renfrow, R. A.; Tia, P. R. *J. Am. Chem. Soc.* **1986**, 108, 4541.
- (12) Bernasconi, C. F.; Renfrow, R. A. *J. Org. Chem.* **1987**, 52, 3035.
- (13) Bernasconi, C. F. *Tetrahedron* **1989**, 45, 4017.
- (14) Bernasconi, C. F.; Fox, J. P.; Fornarini, S. *J. Am. Chem. Soc.* **1980**, 102, 2810.
- (15) Handoo, K. L.; Lu, Y.; Zhao, Y.; Parker, V. D. *Org. Biomol. Chem.* **2003**, 1, 24-26.
- (16) Handoo, K. L.; Lu, Y.; Parker, V. D. *J. Am. Chem. Soc.* **2003**, 125, 9381.
- (17) Parker, V. D.; Li, Z.; Handoo, K. L.; Hao, W.; Cheng, J.-P. *J. Org. Chem.* **2011**, 76, 1250-1256.

- (18) Li, Z.; Cheng, J.-P.; Parker, V. D. *Org. Biomol. Chem.* **2011**, 9, 4563.
- (19) Parker, V. D.; Zhao, Y. *J. Phys. Org. Chem.* **2001**, 14, 604.
- (20) Parker, V. D. *Pure Appl. Chem.* **2005**, 77, 1823-1833.

CHAPTER 8

THE S_N2 DISPLACEMENT OF HALIDE IONS BY 4-NITROPHENOXIDE ION**Abstract**

The S_N2 reactions of *p*-nitrophenoxide ion (PNPO⁻) with *m*- or *p*-nitrobenzyl bromide (MNBBBr or PNBBBr) in acetonitrile were studied by instantaneous rate constant analysis and other non-steady-state kinetic methods under pseudo-first-order conditions. All of the kinetic data clearly show the behavior expected for the pre-association mechanism involving the reversible formation of a kinetically significant “reactant complex”. The latter is kinetically significant and gives rise to large deviations from first-order kinetics.

Introduction

An accepted definition of the S_N2 mechanism for a reaction in solution is: “The nucleophile approaches the substrate from the backside, 180° away from the leaving group. The reaction is a concerted process with no intermediate.” Since the mechanism was named in 1937 by Hughes and Ingold¹ this statement has been accepted as fact with very little discussion to the contrary.

Gas-phase experiments have contributed significantly to the current revival of interest in solvent effects on bimolecular substitution reactions. These investigations have provided striking evidence of the profound influence of solvation on rates and orders of nucleophilicity for S_N2 reactions of anions with alkyl halides. The kinetic data and quantum mechanical calculations have also revealed that the gas-phase reactions have double-well energy surfaces featuring ion-dipole complexes as minima.²⁻⁶ In contrast, the detailed shapes of

the energy surfaces for these important reactions in solution are largely a matter of conjecture. Unimodal, concerted profiles without intermediates are widely assumed in the literature.⁷⁻¹⁰

Calculations by Jorgensen¹¹⁻¹³ on the reaction between chloride ion and methyl chloride ($\text{Cl}^- + \text{CH}_3\text{Cl}$) in dimethylformamide (DMF) suggested that the corresponding ion-dipole complex appears as an energy minimum (Figure 8-1). His results lead one to question the likelihood of concerted $\text{S}_{\text{N}}2$ reactions in non-aqueous media, *i.e.*, proceeding without the presence of intermediates.¹⁴ Analyses of Brønsted plots for $\text{S}_{\text{N}}2$ reactions in DMSO have also been recently interpreted in terms of a two-stage mechanism.¹⁵

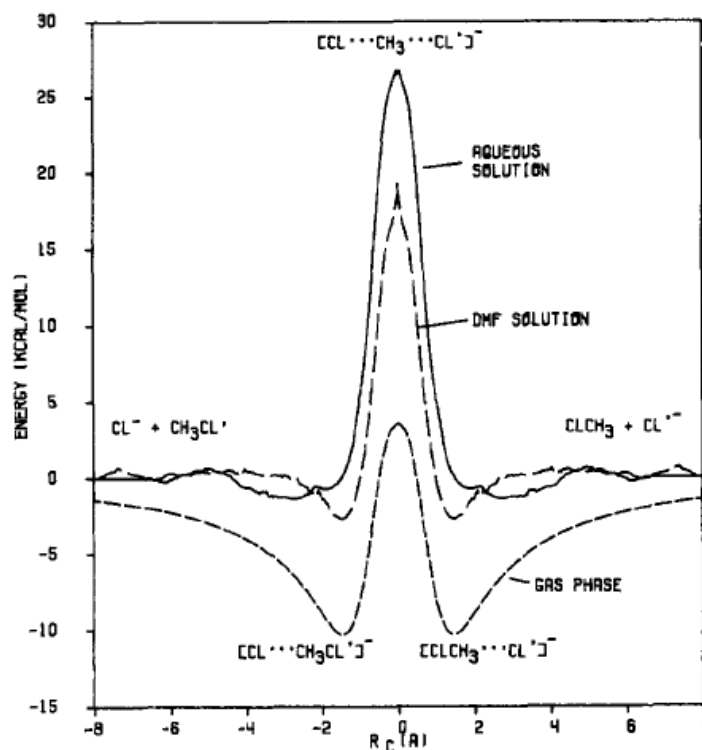


FIGURE 8-1. Calculated internal energies in the gas phase (short dashes) and the potential of mean force in DMF (long dashes) and in aqueous solution (solid curve) for the reaction of Cl^- with CH_3Cl as a function of the reaction coordinate, R_{C} , in angstroms.

A recent study shows¹⁶ that the details of the S_N2 mechanism are still of major interest. But in that study, Jorgensen no longer mentioned the intermediate ion-dipole complexes. That study dealt with the steric and solvation effects in the reactions of chloride ion with a series of alkyl chloronitriles with widely differing steric environment of the chloro bearing C atom. The solution kinetics were carried out in dimethyl formamide with tetraethylammonium ion as supporting counter ion. An interesting conclusion from this study is that the magnitude of the steric effect is not significantly different in the gas phase and in solution. The S_N2 potential energy surfaces proposed in that study are shown in Figure 8-2. It was suggested that the smaller ionic nucleophile (X^-) is solvated much better than the transition state, which is a large and dispersed ion.

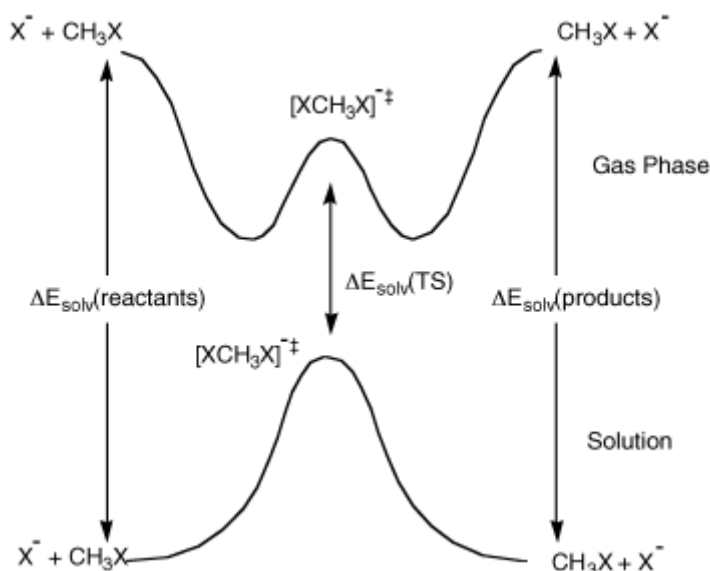
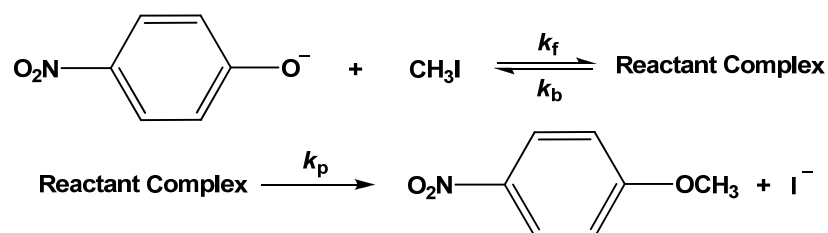


FIGURE 8-2. Comparison of gas-phase and solution-phase S_N2 potential energy surfaces.

Although the ion-dipole mechanism was suggested for some reactions of carbanion nucleophiles,¹⁷ there has not been much activity among organic chemists to test the generality of the latter. We have observed that the kinetics of the reaction between *p*-nitrophenoxide ion and methyl iodide in acetonitrile or aqueous acetonitrile are inconsistent with the simple one-step S_N2 mechanism and suggested the possibility of the formation of a kinetically significant intermediate (Scheme 7-1).¹⁸⁻¹⁹ Although significant, the results were presented in terms that are somewhat unfamiliar to most organic chemists in ionic S_N2 reactions.

SCHEME 8-1. The Mechanism for the Reaction Between PNPO⁻ and Methyl Iodide in Acetonitrile



We have now obtained definitive kinetic evidence that the displacement of halide ion from *m*-nitrobenzyl bromide (MNBBBr) or *p*-nitrobenzyl bromide (PNBBBr) by PNPO⁻ in acetonitrile takes place by a two-step pre-association mechanism. This evidence includes instantaneous rate constant (IRC) studies as well as conventional pseudo-first-order kinetic studies.

Results and Discussion

The spectra illustrated in Figure 8-3 were obtained during the reaction of PNPO⁻ (0.06 mM) with MNBBBr (0.04 M) in acetonitrile at 298 K. The absorbance

due to reactant indicated by the downward arrow decreases in the expected manner. The reactions were monitored by stopped-flow spectrophotometry at 10 nm intervals over the entire wavelength region of the broad absorbance band due to *p*-nitrophenoxide ion from 410 nm to 460 nm.

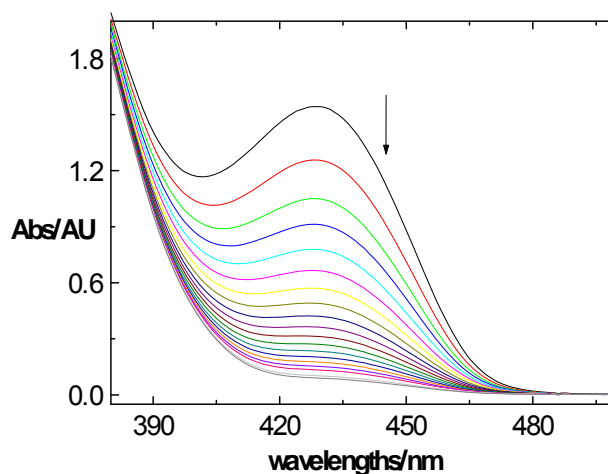


FIGURE 8-3. UV/Vis spectra during the reaction of PNPO^- (0.06 mM) with MNBBBr (0.04 M) in acetonitrile at 298 K. Time between spectra equals 120 s. The last spectrum shown is the 20th recorded at 2400s.

In this chapter, we will elucidate the actual mechanism of the topical displacement reaction in terms of the experimental kinetic data which were analyzed using the same methods as the previous chapters. The first analysis method we used in this chapter is the numerical mechanism probes. The mechanism probes, time ratio $t_{0.50}/t_{0.05}$ and rate constant ratio $k_{\text{init}}/k_{\text{s.s.}}$ provide a quantitative measure of the deviation from one-step behavior.²⁰ Table 8-1 summarizes the mechanism probe parameters observed for the displacement reaction between MNBBBr and PNPO^- in acetonitrile at 298 K along with values of the steady-state rate constants ($k_{\text{s.s.}}$) as a function of the wavelength of the

measurement. Under two different concentrations of MNBBBr (0.04 M and 0.08 M), all of the time ratios $t_{0.50}/t_{0.05}$ are significantly greater than 13.5, and the rate constant ratios $k_{\text{init}}/k_{\text{s.s.}}$ are significantly greater than unity observed while monitoring reactant decay over the entire applicable wavelengths. The results are consistent with the pre-association mechanism involving the reversible formation of a kinetically significant “reactant complex.” The wavelength dependent time and rate constant ratios also indicate that the reaction involves an intermediate. The values of $k_{\text{s.s.}}$ with 0.08 M MNBBBr are almost two times of those at 0.04 M MNBBBr.

TABLE 8-1. Time and Rate Constant Ratios for the Displacement Reaction Between MNBBBr and PNPO⁻ in Acetonitrile at 298K over a Range of Wavelengths

λ/nm	$t_{0.50}/t_{0.05}^a$	$k_{\text{init}}/k_{\text{s.s.}}^a$	$k_{\text{s.s.}}/\text{s}^{-1}^a$
410	21.8	2.06	0.00171
420	21.6	1.90	0.00175
430	18.1	1.52	0.00175
440	17.4	1.52	0.00177
450	17.6	1.55	0.00178
460	19.3	1.62	0.00169

λ/nm	$t_{0.50}/t_{0.05}^b$	$k_{\text{init}}/k_{\text{s.s.}}^b$	$k_{\text{s.s.}}/\text{s}^{-1}^b$
410	17.7	1.63	0.00339
420	17.9	1.81	0.00345
430	18.3	1.59	0.00349
440	20.3	2.01	0.00359
450	18.1	1.69	0.00350
460	16.3	1.48	0.00341

^a [MNBBBr] = 0.04 M, [PNPO⁻] = 0.06 mM. ^b [MNBBBr] = 0.08 M, [PNPO⁻] = 0.06 mM.

Similar results were obtained for the displacement reaction between PNBBBr and PNPO⁻ in acetonitrile at 298 K and are summarized in Table 8-2. The variance in both the time and the rate constant ratios as a function of wavelength

is most likely due to changes in the reactant/intermediate extinction coefficients with wavelength. The values of $k_{s.s.}$ for PNBBr are 10% greater than those for MNBBr with the concentration of 0.04 M. With the higher concentration 0.08 M, the difference is even larger (31%).

TABLE 8-2. Time and Rate Constant Ratios for the Displacement Reaction Between PNBBr and PNPO^- in Acetonitrile at 298K over a Range of Wavelengths

λ/nm	$t_{0.50}/t_{0.05}^a$	$k_{\text{init}}/k_{s.s.}^a$	$k_{s.s.}/\text{s}^{-1}^a$
420	17.1	1.57	0.00189
430	17.0	1.41	0.00190
440	18.4	1.57	0.00189
450	15.7	1.52	0.00195
460	15.4	1.31	0.00194

λ/nm	$t_{0.50}/t_{0.05}^b$	$k_{\text{init}}/k_{s.s.}^b$	$k_{s.s.}/\text{s}^{-1}^b$
420	16.2	2.16	0.00451
430	19.2	1.94	0.00468
440	23.7	2.83	0.00464
450	23.2	2.74	0.00455
460	20.2	2.77	0.00437

λ/nm	$t_{0.50}/t_{0.05}^c$	$k_{\text{init}}/k_{s.s.}^c$	$k_{s.s.}/\text{s}^{-1}^c$
420	28.6	3.18	0.00716
430	27.8	2.77	0.00726
440	29.7	3.02	0.00709
450	21.9	2.02	0.00692
460	23.0	2.00	0.00681

^a [PNBBr] = 0.04 M, [PNPO⁻] = 0.06 mM. ^b [PNBBr] = 0.08 M, [PNPO⁻] = 0.06 mM. ^c [PNBBr] = 0.16 M, [PNPO⁻] = 0.06 mM.

The second analysis method is the 24-point sequential pseudo-first-order kinetics analysis. The apparent rate constants for the displacement reactions between MNBBr/PNBBr and PNPO⁻ in acetonitrile at 298 K obtained using the successive correlation method are summarized in Tables 8-3 and 8-4 as well as in Tables A-33 – A-40. It is obvious that the k_{app} – time profiles begin at relatively

high values of k_{app} and decay with time toward steady-state values at all of the wavelengths. At 420 nm, the value of k_{app} in segment 1 was observed to be equal to 0.00640 s^{-1} and then was observed to decrease steadily to 0.00175 s^{-1} at segment 24 when the reactant is MNBBBr. A similar pattern of k_{app} as a function of time in the analysis was observed when the reactant is PNBBBr, but in this case the k_{app} decreases from 0.00798 s^{-1} to 0.00189 s^{-1} over the same range of degree of reaction (over the first half-life). The expected result of the sequential 24-point procedure for the simple one-step mechanism is a rate constant, independent of time and of the particular time segment analyzed.

The apparent instantaneous rate constants (k_{IRC}) – time profiles for the displacement reactions between MNBBBr/PNBBBr and PNPO^- in acetonitrile are illustrated by the plots in Figure 8-4. The k_{IRC} – time profiles have the form expected for reactant decay in a complex mechanism decreasing rapidly from an initial value of close to 0.009 s^{-1} when the reactant is MNBBBr at 0.04 M (a), and 0.05 s^{-1} when the reactant is PNBBBr at 0.08 M (b), respectively, which decay toward steady-state values, while that expected for the simple one-step mechanism is a straight line with zero slopes.

The data presented in Tables 8-1 – 8-4 and Figure 8-4 provide indisputable evidence that none of the reactions studied take place by a simple one-step mechanism. All of the data observed are consistent with the pre-association mechanism. The only evidence that is available with regard to the structure of the intermediate is that it is reactant-like, absorbing over the entire wavelength region where the reactant absorbs. This suggests that the

intermediate is a non-covalent bonded complex and the ion-dipole complex (Scheme 8-2) is one possibility. The ion-dipole structure has previously been suggested for the intermediate in the pre-association S_N2 reaction of PNPO^- with methyl iodide.⁵

TABLE 8-3. Apparent Rate Constants for the Displacement Reaction Between MNBBBr (0.04 M) and PNPO^- (0.06 mM) in Acetonitrile over the First Half-Life at 298K as a Function of Wavelengths^a

time/s	410 nm		420 nm		430 nm		Segment
	$k_{\text{app}}/\text{s}^{-1}$	\pm	$k_{\text{app}}/\text{s}^{-1}$	\pm	$k_{\text{app}}/\text{s}^{-1}$	\pm	
1.1	0.00747	0.00209	0.00640	0.00240	0.00673	0.00258	1
2.1	0.00466	0.00084	0.00372	0.00120	0.00364	0.00117	2
3.1	0.00367	0.00057	0.00301	0.00073	0.00281	0.00083	3
4.1	0.00329	0.00048	0.00285	0.00059	0.00246	0.00076	4
5.1	0.00304	0.00038	0.00280	0.00053	0.00234	0.00064	5
10.1	0.00271	0.00033	0.00286	0.00048	0.00231	0.00040	6
20.1	0.00256	0.00031	0.00285	0.00029	0.00231	0.00016	7
30.1	0.00238	0.00023	0.00258	0.00021	0.00220	0.00010	8
40.1	0.00223	0.00017	0.00235	0.00014	0.00208	0.00007	9
50.1	0.00211	0.00011	0.00221	0.00011	0.00199	0.00006	10
60.1	0.00203	0.00009	0.00210	0.00009	0.00194	0.00005	11
70.1	0.00198	0.00009	0.00203	0.00008	0.00190	0.00004	12
80.1	0.00194	0.00008	0.00197	0.00007	0.00187	0.00004	13
90.1	0.00189	0.00007	0.00192	0.00006	0.00184	0.00004	14
100.1	0.00186	0.00006	0.00189	0.00006	0.00182	0.00003	15
110.1	0.00183	0.00005	0.00186	0.00005	0.00181	0.00003	16
120.1	0.00181	0.00005	0.00184	0.00005	0.00180	0.00003	17
130.1	0.00179	0.00004	0.00182	0.00004	0.00178	0.00003	18
140.1	0.00177	0.00004	0.00181	0.00004	0.00177	0.00003	19
150.1	0.00176	0.00004	0.00179	0.00004	0.00177	0.00003	20
160.1	0.00174	0.00003	0.00178	0.00004	0.00176	0.00003	21
170.1	0.00173	0.00003	0.00177	0.00004	0.00176	0.00003	22
180.1	0.00172	0.00003	0.00176	0.00003	0.00175	0.00003	23
190.1	0.00171	0.00003	0.00175	0.00003	0.00175	0.00003	24

^a Average of 10 stopped-flow repetitions.

TABLE 8-4. Apparent Rate Constants for the Displacement Reaction Between PNBBr (0.04 M) and PNPO⁻ (0.06 mM) in Acetonitrile over the First Half-Life at 298K as a Function of Wavelengths^a

time/s	420 nm		430 nm		440 nm		Segment
	k_{app}/s^{-1}	\pm	k_{app}/s^{-1}	\pm	k_{app}/s^{-1}	\pm	
1.1	0.00798	0.00309	0.00495	0.00219	0.00438	0.00199	1
2.1	0.00338	0.00183	0.00300	0.00104	0.00331	0.00096	2
3.1	0.00241	0.00103	0.00277	0.00065	0.00294	0.00073	3
4.1	0.00225	0.00055	0.00266	0.00046	0.00269	0.00065	4
5.1	0.00220	0.00034	0.00257	0.00035	0.00257	0.00055	5
10.1	0.00234	0.00025	0.00250	0.00013	0.00260	0.00025	6
20.1	0.00253	0.00018	0.00249	0.00021	0.00265	0.00028	7
30.1	0.00242	0.00013	0.00237	0.00015	0.00247	0.00022	8
40.1	0.00231	0.00009	0.00227	0.00010	0.00232	0.00017	9
50.1	0.00220	0.00007	0.00218	0.00007	0.00222	0.00013	10
60.1	0.00213	0.00006	0.00211	0.00006	0.00216	0.00010	11
70.1	0.00208	0.00005	0.00207	0.00004	0.00211	0.00008	12
80.1	0.00204	0.00005	0.00203	0.00003	0.00206	0.00007	13
90.1	0.00200	0.00004	0.00200	0.00003	0.00203	0.00006	14
100.1	0.00198	0.00004	0.00198	0.00002	0.00200	0.00005	15
110.1	0.00196	0.00004	0.00196	0.00002	0.00198	0.00004	16
120.1	0.00194	0.00003	0.00195	0.00001	0.00196	0.00003	17
130.1	0.00193	0.00003	0.00194	0.00001	0.00194	0.00003	18
140.1	0.00192	0.00003	0.00193	0.00001	0.00193	0.00003	19
150.1	0.00192	0.00003	0.00193	0.00001	0.00192	0.00002	20
160.1	0.00191	0.00003	0.00192	0.00001	0.00191	0.00002	21
170.1	0.00190	0.00002	0.00191	0.00001	0.00190	0.00002	22
180.1	0.00190	0.00002	0.00191	0.00001	0.00189	0.00002	23
190.1	0.00189	0.00002	0.00190	0.00001	0.00189	0.00002	24

^a Average of 10 stopped-flow repetitions.

In addition, the fact that the form of the kinetic data for the reactions of PNPO⁻ with bromoacetonitrile and phenoxide ion (PO⁻) with bromoacetonitrile (BrAN) or methyl iodide (MeI) very closely resembles that for the corresponding reactions of PNPO⁻ with MNBBBr, suggests that the same mechanism is followed in all of the displacement reactions studied.

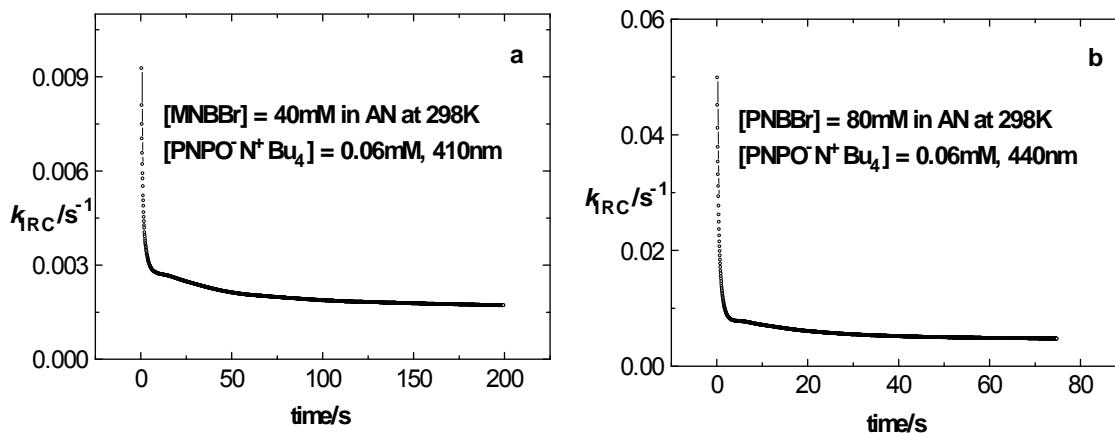
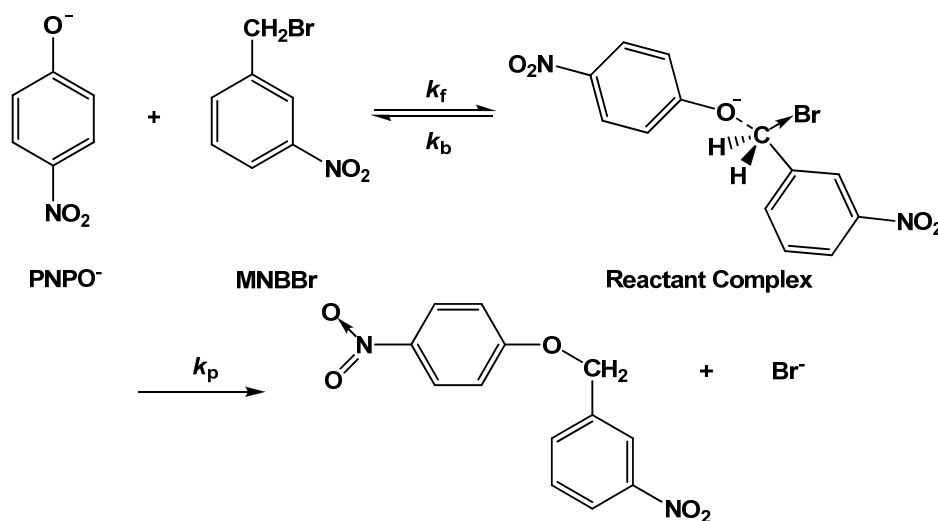


FIGURE 8-4. Apparent instantaneous rate constants (k_{IRC}) – time plots for the displacement reactions between MNBBr (40 mM, a)/PNBBr (80 mM, b) and $PNPO^-$ in acetonitrile at 298K.

SCHEME 8-2. The Proposed Mechanism for the Reaction Between $PNPO^-$ and MNBBr in Acetonitrile



Conclusions

The S_N2 displacement reactions of *p*-nitrophenoxide ion ($PNPO^-$) with *m*- or *p*-nitrobenzyl bromide (MNBBr or PNBBr) in acetonitrile take place by the pre-association mechanism in which the intermediates are kinetically significant (Scheme 8-2). One possibility for the intermediate which is called the reactant

complex in this dissertation is an ion-dipole complex. The kinetic data we have obtained deviate from the first-order kinetics for all of the displacement reactions studied which include the reactions of PNPO^- with MNBBr , PNPO^- with PNBBr , PNPO^- with MeI , PNPO^- with BrAN , PO^- with BrAN , and PO^- with MeI . As a result of the extensive studies on this broad pairs of reactants we predict that the single transition-state model is not appropriate for the $\text{S}_{\text{N}}2$ displacement reactions. The pre-association mechanism fits the data used in our pseudo-first-order rate constant analysis and is therefore the most suitable mechanism for the displacement reactions.

Experimental Section

Materials. *m*-Nitrobenzyl bromide (MNBBr) and *p*-nitrobenzyl bromide (PNBBr) were obtained commercially from Aldrich and recrystallized from isopropanol for at least four times before use. Bromoacetonitrile (BrAN) and methyl iodide (MeI) were also obtained commercially from Aldrich and redistilled before use. Acetonitrile was refluxed and distilled over P_2O_5 under a nitrogen atmosphere and passed through an Al_2O_3 column before transferring into the glove box. *p*-Nitrophenoxide tetrabutylammonium (PNPO^-) was synthesized from *p*-nitrophenyl acetate and tetrabutylammonium hydroxide (40 wt. % solution in water) in dichloromethane. After removing the solvent, yellow solid was obtained. The product was identified by ^1H NMR.

The Procedure for the Displacement Reactions. *m*-Nitrobenzyl bromide (MNBBr , 0.001mol) was allowed to react with *p*-nitrophenoxide ion ($\text{PNPO}^-\text{N}^+\text{Bu}_4$, 0.0015mol) in 25 ml acetonitrile at room temperature. After stirring for about one

week, the solvent was removed. The yellow residual was dissolved in ether. The solution was then filtered to remove excess PNPO^- (because PNPO^- is insoluble in ether). After removing the solvent, it gave yellow solid including a little bit white solid on the flask wall (the white solid is $\text{Bu}_4\text{N}^+\text{Br}^-$). The resulting yellow solid was washed thoroughly with water and dried to give light yellow solid, the product of the displacement reaction. The ^1H NMR spectra for the product of the displacement reaction between MNBBBr and PNPO^- in CDCl_3 is illustrated in Figure A-35.

Kinetic Experiments. Kinetic experiments were carried out using a Hi-Tech SF-61 DX2 stopped-flow spectrophotometer installed in a glove box and kept under a nitrogen atmosphere. The temperature was controlled at 298 K using a constant temperature flow system connected directly to the reaction cell through a bath situated outside of the glove box. All stopped-flow experiments included the recording of at least 10 absorbance – time profiles over the wavelengths range from 410 nm to 460 nm at 10 nm intervals. Each experiment was repeated at least three times. The 2000-point absorbance – time curve data were collected over one half-life.

References

- (1) Cowdrey, W. A.; Hughes, E. D.; Ingold, C. K.; Masterman, S.; Scott, A. *D. J. Chem. Soc.* **1937**, 1252.
- (2) Carrion, F.; Dewar, M. J. S. *J. Am. Chem. Soc.* **1984**, 106, 3531.
- (3) Dedieu, A.; Veillard, A. *Quantum Theory of Chemical Reactions*; Daudel, R., Pullman, A., Salem, L., Veillard, A., Eds.; D. Reidel

Publishers: New York, 1979; Vol. 1, p 69.

- (4) Wolfe, S.; Mitchell, D. J.; Schlegel, H. B. *J. Am. Chem. Soc.* **1981**, *103*, 7692, 7694.
- (5) Morokuma, K. *J. Am. Chem. Soc.* **1982**, *104*, 3732.
- (6) Urban, M.; Cernusak, I.; Kello, V. *Chem. Phys. Lett.* **1984**, *105*, 625.
- (7) Dougherty, R. C.; Roberts, J. D. *Org. Mass Spectrom.* **1974**, *8*, 77.
- (8) Bohme, D. K.; Mackay, G. I.; Payzant, J. D. *J. Am. Chem. Soc.* **1974**, *96*, 4027, 4030.
- (9) Olmstead, W. N.; Brauman, J. I. *J. Am. Chem. Soc.* **1977**, *99*, 4219.
- (10) Pellerite, M. J.; Brauman, J. I. *J. Am. Chem. Soc.* **1980**, *102*, 5993.
- (11) Chandrasekhar, J.; Jorgensen, W. L. *J. Am. Chem. Soc.* **1985**, *107*, 2974.
- (12) Jorgensen, W. L. *Acc. Chem. Res.* **1989**, *22*, 184.
- (13) Vayner, G.; Houk, K. N.; Jorgensen, W. L.; Bauman, J. I. *J. Am. Chem. Soc.* **2004**, *126*, 9054.
- (14) Gilchrist, T. L.; Storr, R. D. *Organic Reactions and Orbital Symmetry*; Cambridge University Press: Cambridge, 1972.
- (15) Hayami, J.; Tanaka, N.; Hihara, N.; Kaji, A. *Tetrahedron Lett.* **1973**, 385.
- (16) Chen, X.; Regan, C. K.; Craig, S. L.; Krenske, E. H.; Houk, K. N.; Jorgensen, W. L.; Bauman, J. I. *J. Am. Chem. Soc.* **2009**, *131*, 16162.
- (17) Bordwell, F. G.; Hughes, D. L. *J. Am. Chem. Soc.* **1986**, *108*, 7300.
- (18) Lu, Y.; Handoo, K. L.; Parker, V. D. *Org. Biomol. Chem.* **2003**, *1*, 36.

- (19) Parker, V. D.; Lu, Y. *Org. Biomol. Chem.* **2003**, 1, 2621.
- (20) Parker, V. D. *Pure Appl. Chem.* **2005**, 77, 1823.

CHAPTER 9

CONCLUSIONS

My overall conclusion for this dissertation is that the experimental data obtained and the subsequent analyses have shown that several typical fundamental organic chemical reactions previously believed to involve single transition-state processes actually take place by more complex mechanisms. It appears that this conclusion may be general and apply to all of the fundamental reactions in the organic chemistry field. I summarize my conclusions for the reactions that I have investigated in the following way:

(1) The hydride transfer reaction between BNAH and MA^+ in acetonitrile takes place in a three-step mechanism which involves two intermediates: a CT complex and a reactant complex. The two intermediates have no new covalent bonds and are held together by the non-bonding overlap of π -orbitals in the two moieties.

(2) The hydride transfer reaction between MAH and Tr^+ in acetonitrile takes place by a complex mechanism with a kinetically significant intermediate. Gaussian calculations at the M06-2x/6-311++G(d,p) level resulted in the observation of a reactant complex on the reaction coordinate leading to the transition state for hydride transfer.

(3) The most important conclusion for the reaction of MAH with BQCN^+ in AN is that it takes place by a multi-step mechanism. Another conclusion of some general importance is that oxygen takes part in a chain process during this reaction. This leads to the conclusion that the chain pathway of formal hydride

transfer in biological systems in nature may also involve the participation of oxygen.

(4) The cation – anion combination reactions of TMT^+ with acetate salts in acetic acid involve the formation of $\{\text{TMT}^+ \text{HOAc}/\text{AcO}^-\}$, which we regard as a solvent separated ion-pair, during the time of mixing. The intramolecular collapse of the solvent separated ion-pair then takes place by a two-step mechanism involving the formation of a kinetically significant “Reactant Complex” as an intermediate which we propose to be the intimate ion pair, $\{\text{TMT}^+ {}^-\text{OAc}\}$. Our observation that the HOAc/AcO^- solutions are ideal systems to obtain detailed kinetic and mechanism information on these important reactions will eventually provide the means to greatly increase our knowledge of how these reactions take place.

(5) The Michael addition reaction between BNS and nitroethide ion takes place by a pre-association mechanism in which the intermediate is kinetically significant. This conclusion was derived from the experimental kinetic data which upon analysis revealed time dependent apparent rate constants for the reaction. Gaussian calculations at the M06-2x/6-31+G(d) level resulted in the observation of a reactant complex on the reaction coordinate leading to the transition state for the addition.

(6) The $\text{S}_{\text{N}}2$ displacement reactions of *p*-nitrophenoxide ion (PNPO^-) with *m*- or *p*-nitrobenzyl bromide (MNBBBr or PNBBBr) in acetonitrile take place by the pre-association mechanism in which the intermediates are kinetically significant. One possibility for the intermediate which is called the reactant complex in this

dissertation is an ion-dipole complex. The kinetic data we have obtained deviate from the first-order kinetics for all of the displacement reactions studied which include the reactions of PNPO^- with MNBBr , PNPO^- with PNBBr , PNPO^- with MeI , PNPO^- with BrAN , PO^- with BrAN , and PO^- with MeI . As a result of the extensive studies on this broad pairs of reactants we predict that the single transition-state model is not appropriate for the $\text{S}_{\text{N}}2$ displacement reactions. The pre-association mechanism fits the data used in our pseudo-first-order rate constant analysis and is therefore the most suitable mechanism for the displacement reactions.

The reactions discussed in this dissertation belong to three classes of fundamental organic reactions: the hydride transfer reactions between NADH model compounds, combination reactions, and $\text{S}_{\text{N}}2$ displacement reactions. Therefore, the answer to the central question: “Is the single transition-state model appropriate for the fundamental reactions in organic chemistry?” is definitely No!

My research provides a significant re-evaluation of how to view the simple reactions in solution. This will affect theoretical approaches and will contribute to provide a framework to understand how e.g. solvation can affect reactivity. Our findings result in the necessity of revising many of the mechanisms believed to be established over the past seventy years and have a broad effect on the chemistry and biochemistry field.

APPENDICES

Appendix A. Supplementary Information for All of the Reactions
Discussed in this Dissertation

TABLE A-1. Apparent Rate Constants and Standard Deviations for 3 Sets of Experiments (20 Stopped-Flow Shots Each) on the Reaction Between BNAH (7.2 mM) and MA⁺ (0.3 mM) in Acetonitrile at 298 K and 410 nm

time/s	Set 1		Set 2		Set 3		Segment
	k_{app}/s^{-1}	S.D.	k_{app}/s^{-1}	S.D.	k_{app}/s^{-1}	S.D.	
0.008	0.910	0.309	1.473	0.375	1.050	0.567	1
0.012	0.865	0.099	1.075	0.169	0.983	0.239	2
0.016	0.768	0.053	0.969	0.075	0.944	0.095	3
0.019	0.726	0.048	0.868	0.055	0.862	0.069	4
0.023	0.685	0.037	0.803	0.042	0.794	0.051	5
0.041	0.603	0.019	0.657	0.019	0.653	0.022	6
0.077	0.569	0.012	0.588	0.020	0.585	0.015	7
0.113	0.547	0.009	0.552	0.015	0.555	0.011	8
0.150	0.540	0.006	0.539	0.010	0.536	0.008	9
0.186	0.534	0.005	0.531	0.007	0.527	0.006	10
0.222	0.530	0.004	0.525	0.005	0.523	0.006	11
0.258	0.528	0.003	0.521	0.004	0.520	0.005	12
0.294	0.527	0.003	0.519	0.003	0.517	0.004	13
0.331	0.526	0.002	0.516	0.003	0.516	0.004	14
0.367	0.525	0.002	0.515	0.002	0.514	0.004	15
0.403	0.524	0.002	0.513	0.002	0.513	0.004	16
0.439	0.524	0.002	0.512	0.002	0.514	0.004	17
0.475	0.525	0.002	0.512	0.002	0.514	0.004	18
0.512	0.526	0.002	0.512	0.002	0.514	0.004	19
0.548	0.526	0.002	0.512	0.002	0.514	0.004	20
0.584	0.526	0.002	0.511	0.002	0.513	0.004	21
0.620	0.526	0.002	0.510	0.002	0.513	0.004	22
0.656	0.526	0.002	0.510	0.002	0.512	0.004	23
0.693	0.526	0.002	0.509	0.002	0.511	0.004	24

TABLE A-2. Apparent Rate Constants and Standard Deviations for 3 Sets of Experiments (20 Stopped-Flow Shots Each) on the Reaction Between BNAH (7.2 mM) and MA⁺ (0.3 mM) in Acetonitrile at 298 K and 420 nm

time/s	Set 1		Set 2		Set 3		Segment
	k_{app}/s^{-1}	S.D.	k_{app}/s^{-1}	S.D.	k_{app}/s^{-1}	S.D.	
0.008	1.160	0.259	1.120	0.242	1.290	0.399	1
0.012	0.974	0.099	0.928	0.130	1.128	0.156	2
0.016	0.870	0.034	0.827	0.068	0.990	0.084	3
0.019	0.796	0.023	0.765	0.061	0.875	0.061	4
0.023	0.747	0.028	0.721	0.054	0.799	0.037	5
0.041	0.654	0.020	0.623	0.028	0.643	0.019	6
0.077	0.621	0.018	0.598	0.019	0.557	0.013	7
0.113	0.593	0.014	0.564	0.017	0.517	0.009	8
0.150	0.578	0.010	0.548	0.013	0.503	0.006	9
0.186	0.572	0.008	0.539	0.010	0.496	0.005	10
0.222	0.567	0.006	0.536	0.009	0.490	0.004	11
0.258	0.569	0.005	0.535	0.008	0.486	0.003	12
0.294	0.569	0.004	0.532	0.007	0.484	0.003	13
0.331	0.569	0.004	0.530	0.006	0.482	0.003	14
0.367	0.568	0.003	0.527	0.006	0.480	0.003	15
0.403	0.567	0.003	0.525	0.005	0.478	0.002	16
0.439	0.567	0.003	0.524	0.005	0.477	0.002	17
0.475	0.566	0.003	0.522	0.005	0.476	0.002	18
0.512	0.566	0.003	0.521	0.005	0.475	0.002	19
0.548	0.566	0.003	0.519	0.005	0.475	0.002	20
0.584	0.566	0.002	0.518	0.005	0.474	0.002	21
0.620	0.566	0.002	0.517	0.005	0.474	0.002	22
0.656	0.566	0.002	0.516	0.005	0.473	0.002	23
0.693	0.566	0.002	0.516	0.005	0.472	0.002	24

TABLE A-3. Apparent Rate Constants and Standard Deviations for 3 Sets of Experiments (20 Stopped-Flow Shots Each) on the Reaction Between BNAH (7.2 mM) and MA⁺ (0.3 mM) in Acetonitrile at 298 K and 430 nm

time/s	Set 1		Set 2		Set 3		Segment
	k_{app}/s^{-1}	S.D.	k_{app}/s^{-1}	S.D.	k_{app}/s^{-1}	S.D.	
0.008	2.055	0.199	1.865	0.513	1.851	0.493	1
0.012	1.789	0.071	1.752	0.296	1.647	0.324	2
0.015	1.645	0.034	1.558	0.108	1.577	0.152	3
0.019	1.500	0.035	1.354	0.053	1.413	0.065	4
0.023	1.385	0.030	1.187	0.044	1.274	0.041	5
0.042	1.062	0.022	0.792	0.020	0.883	0.022	6
0.079	0.793	0.016	0.628	0.012	0.685	0.023	7
0.117	0.666	0.011	0.552	0.009	0.591	0.013	8
0.155	0.605	0.008	0.518	0.007	0.548	0.010	9
0.192	0.570	0.006	0.501	0.005	0.527	0.008	10
0.230	0.548	0.004	0.495	0.004	0.519	0.007	11
0.267	0.533	0.003	0.489	0.004	0.512	0.006	12
0.305	0.521	0.003	0.484	0.003	0.505	0.005	13
0.343	0.513	0.002	0.481	0.003	0.501	0.005	14
0.380	0.506	0.002	0.478	0.003	0.498	0.005	15
0.418	0.501	0.002	0.476	0.003	0.495	0.004	16
0.455	0.496	0.002	0.474	0.003	0.492	0.004	17
0.493	0.493	0.002	0.472	0.003	0.491	0.004	18
0.531	0.490	0.002	0.471	0.003	0.489	0.004	19
0.568	0.486	0.002	0.470	0.003	0.487	0.004	20
0.606	0.484	0.002	0.468	0.003	0.486	0.004	21
0.643	0.481	0.002	0.467	0.003	0.485	0.004	22
0.681	0.478	0.002	0.467	0.003	0.484	0.004	23
0.719	0.476	0.002	0.466	0.003	0.484	0.004	24

TABLE A-4. Apparent Rate Constants and Standard Deviations for 3 Sets of Experiments (20 Stopped-Flow Shots Each) on the Reaction Between BNAH (7.2 mM) and MA⁺ (0.6 mM) in Acetonitrile at 298 K and 440 nm

time/s	Set 1		Set 2		Set 3		Segment
	k_{app}/s^{-1}	S.D.	k_{app}/s^{-1}	S.D.	k_{app}/s^{-1}	S.D.	
0.008	1.492	0.234	1.341	0.322	1.209	0.455	1
0.012	1.261	0.088	1.159	0.085	0.915	0.193	2
0.015	1.145	0.041	1.026	0.064	0.788	0.089	3
0.019	1.059	0.036	0.943	0.041	0.722	0.061	4
0.023	0.984	0.032	0.871	0.030	0.679	0.043	5
0.042	0.778	0.022	0.695	0.030	0.600	0.021	6
0.079	0.641	0.014	0.605	0.017	0.583	0.014	7
0.117	0.585	0.012	0.555	0.015	0.572	0.013	8
0.155	0.560	0.008	0.535	0.011	0.560	0.010	9
0.192	0.544	0.006	0.523	0.008	0.554	0.007	10
0.230	0.534	0.005	0.516	0.006	0.551	0.006	11
0.267	0.527	0.005	0.510	0.005	0.550	0.005	12
0.305	0.523	0.004	0.508	0.004	0.547	0.004	13
0.343	0.519	0.004	0.506	0.004	0.545	0.004	14
0.380	0.516	0.004	0.503	0.003	0.542	0.003	15
0.418	0.512	0.003	0.501	0.003	0.540	0.003	16
0.455	0.509	0.003	0.499	0.003	0.537	0.003	17
0.493	0.506	0.003	0.497	0.003	0.536	0.002	18
0.531	0.504	0.003	0.495	0.003	0.534	0.002	19
0.568	0.501	0.003	0.494	0.003	0.532	0.002	20
0.606	0.499	0.003	0.492	0.003	0.531	0.002	21
0.643	0.497	0.003	0.491	0.003	0.529	0.002	22
0.681	0.495	0.003	0.490	0.003	0.529	0.002	23
0.719	0.494	0.003	0.489	0.003	0.528	0.002	24

TABLE A-5. Apparent Rate Constants and Standard Deviations for 3 Sets of Experiments (20 Stopped-Flow Shots Each) on the Reaction Between BNAH (7.2 mM) and MA⁺ (0.6 mM) in Acetonitrile at 298 K and 450 nm

time/s	Set 1		Set 2		Set 3		Segment
	k_{app}/s^{-1}	S.D.	k_{app}/s^{-1}	S.D.	k_{app}/s^{-1}	S.D.	
0.008	1.503	0.168	1.303	0.470	1.466	0.147	1
0.012	1.316	0.080	1.227	0.163	1.320	0.083	2
0.015	1.140	0.046	1.134	0.070	1.158	0.052	3
0.019	1.033	0.032	1.045	0.047	1.064	0.041	4
0.023	0.940	0.027	0.968	0.035	0.988	0.030	5
0.042	0.769	0.033	0.781	0.028	0.800	0.039	6
0.079	0.685	0.016	0.677	0.016	0.701	0.020	7
0.117	0.624	0.008	0.616	0.014	0.632	0.011	8
0.155	0.590	0.006	0.585	0.010	0.596	0.009	9
0.192	0.570	0.005	0.566	0.008	0.574	0.007	10
0.230	0.556	0.004	0.553	0.006	0.559	0.006	11
0.267	0.546	0.004	0.545	0.005	0.550	0.005	12
0.305	0.538	0.003	0.538	0.004	0.542	0.004	13
0.343	0.532	0.003	0.533	0.003	0.535	0.004	14
0.380	0.527	0.003	0.528	0.003	0.530	0.003	15
0.418	0.522	0.003	0.524	0.003	0.526	0.003	16
0.455	0.518	0.003	0.520	0.003	0.522	0.003	17
0.493	0.515	0.003	0.517	0.003	0.518	0.003	18
0.531	0.512	0.003	0.514	0.002	0.515	0.003	19
0.568	0.510	0.003	0.512	0.002	0.513	0.003	20
0.606	0.508	0.003	0.510	0.002	0.511	0.003	21
0.643	0.506	0.003	0.508	0.002	0.509	0.003	22
0.681	0.504	0.003	0.506	0.002	0.507	0.003	23
0.719	0.503	0.003	0.505	0.002	0.506	0.003	24

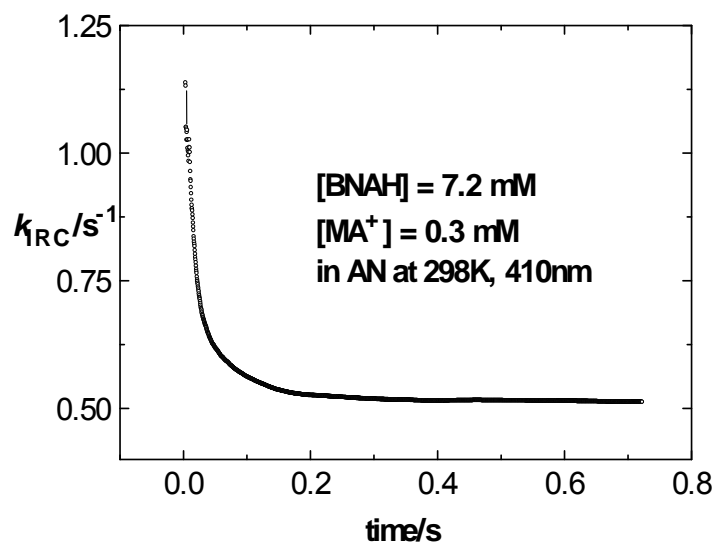


FIGURE A-1. Apparent instantaneous rate constants (k_{IRC}) – time plot for the reaction between BNAH and MA^+ in AN at 298K and 410 nm.

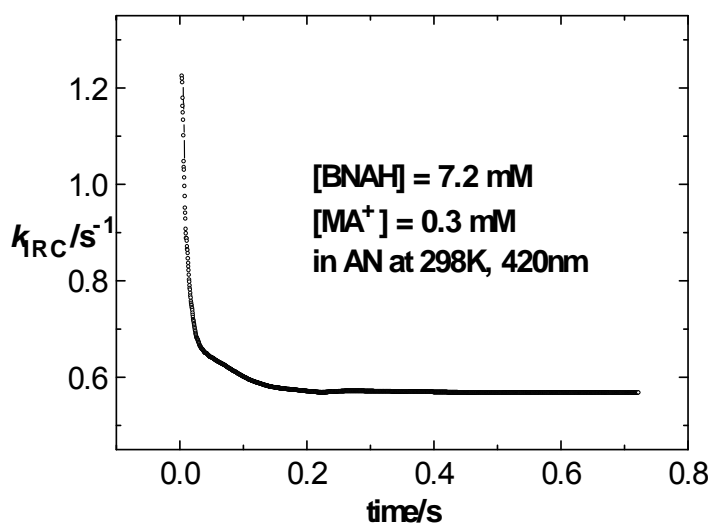


FIGURE A-2. Apparent instantaneous rate constants (k_{IRC}) – time plot for the reaction between BNAH and MA^+ in AN at 298K and 420 nm.

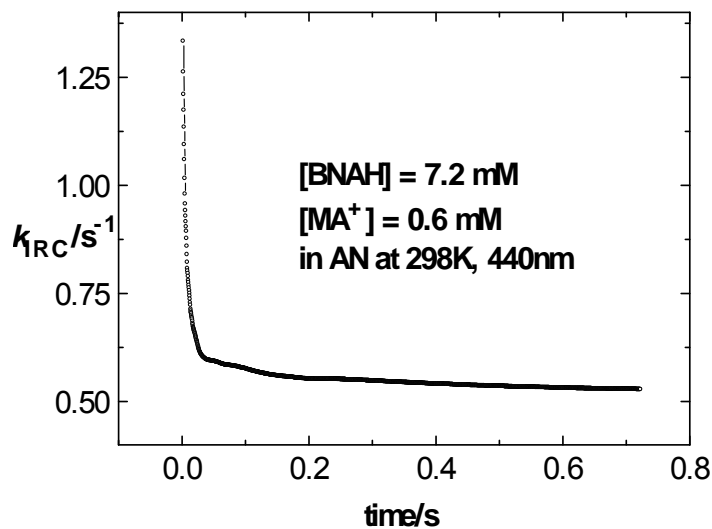


FIGURE A-3. Apparent instantaneous rate constants (k_{IRC}) – time plot for the reaction between BNAH and MA^+ in AN at 298K and 440 nm.

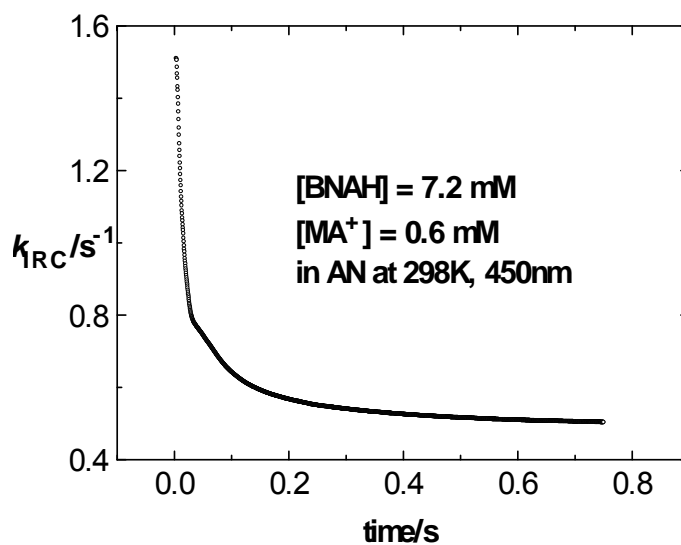


FIGURE A-4. Apparent instantaneous rate constants (k_{IRC}) – time plot for the reaction between BNAH and MA^+ in AN at 298K and 450nm.

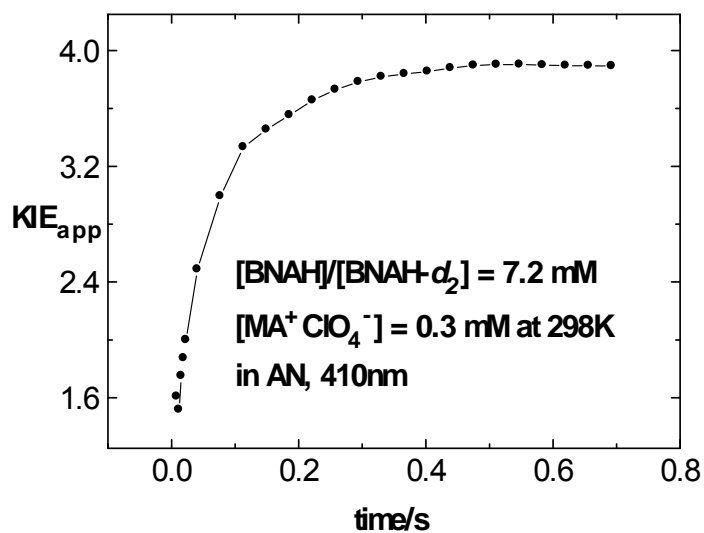


FIGURE A-5. Apparent KIE for the reactions between BNAH/BNAH- d_2 and MA^+ in AN at 298K and 410 nm as a function of reaction time.

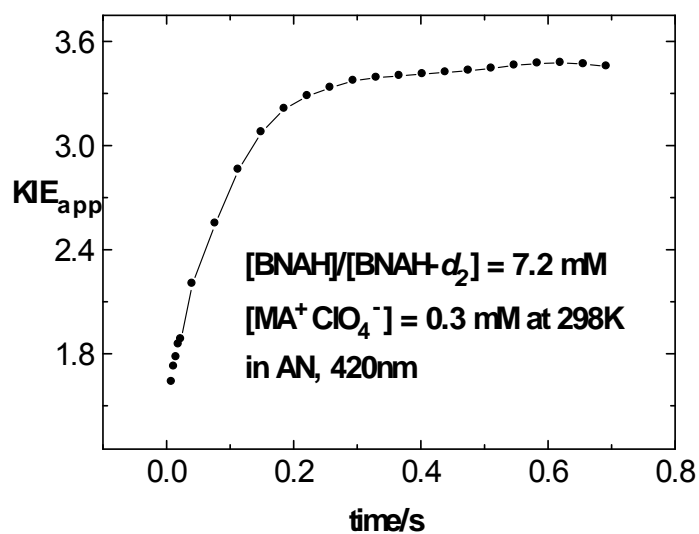


FIGURE A-6. Apparent KIE for the reactions between BNAH/BNAH- d_2 and MA^+ in AN at 298K and 420 nm as a function of reaction time.

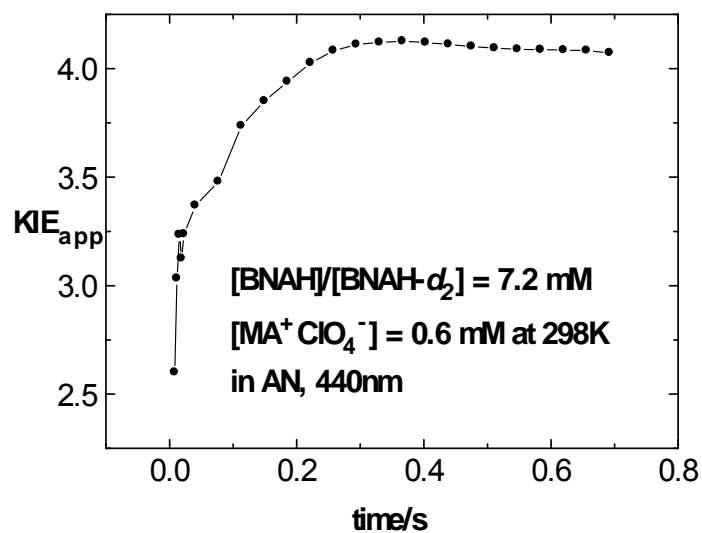


FIGURE A-7. Apparent KIE for the reactions between BNAH/BNAH- d_2 and MA^+ in AN at 298K and 440 nm as a function of reaction time.

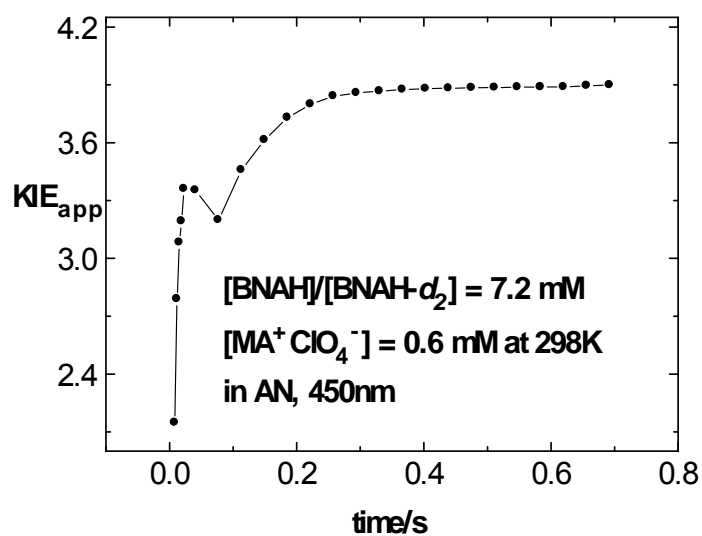


FIGURE A-8. Apparent KIE for the reactions between BNAH/BNAH- d_2 and MA^+ in AN at 298K and 450 nm as a function of reaction time.

TABLE A-6. Rate Constants for the Reaction Between BNAH (7.2 mM) and MA⁺ (0.6 mM) in Acetonitrile at Various Temperatures

T/K	$k_{s.s.}/s^{-1}$	$k_2/M^{-1} s^{-1}$	$\Delta H^\ddagger = 6.47 \text{ kcal mol}^{-1}$ $\Delta S^\ddagger = -28.3 \text{ cal mol}^{-1} \text{ K}^{-1}$ $\Delta G^\ddagger = 14.9 \text{ kcal mol}^{-1}$
293	0.426	59.2	
298	0.527	73.2	
303	0.642	89.2	
313	0.949	131.8	
323	1.314	182.4	

TABLE A-7. Changes in the Slopes and the Intercepts with the Extent of Reaction during Conventional Pseudo-First-Order Analysis for the Reaction of MAH (0.2 mM) with Tr⁺ (0.05 M) in Acetonitrile at 298K and 400 nm

Number of HL	k_{app}/s^{-1}	intercept/ s^{-1}
0.5	0.193	-0.00190
1.0	0.189	0.00203
2.0	0.183	0.0122
3.0	0.176	0.0350
4.0	0.166	0.0847

TABLE A-8. Changes in the Slopes and the Intercepts with the Extent of Reaction during Conventional Pseudo-First-Order Analysis for the Reaction of MAH (0.2 mM) with Tr⁺ (0.05 M) in Acetonitrile at 298K and 410 nm

Number of HL	k_{app}/s^{-1}	intercept/ s^{-1}
0.5	0.185	-0.00657
1.0	0.184	-0.00556
2.0	0.180	0.00348
3.0	0.173	0.0248
4.0	0.162	0.0828

TABLE A-9. Changes in the Slopes and the Intercepts with the Extent of Reaction during Conventional Pseudo-First-Order Analysis for the Reaction of MAH (0.2 mM) with Tr^+ (0.05 M) in Acetonitrile at 298K and 420 nm

Number of HL	$k_{\text{app}}/\text{s}^{-1}$	intercept/ s^{-1}
0.5	0.195	-0.00167
1.0	0.190	0.00254
2.0	0.183	0.0146
3.0	0.176	0.0366
4.0	0.165	0.0898

TABLE A-10. Changes in the Slopes and the Intercepts with the Extent of Reaction during Conventional Pseudo-First-Order Analysis for the Reaction of MAH (0.4 mM) with Tr^+ (0.05 M) in Acetonitrile at 298K and 430 nm

Number of HL	$k_{\text{app}}/\text{s}^{-1}$	intercept/ s^{-1}
0.5	0.242	0.00642
1.0	0.224	0.0185
2.0	0.207	0.0454
3.0	0.192	0.0883
4.0	0.173	0.173

TABLE A-11. Changes in the Slopes and the Intercepts with the Extent of Reaction during Conventional Pseudo-First-Order Analysis for the Reaction of MAH (0.4 mM) with Tr^+ (0.05 M) in Acetonitrile at 298K and 440 nm

Number of HL	$k_{\text{app}}/\text{s}^{-1}$	intercept/ s^{-1}
0.5	0.242	0.00717
1.0	0.221	0.0214
2.0	0.199	0.0565
3.0	0.180	0.115
4.0	0.147	0.281

TABLE A-12. Apparent Rate Constants and Standard Deviations for 3 Sets of Experiments (20 Stopped-Flow Shots Each) on the Reaction Between MAH (0.2 mM) and Tr^+ (0.05 M) in Acetonitrile at 298 K and 400 nm

time/s	Set 1		Set 2		Set 3		Segment
	$k_{\text{app}}/\text{s}^{-1}$	S.D.	$k_{\text{app}}/\text{s}^{-1}$	S.D.	$k_{\text{app}}/\text{s}^{-1}$	S.D.	
0.017	0.270	0.024	0.217	0.033	0.220	0.015	1
0.027	0.250	0.021	0.229	0.012	0.223	0.012	2
0.037	0.242	0.013	0.227	0.008	0.222	0.007	3
0.047	0.240	0.010	0.220	0.005	0.218	0.006	4
0.057	0.234	0.007	0.217	0.005	0.215	0.005	5
0.107	0.219	0.005	0.208	0.004	0.207	0.002	6
0.207	0.211	0.003	0.203	0.002	0.204	0.001	7
0.307	0.208	0.002	0.203	0.001	0.203	0.001	8
0.407	0.206	0.002	0.204	0.001	0.203	0.001	9
0.507	0.204	0.001	0.205	0.001	0.203	0.001	10
0.607	0.203	0.001	0.206	0.001	0.204	0.001	11
0.707	0.202	0.001	0.206	0.001	0.204	0.001	12
0.807	0.201	0.001	0.206	0.001	0.204	0.001	13
0.907	0.200	0.001	0.206	0.001	0.204	0.001	14
1.007	0.200	0.001	0.206	0.001	0.204	0.001	15
1.107	0.199	0.001	0.206	0.001	0.204	0.001	16
1.207	0.199	0.001	0.206	0.001	0.204	0.001	17
1.307	0.198	0.001	0.206	0.001	0.204	0.001	18
1.407	0.198	0.001	0.206	0.001	0.204	0.001	19
1.507	0.197	0.001	0.206	0.001	0.204	0.001	20
1.607	0.197	0.001	0.206	0.001	0.204	0.001	21
1.707	0.196	0.001	0.206	0.001	0.204	0.001	22
1.807	0.196	0.001	0.206	0.001	0.204	0.001	23
1.907	0.196	0.001	0.206	0.001	0.203	0.001	24

TABLE A-13. Apparent Rate Constants and Standard Deviations for 3 Sets of Experiments (20 Stopped-Flow Shots Each) on the Reaction Between MAH (0.2 mM) and Tr⁺ (0.05 M) in Acetonitrile at 298 K and 410 nm

time/s	Set 1		Set 2		Set 3		Segment
	k_{app}/s^{-1}	S.D.	k_{app}/s^{-1}	S.D.	k_{app}/s^{-1}	S.D.	
0.017	0.241	0.089	0.230	0.030	0.226	0.021	1
0.027	0.239	0.054	0.225	0.012	0.227	0.009	2
0.037	0.236	0.043	0.220	0.009	0.222	0.005	3
0.047	0.237	0.029	0.217	0.005	0.213	0.004	4
0.057	0.228	0.022	0.216	0.004	0.210	0.004	5
0.107	0.211	0.010	0.208	0.002	0.203	0.003	6
0.207	0.203	0.006	0.204	0.001	0.200	0.001	7
0.307	0.202	0.004	0.205	0.001	0.200	0.001	8
0.407	0.203	0.002	0.205	0.001	0.200	0.001	9
0.507	0.204	0.002	0.206	0.001	0.200	0.001	10
0.607	0.205	0.002	0.206	0.001	0.200	0.001	11
0.707	0.205	0.001	0.206	0.001	0.201	0.001	12
0.807	0.205	0.001	0.206	0.001	0.201	0.001	13
0.907	0.205	0.001	0.206	0.001	0.201	0.001	14
1.007	0.205	0.001	0.206	0.001	0.201	0.001	15
1.107	0.205	0.001	0.206	0.001	0.200	0.001	16
1.207	0.205	0.001	0.206	0.001	0.200	0.001	17
1.307	0.205	0.001	0.206	0.001	0.200	0.001	18
1.407	0.205	0.001	0.206	0.001	0.200	0.001	19
1.507	0.204	0.001	0.206	0.001	0.200	0.001	20
1.607	0.205	0.001	0.206	0.001	0.200	0.001	21
1.707	0.205	0.001	0.206	0.001	0.200	0.001	22
1.807	0.204	0.001	0.206	0.001	0.200	0.001	23
1.907	0.204	0.001	0.206	0.001	0.200	0.001	24

TABLE A-14. Apparent Rate Constants and Standard Deviations for 3 Sets of Experiments (20 Stopped-Flow Shots Each) on the Reaction Between MAH (0.2 mM) and Tr⁺ (0.05 M) in Acetonitrile at 298 K and 420 nm

time/s	Set 1		Set 2		Set 3		Segment
	k_{app}/s^{-1}	S.D.	k_{app}/s^{-1}	S.D.	k_{app}/s^{-1}	S.D.	
0.017	0.257	0.041	0.226	0.027	0.228	0.017	1
0.027	0.253	0.024	0.224	0.011	0.223	0.008	2
0.037	0.249	0.013	0.224	0.008	0.223	0.006	3
0.047	0.239	0.011	0.219	0.006	0.221	0.004	4
0.057	0.234	0.010	0.216	0.006	0.217	0.004	5
0.107	0.220	0.005	0.206	0.003	0.209	0.002	6
0.207	0.212	0.003	0.202	0.002	0.205	0.001	7
0.307	0.208	0.002	0.202	0.002	0.204	0.001	8
0.407	0.205	0.002	0.202	0.002	0.204	0.000	9
0.507	0.204	0.001	0.202	0.001	0.205	0.000	10
0.607	0.203	0.001	0.202	0.001	0.205	0.000	11
0.707	0.202	0.001	0.203	0.001	0.205	0.000	12
0.807	0.201	0.001	0.202	0.001	0.205	0.000	13
0.907	0.200	0.001	0.202	0.001	0.205	0.000	14
1.007	0.199	0.001	0.202	0.001	0.205	0.000	15
1.107	0.198	0.001	0.202	0.001	0.205	0.000	16
1.207	0.198	0.001	0.202	0.001	0.205	0.000	17
1.307	0.197	0.001	0.202	0.001	0.205	0.000	18
1.407	0.196	0.001	0.202	0.001	0.205	0.000	19
1.507	0.196	0.001	0.202	0.001	0.205	0.000	20
1.607	0.195	0.001	0.202	0.001	0.205	0.000	21
1.707	0.195	0.001	0.202	0.001	0.205	0.000	22
1.807	0.195	0.001	0.201	0.001	0.205	0.000	23
1.907	0.194	0.001	0.201	0.001	0.205	0.000	24

TABLE A-15. Apparent Rate Constants and Standard Deviations for 3 Sets of Experiments (20 Stopped-Flow Shots Each) on the Reaction Between MAH (0.4 mM) and Tr^+ (0.05 M) in Acetonitrile at 298 K and 430 nm

time/s	Set 1		Set 2		Set 3		Segment
	$k_{\text{app}}/\text{s}^{-1}$	S.D.	$k_{\text{app}}/\text{s}^{-1}$	S.D.	$k_{\text{app}}/\text{s}^{-1}$	S.D.	
0.017	0.219	0.013	0.208	0.018	0.242	0.015	1
0.027	0.224	0.009	0.212	0.005	0.246	0.008	2
0.037	0.222	0.005	0.215	0.005	0.243	0.006	3
0.047	0.220	0.003	0.213	0.003	0.238	0.005	4
0.057	0.217	0.003	0.209	0.002	0.234	0.004	5
0.107	0.209	0.001	0.200	0.002	0.224	0.001	6
0.207	0.206	0.001	0.197	0.001	0.218	0.001	7
0.307	0.205	0.001	0.196	0.001	0.216	0.001	8
0.407	0.205	0.001	0.195	0.001	0.215	0.000	9
0.507	0.206	0.001	0.195	0.001	0.214	0.000	10
0.607	0.206	0.001	0.195	0.001	0.213	0.000	11
0.707	0.206	0.001	0.195	0.001	0.213	0.000	12
0.807	0.206	0.001	0.195	0.001	0.212	0.000	13
0.907	0.206	0.001	0.194	0.001	0.212	0.000	14
1.007	0.206	0.001	0.194	0.002	0.212	0.000	15
1.107	0.206	0.001	0.194	0.002	0.212	0.000	16
1.207	0.206	0.001	0.193	0.002	0.211	0.000	17
1.307	0.206	0.001	0.193	0.002	0.211	0.000	18
1.407	0.206	0.001	0.192	0.002	0.211	0.000	19
1.507	0.206	0.001	0.192	0.002	0.211	0.001	20
1.607	0.206	0.001	0.192	0.002	0.210	0.001	21
1.707	0.206	0.001	0.191	0.002	0.210	0.001	22
1.807	0.206	0.001	0.191	0.002	0.210	0.001	23
1.907	0.205	0.001	0.190	0.002	0.210	0.001	24

TABLE A-16. Apparent Rate Constants and Standard Deviations for 3 Sets of Experiments (20 Stopped-Flow Shots Each) on the Reaction Between MAH (0.4 mM) and Tr^+ (0.05 M) in Acetonitrile at 298 K and 440 nm

time/s	Set 1		Set 2		Set 3		Segment
	$k_{\text{app}}/\text{s}^{-1}$	S.D.	$k_{\text{app}}/\text{s}^{-1}$	S.D.	$k_{\text{app}}/\text{s}^{-1}$	S.D.	
0.017	0.221	0.019	0.228	0.035	0.248	0.013	1
0.027	0.218	0.010	0.224	0.010	0.246	0.008	2
0.037	0.218	0.006	0.220	0.007	0.242	0.004	3
0.047	0.215	0.005	0.215	0.005	0.238	0.004	4
0.057	0.213	0.004	0.210	0.004	0.235	0.003	5
0.107	0.208	0.003	0.200	0.002	0.225	0.002	6
0.207	0.205	0.001	0.195	0.002	0.218	0.001	7
0.307	0.204	0.001	0.195	0.002	0.215	0.001	8
0.407	0.204	0.001	0.194	0.002	0.214	0.000	9
0.507	0.204	0.001	0.195	0.001	0.213	0.000	10
0.607	0.204	0.001	0.194	0.001	0.212	0.000	11
0.707	0.204	0.001	0.194	0.001	0.211	0.000	12
0.807	0.204	0.001	0.194	0.001	0.211	0.000	13
0.907	0.204	0.001	0.194	0.001	0.210	0.000	14
1.007	0.204	0.001	0.194	0.001	0.210	0.001	15
1.107	0.204	0.001	0.193	0.001	0.210	0.001	16
1.207	0.204	0.001	0.193	0.001	0.209	0.001	17
1.307	0.204	0.001	0.193	0.001	0.209	0.001	18
1.407	0.204	0.001	0.192	0.001	0.209	0.001	19
1.507	0.204	0.001	0.192	0.001	0.209	0.001	20
1.607	0.204	0.001	0.192	0.001	0.209	0.001	21
1.707	0.204	0.001	0.192	0.001	0.208	0.001	22
1.807	0.204	0.001	0.191	0.001	0.208	0.001	23
1.907	0.204	0.001	0.191	0.001	0.208	0.001	24

TABLE A-17. Apparent Rate Constants and Standard Deviations for 3 Sets of Experiments (20 Stopped-Flow Shots Each) on the Reaction Between MAH (0.4 mM) and Tr⁺ (0.05 M) in Acetonitrile at 298 K and 450 nm

time/s	Set 1		Set 2		Set 3		Segment
	k_{app}/s^{-1}	S.D.	k_{app}/s^{-1}	S.D.	k_{app}/s^{-1}	S.D.	
0.017	0.227	0.030	0.262	0.036	0.255	0.027	1
0.027	0.228	0.010	0.245	0.014	0.249	0.016	2
0.037	0.229	0.012	0.240	0.011	0.243	0.011	3
0.047	0.226	0.011	0.233	0.013	0.238	0.010	4
0.057	0.220	0.009	0.233	0.035	0.231	0.010	5
0.107	0.208	0.004	0.213	0.006	0.218	0.007	6
0.207	0.203	0.003	0.209	0.005	0.213	0.003	7
0.307	0.202	0.002	0.207	0.004	0.210	0.003	8
0.407	0.203	0.001	0.206	0.004	0.209	0.002	9
0.507	0.203	0.001	0.206	0.004	0.208	0.002	10
0.607	0.204	0.001	0.206	0.004	0.208	0.002	11
0.707	0.204	0.001	0.205	0.004	0.207	0.002	12
0.807	0.204	0.001	0.205	0.004	0.207	0.002	13
0.907	0.204	0.001	0.204	0.004	0.206	0.002	14
1.007	0.204	0.001	0.204	0.004	0.206	0.002	15
1.107	0.204	0.001	0.204	0.003	0.205	0.002	16
1.207	0.204	0.001	0.203	0.003	0.205	0.002	17
1.307	0.204	0.001	0.203	0.003	0.205	0.002	18
1.407	0.204	0.001	0.202	0.003	0.204	0.002	19
1.507	0.204	0.001	0.202	0.003	0.204	0.002	20
1.607	0.204	0.001	0.202	0.003	0.203	0.002	21
1.707	0.203	0.001	0.201	0.003	0.203	0.002	22
1.807	0.203	0.001	0.201	0.003	0.203	0.002	23
1.907	0.203	0.001	0.201	0.003	0.202	0.002	24

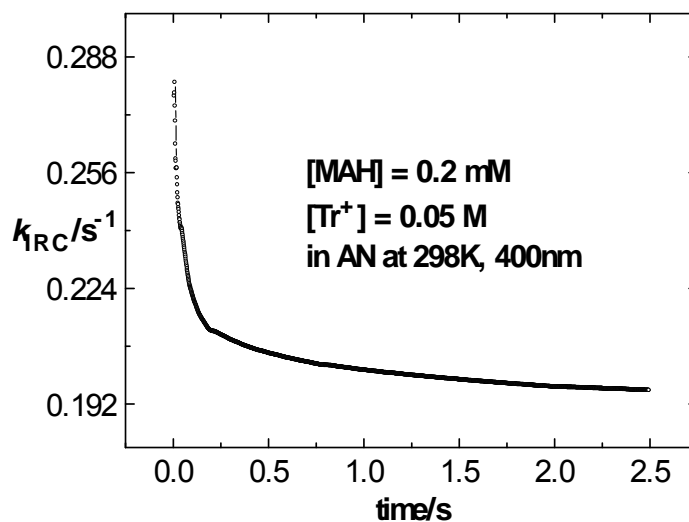


FIGURE A-9. Apparent instantaneous rate constants (k_{IRC}) – time plot for the reaction between MAH and Tr^+ in AN at 298K and 400 nm.

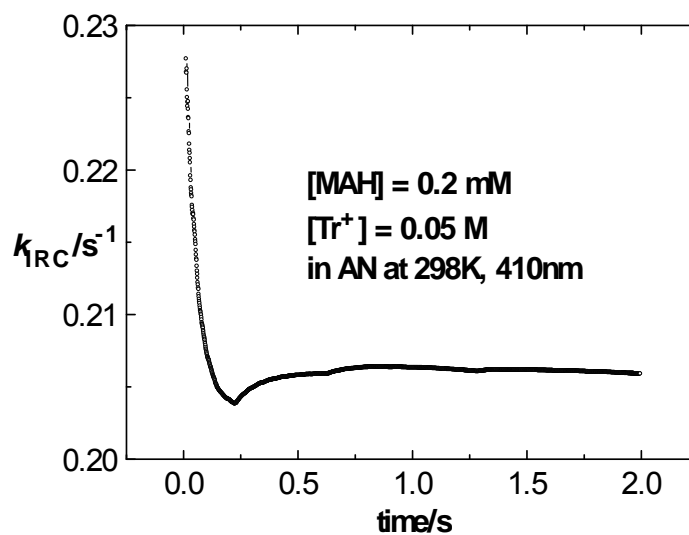


FIGURE A-10. Apparent instantaneous rate constants (k_{IRC}) – time plot for the reaction between MAH and Tr^+ in AN at 298K and 410 nm.

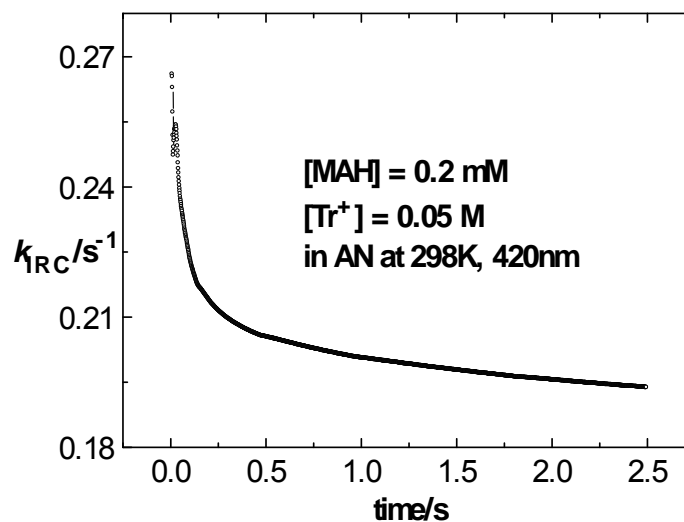


FIGURE A-11. Apparent instantaneous rate constants (k_{IRC}) – time plot for the reaction between MAH and Tr^+ in AN at 298K and 420 nm.

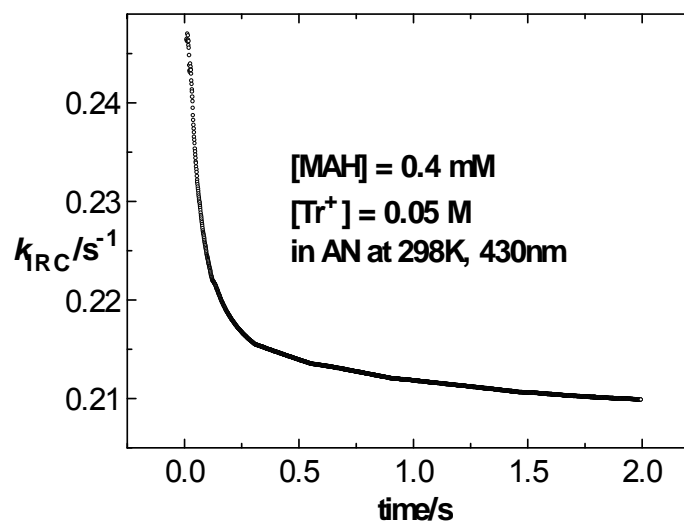


FIGURE A-12. Apparent instantaneous rate constants (k_{IRC}) – time plot for the reaction between MAH and Tr^+ in AN at 298K and 430 nm.

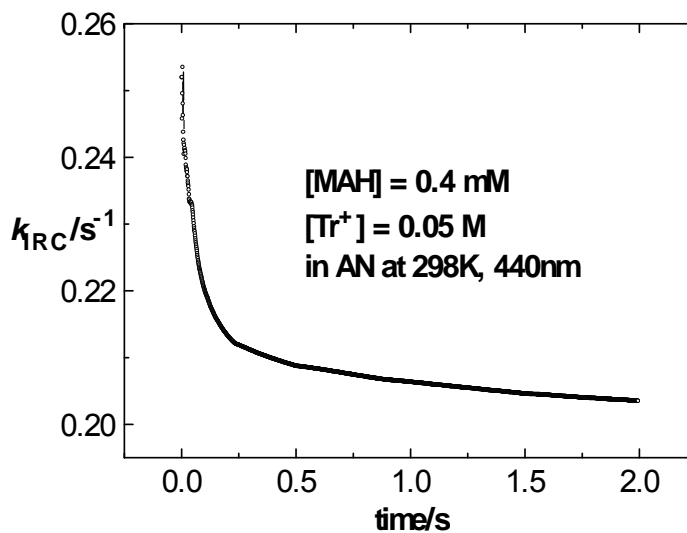


FIGURE A-13. Apparent instantaneous rate constants (k_{IRC}) – time plot for the reaction between MAH and Tr^+ in AN at 298K and 440 nm.

TABLE A-18. Rate Constants for the Reaction Between MAH (0.4 mM) and Tr^+ (0.05 M) in Acetonitrile at Various Temperatures

T/K	$k_{\text{s.s.}}/\text{s}^{-1}$	$k_2/\text{M}^{-1} \text{s}^{-1}$	$\Delta H^\ddagger = 11.0 \text{ kcal mol}^{-1}$ $\Delta S^\ddagger = -18.7 \text{ cal mol}^{-1} \text{K}^{-1}$ $\Delta G^\ddagger = 16.6 \text{ kcal mol}^{-1}$
288	0.103	2.06	
298	0.207	4.14	
308	0.387	7.74	
318	0.703	14.1	

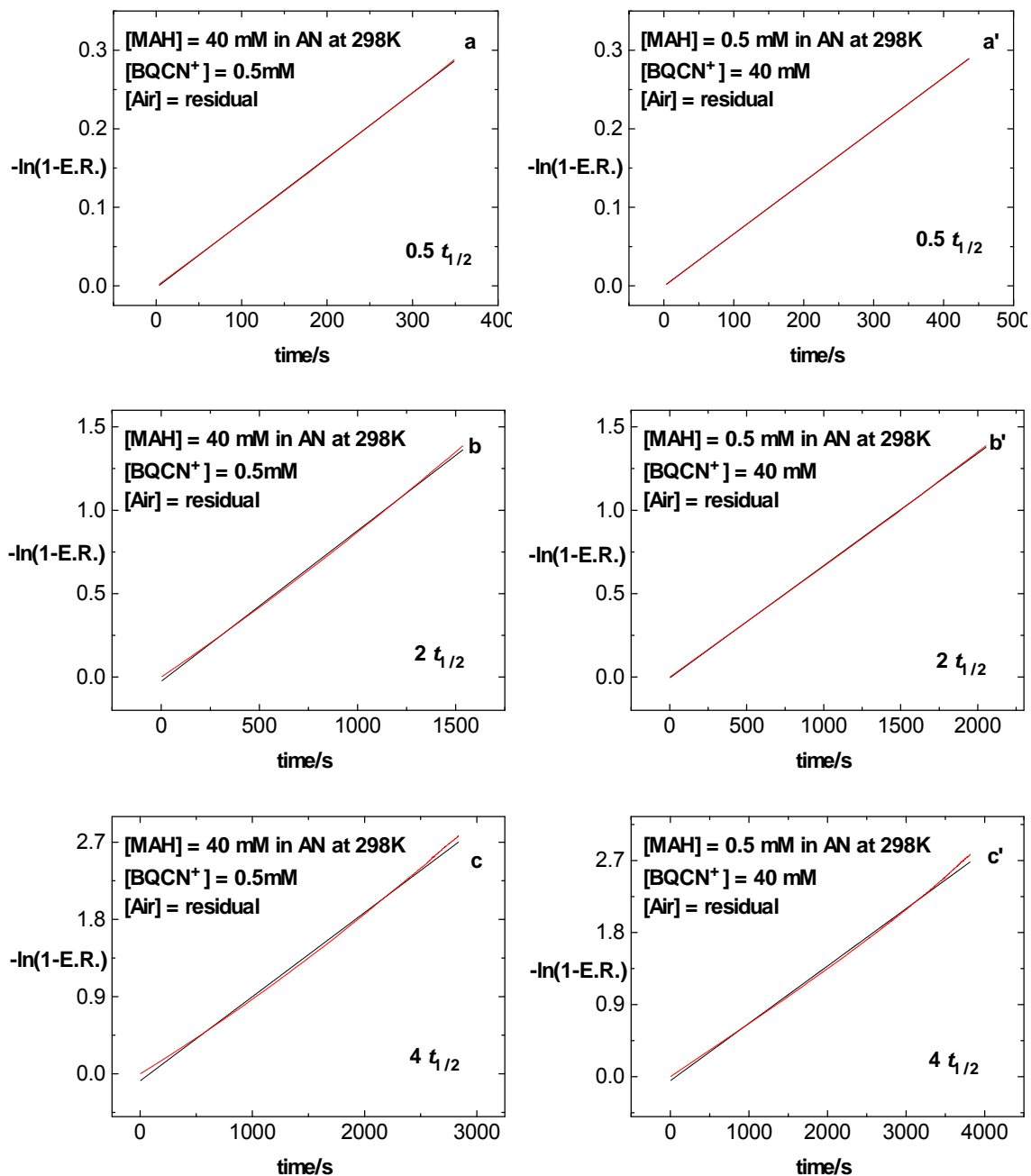


FIGURE A-14. A comparison pseudo-first-order plots for the reactions of MAH (40 mM) with BQCN⁺ (0.50 mM) (a, b and c) to those of MAH (0.5 mM) with BQCN⁺ (40 mM) (a', b' and c') in AN in the presence of residual oxygen at 298 K and 430 nm.

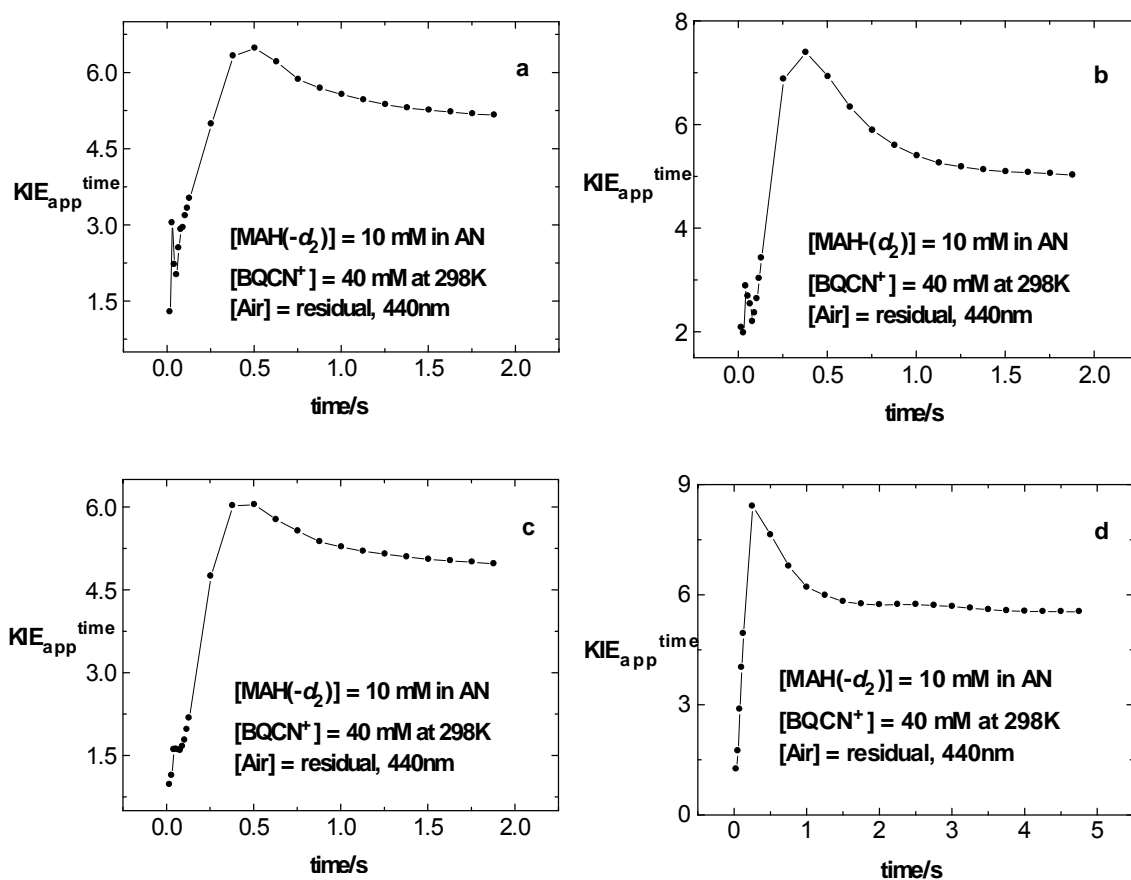


FIGURE A-15. Apparent KIE for the reactions of MAH/MAH- d_2 (10 mM) with BQCN $^+$ (40 mM) in AN in the presence of residual oxygen at 298 K and 440 nm as a function of reaction time.

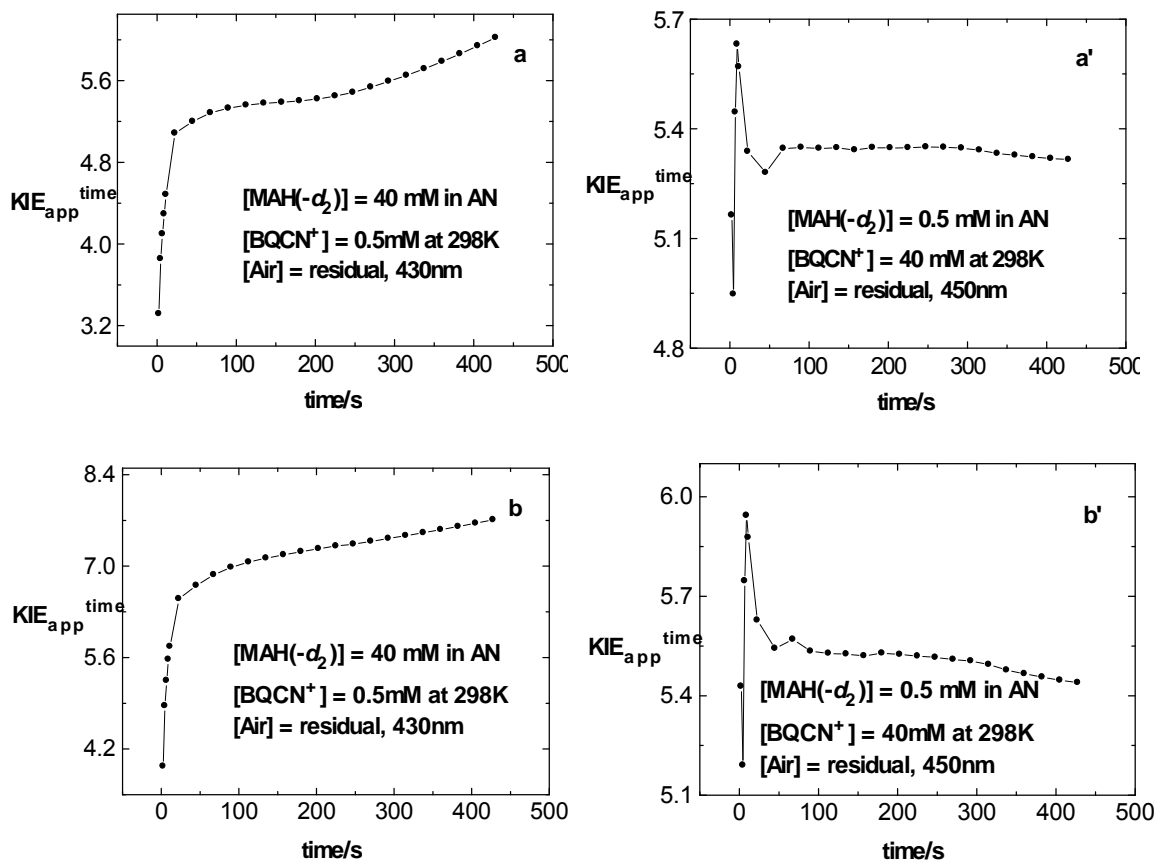


FIGURE A-16. Apparent KIE for the reactions of MAH/MAH- d_2 (40 mM) with BQCN⁺ (0.50 mM) (a and b) and MAH/MAH- d_2 (0.5 mM) with BQCN⁺ (40 mM) (a' and b') in AN in the presence of residual oxygen at 298 K and 430 nm or 450 nm as a function of reaction time.

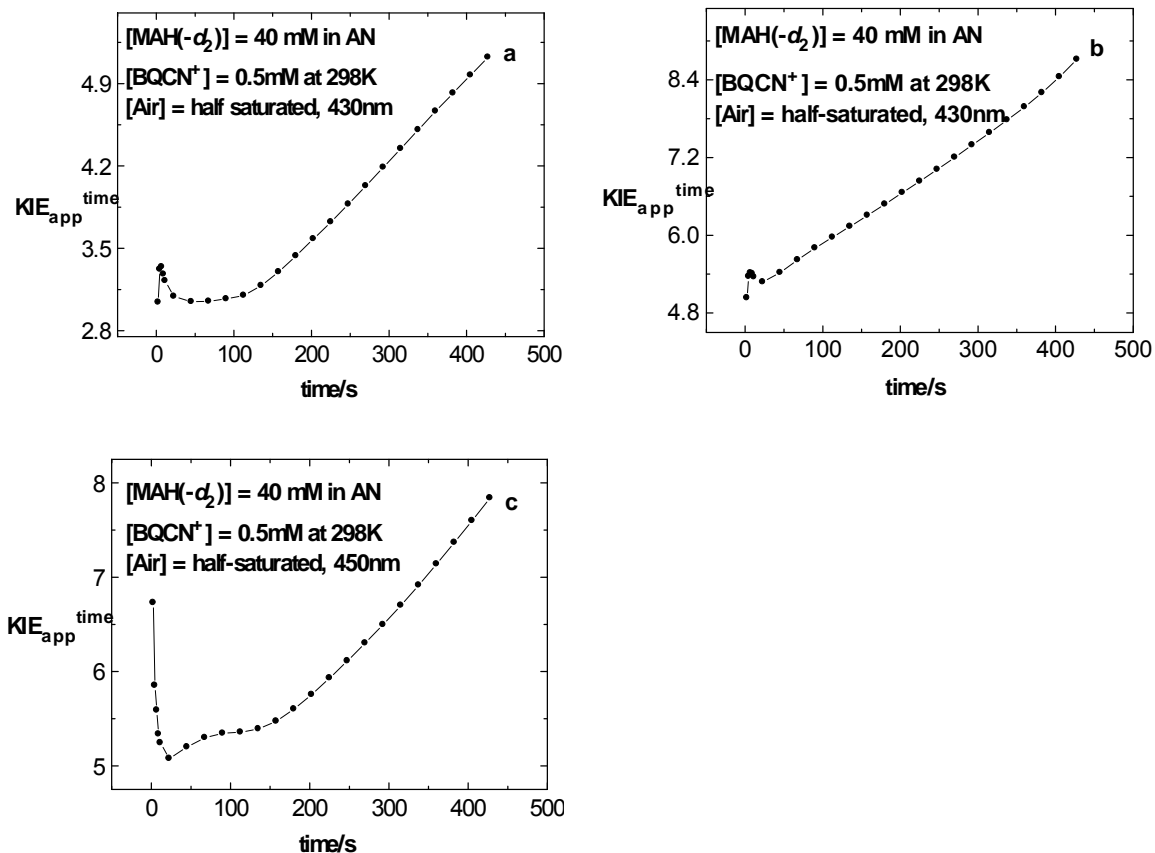


FIGURE A-17. Apparent KIE for the reactions of MAH/MAH- d_2 (40 mM) with BQCN $^+$ (0.50 mM) in AN half-saturated with air at 298 K and 430 nm or 450 nm as a function of reaction time.

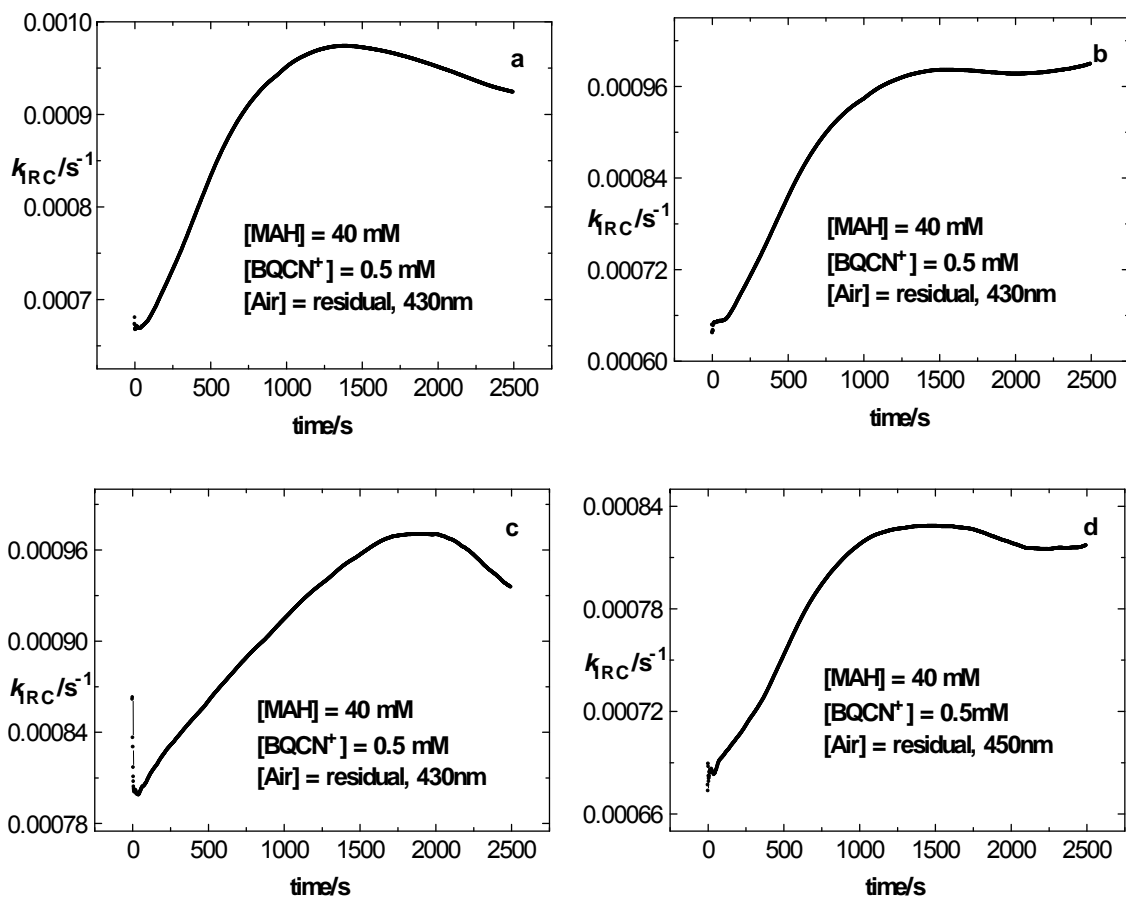


FIGURE A-18. Apparent instantaneous rate constants (k_{IRC}) – time plots for the reaction of MAH (40 mM) with BQCN⁺ (0.50 mM) in AN in the presence of residual oxygen at 298 K and 430 nm or 450nm (four sets).

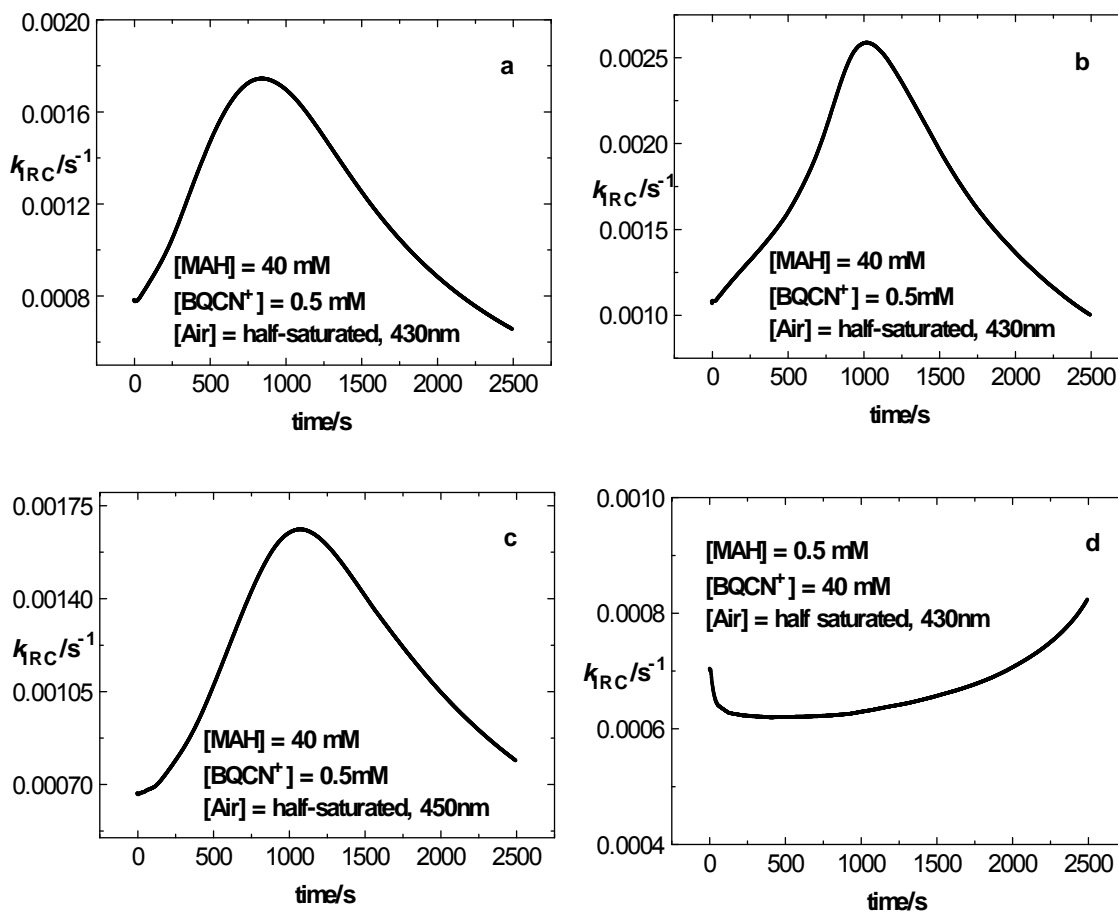


FIGURE A-19. Apparent instantaneous rate constants (k_{IRC}) – time plots for the reactions of MAH (40 mM) with BQCN⁺ (0.50 mM) (a, b and c) and MAH (0.5 mM) with BQCN⁺ (40 mM) (d) in AN half-saturated with air at 298 K and 430 nm or 450 nm.

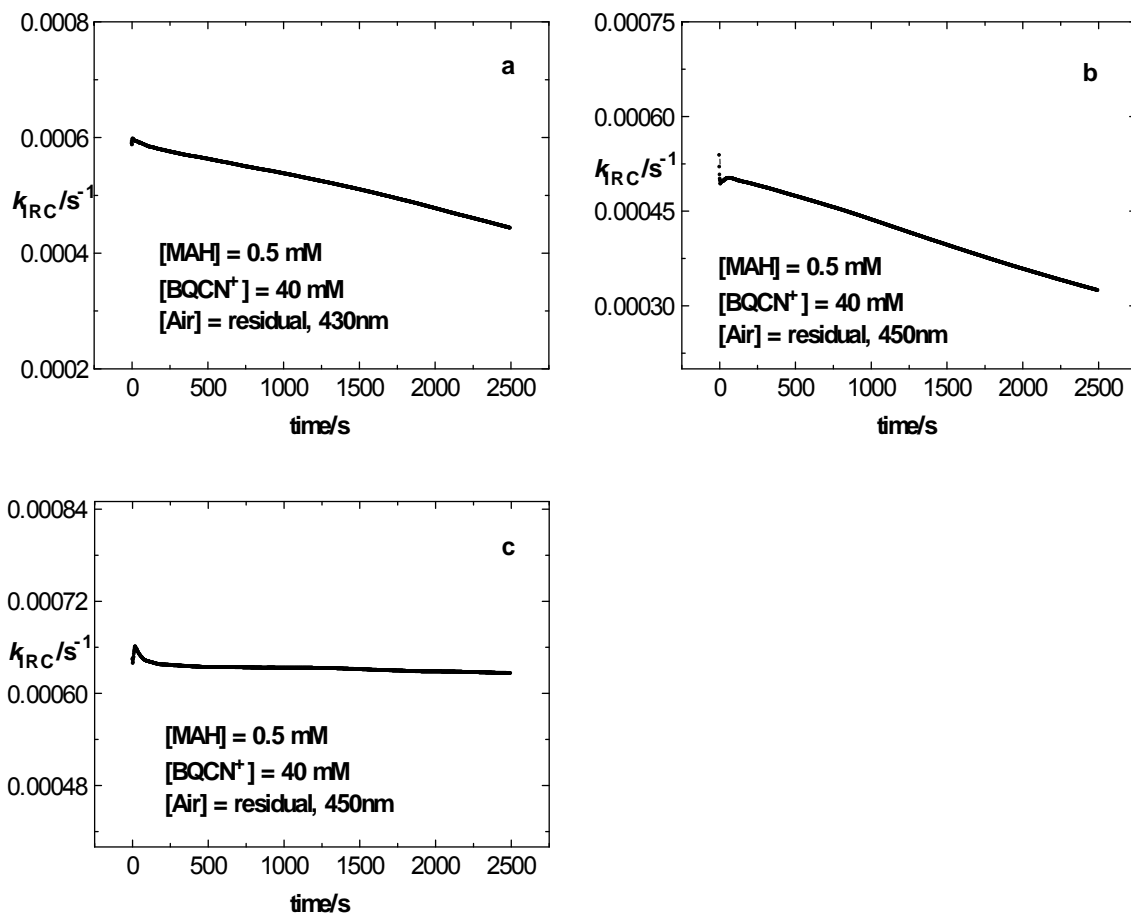


FIGURE A-20. Apparent instantaneous rate constants (k_{IRC}) – time plots for the reaction of MAH (0.5 mM) with BQCN⁺ (40 mM) in AN in the presence of residual oxygen at 298 K and 430 nm or 450nm (three sets).

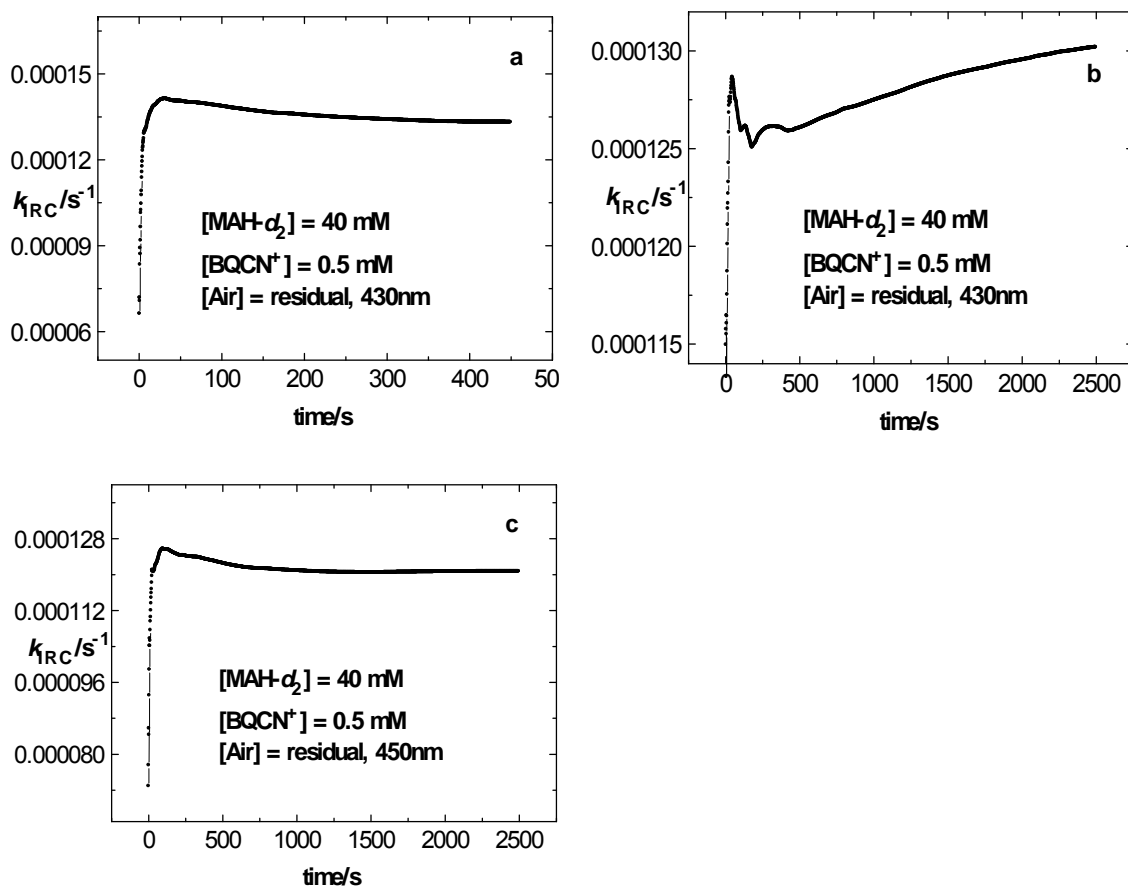


FIGURE A-21. Apparent instantaneous rate constants (k_{IRC}) – time plots for the reaction of MAH- d_2 (40 mM) with BQCN⁺ (0.50 mM) in AN in the presence of residual oxygen at 298 K and 430 nm or 450nm (three sets).

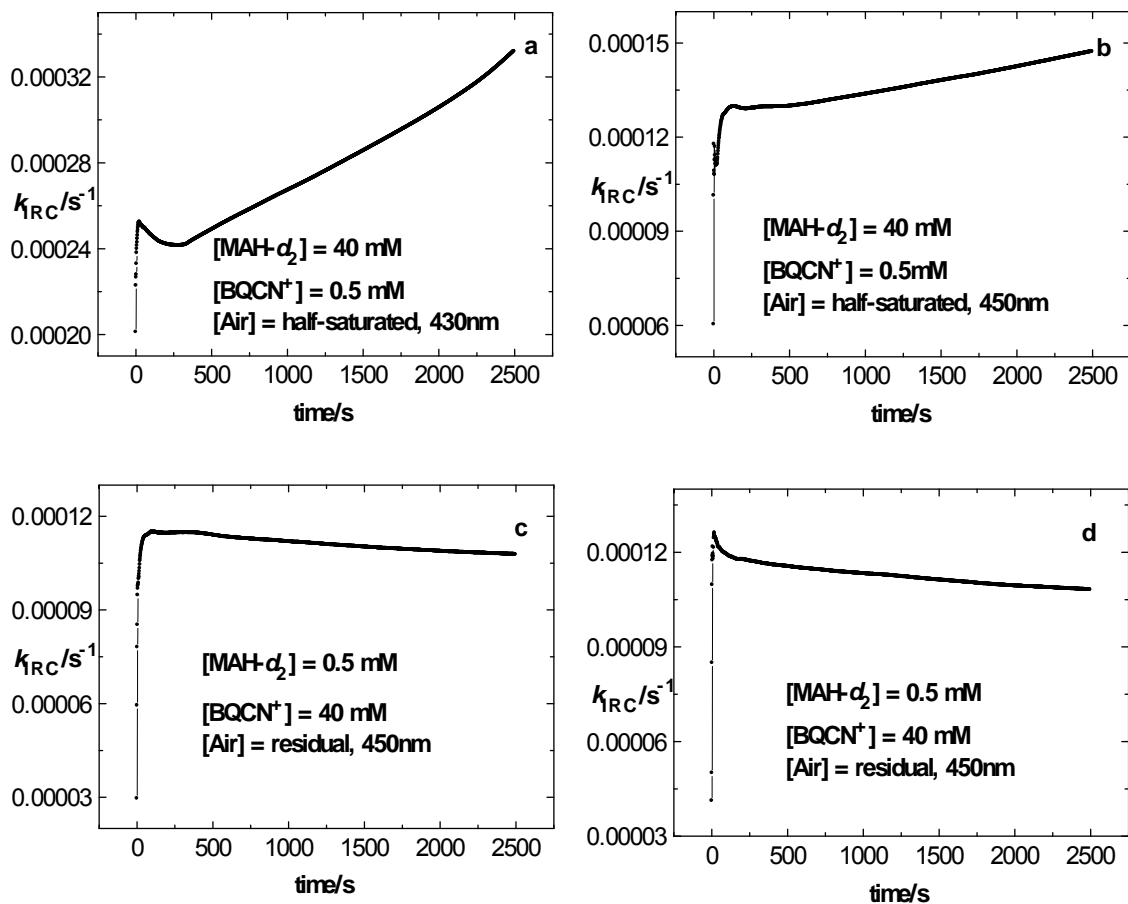


FIGURE A-22. Apparent instantaneous rate constants (k_{IRC}) – time plots for the reactions of $MAH-d_2$ (40 mM) with $BQCN^+$ (0.50 mM) in AN half-saturated with air at 430nm or 450 nm (a and b) and $MAH-d_2$ (0.5 mM) with $BQCN^+$ (40 mM) in the presence of residual oxygen at 298 K and 450 nm (c and d).

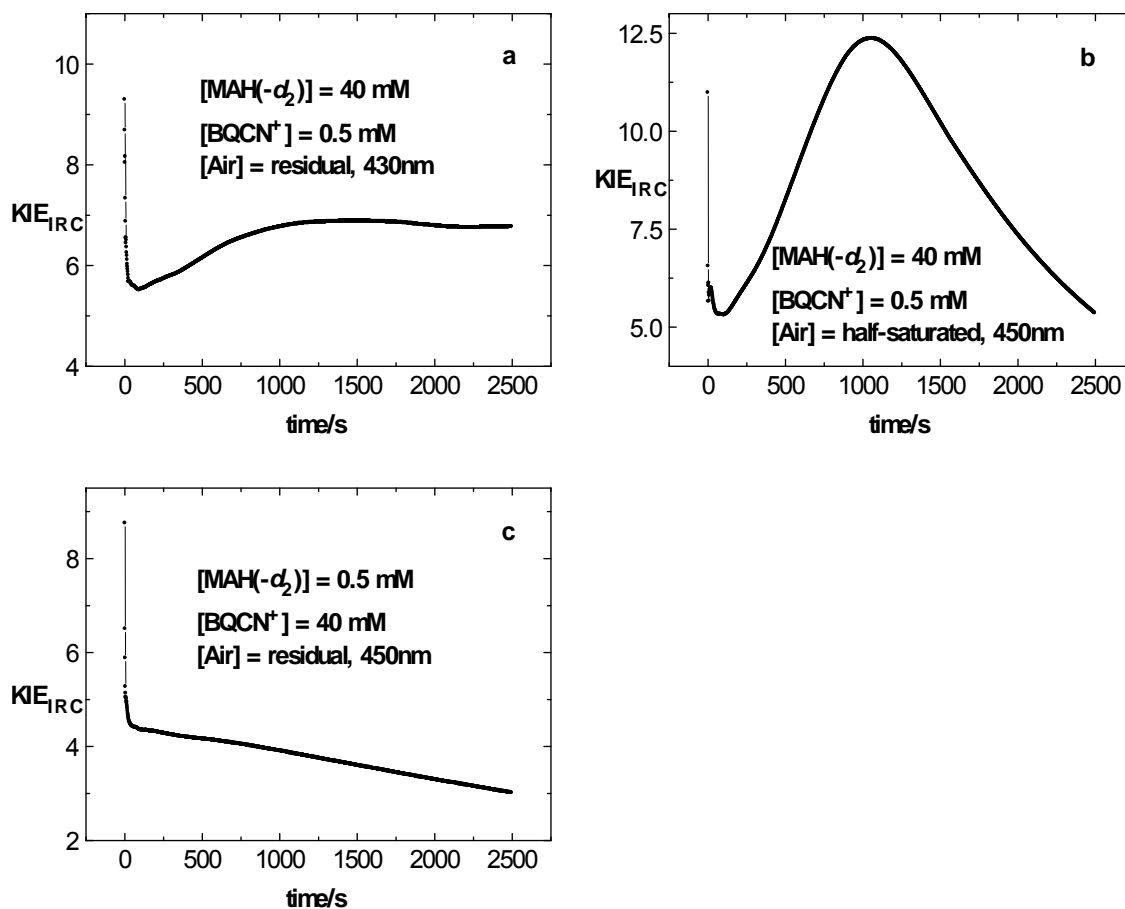


FIGURE A-23. KIE_{IRC} plots for the reactions of MAH/MAH-*d*₂ (40 mM) with BQCN⁺ (0.50 mM) in AN in the presence of residual oxygen (a) and half-saturated with air (b) and MAH/MAH-*d*₂ (0.5 mM) with BQCN⁺ (40 mM) in the presence of residual oxygen (c) at 298 K and 450 nm.

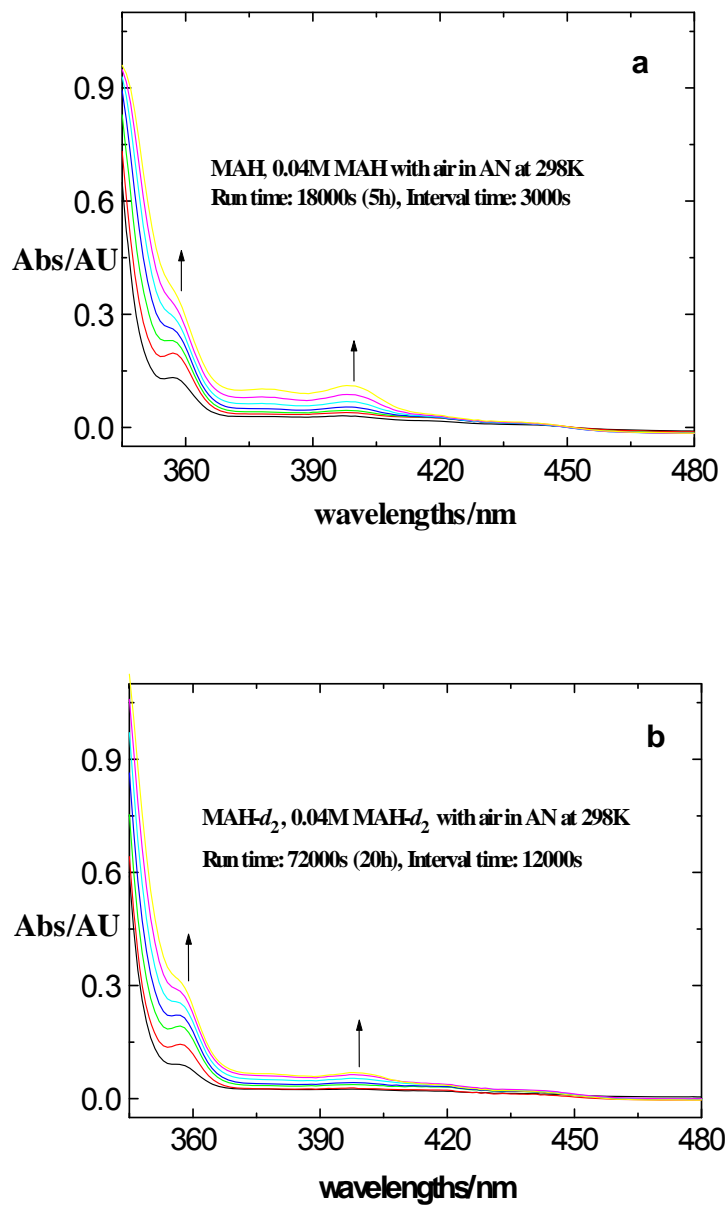


FIGURE A-24. UV/Vis absorption spectra for the reactions of MAH with air (a) and MAH- d_2 with air (b) at 298K.

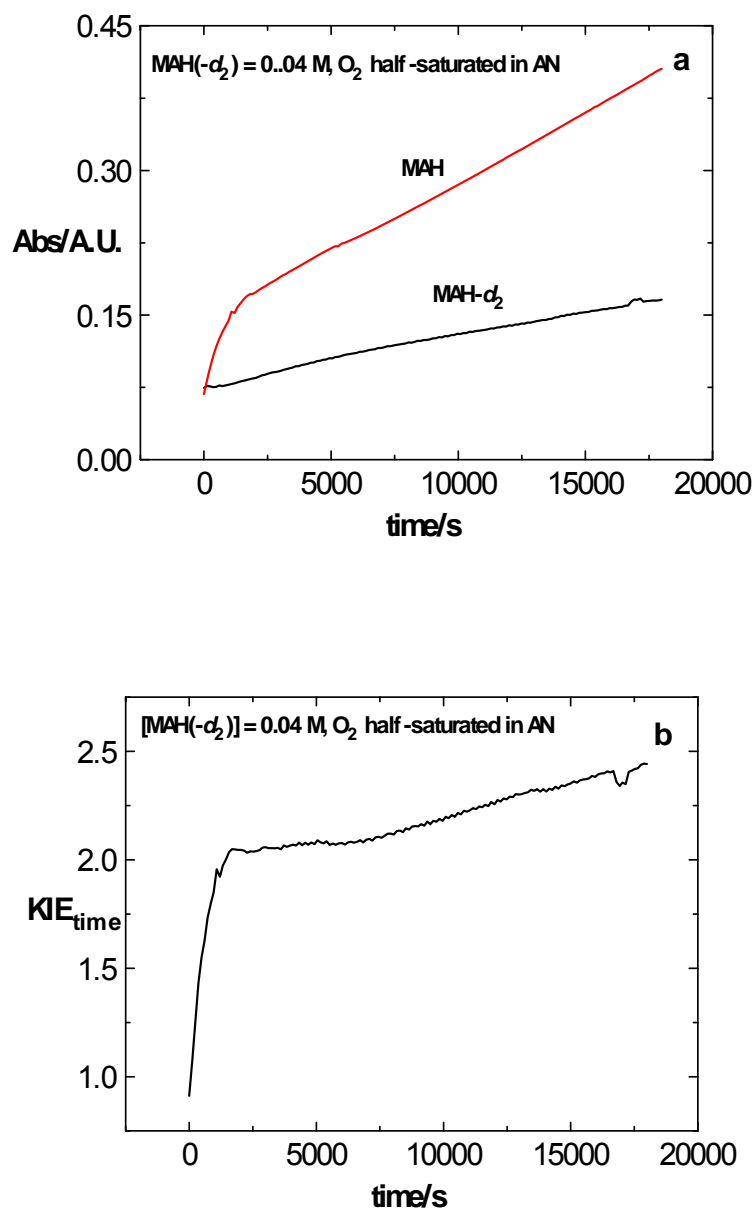


FIGURE A-25. Absorbance – time curves (a) and KIE_{time} – time plot (b) for the reactions of MAH/MAH- d_2 with oxygen in AN half-saturated with air at 298K.

TABLE A-19. Apparent Steady-State Rate Constants for 3 Sets of Experiments (20 Stopped-Flow Shots Each) on the Reaction Between TMT⁺ (0.02 mM) and NaOAc (0.5 M) in Acetic Acid at Various Temperatures and 480 nm

T/K	$k_{s.s.}/s^{-1}$			
	Set 1	Set 2	Set 3	Average
293	0.0552	0.0561	0.0697	0.0603
303	0.112	0.121	0.132	0.122
313	0.279	0.209	0.235	0.241
323	0.496	0.433	0.470	0.466

TABLE A-20. Equilibrium Constants (K_4) for 3 Sets of Experiments (20 Stopped-Flow Shots Each) on the Reaction Between TMT⁺ (0.02 mM) and NaOAc (0.5 M) in Acetic Acid at Various Temperatures and 480 nm

T/K	K_4			
	Set 1	Set 2	Set 3	Average
293	1.144	1.262	1.203	1.203
303	0.814	1.212	0.805	0.944
313	0.820	0.728	0.774	0.774
323	0.489	0.659	0.677	0.608

TABLE A-21. Apparent Steady-State Rate Constants for 3 Sets of Experiments (20 Stopped-Flow Shots Each) on the Reaction Between TMT⁺ (0.02 mM) and Bu₄N⁺ HOAc/AcO⁻ (0.005 M) in HOAc/AN (1/1, v/v) at Various Temperatures and 480 nm

T/K	$k_{s.s.}/s^{-1}$			
	Set 1	Set 2	Set 3	Average
298	0.0204	0.0158	0.0155	0.0172
303	0.0245	0.0220	0.0262	0.0242
313	0.0655	0.0584	0.0510	0.0583
323	0.0908	0.112	0.118	0.107

TABLE A-22. Equilibrium Constants (K_4) for 3 Sets of Experiments (20 Stopped-Flow Shots Each) on the Reaction Between TMT^+ (0.02 mM) and $\text{Bu}_4\text{N}^+ \text{HOAc}/\text{AcO}^-$ (0.005 M) in HOAc/AN (1/1, v/v) at Various Temperatures and 480 nm

T/K	K_4			
	Set 1	Set 2	Set 3	Average
298	0.672	0.776	0.838	0.762
303	0.568	0.861	0.818	0.749
313	0.570	0.693	0.849	0.704
323	0.548	0.597	0.757	0.634

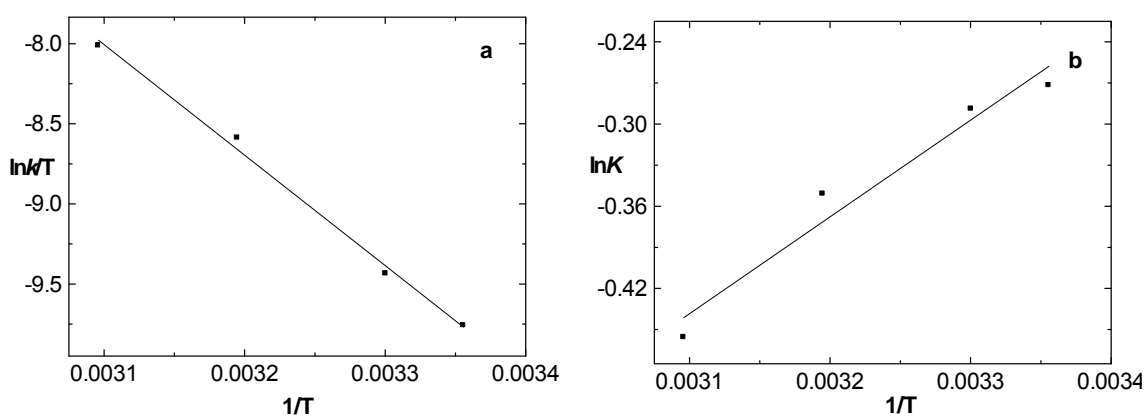


FIGURE A-26. Eyring plot for the collapse of the ion pair in HOAc/AN (1/1, v/v) (a) and Van't Hoff type plot for equilibrium (4) in HOAc/AN (1/1, v/v) (b).

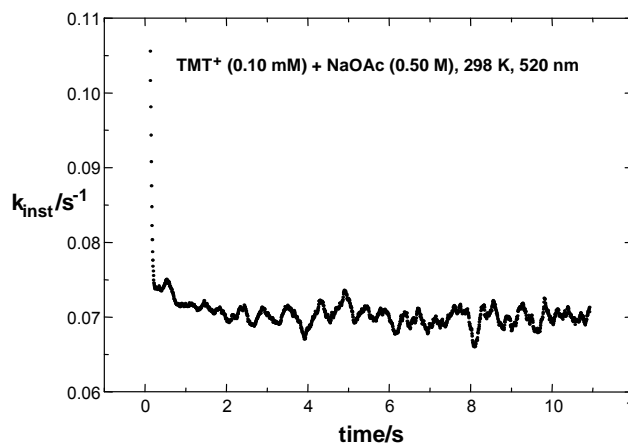


FIGURE A-27. Sliding 51 point IRC analysis over the first half-life of the reaction of TMT^+ (0.1 mM) with NaOAc (0.5 M) at 298 K and 520 nm.

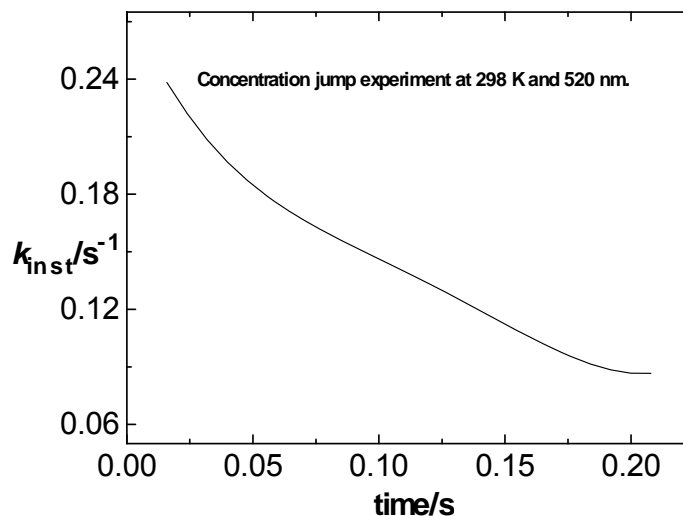


FIGURE A-28. IRC analysis of the first 3% of the extent of reaction – time profile for the concentration jump experiment on the reaction of TMT^+ (0.22 mM) with NaOAc (0.5 M) carried out at 298 K and 520 nm.

In order to insure that the more rapid initial reaction is not due to a small amount of reactive impurity in the acetate solution, the latter was treated with a sufficient quantity of TMT^+ to result in an equilibrium concentration of 0.02 mM for the combined $\text{TMT}^+/\text{TMT-OAc}$ species. This solution was then used in the second reactant syringe during a stopped-flow experiment at 520 nm and 298 K in which $[\text{TMT}^+]$ was jumped from 0.02 to 0.22 mM. (Reference for Instantaneous Rate Constant Analysis: in Chapter 6 (33) Parker, V. D. *J. Phys. Org. Chem.* **2006**, 19, 714.)

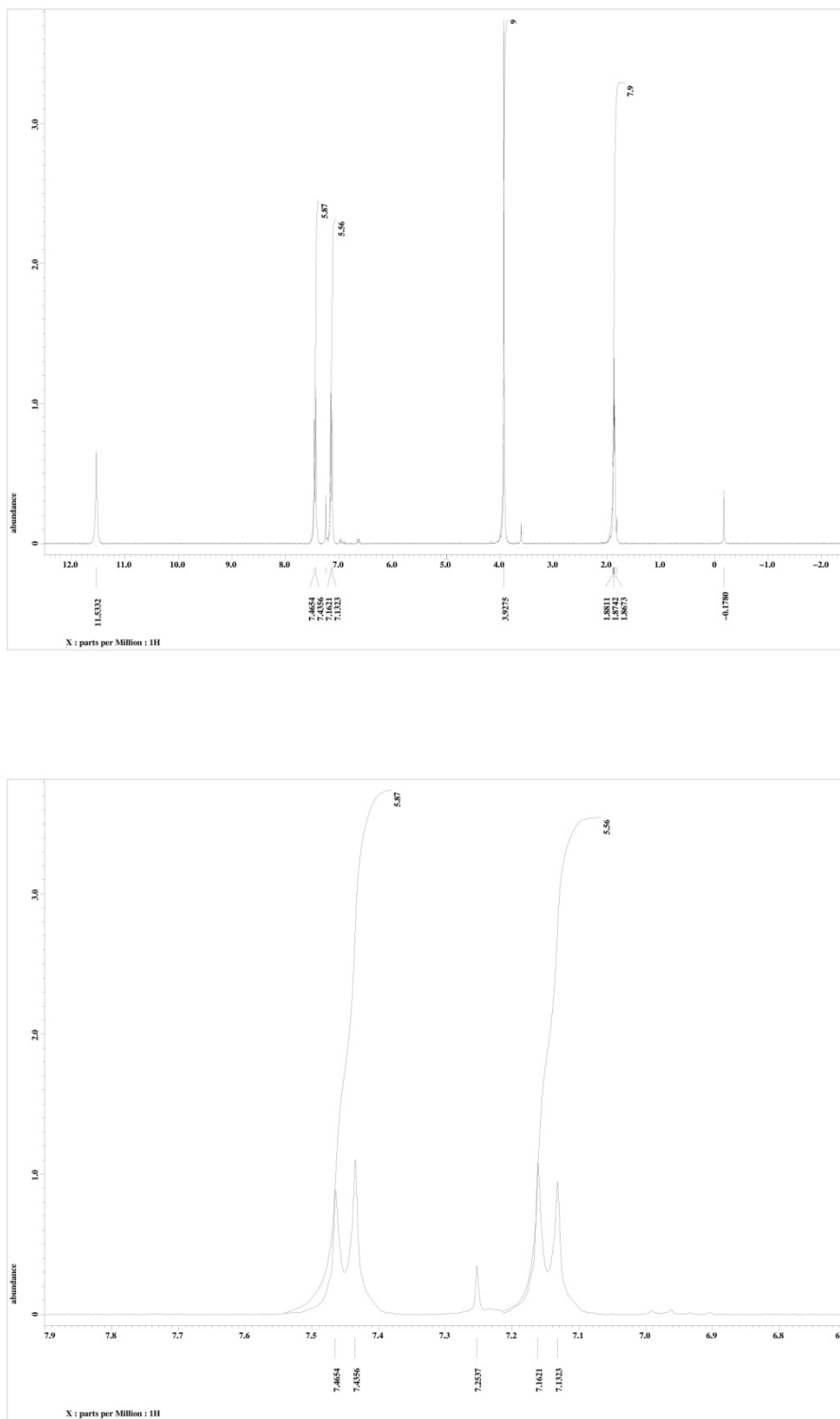


FIGURE A-29. ^1H NMR spectra of $\text{TMT}^+\text{ClO}_4^-$ in $\text{CD}_3\text{CO}_2\text{D}/\text{CDCl}_3$ (1/2).

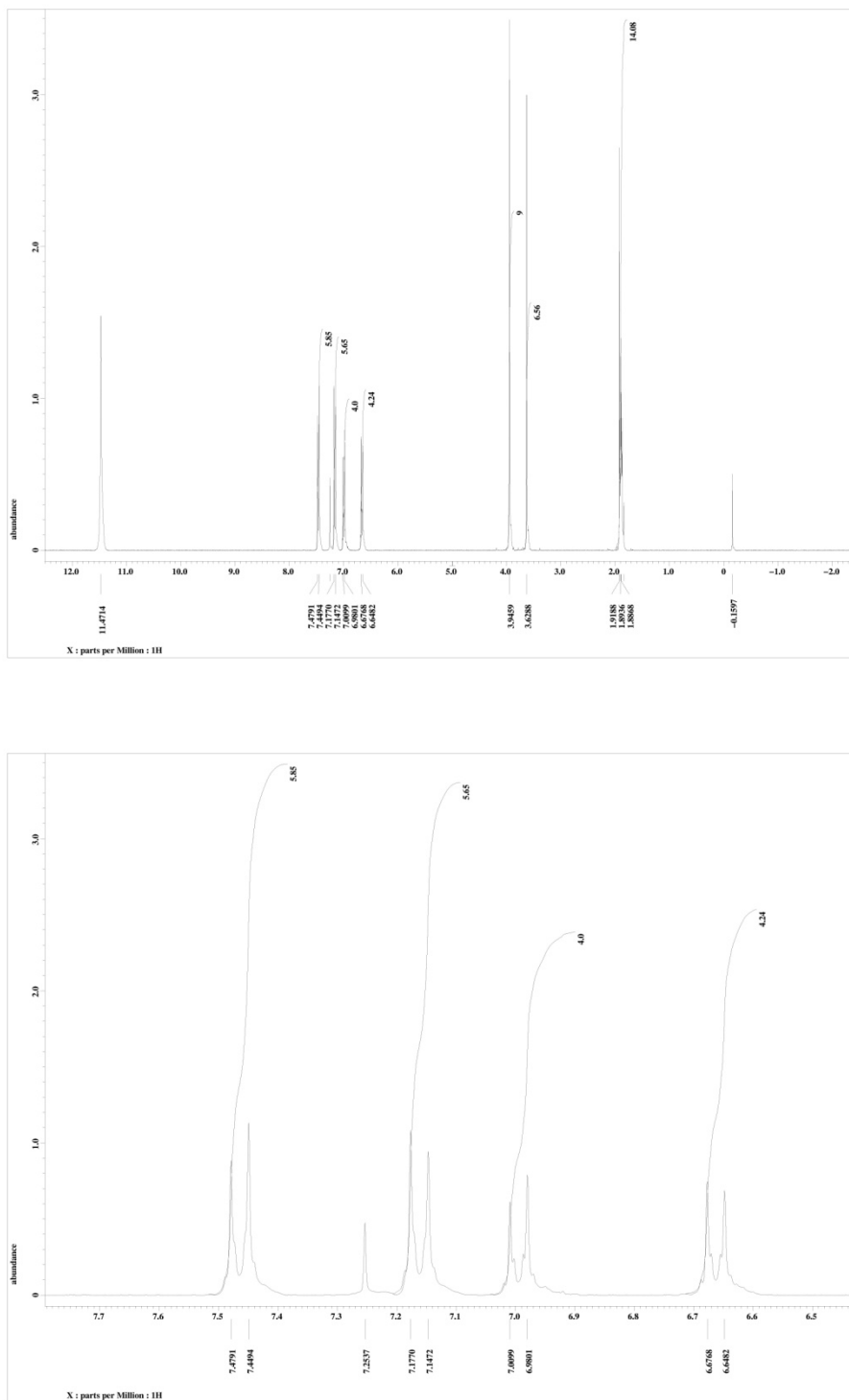


TABLE A-23. Changes in the Slopes and the Intercepts with the Extent of Reaction during Conventional Pseudo-First-Order Analysis for the Reaction of BNS with Nitroethide Ion in Two Different Solvents at 298K and 320 nm

Number of HL	in AN/Water (3/1, v/v) ^a		in DMSO/Water (3/1, v/v) ^b	
	k_{app}/s^{-1}	intercept/ s^{-1}	k_{app}/s^{-1}	intercept/ s^{-1}
0.5	0.0449	0.00524	0.835	-0.000234
1.0	0.0442	0.00756	0.819	-0.00076
2.0	0.0432	0.0154	0.790	0.0134
3.0	0.0418	0.0347	0.749	0.0365
4.0	0.0394	0.0841	0.651	0.255

^a [BNS] = 0.1 mM, [Nitroethide] = 0.04 M; ^b [BNS] = 0.05 mM, [Nitroethide] = 5.0 mM.

TABLE A-24. Changes in the Slopes and the Intercepts with the Extent of Reaction during Conventional Pseudo-First-Order Analysis for the Reaction of BNS with Nitroethide Ion in Two Different Solvents at 298K and 330 nm

Number of HL	in AN/Water (3/1, v/v)		in DMSO/Water (3/1, v/v)	
	k_{app}/s^{-1}	intercept/ s^{-1}	k_{app}/s^{-1}	intercept/ s^{-1}
0.5	0.0445	0.000640	0.820	-0.00446
1.0	0.0436	0.00383	0.806	-0.00162
2.0	0.0428	0.0102	0.780	0.0104
3.0	0.0417	0.0249	0.734	0.0465
4.0	0.0396	0.0682	0.631	0.175

TABLE A-25. Changes in the Slopes and the Intercepts with the Extent of Reaction during Conventional Pseudo-First-Order Analysis for the Reaction of BNS with Nitroethide Ion in Two Different Solvents at 298K and 340 nm

Number of HL	in AN/Water (3/1, v/v)		in DMSO/Water (3/1, v/v)	
	k_{app}/s^{-1}	intercept/ s^{-1}	k_{app}/s^{-1}	intercept/ s^{-1}
0.5	0.0447	0.0000898	0.818	-0.00454
1.0	0.0443	0.00142	0.804	-0.00176
2.0	0.0435	0.00783	0.775	0.0114
3.0	0.0423	0.0245	0.721	0.0548
4.0	0.0403	0.0645	0.585	0.235

TABLE A-26. Changes in the Slopes and the Intercepts with the Extent of Reaction during Conventional Pseudo-First-Order Analysis for the Reaction of BNS with Nitroethide Ion in Two Different Solvents at 298K and 350 nm

Number of HL	in AN/Water (3/1, v/v)		in DMSO/Water (3/1, v/v)	
	k_{app}/s^{-1}	intercept/ s^{-1}	k_{app}/s^{-1}	intercept/ s^{-1}
0.5	0.0453	0.000912	0.831	-0.00590
1.0	0.0446	0.00329	0.802	-0.000401
2.0	0.0436	0.0110	0.767	0.0157
3.0	0.0424	0.0286	0.706	0.0654
4.0	0.0398	0.0806	0.553	0.275

TABLE A-27. Changes in the Slopes and the Intercepts with the Extent of Reaction during Conventional Pseudo-First-Order Analysis for the Reaction of BNS with Nitroethide Ion in Two Different Solvents at 298K and 360 nm

Number of HL	in AN/Water (3/1, v/v)		in DMSO/Water (3/1, v/v)	
	k_{app}/s^{-1}	intercept/ s^{-1}	k_{app}/s^{-1}	intercept/ s^{-1}
0.5	0.0453	0.00701	0.899	-0.00863
1.0	0.0442	0.00991	0.877	-0.00510
2.0	0.0434	0.0172	0.867	-0.00117
3.0	0.0419	0.0377	0.856	0.00593
4.0	0.0389	0.0997	0.840	0.0218

TABLE A-28. Apparent Rate Constants and Standard Deviations Obtained by the Sequential Pseudo-First-Order Analysis for the Reaction of BNS with Nitroethide Ion in AN/Water (3/1, v/v) and DMSO/Water (3/1, v/v) over the First Half-Life at 298K and 330 nm

AN/W (3/1, v/v) ^a			DMSO/W (3/1, v/v) ^b			Segment
time/s	k_{app}/s^{-1}	\pm	time/s	k_{app}/s^{-1}	\pm	
0.047	0.0795	0.0093	0.002	1.164	0.225	1
0.089	0.0717	0.0057	0.005	0.903	0.185	2
0.132	0.0618	0.0020	0.007	0.906	0.175	3
0.174	0.0571	0.0009	0.009	0.915	0.132	4
0.217	0.0543	0.0011	0.011	0.880	0.098	5
0.429	0.0490	0.0007	0.023	0.829	0.044	6
0.854	0.0468	0.0008	0.045	0.838	0.013	7
1.279	0.0461	0.0008	0.067	0.843	0.011	8
1.704	0.0460	0.0007	0.090	0.836	0.010	9
2.129	0.0459	0.0007	0.112	0.829	0.008	10
2.554	0.0457	0.0007	0.135	0.825	0.006	11
2.979	0.0456	0.0007	0.157	0.822	0.005	12
3.404	0.0455	0.0007	0.179	0.819	0.005	13
3.829	0.0454	0.0007	0.202	0.817	0.004	14
4.254	0.0454	0.0007	0.224	0.815	0.004	15
4.679	0.0454	0.0008	0.247	0.813	0.004	16
5.104	0.0453	0.0008	0.269	0.811	0.004	17
5.529	0.0453	0.0008	0.291	0.809	0.004	18
5.954	0.0453	0.0008	0.314	0.808	0.004	19
6.379	0.0453	0.0008	0.336	0.806	0.004	20
6.804	0.0452	0.0008	0.359	0.805	0.004	21
7.229	0.0452	0.0009	0.381	0.804	0.004	22
7.654	0.0452	0.0009	0.403	0.802	0.004	23
8.079	0.0452	0.0009	0.426	0.801	0.004	24

^a [BNS] = 0.1 mM, [Nitroethide] = 0.04 M; ^b [BNS] = 0.05 mM, [Nitroethide] = 5.0 mM. Average of 3 sets of 20 stopped-flow repetitions.

TABLE A-29. Apparent Rate Constants and Standard Deviations Obtained by the Sequential Pseudo-First-Order Analysis for the Reaction of BNS with Nitroethide Ion in AN/Water (3/1, v/v) and DMSO/Water (3/1, v/v) over the First Half-Life at 298K and 340 nm

AN/W (3/1, v/v) ^a			DMSO/W (3/1, v/v) ^b			Segment
time/s	k_{app}/s^{-1}	\pm	time/s	k_{app}/s^{-1}	\pm	
0.047	0.0853	0.0048	0.002	1.069	0.268	1
0.089	0.0798	0.0046	0.005	0.969	0.226	2
0.132	0.0672	0.0027	0.007	0.937	0.184	3
0.174	0.0607	0.0015	0.009	0.887	0.108	4
0.217	0.0566	0.0013	0.011	0.879	0.089	5
0.429	0.0499	0.0005	0.023	0.810	0.046	6
0.854	0.0475	0.0007	0.045	0.843	0.016	7
1.279	0.0467	0.0007	0.067	0.846	0.013	8
1.704	0.0462	0.0005	0.090	0.837	0.011	9
2.129	0.0460	0.0005	0.112	0.830	0.009	10
2.554	0.0458	0.0004	0.135	0.823	0.007	11
2.979	0.0457	0.0004	0.157	0.819	0.006	12
3.404	0.0456	0.0004	0.179	0.815	0.005	13
3.829	0.0456	0.0004	0.202	0.813	0.004	14
4.254	0.0456	0.0004	0.224	0.811	0.003	15
4.679	0.0455	0.0004	0.247	0.809	0.003	16
5.104	0.0455	0.0004	0.269	0.807	0.003	17
5.529	0.0455	0.0004	0.291	0.806	0.002	18
5.954	0.0455	0.0005	0.314	0.804	0.002	19
6.379	0.0455	0.0005	0.336	0.803	0.002	20
6.804	0.0454	0.0005	0.359	0.801	0.002	21
7.229	0.0454	0.0005	0.381	0.800	0.002	22
7.654	0.0454	0.0005	0.403	0.799	0.002	23
8.079	0.0454	0.0005	0.426	0.797	0.002	24

^a [BNS] = 0.1 mM, [Nitroethide] = 0.04 M; ^b [BNS] = 0.05 mM, [Nitroethide] = 5.0 mM. Average of 3 sets of 20 stopped-flow repetitions.

TABLE A-30. Apparent Rate Constants and Standard Deviations Obtained by the Sequential Pseudo-First-Order Analysis for the Reaction of BNS with Nitroethide Ion in AN/Water (3/1, v/v) and DMSO/Water (3/1, v/v) over the First Half-Life at 298K and 350 nm

AN/W (3/1, v/v) ^a			DMSO/W (3/1, v/v) ^b			Segment
time/s	k_{app}/s^{-1}	\pm	time/s	k_{app}/s^{-1}	\pm	
0.047	0.0957	0.0033	0.002	1.513	0.234	1
0.089	0.0912	0.0051	0.005	1.049	0.145	2
0.132	0.0783	0.0016	0.007	0.974	0.107	3
0.174	0.0695	0.0016	0.009	0.882	0.114	4
0.217	0.0643	0.0023	0.011	0.854	0.109	5
0.429	0.0544	0.0036	0.023	0.816	0.053	6
0.854	0.0497	0.0029	0.045	0.856	0.026	7
1.279	0.0480	0.0019	0.067	0.882	0.023	8
1.704	0.0471	0.0012	0.090	0.872	0.018	9
2.129	0.0465	0.0009	0.112	0.859	0.014	10
2.554	0.0461	0.0008	0.135	0.852	0.012	11
2.979	0.0459	0.0007	0.157	0.846	0.010	12
3.404	0.0458	0.0007	0.179	0.841	0.009	13
3.829	0.0457	0.0007	0.202	0.836	0.008	14
4.254	0.0456	0.0007	0.224	0.833	0.007	15
4.679	0.0456	0.0007	0.247	0.831	0.006	16
5.104	0.0455	0.0007	0.269	0.829	0.006	17
5.529	0.0455	0.0007	0.291	0.827	0.006	18
5.954	0.0454	0.0008	0.314	0.825	0.005	19
6.379	0.0454	0.0008	0.336	0.823	0.005	20
6.804	0.0454	0.0008	0.359	0.822	0.005	21
7.229	0.0454	0.0008	0.381	0.820	0.005	22
7.654	0.0454	0.0008	0.403	0.819	0.005	23
8.079	0.0453	0.0008	0.426	0.817	0.005	24

^a [BNS] = 0.1 mM, [Nitroethide] = 0.04 M; ^b [BNS] = 0.05 mM, [Nitroethide] = 5.0 mM. Average of 3 sets of 20 stopped-flow repetitions.

TABLE A-31. Apparent Rate Constants and Standard Deviations Obtained by the Sequential Pseudo-First-Order Analysis for the Reaction of BNS with Nitroethide Ion in AN/Water (3/1, v/v) and DMSO/Water (3/1, v/v) over the First Half-Life at 298K and 360 nm

AN/W (3/1, v/v) ^a			DMSO/W (3/1, v/v) ^b			Segment
time/s	k_{app}/s^{-1}	\pm	time/s	k_{app}/s^{-1}	\pm	
0.047	0.1131	0.0148	0.002	2.359	0.255	1
0.089	0.1064	0.0125	0.005	1.266	0.196	2
0.132	0.0872	0.0064	0.007	0.990	0.110	3
0.174	0.0760	0.0044	0.009	0.902	0.053	4
0.217	0.0695	0.0044	0.011	0.926	0.033	5
0.429	0.0557	0.0035	0.023	0.822	0.022	6
0.854	0.0489	0.0010	0.045	0.891	0.023	7
1.279	0.0469	0.0004	0.067	0.921	0.039	8
1.704	0.0461	0.0004	0.090	0.914	0.042	9
2.129	0.0456	0.0004	0.112	0.905	0.034	10
2.554	0.0453	0.0004	0.135	0.897	0.030	11
2.979	0.0452	0.0004	0.157	0.892	0.025	12
3.404	0.0451	0.0004	0.179	0.888	0.022	13
3.829	0.0450	0.0004	0.202	0.884	0.019	14
4.254	0.0449	0.0004	0.224	0.880	0.017	15
4.679	0.0449	0.0004	0.247	0.878	0.016	16
5.104	0.0448	0.0004	0.269	0.876	0.015	17
5.529	0.0448	0.0004	0.291	0.875	0.014	18
5.954	0.0448	0.0004	0.314	0.874	0.013	19
6.379	0.0447	0.0004	0.336	0.872	0.013	20
6.804	0.0447	0.0005	0.359	0.871	0.013	21
7.229	0.0446	0.0005	0.381	0.870	0.013	22
7.654	0.0446	0.0005	0.403	0.869	0.012	23
8.079	0.0446	0.0005	0.426	0.868	0.012	24

^a [BNS] = 0.1 mM, [Nitroethide] = 0.04 M; ^b [BNS] = 0.05 mM, [Nitroethide] = 5.0 mM. Average of 3 sets of 20 stopped-flow repetitions.

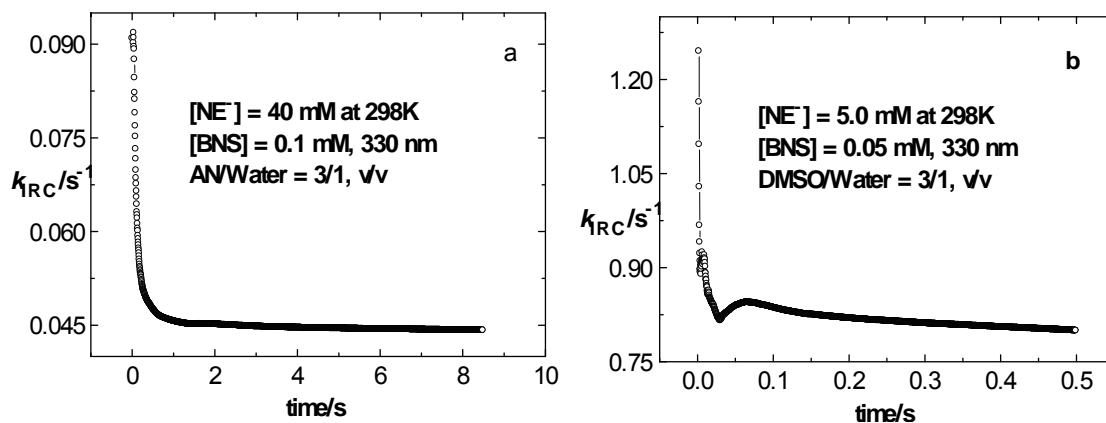


FIGURE A-31. Apparent instantaneous rate constants (k_{IRC}) – time plots for the reaction between BNS and nitroethide ion in AN/Water (3/1, v/v) (a) and DMSO/Water (3/1, v/v) (b) at 298K and 330 nm.

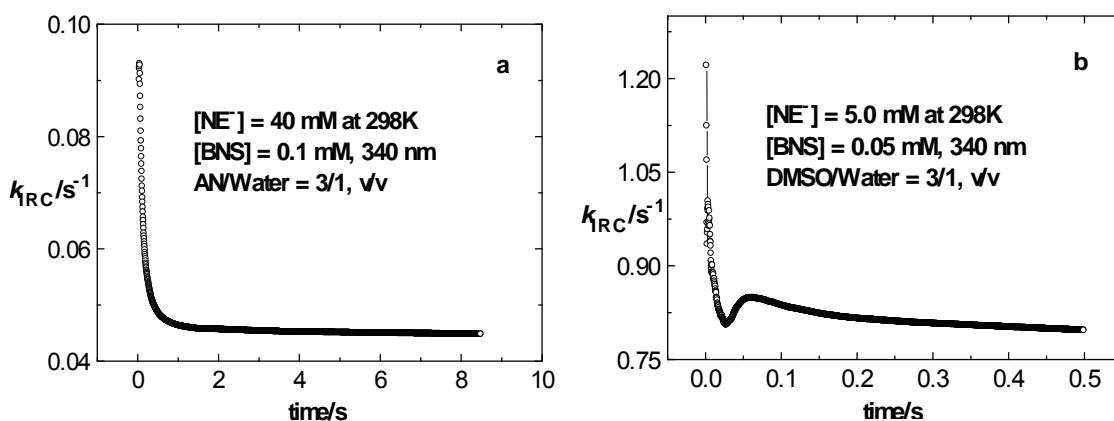


FIGURE A-32. Apparent instantaneous rate constants (k_{IRC}) – time plots for the reaction between BNS and nitroethide ion in AN/Water (3/1, v/v) (a) and DMSO/Water (3/1, v/v) (b) at 298K and 340 nm.

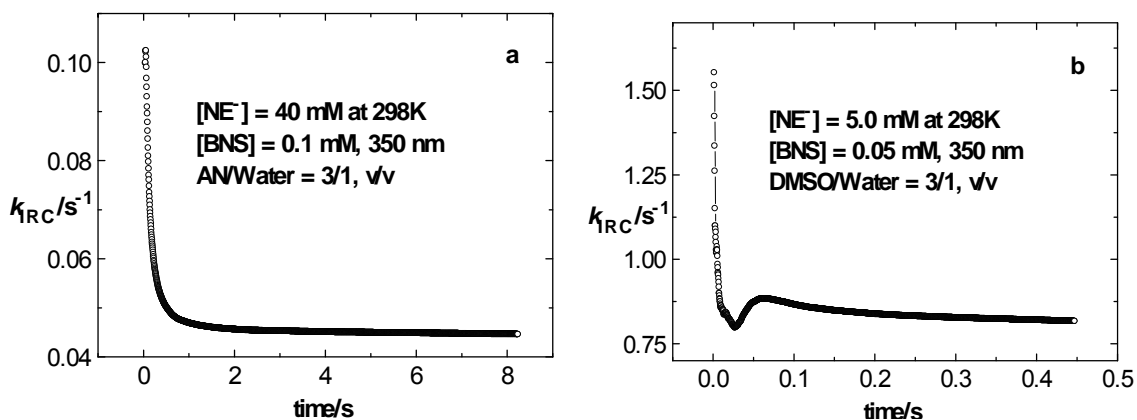


FIGURE A-33. Apparent instantaneous rate constants (k_{IRC}) – time plots for the reaction between BNS and nitroethide ion in AN/Water (3/1, v/v) (a) and DMSO/Water (3/1, v/v) (b) at 298K and 350 nm.

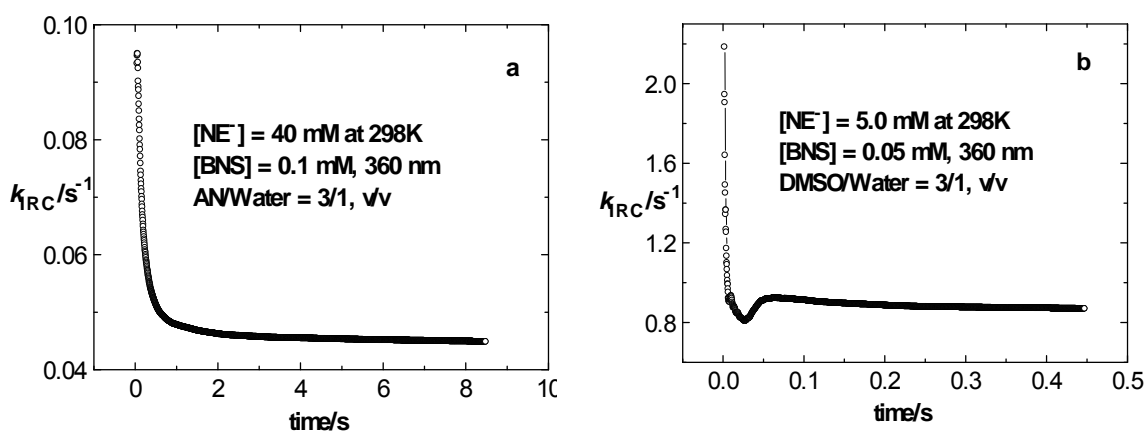


FIGURE A-34. Apparent instantaneous rate constants (k_{IRC}) – time plots for the reaction between BNS and nitroethide ion in AN/Water (3/1, v/v) (a) and DMSO/Water (3/1, v/v) (b) at 298K and 360 nm.

TABLE A-32. Second-Order Rate Constants for 3 Sets of Experiments (20 Stopped-Flow Shots Each) on the Reaction Between BNS (0.1 mM) and Nitroethide Ion (0.04 M) in AN/Water (3/1, v/v) at Various Temperatures and 320 nm

T/K	$k_2/\text{M}^{-1} \text{s}^{-1}$				
	Set 1	Set 2	Set 3	Average	
293	0.76	0.78	0.74	0.76	$\Delta H^\ddagger = 14.8 \text{ kcal mol}^{-1}$ $\Delta S^\ddagger = -8.37 \text{ cal mol}^{-1} \text{K}^{-1}$ $\Delta G^\ddagger = 17.3 \text{ kcal mol}^{-1}$
303	1.84	1.81	1.80	1.82	
313	4.20	4.18	4.18	4.19	
323	9.10	8.83	8.78	8.90	

TABLE A-33. Apparent Rate Constants for the Displacement Reaction Between MNBB⁺ (0.04 M) and PNPO⁻ (0.06 mM) in Acetonitrile over the First Half-Life at 298K as a Function of Wavelengths^a

time/s	440 nm		450 nm		460 nm		Segment
	$k_{\text{app}}/\text{s}^{-1}$	\pm	$k_{\text{app}}/\text{s}^{-1}$	\pm	$k_{\text{app}}/\text{s}^{-1}$	\pm	
1.1	0.00485	0.00216	0.00804	0.00213	0.00676	0.00173	1
2.1	0.00283	0.00114	0.00332	0.00077	0.00393	0.00095	2
3.1	0.00242	0.00085	0.00252	0.00076	0.00321	0.00062	3
4.1	0.00227	0.00069	0.00233	0.00074	0.00291	0.00043	4
5.1	0.00225	0.00054	0.00231	0.00065	0.00276	0.00033	5
10.1	0.00232	0.00036	0.00249	0.00038	0.00248	0.00023	6
20.1	0.00239	0.00026	0.00248	0.00016	0.00239	0.00019	7
30.1	0.00228	0.00016	0.00233	0.00009	0.00221	0.00012	8
40.1	0.00215	0.00008	0.00220	0.00006	0.00208	0.00008	9
50.1	0.00206	0.00004	0.00210	0.00005	0.00199	0.00006	10
60.1	0.00200	0.00003	0.00203	0.00004	0.00193	0.00004	11
70.1	0.00195	0.00004	0.00198	0.00003	0.00188	0.00004	12
80.1	0.00191	0.00004	0.00194	0.00003	0.00184	0.00003	13
90.1	0.00189	0.00004	0.00191	0.00002	0.00182	0.00003	14
100.1	0.00187	0.00004	0.00189	0.00002	0.00179	0.00003	15
110.1	0.00186	0.00004	0.00186	0.00002	0.00177	0.00002	16
120.1	0.00184	0.00004	0.00185	0.00002	0.00176	0.00002	17
130.1	0.00183	0.00004	0.00183	0.00002	0.00174	0.00002	18
140.1	0.00182	0.00003	0.00182	0.00002	0.00173	0.00002	19
150.1	0.00181	0.00003	0.00181	0.00002	0.00172	0.00002	20
160.1	0.00180	0.00003	0.00180	0.00002	0.00172	0.00002	21
170.1	0.00179	0.00002	0.00179	0.00002	0.00171	0.00002	22
180.1	0.00178	0.00002	0.00179	0.00002	0.00170	0.00002	23
190.1	0.00177	0.00002	0.00178	0.00002	0.00169	0.00002	24

^a Average of 10 stopped-flow repetitions.

TABLE A-34. Apparent Rate Constants for the Displacement Reaction Between PNBBr (0.04 M) and PNPO⁻ (0.06 mM) in Acetonitrile over the First Half-Life at 298K as a Function of Wavelengths^a

time/s	450 nm		460 nm		Segment
	k_{app}/s^{-1}	\pm	k_{app}/s^{-1}	\pm	
1.1	0.00694	0.00144	0.00561	0.00181	1
2.1	0.00369	0.00074	0.00278	0.00082	2
3.1	0.00274	0.00062	0.00229	0.00051	3
4.1	0.00232	0.00076	0.00219	0.00038	4
5.1	0.00213	0.00075	0.00215	0.00041	5
10.1	0.00212	0.00039	0.00228	0.00040	6
20.1	0.00249	0.00021	0.00235	0.00023	7
30.1	0.00243	0.00015	0.00226	0.00015	8
40.1	0.00232	0.00012	0.00219	0.00010	9
50.1	0.00224	0.00009	0.00213	0.00007	10
60.1	0.00217	0.00008	0.00209	0.00005	11
70.1	0.00213	0.00006	0.00206	0.00004	12
80.1	0.00209	0.00006	0.00204	0.00004	13
90.1	0.00206	0.00005	0.00202	0.00003	14
100.1	0.00204	0.00004	0.00200	0.00003	15
110.1	0.00202	0.00004	0.00199	0.00002	16
120.1	0.00201	0.00003	0.00198	0.00002	17
130.1	0.00199	0.00003	0.00197	0.00002	18
140.1	0.00198	0.00003	0.00196	0.00002	19
150.1	0.00197	0.00003	0.00196	0.00002	20
160.1	0.00196	0.00003	0.00195	0.00002	21
170.1	0.00196	0.00002	0.00195	0.00002	22
180.1	0.00195	0.00002	0.00194	0.00002	23
190.1	0.00195	0.00002	0.00194	0.00001	24

^a Average of 10 stopped-flow repetitions.

TABLE A-35. Apparent Rate Constants for the Displacement Reaction Between MNBB⁺ (0.08 M) and PNPO⁻ (0.06 mM) in Acetonitrile over the First Half-Life at 298K as a Function of Wavelengths (1)^a

time/s	410 nm		420 nm		430 nm		Segment
	k_{app}/s^{-1}	\pm	k_{app}/s^{-1}	\pm	k_{app}/s^{-1}	\pm	
0.6	0.00899	0.00893	0.00817	0.00523	0.01281	0.00789	1
1.1	0.00416	0.00375	0.00464	0.00323	0.00732	0.00272	2
1.6	0.00336	0.00250	0.00398	0.00215	0.00537	0.00170	3
2.2	0.00348	0.00213	0.00384	0.00145	0.00466	0.00136	4
2.7	0.00373	0.00170	0.00392	0.00108	0.00436	0.00111	5
5.3	0.00459	0.00057	0.00460	0.00075	0.00469	0.00089	6
10.6	0.00452	0.00040	0.00470	0.00045	0.00485	0.00056	7
15.8	0.00422	0.00035	0.00432	0.00027	0.00451	0.00036	8
21.1	0.00402	0.00030	0.00405	0.00020	0.00425	0.00028	9
26.3	0.00388	0.00024	0.00390	0.00016	0.00406	0.00023	10
31.6	0.00376	0.00019	0.00379	0.00014	0.00396	0.00019	11
36.8	0.00368	0.00015	0.00371	0.00012	0.00387	0.00016	12
42.1	0.00362	0.00013	0.00365	0.00010	0.00380	0.00014	13
47.3	0.00357	0.00010	0.00361	0.00009	0.00374	0.00012	14
52.6	0.00353	0.00009	0.00357	0.00008	0.00369	0.00011	15
57.8	0.00350	0.00008	0.00355	0.00007	0.00365	0.00009	16
63.1	0.00347	0.00007	0.00353	0.00006	0.00362	0.00008	17
68.3	0.00345	0.00006	0.00352	0.00006	0.00359	0.00008	18
73.6	0.00344	0.00006	0.00350	0.00005	0.00357	0.00007	19
78.8	0.00343	0.00005	0.00349	0.00005	0.00355	0.00006	20
84.1	0.00342	0.00004	0.00348	0.00004	0.00353	0.00006	21
89.3	0.00341	0.00004	0.00347	0.00004	0.00351	0.00005	22
94.6	0.00340	0.00004	0.00346	0.00004	0.00350	0.00005	23
99.8	0.00339	0.00003	0.00345	0.00003	0.00349	0.00005	24

^a Average of 10 stopped-flow repetitions.

TABLE A-36. Apparent Rate Constants for the Displacement Reaction Between MNBB⁺ (0.08 M) and PNPO⁻ (0.06 mM) in Acetonitrile over the First Half-Life at 298K as a Function of Wavelengths (2)^a

time/s	440 nm		450 nm		460 nm		Segment
	k_{app}/s^{-1}	\pm	k_{app}/s^{-1}	\pm	k_{app}/s^{-1}	\pm	
0.6	0.01574	0.01126	0.01275	0.00537	0.01786	0.01195	1
1.1	0.00727	0.00517	0.00670	0.00273	0.00803	0.00550	2
1.6	0.00534	0.00314	0.00553	0.00239	0.00512	0.00342	3
2.2	0.00452	0.00224	0.00495	0.00172	0.00406	0.00203	4
2.7	0.00433	0.00187	0.00476	0.00126	0.00366	0.00118	5
5.3	0.00539	0.00118	0.00499	0.00074	0.00403	0.00070	6
10.6	0.00522	0.00042	0.00500	0.00044	0.00438	0.00052	7
15.8	0.00480	0.00025	0.00465	0.00034	0.00423	0.00036	8
21.1	0.00451	0.00020	0.00437	0.00027	0.00405	0.00029	9
26.3	0.00431	0.00017	0.00417	0.00022	0.00391	0.00023	10
31.6	0.00416	0.00014	0.00403	0.00018	0.00380	0.00019	11
36.8	0.00405	0.00012	0.00393	0.00015	0.00372	0.00016	12
42.1	0.00396	0.00011	0.00385	0.00013	0.00366	0.00014	13
47.3	0.00389	0.00010	0.00378	0.00011	0.00362	0.00012	14
52.6	0.00383	0.00009	0.00373	0.00010	0.00358	0.00011	15
57.8	0.00379	0.00008	0.00368	0.00009	0.00355	0.00010	16
63.1	0.00375	0.00007	0.00365	0.00008	0.00353	0.00009	17
68.3	0.00372	0.00006	0.00362	0.00007	0.00350	0.00008	18
73.6	0.00369	0.00006	0.00359	0.00007	0.00348	0.00007	19
78.8	0.00366	0.00006	0.00357	0.00006	0.00347	0.00007	20
84.1	0.00364	0.00005	0.00355	0.00005	0.00345	0.00006	21
89.3	0.00362	0.00005	0.00353	0.00005	0.00344	0.00006	22
94.6	0.00360	0.00005	0.00352	0.00005	0.00342	0.00006	23
99.8	0.00359	0.00004	0.00350	0.00005	0.00341	0.00005	24

^a Average of 10 stopped-flow repetitions.

TABLE A-37. Apparent Rate Constants for the Displacement Reaction Between PNBBr (0.08 M) and PNPO⁻ (0.06 mM) in Acetonitrile over the First Half-Life at 298K as a Function of Wavelengths (1)^a

time/s	420 nm		430 nm		Segment
	k_{app}/s^{-1}	\pm	k_{app}/s^{-1}	\pm	
0.4	0.01810	0.01051	0.02758	0.01267	1
0.8	0.01276	0.00438	0.01468	0.00618	2
1.2	0.00988	0.00360	0.01070	0.00484	3
1.5	0.00845	0.00314	0.00928	0.00328	4
1.9	0.00745	0.00274	0.00861	0.00223	5
3.8	0.00593	0.00116	0.00827	0.00122	6
7.5	0.00621	0.00064	0.00778	0.00103	7
11.3	0.00602	0.00051	0.00705	0.00080	8
15.0	0.00572	0.00043	0.00648	0.00063	9
18.8	0.00547	0.00038	0.00607	0.00052	10
22.5	0.00528	0.00034	0.00578	0.00043	11
26.3	0.00513	0.00029	0.00555	0.00037	12
30.0	0.00501	0.00025	0.00537	0.00032	13
33.8	0.00491	0.00022	0.00524	0.00028	14
37.5	0.00484	0.00020	0.00514	0.00025	15
41.3	0.00477	0.00018	0.00506	0.00022	16
45.0	0.00471	0.00016	0.00498	0.00020	17
48.8	0.00467	0.00015	0.00492	0.00018	18
52.5	0.00463	0.00014	0.00487	0.00017	19
56.3	0.00460	0.00013	0.00482	0.00015	20
60.0	0.00458	0.00012	0.00477	0.00014	21
63.8	0.00455	0.00011	0.00474	0.00014	22
67.5	0.00453	0.00010	0.00470	0.00013	23
71.3	0.00451	0.00009	0.00468	0.00012	24

^a Average of 10 stopped-flow repetitions.

TABLE A-38. Apparent Rate Constants for the Displacement Reaction Between PNBBr (0.08 M) and PNPO⁻ (0.06 mM) in Acetonitrile over the First Half-Life at 298K as a Function of Wavelengths (2)^a

time/s	440 nm		450 nm		460 nm		Segment
	k_{app}/s^{-1}	\pm	k_{app}/s^{-1}	\pm	k_{app}/s^{-1}	\pm	
0.4	0.03779	0.01385	0.02809	0.01265	0.04331	0.01540	1
0.8	0.02143	0.00636	0.01824	0.00650	0.02366	0.00805	2
1.2	0.01500	0.00411	0.01361	0.00459	0.01609	0.00540	3
1.5	0.01184	0.00308	0.01135	0.00326	0.01224	0.00398	4
1.9	0.01012	0.00237	0.00996	0.00248	0.01014	0.00317	5
3.8	0.00781	0.00078	0.00763	0.00115	0.00771	0.00131	6
7.5	0.00741	0.00081	0.00728	0.00075	0.00727	0.00055	7
11.3	0.00686	0.00072	0.00681	0.00073	0.00656	0.00036	8
15.0	0.00643	0.00058	0.00635	0.00065	0.00602	0.00030	9
18.8	0.00605	0.00048	0.00598	0.00055	0.00564	0.00027	10
22.5	0.00576	0.00041	0.00568	0.00047	0.00538	0.00024	11
26.3	0.00554	0.00036	0.00546	0.00040	0.00517	0.00021	12
30.0	0.00536	0.00031	0.00528	0.00034	0.00501	0.00019	13
33.8	0.00522	0.00028	0.00515	0.00029	0.00489	0.00017	14
37.5	0.00511	0.00025	0.00504	0.00025	0.00479	0.00015	15
41.3	0.00502	0.00022	0.00494	0.00022	0.00471	0.00014	16
45.0	0.00494	0.00020	0.00487	0.00020	0.00464	0.00013	17
48.8	0.00488	0.00018	0.00480	0.00018	0.00458	0.00012	18
52.5	0.00482	0.00017	0.00474	0.00016	0.00454	0.00011	19
56.3	0.00478	0.00015	0.00469	0.00014	0.00449	0.00010	20
60.0	0.00474	0.00014	0.00465	0.00013	0.00446	0.00009	21
63.8	0.00470	0.00013	0.00461	0.00012	0.00443	0.00009	22
67.5	0.00467	0.00012	0.00458	0.00011	0.00440	0.00008	23
71.3	0.00464	0.00011	0.00455	0.00010	0.00437	0.00008	24

^a Average of 10 stopped-flow repetitions.

TABLE A-39. Apparent Rate Constants for the Displacement Reaction Between PNBBr (0.16 M) and PNPO⁻ (0.06 mM) in Acetonitrile over the First Half-Life at 298K as a Function of Wavelengths (1)^a

time/s	420 nm		430 nm		440 nm		Segment
	k_{app}/s^{-1}	\pm	k_{app}/s^{-1}	\pm	k_{app}/s^{-1}	\pm	
0.3	0.09673	0.02018	0.06606	0.02541	0.08439	0.02087	1
0.5	0.04746	0.01131	0.03618	0.01553	0.04379	0.00973	2
0.7	0.03017	0.00833	0.02369	0.01104	0.02958	0.00600	3
1.0	0.02211	0.00684	0.01823	0.00877	0.02294	0.00462	4
1.2	0.01830	0.00569	0.01585	0.00702	0.01953	0.00412	5
2.4	0.01533	0.00229	0.01485	0.00367	0.01539	0.00400	6
4.8	0.01316	0.00148	0.01280	0.00189	0.01255	0.00177	7
7.1	0.01147	0.00116	0.01123	0.00125	0.01094	0.00089	8
9.5	0.01033	0.00093	0.01014	0.00093	0.00992	0.00061	9
11.9	0.00955	0.00075	0.00942	0.00075	0.00923	0.00049	10
14.3	0.00903	0.00060	0.00891	0.00061	0.00875	0.00041	11
16.6	0.00864	0.00049	0.00854	0.00051	0.00839	0.00034	12
19.0	0.00834	0.00040	0.00827	0.00044	0.00812	0.00029	13
21.4	0.00811	0.00034	0.00806	0.00038	0.00792	0.00025	14
23.8	0.00793	0.00028	0.00791	0.00034	0.00775	0.00022	15
26.1	0.00777	0.00024	0.00779	0.00030	0.00762	0.00020	16
28.5	0.00765	0.00021	0.00769	0.00026	0.00751	0.00018	17
30.9	0.00754	0.00019	0.00760	0.00023	0.00742	0.00016	18
33.3	0.00745	0.00017	0.00753	0.00021	0.00735	0.00014	19
35.6	0.00738	0.00015	0.00746	0.00019	0.00729	0.00013	20
38.0	0.00732	0.00013	0.00740	0.00017	0.00723	0.00012	21
40.4	0.00726	0.00012	0.00735	0.00016	0.00718	0.00011	22
42.8	0.00721	0.00011	0.00730	0.00015	0.00713	0.00010	23
45.1	0.00716	0.00010	0.00726	0.00014	0.00709	0.00010	24

^a Average of 10 stopped-flow repetitions.

TABLE A-40. Apparent Rate Constants for the Displacement Reaction Between PNBBr (0.16 M) and PNPO⁻ (0.06 mM) in Acetonitrile over the First Half-Life at 298K as a Function of Wavelengths (2)^a

time/s	450 nm		460 nm		Segment
	k_{app}/s^{-1}	\pm	k_{app}/s^{-1}	\pm	
0.3	0.03549	0.01566	0.04803	0.02900	1
0.5	0.01897	0.01414	0.02705	0.01512	2
0.7	0.01381	0.00921	0.01844	0.00877	3
1.0	0.01198	0.00631	0.01506	0.00484	4
1.2	0.01150	0.00473	0.01382	0.00331	5
2.4	0.01176	0.00223	0.01264	0.00299	6
4.8	0.01027	0.00106	0.01054	0.00173	7
7.1	0.00936	0.00081	0.00947	0.00123	8
9.5	0.00870	0.00060	0.00877	0.00093	9
11.9	0.00827	0.00047	0.00829	0.00073	10
14.3	0.00796	0.00037	0.00796	0.00059	11
16.6	0.00773	0.00030	0.00771	0.00049	12
19.0	0.00756	0.00025	0.00752	0.00041	13
21.4	0.00745	0.00021	0.00738	0.00035	14
23.8	0.00735	0.00018	0.00727	0.00031	15
26.1	0.00727	0.00016	0.00718	0.00027	16
28.5	0.00720	0.00014	0.00711	0.00024	17
30.9	0.00714	0.00012	0.00705	0.00021	18
33.3	0.00709	0.00011	0.00699	0.00019	19
35.6	0.00705	0.00010	0.00694	0.00017	20
38.0	0.00701	0.00009	0.00690	0.00016	21
40.4	0.00697	0.00008	0.00687	0.00014	22
42.8	0.00694	0.00007	0.00684	0.00013	23
45.1	0.00692	0.00007	0.00681	0.00013	24

^a Average of 10 stopped-flow repetitions.

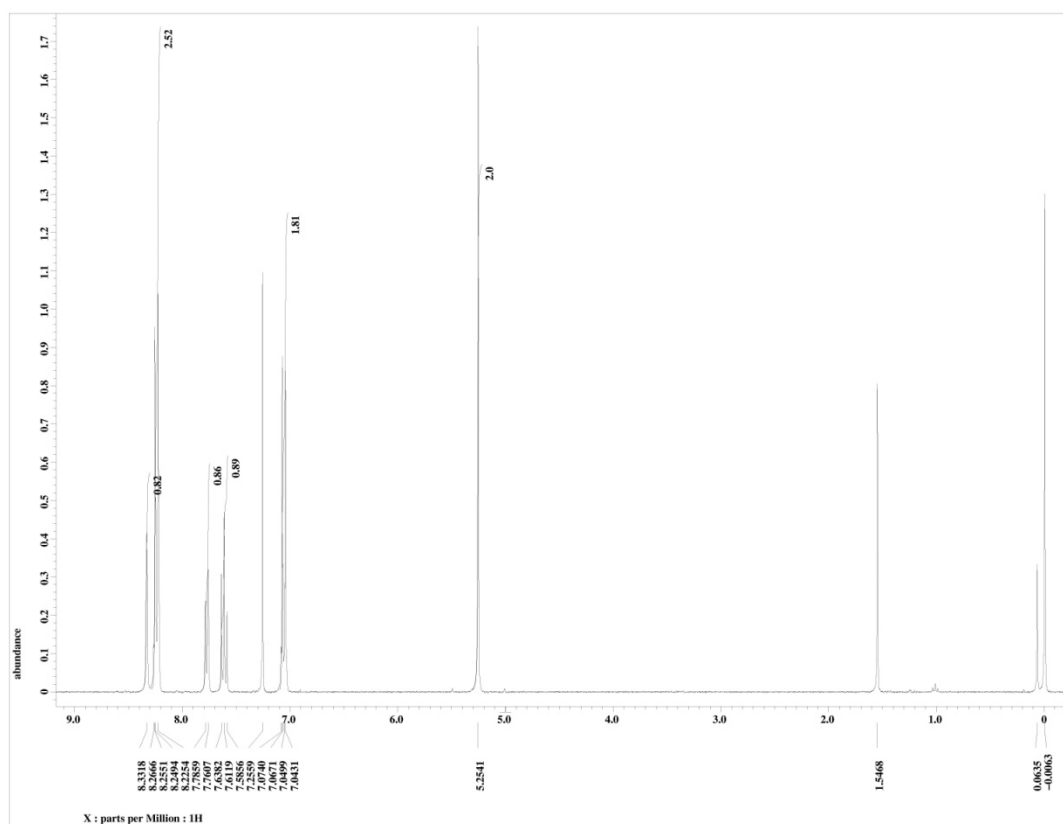


FIGURE A-35. ^1H NMR spectra for the product of the displacement reaction between MNBBBr and PNPO^- in CDCl_3 .

Appendix B. Copyright Permissions

JOHN WILEY AND SONS LICENSE TERMS AND CONDITIONS

Mar 06, 2012

This is a License Agreement between Weifang Hao ("You") and John Wiley and Sons ("John Wiley and Sons") provided by Copyright Clearance Center ("CCC"). The license consists of your order details, the terms and conditions provided by John Wiley and Sons, and the payment terms and conditions.

All payments must be made in full to CCC. For payment instructions, please see information listed at the bottom of this form.

License Number	2863351213455
License date	Mar 06, 2012
Licensed content publisher	John Wiley and Sons
Licensed content publication	International Journal of Chemical Kinetics
Licensed content title	Nonconventional versus conventional application of pseudo-first-order kinetics to fundamental organic reactions
Licensed content author	Vernon D. Parker, Weifang Hao, Zhao Li, Russell Scow
Licensed content date	Jan 1, 2012
Start page	2
End page	12
Type of use	Dissertation/Thesis
Requestor type	Author of this Wiley article
Format	Print and electronic
Portion	Full article
Will you be translating?	No
Order reference number	
Total	0.00 USD

Terms and Conditions

TERMS AND CONDITIONS

This copyrighted material is owned by or exclusively licensed to John Wiley & Sons, Inc. or one of its group companies (each a "Wiley Company") or a society for whom a Wiley Company has exclusive publishing rights in relation to a particular journal (collectively WILEY). By clicking "accept" in connection with completing this licensing transaction, you agree that the following terms and conditions apply to this transaction (along with the billing and payment terms and conditions established by the Copyright Clearance Center Inc., ("CCC's Billing and Payment terms and conditions"), at the time that you opened your Rightslink account (these are available at any time at <http://myaccount.copyright.com>)

Terms and Conditions

1. The materials you have requested permission to reproduce (the "Materials") are protected by copyright.

2. You are hereby granted a personal, non-exclusive, non-sublicensable, non-transferable, worldwide, limited license to reproduce the Materials for the purpose specified in the licensing process. This license is for a one-time use only with a maximum distribution equal to the number that you identified in the licensing process. Any form of republication granted by this license must be completed within two years of the date of the grant of this license (although copies prepared before may be distributed thereafter). The Materials shall not be used in any other manner or for any other purpose. Permission is granted subject to an appropriate acknowledgement given to the author, title of the material/book/journal and the publisher. You shall also duplicate the copyright notice that appears in the Wiley publication in your use of the Material. Permission is also granted on the understanding that nowhere in the text is a previously published source acknowledged for all or part of this Material. Any third party material is expressly excluded from this permission.

3. With respect to the Materials, all rights are reserved. Except as expressly granted by the terms of the license, no part of the Materials may be copied, modified, adapted (except for minor reformatting required by the new Publication), translated, reproduced, transferred or distributed, in any form or by any means, and no derivative works may be made based on the Materials without the prior permission of the respective copyright owner. You may not alter, remove or suppress in any manner any copyright, trademark or other notices displayed by the Materials. You may not license, rent, sell, loan, lease, pledge, offer as security, transfer or assign the Materials, or any of the rights granted to you hereunder to any other person.

4. The Materials and all of the intellectual property rights therein shall at all times remain the exclusive property of John Wiley & Sons Inc or one of its related companies (WILEY) or their respective licensors, and your interest therein is only that of having possession of and the right to reproduce the Materials pursuant to Section 2 herein during the continuance of this Agreement. You agree that you own no right, title or interest in or to the Materials or any of the intellectual property rights therein. You shall have no rights hereunder other than the license as provided for above in Section 2. No right, license or interest to any trademark, trade name, service mark or other branding ("Marks") of WILEY or its licensors is granted hereunder, and you agree that you shall not assert any such right, license or interest with respect thereto.

5. NEITHER WILEY NOR ITS LICENSORS MAKES ANY WARRANTY OR REPRESENTATION OF ANY KIND TO YOU OR ANY THIRD PARTY, EXPRESS, IMPLIED OR STATUTORY, WITH RESPECT TO THE MATERIALS OR THE ACCURACY OF ANY INFORMATION CONTAINED IN THE MATERIALS, INCLUDING, WITHOUT LIMITATION, ANY IMPLIED WARRANTY OF MERCHANTABILITY, ACCURACY, SATISFACTORY QUALITY, FITNESS FOR A PARTICULAR PURPOSE, USABILITY, INTEGRATION OR NON-INFRINGEMENT AND ALL SUCH WARRANTIES ARE HEREBY EXCLUDED BY WILEY AND ITS LICENSORS AND WAIVED BY YOU.

6. WILEY shall have the right to terminate this Agreement immediately upon breach of this Agreement by you.

7. You shall indemnify, defend and hold harmless WILEY, its Licensors and their respective directors, officers, agents and employees, from and against any actual or threatened claims, demands, causes of action or proceedings arising from any breach of this Agreement by you.

8. IN NO EVENT SHALL WILEY OR ITS LICENSORS BE LIABLE TO YOU OR ANY OTHER PARTY OR ANY OTHER PERSON OR ENTITY FOR ANY SPECIAL, CONSEQUENTIAL, INCIDENTAL, INDIRECT, EXEMPLARY OR PUNITIVE DAMAGES, HOWEVER CAUSED, ARISING OUT OF OR IN CONNECTION WITH THE DOWNLOADING, PROVISIONING, VIEWING OR USE OF THE MATERIALS REGARDLESS OF THE FORM OF ACTION, WHETHER FOR BREACH OF CONTRACT, BREACH OF WARRANTY, TORT, NEGLIGENCE, INFRINGEMENT OR OTHERWISE (INCLUDING, WITHOUT LIMITATION, DAMAGES BASED ON LOSS OF PROFITS, DATA, FILES, USE, BUSINESS OPPORTUNITY OR CLAIMS OF THIRD PARTIES), AND WHETHER OR NOT THE PARTY HAS BEEN ADVISED OF THE POSSIBILITY OF SUCH DAMAGES. THIS LIMITATION SHALL APPLY NOTWITHSTANDING ANY FAILURE OF ESSENTIAL PURPOSE OF ANY LIMITED REMEDY PROVIDED HEREIN.

9. Should any provision of this Agreement be held by a court of competent jurisdiction to be illegal, invalid, or unenforceable, that provision shall be deemed amended to achieve as nearly as possible the same economic effect as the original provision, and the legality, validity and enforceability of the remaining provisions of this Agreement shall not be affected or impaired.

thereby.

10. The failure of either party to enforce any term or condition of this Agreement shall not constitute a waiver of either party's right to enforce each and every term and condition of this Agreement. No breach under this agreement shall be deemed waived or excused by either party unless such waiver or consent is in writing signed by the party granting such waiver or consent. The waiver by or consent of a party to a breach of any provision of this Agreement shall not operate or be construed as a waiver of or consent to any other or subsequent breach by such other party.

11. This Agreement may not be assigned (including by operation of law or otherwise) by you without WILEY's prior written consent.

12. Any fee required for this permission shall be non-refundable after thirty (30) days from receipt.

13. These terms and conditions together with CCC's Billing and Payment terms and conditions (which are incorporated herein) form the entire agreement between you and WILEY concerning this licensing transaction and (in the absence of fraud) supersedes all prior agreements and representations of the parties, oral or written. This Agreement may not be amended except in writing signed by both parties. This Agreement shall be binding upon and inure to the benefit of the parties' successors, legal representatives, and authorized assigns.

14. In the event of any conflict between your obligations established by these terms and conditions and those established by CCC's Billing and Payment terms and conditions, these terms and conditions shall prevail.

15. WILEY expressly reserves all rights not specifically granted in the combination of (i) the license details provided by you and accepted in the course of this licensing transaction, (ii) these terms and conditions and (iii) CCC's Billing and Payment terms and conditions.

16. This Agreement will be void if the Type of Use, Format, Circulation, or Requestor Type was misrepresented during the licensing process.

17. This Agreement shall be governed by and construed in accordance with the laws of the State of New York, USA, without regards to such state's conflict of law rules. Any legal action, suit or proceeding arising out of or relating to these Terms and Conditions or the breach thereof shall be instituted in a court of competent jurisdiction in New York County in the State of New York in the United States of America and each party hereby consents and submits to the personal jurisdiction of such court, waives any objection to venue in such court and consents to service of process by registered or certified mail, return receipt requested, at the last known address of such party.

Wiley Open Access Terms and Conditions

All research articles published in Wiley Open Access journals are fully open access: immediately freely available to read, download and share. Articles are published under the terms of the [Creative Commons Attribution Non Commercial License](#), which permits use, distribution and reproduction in any medium, provided the original work is properly cited and is not used for commercial purposes. The license is subject to the Wiley Open Access terms and conditions: Wiley Open Access articles are protected by copyright and are posted to repositories and websites in accordance with the terms of the [Creative Commons Attribution Non Commercial License](#). At the time of deposit, Wiley Open Access articles include all changes made during peer review, copyediting, and publishing. Repositories and websites that host the article are responsible for incorporating any publisher-supplied amendments or retractions issued subsequently. Wiley Open Access articles are also available without charge on Wiley's publishing platform, **Wiley Online Library** or any successor sites.

Use by non-commercial users

For non-commercial and non-promotional purposes individual users may access, download, copy, display and redistribute to colleagues Wiley Open Access articles, as well as adapt, translate, text-

and data-mine the content subject to the following conditions:

- The authors' moral rights are not compromised. These rights include the right of "paternity" (also known as "attribution" - the right for the author to be identified as such) and "integrity" (the right for the author not to have the work altered in such a way that the author's reputation or integrity may be impugned).
- Where content in the article is identified as belonging to a third party, it is the obligation of the user to ensure that any reuse complies with the copyright policies of the owner of that content.
- If article content is copied, downloaded or otherwise reused for non-commercial research and education purposes, a link to the appropriate bibliographic citation (authors, journal, article title, volume, issue, page numbers, DOI and the link to the definitive published version on Wiley Online Library) should be maintained. Copyright notices and disclaimers must not be deleted.
- Any translations, for which a prior translation agreement with Wiley has not been agreed, must prominently display the statement: "This is an unofficial translation of an article that appeared in a Wiley publication. The publisher has not endorsed this translation."

Use by commercial "for-profit" organisations

Use of Wiley Open Access articles for commercial, promotional, or marketing purposes requires further explicit permission from Wiley and will be subject to a fee. Commercial purposes include:

- Copying or downloading of articles, or linking to such articles for further redistribution, sale or licensing;
- Copying, downloading or posting by a site or service that incorporates advertising with such content;
- The inclusion or incorporation of article content in other works or services (other than normal quotations with an appropriate citation) that is then available for sale or licensing, for a fee (for example, a compilation produced for marketing purposes, inclusion in a sales pack)
- Use of article content (other than normal quotations with appropriate citation) by for-profit organisations for promotional purposes
- Linking to article content in e-mails redistributed for promotional, marketing or educational purposes;
- Use for the purposes of monetary reward by means of sale, resale, licence, loan, transfer or other form of commercial exploitation such as marketing products
- Print reprints of Wiley Open Access articles can be purchased from: corporate-sales@wiley.com

Other Terms and Conditions:

BY CLICKING ON THE "I AGREE..." BOX, YOU ACKNOWLEDGE THAT YOU HAVE READ AND FULLY UNDERSTAND EACH OF THE SECTIONS OF AND PROVISIONS SET FORTH IN THIS AGREEMENT AND THAT YOU ARE IN AGREEMENT WITH AND ARE WILLING TO ACCEPT ALL OF YOUR OBLIGATIONS AS SET FORTH IN THIS AGREEMENT.

v1.7

If you would like to pay for this license now, please remit this license along with your

payment made payable to "COPYRIGHT CLEARANCE CENTER" otherwise you will be invoiced within 48 hours of the license date. Payment should be in the form of a check or money order referencing your account number and this invoice number RLNK500734106.

Once you receive your invoice for this order, you may pay your invoice by credit card. Please follow instructions provided at that time.

Make Payment To:
Copyright Clearance Center
Dept 001
P.O. Box 843006
Boston, MA 02284-3006

For suggestions or comments regarding this order, contact RightsLink Customer Support: customercare@copyright.com or +1-877-622-5543 (toll free in the US) or +1-978-646-2777.

Gratis licenses (referencing \$0 in the Total field) are free. Please retain this printable license for your reference. No payment is required.

Zhao Li
Dept. of Chemistry and Biochemistry
Utah State University
0300 Old Main Hill
Logan, UT 84322-0300

I, Zhao Li, do hereby grant Weifang Hao permission to reprint the articles I coauthored in her doctoral dissertation.

Article: "Non-conventional vs. conventional application of pseudo-first-order kinetics to fundamental organic reactions" coauthored by Vernon D. Parker, Weifang Hao and Russell Scow, *Int. J. Chem. Kinet.*, **2012**, *44*, 2-12.



Date 03-05-2012

Zhao Li

Russell Scow
Utah State University Alumni
4645 Sunstone Rd #36
Taylorsville, Utah 84123

I, Russell Scow, do hereby grant Weifang Hao permission to reprint the articles I coauthored in her doctoral dissertation.

Article: "Non-conventional vs. conventional application of pseudo-first-order kinetics to fundamental organic reactions" coauthored by Vernon D. Parker, Weifang Hao and Zhao Li, *Int. J. Chem. Kinet.* **2012**, 44, 2-12.



Date 2/11/12

Russell Scow



RightsLink®

Home

Account
Info

Help



ACS Publications
High quality. High impact.

Title: Rapid Formation and Slow
Collapse of a Carbocation–Anion
Pair to a Neutral Molecule
Author: Weifang Hao et al.
Publication: The Journal of Organic
Chemistry
Publisher: American Chemical Society
Date: Jan 1, 2008
Copyright © 2008, American Chemical Society

Logged in as:
Weifang Hao

LOGOUT

PERMISSION/LICENSE IS GRANTED FOR YOUR ORDER AT NO CHARGE

This type of permission/license, instead of the standard Terms & Conditions, is sent to you because no fee is being charged for your order. Please note the following:

- Permission is granted for your request in both print and electronic formats.
- If figures and/or tables were requested, they may be adapted or used in part.
- Please print this page for your records and send a copy of it to your publisher/graduate school.
- Appropriate credit for the requested material should be given as follows: "Reprinted (adapted) with permission from (COMPLETE REFERENCE CITATION). Copyright (YEAR) American Chemical Society." Insert appropriate information in place of the capitalized words.
- One-time permission is granted only for the use specified in your request. No additional uses are granted (such as derivative works or other editions). For any other uses, please submit a new request.

BACK

CLOSE WINDOW

Copyright © 2012 Copyright Clearance Center, Inc. All Rights Reserved. [Privacy statement](#).
Comments? We would like to hear from you. E-mail us at customercare@copyright.com

CURRICULUM VITAE

Weifang Hao

Department of Chemistry and Biochemistry

Utah State University, Logan, UT 84322-0300

Cell phone: (435)754-6149

E-mail: weifang.hao@aggiemail.usu.edu**EDUCATION**

Ph.D., Organic Chemistry, Utah State University, Logan, Utah	May 2012
Ph.D., Organic Chemistry, Nankai University, P. R. China	July 2005
B.S., Chemistry, Zhengzhou University, P. R. China	July 2000

TEACHING EXPERIENCE**Teaching Assistant**

Utah State University, Logan, Utah	August 2007-May 2009
------------------------------------	----------------------

Developed curriculum in all areas including illustration, grading, preparing quizzes, holding office hours, and assigning final grades

- General Chemistry Lab 1215 Spring 2008, Fall 2008, Spring 2009
- Organic Chemistry Lab 2315 Fall 2007

Nankai University, Tianjin, P.R.China	August 2001-July 2002
---------------------------------------	-----------------------

- Organic Chemistry Lab

Grader

Utah State University, Logan, Utah	August 2008-December 2008
------------------------------------	---------------------------

- Organic Chemistry 2310

TRAINING EXPERIENCE

- Supervised three undergraduate students' innovation projects related to the biological active molecules NO and NADH at Nankai University
- Conducted the training of ten undergraduate and graduate students performing kinetics on several organic reaction systems during their research at Utah State University

RESEARCH EXPERIENCE

Postdoctoral Research Fellow, Advisor: Prof. Vernon D. Parker,
Department of Chemistry & Biochemistry, Utah State University, Logan, Utah,
July 2005-July 2007

- Employed the non-steady-state kinetic methods developed in the Parker's lab to clarify the detailed mechanisms of various fundamental organic reactions and to confirm the existence of more than one transition state on the reaction coordinate of these important reactions
- Developed novel analysis methods to unambiguously distinguish between simple single-step and multi-step complex reaction mechanisms

Ph.D. Graduate Student, Advisors: Prof. Jin-Pei Cheng & Prof. Xiao-Qing Zhu,
State Key Laboratory of Elemento-Organic Chemistry, Nankai University,
Tianjin, P. R. China September 2000-July 2005

- Determine the N-NO bond dissociation energies of nitrosoamines, performed the thermodynamics and kinetics investigation on the NO transfer mechanism from its donor to substrates

- Synthesized the metalloporphyrins and nitrosylmetalloporphyrin complexes, determined the metal-NO bond dissociation energies of nitrosylmetalloporphyrin complexes, analyzed the charge distribution on the metal-NO bond in nitrosylmetalloporphyrin complexes
- Designed and synthesized the NADH coenzyme model compounds, performed the thermodynamics and kinetics investigations on the hydride transfer mechanism from NADH models to substrates
- Performed kinetic investigation on the oxidation mechanism of NADH models Hantzsch 1,4-dihydropyridines by RSNO

TECHNIQUES AND EXPERTISE

- Hi-Tech Stopped-Flow Spectroscopy
- BAS-100B Electrochemical Analyzer
- Agilent UV-Vis Spectrophotometer
- Tronac-450 Thermal Titration Calorimetry
- Jeol ECX-300NMR Instrument
- ITC-4200 Isothermal Titration Calorimetry
- IR Spectrophotometer
- Glove Box, *etc.*

PUBLICATIONS

- Vernon D. Parker, Weifang Hao, Zhao Li and Russell Scow, "Nonconventional versus Conventional Application of Pseudo-First-Order Kinetics to Fundamental Organic Reactions", *International Journal of Chemical Kinetics*, **2012**, 44(1), 2-12;
- Vernon D. Parker, Zhao Li, Kishan L. Handoo, Weifang Hao and Jin-Pei Cheng, "The Reversible Consecutive Mechanism for the Reaction of Trinitroanisole with Methoxide Ion", *The Journal of Organic Chemistry*, **2011**, 76(5), 1250-1256;

- **Weifang Hao** and Vernon D. Parker, “Rapid Formation and Slow Collapse of a Carbocation-Anion Pair to a Neutral Molecule”, *The Journal of Organic Chemistry (Featured Article)*, **2008**, 73(1), 48-55;
- Xiao-Qing Zhu, **Weifang Hao**, Hui Tang, Chun-Hua Wang and Jin-Pei Cheng, “Determination of N-NO Bond Dissociation Energies of *N*-Methyl-*N*-Nitrosobenzene sulfonamides in Acetonitrile and Application in the Mechanism Analyses on NO Transfer”, *Journal of the American Chemical Society*, **2005**, 127(8), 2696-2708;
- Xiao-Qing Zhu, Qian Li, **Weifang Hao** and Jin-Pei Cheng, “Dissociation Energies and Charge Distribution of the Co-NO Bond for Nitrosyl- $\alpha,\beta,\gamma,\delta$ -tetraphenylporphinato-cobalt(II) and Nitrosyl- $\alpha,\beta,\gamma,\delta$ -tetraphenylporphinatocobalt(III) in Benzonitrile Solution”, *Journal of the American Chemical Society*, **2002**, 124(33), 9887-9893;
- **Weifang Hao**, Hui Tang, Xiao-Qing Zhu and Jin-Pei Cheng, “Heterolytic and Homolytic N-NO Bond Dissociation Energies of *N*-Nitrosobenzenesulfonylmethylamines in Acetonitrile”, *Chinese Journal of Organic Chemistry*, **2003**, 23, Suppl., 172;
- **Weifang Hao**, Xiao-Qing Zhu and Jin-Pei Cheng, “Oxidation Mechanisms of NAD(P)H Model Hantzsch 1,4-Dihydropyridines by RSNO”, *Chinese Journal of Organic Chemistry*, **2003**, 23, Suppl., 171.

PRESENTATION

- **Weifang Hao**, Xiao-Qing Zhu and Jin-Pei Cheng, *Twelfth Fechem Conference on Heterocycles in Bio-organic Chemistry*, Siena, Italy, **2004**, PO-55, 192-193.

POSTERS

- **Weifang Hao** and Vernon D. Parker, "The Mechanism of the Hydride Transfer Reaction between 1-Benzyl-3-cyanoquinolinium Ion with *N*-Methyl-9,10-dihydroacridine in Acetonitrile", *The 33rd Reaction Mechanisms Conference*, University of Massachusetts Amherst, June 23-26, **2010**, 55;
- **Weifang Hao**, Lan Ban, Xiao-Qing Zhu and Jin-Pei Cheng, "Kinetic and Mechanistic Investigation of the Oxidation of Hantzsch 1,4-Dihydropyridines Derivatives by *N*-Benzylphenothiazine Radical Cation in Acetonitrile", *The 24th Chinese Chemical Society Conference*, Changsha, China, **2004**;
- Qian Li, **Weifang Hao**, Juan Cheng, Xiao-Qing Zhu, Jia-Qi He and Jin-Pei Cheng, *The Second National Organic Chemistry Science Conference*, Hangzhou, China, **2001**, 586;
- Qian Li, Juan Cheng, **Weifang Hao**, Xiao-Qing Zhu, Jia-Qi He and Jin-Pei Cheng, *The Second National Organic Chemistry Science Conference*, Hangzhou, China, **2001**, 587.